THE UNIVERSITY *of* EDINBURGH

Nonequilibrium Emergent Interactions between Run-and-Tumble Random Walkers

Alexander Slowman

Doctor of Philosophy
The University of Edinburgh
October 2017

Lay Summary

This thesis presents the study of a theoretical model inspired by the way certain species of bacteria swim, where they propel themselves, or *run*, in a reasonably straight line and, every so often, randomly change their direction in a process known as *tumbling*. They are termed *run-and-tumble random walkers*. The randomness comes from the times at which they change direction, which are not predetermined but governed by probabilistic rules.

The work in this thesis contributes to the study of particles that use their own on-board supply of energy to propel themselves. This *activity* distinguishes them from *passive* particles, which move only according to ambient thermal fluctuations. For example, pollen grains on the surface of water, if looked at closely, move in random directions with very rapid fluctuations. This movement is due to microscopic water particles, which themselves only have energy from the ambient environment, bombarding the grains from many different directions. When particles are at the mercy of these thermal fluctuations, they are known as *equilibrium* matter. In contrast, bacteria, although they also experience the effects of thermal fluctuations, can move themselves in a definite direction using their tail-like appendages called *flagella*. Hence they are *out of equilibrium*.

The focus of this thesis is the behaviour of nonequilibrium run-and-tumble random walkers when they are subject to a simple rule known as an *exclusion* interaction: they may not occupy the same region of space at the same time. The principal finding is that the equations describing the long-time motion of two of these particles show that they spend much of the time close together, as if attracted to each other. This might appear surprising as the particles only interact repulsively via exclusion. Thus this attraction *emerges* from the combination of run-and-tumble motion and exclusion. These results may help explain why, when there are large numbers of run-and-tumble particles, they tend to congregate together in clusters, which other works have previously observed.

Abstract

Nonequilibrium statistical physics involves the study of many-particle systems that break time reversibility—also known as detailed balance—at some scale. For states in thermal equilibrium, which must respect detailed balance, the comprehensive theory of statistical mechanics was developed to explain how their macroscopic properties arise from interactions between their microscopic constituent particles; for nonequilibrium states no such theory exists. The study of active matter, made up of particles that individually transduce free energy to produce systematic movement, provides a paradigm in which to develop an understanding of nonequilibrium behaviours. In this thesis, we are interested in particular in the microscopic interactions that generate the clustering of active particles that has been widely observed in simulations, and may have biological relevance to the formation of bacterial assemblages known as biofilms, which are an important source of human infection.

The focus of this thesis is a microscopic lattice-based model of two random walkers interacting under mutual exclusion and undergoing the run-and-tumble dynamics that characterise the motion of certain species of bacteria, notably *Escherichia coli*. I apply perturbative and exact analytic approaches from statistical physics to three variants of the model in order to find the probability distributions of their nonequilibrium steady states and elucidate the emergent interactions that manifest.

I first apply a generating function approach to the model on a one-dimensional periodic lattice where the particles perform straight line *runs* randomly interspersed by instantaneous velocity reversals or *tumbles*, and find an exact solution to the stationary probability distribution. The distribution can be interpreted as an effective non-equilibrium pair potential that leads to a finite-range attraction in addition to jamming between the random walkers. The finite-range attraction collapses to a delta function in the limit of continuous space and

time, but the combination of this jamming and attraction is sufficiently strong that even in this continuum limit the particles spend a finite fraction of time next to each other. Thus, although the particles only interact directly through repulsive hard-core exclusion, the activity of the particles causes the emergence of attractive interactions, which do not arise between passive particles with repulsive interactions and dynamics respecting detailed balance.

I then relax the unphysical assumption of instantaneous tumbling and extend the interacting run-and-tumble model to incorporate a finite tumbling duration, where a tumbling particle remains stationary on its site. Here the exact solution for the nonequilibrium stationary state is derived using a generalisation of the previous generating function approach. This steady state is characterised by two lengthscales, one arising from the jamming of approaching particles, familiar from the instant tumbling model, and the other from one particle moving when the other is tumbling. The first of these lengthscales vanishes in a scaling limit where continuum dynamics is recovered. However, the second, entirely new, lengthscale remains finite. These results show that the feature of a finite tumbling duration is relevant to the physics of run-and-tumble interactions.

Finally, I explore the effect of walls on the interacting run-and-tumble model by applying a perturbative graph-theoretic approach to the model with reflecting boundaries. Confining the particles in this way leads to a probability distribution in the low tumble limit with a much richer structure than the corresponding limit for the model on a periodic lattice. This limiting probability distribution indicates that an interaction over a finite distance emerges not just between the particles, but also between the particles and the reflecting boundaries.

Together, these works provide a potential pathway towards understanding the clustering of self-propelled particles widely observed in active matter from a microscopic perspective.

Acknowledgements

I would like to express my deepest thanks to my principal supervisor, Richard Blythe, and to my second supervisor, Martin Evans, for their support and guidance throughout all the work presented in this thesis.

I would also like to express my gratitude to the School of Physics and Astronomy, and in particular to the members of the Statistical Physics and Soft Matter groups, for making Edinburgh such a wonderful place to work and study.

I acknowledge funding for my studies through an EPSRC studentship.

Declaration

I declare that this thesis was composed by myself, that the work contained herein is my own except where explicitly stated otherwise in the text, and that this work has not been submitted for any other degree or professional qualification except as specified.

Parts of this work have been published in

A. B. Slowman, M. R. Evans, and R. A. Blythe. Jamming and attraction of interacting run-and-tumble random walkers. *Phys. Rev. Lett.*, 116:218101, 2016.

A. B. Slowman, M. R. Evans, and R. A. Blythe. Exact solution of two interacting run-and-tumble random walkers with finite tumble duration. *Journal of Physics A: Mathematical and Theoretical*, 50:375601, 2017.

(*Alexander Slowman,* October 2017)

Contents

List of Figures

List of Tables

Chapter 1

Introduction: statistical mechanics and bacterial dynamics

The problem of bacterial dynamics sits at the crossroads of statistical mechanics and biology. The ability of some bacteria to swim via self-propulsion, and the interactions mediated by this motion, are the subjects of intense research in both microbiology and biophysics [1–5]. From a physical perspective, the key feature of bacterial self-propulsion is that it derives from the conversion of on-board chemical energy into directed motion [3]. In biophysical communities, this process marks bacteria as constituents of *active matter* [2], whose macroscopic characteristics can differ strongly from the more traditional passive matter that rests in thermal equilibrium with its environment [6–10]. The distinction between active and passive matter is reflected at the scale of microscopic theory: self-propulsion, for which there is forward motion without corresponding reversals, necessarily breaks time-reversal symmetry, which is characteristic of systems in equilibrium [3]. Therefore bacterial dynamics is, at the fundamental theoretical level, also part of the family of inherently nonequilibrium processes that are the focus of modern statistical mechanics.

A major theoretical goal in nonequilibrium statistical mechanics is to identify how the Boltzmann distribution of particle configurations generalises beyond equilibrium conditions. In equilibrium systems, forces derive from a potential, energy is exchanged reversibly with the environment and the probability of a particle configuration is entirely determined by the potential. In nonequilibrium systems, where energy is exchanged irreversibly with the environment, there is

no one-to-one relationship between a potential that governs interparticle forces and the probability distribution, even in a *stationary*, or *steady*, state where the probability does not change in time. This means that *effective* forces between particles can emerge [3]. It is such nonequilibrium effective interactions, specifically those that can manifest in models of bacterial dynamics, that are the subject of this thesis.

In this work, I present the analytic solutions of variants of a theoretical model inspired by the dynamics of interacting bacteria. From these analytic solutions, we identify emergent interactions between the particles, which are qualitatively completely different from the much simpler *bare* interactions that serve as inputs to the model. In this chapter we examine the background to this model, and where it sits within the wider context of biology, biophysics and statistical mechanics.

The model studied in this thesis is a lattice-based interacting random walk. I trace the emerging relationship between the theory of random walks and the study of active matter in section 1.1 of this introductory chapter. Within active matter there has been particular interest in a type of bacterial motion known as *run-and-tumble dynamics*, which has been extensively studied in experiments as detailed in section 1.2. These observations have served as inspiration for a prototypical model of active random walks introduced in section 1.3. Section 1.4 describes how this run-and-tumble random walk model with *interactions* has been used to investigate the striking clustering phenomena collectively known as *motility-induced phase separation*. Recent efforts to elucidate the form of the effective interactions that lead to such clustering are summarised in section 1.5, setting the stage for the investigations of interacting run-and-tumble random walkers presented in this thesis. Finally, in section 1.6, I outline the structure of the remaining thesis chapters.

1.1 Random walks of active particles

A *random walk* is generated by a sequence of displacements whose magnitude and direction are governed by probabilistic rules [11]. The role of random walks in systems of statistical physics has its origins in the stochastic formulation of *Brownian* motion [11, 12]. Brownian motion is concerned with the irregular movement presented by particles of colloidal size immersed in a fluid. An example of such particles are pollen grains, which were the subject of the experiments of

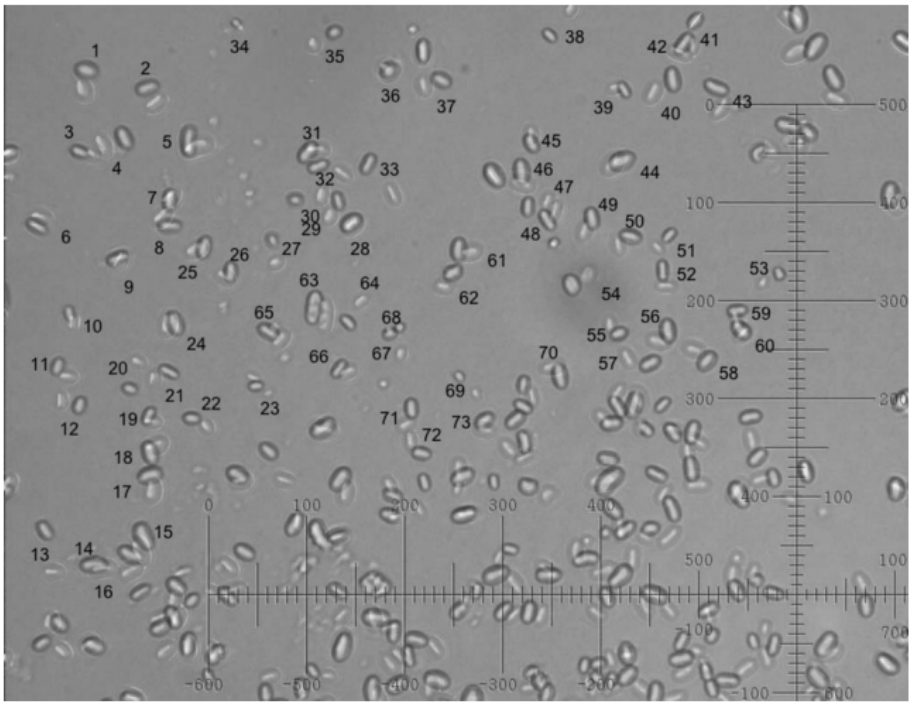

Figure 1.1 *(Reproduced from [14]) Two superimposed photos of Clarkia pulchella pollen taken 1 minute apart. The scale is 2 μm per division.*

Robert Brown who would give his name to their "rapid oscillatory motion" [13]. A picture of *Clarkia pulchella* pollen, whose grains are of the type Brown observed in his pioneering investigations, is shown in Figure 1.1.

The motion of a Brownian particle is maintained by fluctuations in the collisions with molecules in the surrounding fluid. These collisions are so frequent, each having a tiny effect on the path of the particle, that collisions can neither be separated from each other, nor can the effect of any single collision be resolved [15]. Thus the motion of a Brownian particle is modelled in two parts: a systematic part relating to its instantaneous velocity, $\mathbf{u}$, and second part independent of its velocity that fluctuates extremely rapidly compared to $\mathbf{u}$, and has only statistically defined properties [11]. A description of such a statistically defined process is known as *stochastic* modelling.

The most common way to describe a Brownian particle is through a stochastic form of Newton's second law known as a *Langevin* description [16]. Following [16], the time evolution of the Brownian particle with velocity $\mathbf{u}$ at position $\mathbf{r}$ is written

(rescaling so that mass is equal to one) as

$$\frac{\mathrm{d}\mathbf{u}}{\mathrm{d}t} = -\gamma\mathbf{u} - \nabla V(\mathbf{r}) + F(t) \tag{1.1}$$

where $\gamma\mathbf{u}$ is the Stokes friction, which is the drag force exerted on spherical objects in small Reynolds number flow where viscous forces are dominant, $V(\mathbf{r})$ is some space-dependent potential (that may be zero) and $F(t)$ is some short-correlated random force. This force is Gaussian-distributed with independent components and δ-correlated time dependence:

$$\langle F(t)\rangle = 0 \tag{1.2}$$

$$\langle F_i(t)F_j(t)\rangle = 2D'\delta_{i,j}\delta(t-t') \quad i,j = x,y,z, \tag{1.3}$$

where D' is the intensity of the noise. In turn, a solution to (1.1) is expressed as a distribution over all possible positions. This description transforms an initial (intractable) deterministic description of the many interacting water and pollen particles, and replaces it with one in terms of probability distributions. Thus this formulation is properly in the realm of statistical physics.

When a system is in thermal equilibrium with its environment, its particles are distributed according to the *Gibbs-Boltzmann* probability weight $p \sim e^{-\beta U}$, where β is the inverse temperature and U is the potential of the system [16, 17]. This enables a connection to be made between the stochastic description of a Brownian particle (shown above in terms of a Langevin equation) and physically measurable quantities. In the classic case of a Brownian particle undergoing diffusion in equilibrium, the diffusion constant (a measure of its mean-squared displacement) may be expressed in terms of physical parameters and constants. Specifically, the diffusion constant, D, given by

$$D = \frac{\bar{x^2}}{2dt} \tag{1.4}$$

where $\bar{x^2}$ is the mean-squared displacement at time t in dimension d, may be expressed as

$$D = \frac{k_\mathrm{B}T}{\gamma} \tag{1.5}$$

where T is the temperature and k_B is the Boltzmann constant [18]. Thus the dynamics of the motion of the particle, characterised by the mean-squared displacement, can be described without dependence on the specific forces maintaining the equilibrium.

The theory of Brownian motion has had enormous success in a wide range of applications from colloidal physics to fluid mechanics [15]. However, implicit in this description is that the Brownian particle is passive: its motion is determined only by collisions. This passive restriction excludes the subject of this thesis, which are particles that self-propel: a system of active matter.

Active matter are driven systems for which energy is supplied directly and independently to the individual constituents: active particles [2, 16]. In general, active particles will, by dissipating this energy, produce some kind of propulsion resulting in systematic movement [2]. These self-propelled particles may be naturally occurring, such as birds, or synthetic, such as photoactivated colloids [19], whose propulsion can be turned on and off with a blue light.

As elucidated by Ramaswamy in his review article [2], it is not just the individual motion of these particles which is of interest, but their collective emergent behaviours. Birds are known to flock and it is this behaviour that has been the subject of some of the earliest investigations in active matter [2]. Reynolds was the first to model birds as orientationally ordered interacting particles that try to align their velocity vectors with their neighbours in the presence of noise [20]. The work of Viscek and collaborators shows that this model presents a phase transition from a disordered state to a flock (see Figure 1.3) with long-range order in the velocities of the 'birds' as the concentration of particles is increased, or the strength of the noise is decreased [6–8, 21]. Work by Andrea Cavagna and collaborators, using a different but related theory to that of Viscek, has explained data from observations of real starling flocks [22]. A picture of such a flocking event is shown in Figure 1.2. Fascinating emergent behaviours have also been observed in the case of photoactivated colloids, where competition between their self-propulsion and an attractive interaction induced by phoretic effects leads to the formation 'living crystals', which form, break, explode, and re-form in a different place [19].

Active matter therefore encompasses an enormous range of natural phenomena, and correspondingly there are diverse theoretical approaches to describing it. The long-range order observed in the flocking models described above was explained using coarse-grained field-theoretic methods by Toner and Tu [6, 8]. Swimming organisms also exhibit fascinating collective motion through their interactions with the surrounding fluid and are another focus of the study of active matter [2]. They may be understood through coupling the dynamical equations of the swimmers and the Navier-Stokes equation describing the velocity field of the

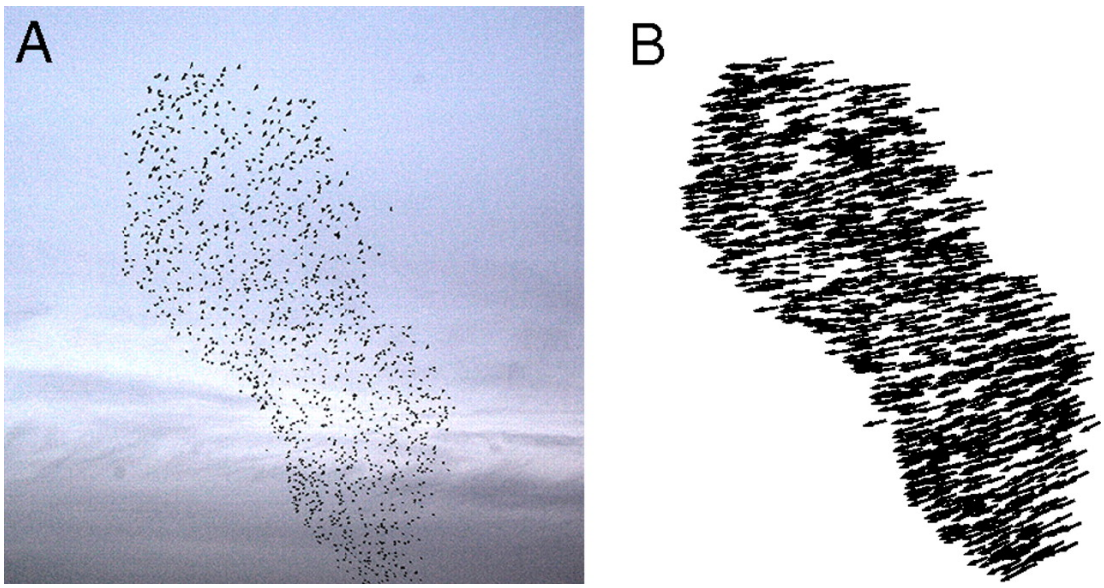

Figure 1.2 *(Reproduced from [23]) (A) One snapshot from a flocking event with 1,246 birds. (B) Instantaneous vector velocities of all the individuals in this snapshot.*

suspension [24]. Separately, there has been much recent progress in active matter that ignores both alignment and hydrodynamic interactions: *scalar active matter* [25–27]. All these works share the common use of continuum models for a system of many interacting constituents described at large scales by only a few fields. They might generally be called *hydrodynamic* approaches to active matter, where this use of the term "hydrodynamics" is not restricted to the study of interactions mediated by a fluid [9].

In contrast to hydrodynamic approaches, microscopic models describe the system at the level of the individual particles of interest without further coarse-graining beyond a stochastic description of individual particle motion. In studies using simulations, a microscopic formulation provides a test of coarse-grained theories, and often presents evidence of new emergent phenomena that have not yet be captured by existing analytic theories [28–30]. Complementing computational work, analytic investigations of microscopic models present the opportunity to more deeply understand the origin of behaviours predicted by coarse-grained methods. It is here that the theory of random walks provides a natural framework in which to study self-propelled particles [1].

There are two prototypical microscopic models of self-propelled particles: *active Brownian particles* and run-and-tumble particles [16, 31]. Active Brownian particles inherit from the Langevin description of Eq. (1.1). They self-propel at a

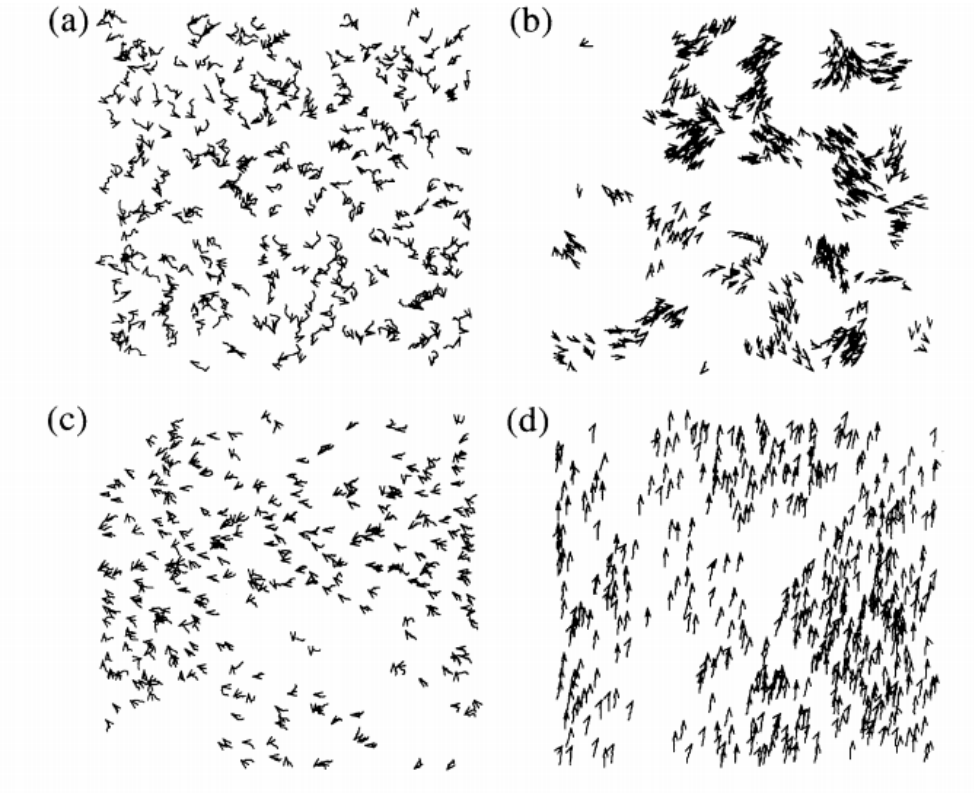

Figure 1.3 *(Reproduced from [21]) The velocities of self-propelled particles driven with a constant speed. At each time step the particles assume the average direction of nearby particles subject to a random perturbation. The figures show the system at different densities and subject to different levels of the random perturbative noise. (a) displays an initial configuration. (b) shows that when both the density and noise are small the particles form small groups and move collectively in different directions. In (c) the noise and density are higher than in (b), and the particles move randomly with some correlation. The highest density with small noise is shown in (d), where the motion is ordered.*

fixed speed along a body-axis that reorients through slow angular diffusion [31]. The self-propulsion occurs through a constant external force applied to each particle along its swim direction $\mathbf{u}$. In this minimal model, the only dynamics in addition to self-propulsion comes from continuous angular diffusion from the same stochastic source as for passive Brownian motion. Following [16], the evolution of an active Brownian particle (again taking mass equal to 1) is governed by the equation

$$\frac{\mathrm{d}\mathbf{u}}{\mathrm{d}t} = -\gamma(\mathbf{r},\mathbf{u})\mathbf{u} - \nabla V(\mathbf{r}) + F(t) \tag{1.6}$$

where the coefficient of the dissipative force, γ, is now dependent on the position and velocity of the particle, and $F(t)$ remains governed by the relation (1.3),

which is now independent of the parameters in the dissipative force $-\gamma(\mathbf{r}, \mathbf{u})\mathbf{u}$. In the case of a particle moving at a constant velocity, u_0, in two dimensions with velocity parameterised as

$$\mathbf{u} = \{u_0 \cos\theta(t), u_0 \sin\theta(t)\} \tag{1.7}$$

the angular reorientation is described by

$$\frac{\mathrm{d}}{\mathrm{d}t}\theta = \frac{1}{u_0}\sqrt{2D'\xi(t)}. \tag{1.8}$$

Inspired by experiments with synthetic colloids [32–34], microscopic computational models have elucidated many nonequilibrium behaviours in systems of active Brownian particles. These include the pressure exerted by a suspension of the particles [35], or the phase diagrams of active Brownian particles with soft repulsive interactions that exhibit clustering [36].

The second prototypical model describes run-and-tumble particles. Their interactions are the focus of this thesis. The dynamics of run-and-tumble particles differ from active Brownian particles only in the details of their angular relaxation, which involve discrete changes in direction that characterise tumbling events [31]. Before detailing this model of run-and-tumble particles in section 1.3, we first consider the experimental background to this model in the context of the most well-known organism that performs run-and-tumble motion: the bacterium *Escherichia coli*.

1.2 Run-and-tumble dynamics of Escherichia coli

Although we are concerned principally with the run-and-tumble model we will meet in the next section as a way to understand features of nonequilibrium dynamics from a theoretical perspective, the biological and experimental context is valuable for two reasons. First, it is experimental observations that inspired the model. Thus the background in this section will inform the extent to which it can be relevant to understanding real behaviour in nature and, in particular, if the model can be experimentally realised. Secondly, if the model is initially too idealised to accurately predict experimental results, identification of the weakest approximations will be crucial to improving it.

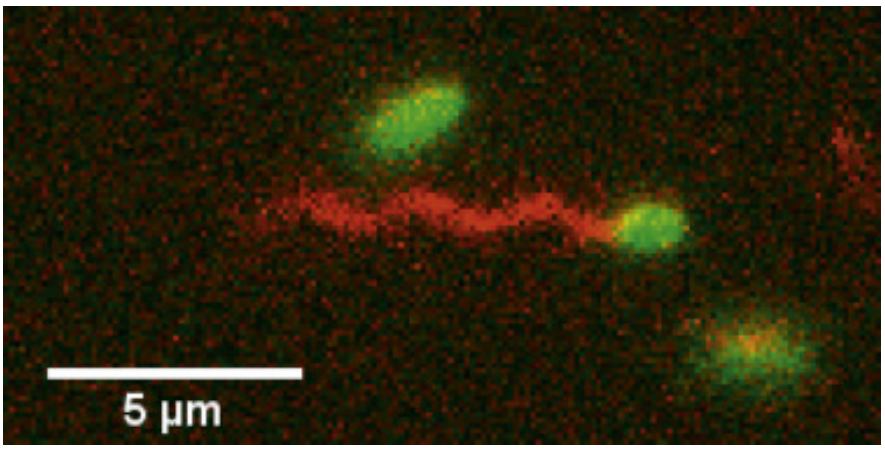

Figure 1.4 *(Reproduced from [37]) Swimming E. coli with fluorescently labelled flagella.*

In this section I describe some of the features of the bacterium *Escherichia coli* (*E. coli*), which is the best known example of a living organism with run-and-tumble dynamics [38]. In fact, it has been described as the best understood living organism on earth today [37]. It is commonly found in the intestine of warm-blooded organisms [39], and is of biological and medical significance [40]. However, it is the motility of *E. coli* that is principally of interest to us here and will serve as the inspiration for the models of interacting run-and-tumble random walkers studied in later chapters.

An *E. coli* bacterium has a rod-shaped body approximately 10^{-4}cm in diameter and 2×10^{-4}cm long [38]. Multiple helical flagella emerge from random points on the cell body [41], extending to approximately three body lengths into the surrounding medium [38]. These flagella are powered by rotary motors that, viewed from behind, can rotate clockwise or anticlockwise [42]. When the flagella rotate anticlockwise, they bundle together to propel the bacterium forward [43]. A picture of swimming *E. coli* is shown in Figure 1.4. When the motors reverse, now rotating clockwise, they cause the flagella to turn independently and unbundle so that the cell moves in a highly erratic manner known as *tumbling* [43], which we will consider in more detail in the following subsection.

1.2.1 Distribution of run and tumble intervals

There are many genetic variants known as *strains* of *E. coli*, which can present different motile behaviours, including ones that do not tumble [44, 45]. Here we are concerned with those variants that retain the dynamics described above, which

are *wild-type*. However, despite the apparent simplicity of this run-and-tumble dynamics, the duration of runs and tumbles are very difficult to measure leading to a range of different reports for their corresponding distributions [43, 46–48]. If we are to build a robust microscopic theory of their motion it is important to understand the limitations of the necessarily highly idealised random walk model we will build. These limitations come not just from approximations made by omitting some experimental observations from the model, but also those aspects for which experiments have yet to determine conclusively.

There is experimental agreement that wild-type cells run for approximately 1s on average, and tumble for an average of about 0.1s, after which they run again more or less in a random new direction [37, 43]. In a pioneering paper on *E. coli* motility [43], Berg and collaborators reported that when swimming in a medium of low viscosity the cells choose a mean angular deviation of 68° from the initial swimming direction, and therefore the direction of swimming chosen after tumbling is biased in favour of the initial, or 'forward', direction. They also report that the distribution of run and tumble intervals is exponential and does not depend on the lengths of the intervals that precede it [43].

However, experiments investigating the behaviour of *E. coli* flagella in [46] found that the distribution for the intervals of the anticlockwise rotations of the flagellar motors of a single cell was not exponential. In [46], Korobkova and collaborators recorded binary time series constructed from the rotations of single motors on an *E. coli* bacterium immobilised onto microscope slides. Given that rotation anticlockwise implies running, and rotation clockwise implies tumbling, the distribution of the intervals of a motor anticlockwise and clockwise rotations corresponds to the distribution of the running and tumbling intervals respectively. The findings in [46] suggested that either the intervals are not independently and identically distributed, or not exponentially distributed (but independently and identically distributed).

This leads to the question of the effect of flagellar correlation and variability [46, 47, 49]. The connection between flagellar dynamics, in particular the relationship between the direction of rotor rotation and propulsion versus tumbling, as reported by Berg and coworkers in [43] appears very straightforward: when the rotors all turn anticlockwise the particle swims smoothly, and when they all reverse, the particle tumbles. However, until recently, direct observation of flagellar dynamics in swimming cells was limited to short durations of about 1s [49–51]. Thus, the natural questions arise: are the flagella rotation intervals

uncorrelated, are there cases when individual flagellar motors rotate in different directions to others, and, if so, what is the effect?

Work by Mears and collaborators in [49] found individual flagella on the same wild-type cell tend to, on average, move in a coordinated way. Therefore, although a single flagellum could sometimes "veto" swimming by rotating in the clockwise direction while the others rotated anticlockwise, the number of flagella involved in any tumble was typically much greater than would be expected if the flagella were acting independently [49]. Even though these tumbles did not involve all the flagella, they were nevertheless of canonical form [47, 49]. Furthermore, they found the correlation persists for about 0.1s—the average duration of a tumble [49]. Mears and collaborators also reported that "swimming is robust against variations in flagellar number but due to inter-flagellar correlations, an 'effective number' of flagella—smaller than the actual number—enters into this relation".

Thus the evidence [47, 49] suggests that the motor rotations are correlated, and therefore that for a single cell the distribution of the intervals for one motor will be approximately those of the others. The run distributions have been found to be predominately exponential [47]. The tumbling intervals are dominated by exponential behaviour [46]. However, both Mears' and Korobokova's works show there is a large amount of intercellular variability [46, 47, 49]. In [47], although the run intervals were predominately exponential, intercelluar variability meant that their distribution had a pronounced *heavy tail* corresponding to very long runs. These very long runs were taken by a large number of cells rather than a few anomalous ones [47]. The investigations of Korobkova and collaborators show that a cell can also have non-exponential run-interval behaviour (they instead found it to be well described by a power law) [46].

Moreover, *higher-order* effects beyond the two state run-and-tumble model have been observed. These include reversal of the swimming direction when the orientation of the flagellar bundle changes [52] and different cell velocities before and after a tumble [43, 47, 49].

1.2.2 Run-and-tumble swimming in one dimension

So far in this section, I have discussed the results of experiments investigating the motility of *E. coli* in a three-dimensional environment [43, 50, 52], although the cells have sometimes been immobilised in some way to better observe their

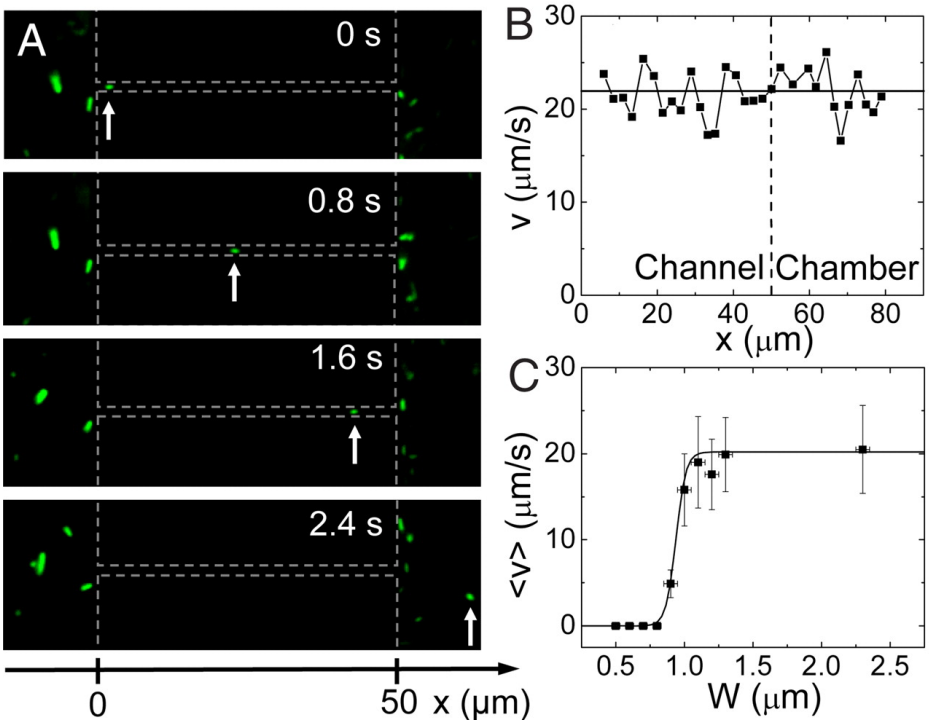

Figure 1.5 *(Reproduced from [54]) A shows time-lapse images of an E. coli bacterium (with position labelled with an arrow) swimming left to right. In the first three images it moves in an 1.2μm wide channel, before entering the chamber in image 4. In B, the velocity of the bacterium in the images in A is shown. In C, the average velocity $< v >$ of bacteria in different channel widths W is depicted. The error bars correspond to the standard deviation of velocities in all the bacteria in a given-size channel. The solid line shows a sigmoidal fit to the data.*

flagellar behaviour [46, 47, 49, 50]. In addition to the three dimensions that bacteria often inhabit, there is also good reason for interest in bacterial movement in confined spaces [53, 54]. Specifically, as outlined in [54], the majority of soil and bedrock bacteria, which make up a large percentage of the earth's biomass [55], live in pores of size 6 micrometer and smaller [56]. It remains, however, largely unknown how bacteria move through pores of very small size [54].

In [54], Mannik and collaborators investigated how narrow channels can be made such that *E. coli* could could still swim through them. They found that for a sufficiently shallow and narrow (but not too narrow) channel, it was possible to create an essentially one-dimensional environment for the bacteria where tumbling leads to only two possible outcomes: reversing of the direction or motion in the same direction [54]. Furthermore, they reported that *E. coli* present their bulk motility pattern in these channels, swimming at the same average speed as when

they were in chambers where they could swim in three dimensions [54]. These results are presented in Figure 1.5.

The work summarised in this section has shown that a reasonable, although idealised, model of *E. coli's* run-and-tumble dynamics could describe the runs and tumbles as exponentially distributed Poisson processes in a one-dimensional environment. We will see that these features presents an opportunity for the theorist to construct a model that is accessible to analytic methods. The minimal variant is known as the *persistent random walker* model, and is discussed in the next section.

1.3 The persistent random walker model

The key to modelling self-propelled particles is how to describe changes in their direction. For a particle moving along a straight line at a constant velocity, the so-called *persistence* effect describes how, after a time interval, the particle may move in the same direction as the previous path or in the opposite direction, according to some probability distribution [57, 58]. Schnitzer [59] was the first to generalise this description to be applicable to the random walks of *E. coli* with an emphasis on the application to the bacterial search for chemical attractants, known as *chemotaxis*.

Schnizter began with differential equations describing the time evolution of the density of run-and-tumble particles with a particular direction in one dimension [59]:

$$\begin{aligned} \frac{\partial R(x,t)}{\partial t} &= -\frac{\partial (vR(x,t))}{\partial x} - \frac{\tilde{\alpha} R(x,t)}{2} + \frac{\tilde{\alpha}(x) L(x,t)}{2} \\ \frac{\partial L(x,t)}{\partial t} &= -\frac{\partial (vL(x,t))}{\partial x} + \frac{\tilde{\alpha} R(x,t)}{2} - \frac{\tilde{\alpha}(x) L(x,t)}{2} \end{aligned} \tag{1.9}$$

where R and L are the densities of particles moving right and left respectively at position x and time t, and $\tilde{\alpha}$ is the rate of tumbling at position x, which occurs instantaneously as a Poisson process. Note that we saw in subsection 1.2.1 that, with caveats, this leads to a reasonable approximation of the run distribution of *E. coli*. This model does make a significant idealisation for the tumbling, which occurs here in zero time. Although justified to the extent tumble durations are much shorter than run durations, in chapter 3 we will see that

a finite tumble duration leads to new features in the model's behaviour when interparticle interactions are present. Turning back to Eq. (1.9), the first term on the right-hand side of each line comes from the spatial distribution of right-moving particles. The remaining terms model the tumbling, which cause right-moving particles to become left-moving particles and vice versa.

By recasting Eq. (1.9) in terms of a local density $\rho = R+L$ and flux $J = v(R-L)$, Schnitzer constructed a differential equation that allowed him to express the flux in terms of the density and model parameters only [59]:

$$J(x) = \frac{-v^2(x)}{\tilde{\alpha}(x)}\frac{\partial \rho}{\partial x} - \frac{v(x)\rho(x)}{\tilde{\alpha}(x)}\frac{\partial v}{\partial x} \tag{1.10}$$

Schnizter generalises this expression for the flux into an effective *Smoluchowski* equation that has tumbling rates dependent on direction and uses it to investigate possible strategies for chemotaxis that involve modulation of the tumble rate [59]. He predicts that particles that perform temporal comparisons of the concentration of a chemical attractant will lower their tumble rate when moving in a favourable direction (along an increasing concentration of attractants).

In the case when attractants are not present, the tumble rate is not modulated and so a specific case of the formulation in Eq. (1.9) is appropriate to model run-and-tumble motion: where the tumble rate is constant. As we seek a minimal model of interactions between walkers, rather than the effect of attractants on them, we will consider this simpler model in more detail.

With the tumble rate constant, the expression in Eq. (1.9) is mathematically equivalent to the dynamics of the voltage and current in power transmission lines as modelled by the telegrapher's equations [60]. The first step is to write Eq. (1.9) in terms of ρ and J:

$$\frac{\partial \rho}{\partial t} = -\frac{\partial J}{\partial x}, \tag{1.11}$$

$$\frac{\partial J}{\partial t} = -v^2\frac{\partial \rho}{\partial x} - \tilde{\alpha}J. \tag{1.12}$$

Differentiating Eqs. (1.11) and (1.12) with respect to time gives the telegrapher's equation for ρ and J. For ρ this is

$$\frac{\partial^2 \rho}{\partial t^2} + \tilde{\alpha}\frac{\partial \rho}{\partial t} = v^2\frac{\partial^2 J}{\partial x^2}. \tag{1.13}$$

Two papers [61, 62] by Angelani have applied this formulation to the problem of run-and-tumble dynamics. In [61], absorption problems for the one-dimensional model with partially reflecting boundaries are considered. He finds the mean time to absorption, τ, for symmetric boundaries at a and b and a reflection coefficient of γ to be

$$\tau = \frac{b}{v\epsilon} + \frac{\tilde{\alpha}b^2}{2v^2} \tag{1.14}$$

where

$$\epsilon = \frac{1-\gamma}{1+\gamma}, \tag{1.15}$$

so that at $\gamma = 0,\ \epsilon = 1$ the boundary is perfectly absorbing, and for $\gamma = 1,\ \epsilon = 0$ the boundary is perfectly reflecting. Interpreting this result, Angelani finds that for boxes small with respect to $v/\tilde{\alpha}$, the first term, which is wave-like, dominates. The second, diffusive-like term characterises the behaviour for larger boxes. The times to absorption for different boundary conditions are also given in [61], as well as the survival probability that the particle has not yet been absorbed at time t.

The case of hard walls is investigated in [62], where Angelani studies a model of persistent random walkers confined to a one-dimensional box. Particles then become stuck at the walls until a tumble event reverses their direction. He finds that this interaction with the walls can result in accumulation through an expression for the particle's probability distribution. In [62], Angelani also finds that the pressure induced by particle collisions with the walls is higher for the first collisions than that in the long-time limit.

Related work on persistent random walkers was undertaken in [63], which derives analytic expressions for the first-passage properties of persistent random walkers under external force fields and chemotactic fields, and in [64], which considered tumbling events governed by a non-Poissonian process. Together these works have relatively well-characterised the single-particle dynamics of the persistent random walker model. The work in this thesis extends the understanding of the persistent random walker model to include the effect of interactions between particles in chapter 2 and 3, and the effect of walls when interparticle interactions are also present in chapter 4. The findings represent a step towards understanding the collective behaviour of interacting persistent random walkers from a microscopic perspective. We examine a striking example of such collective behaviour in the next section.

1.4 Clustering of self-propelled particles

Beyond one-particle dynamics lies the effects of interactions observed in systems of self-propelled particles, some of which I highlighted in section 1.1. Not only are these phenomena interesting in their own right, but at the macroscopic scale they can lead to collective motion that dominates the behaviour of the system. Of particular relevance to the work in this thesis is the finding that self-propelled particles exhibit a tendency to cluster as a consequence of the particle velocity decreasing as the local particle density increases [65]. This phenomenon is known as *motility-induced phase separation* [65]. The interest in the propensity for clusters to form is twofold: on the one hand in the implications for possible applications to design or control real experimental systems and, on the other, to develop a greater understanding of how the underlying nonequilibrium dynamics of individual particles, such as the persistent random walker, can build complex emergent structures.

In the realm of biophysics, there is speculation that this clustering may have practical implications [3, 66]. In particular, bacteria are commonly found in aggregates called *biofilms* which are important sources of human infection [67, 68] and contamination in the food industry [69]. The development of biofilms shows remarkable variety [70], but they are generally described as cells bound together by extracellular polymeric substances and attached to a surface [71]. Their formation involves both cell–surface and cell–cell interactions [70]. Figure 1.6 shows the current paradigmatic model of biofilm formation. According to this theory of biofilm development [72], the early stages of biofilm formation involve single freely swimming cells attaching to the surface. These then proliferate to form small cell clusters [72]. However, it has been suggested [3] that bacteria could down-regulate their swimming activity at high density to add to these clusters through cell–cell communication.

There are a number of different interaction mechanisms that can generate a density-dependent velocity, with the precise form of the density dependence depending on microscopic considerations. Most obviously, particles can interact by direct collisions, resulting in jamming where both particles stop moving. This may be considered an extreme case of density dependence [29, 74, 75]. Other possibilities are density-dependent responses induced by chemotaxis [43] or other signalling molecules [76] (there is evidence for such cell-cell signalling molecules for some biofilms [77]), and hydrodynamic interactions [78]. Specifically, for biofilms

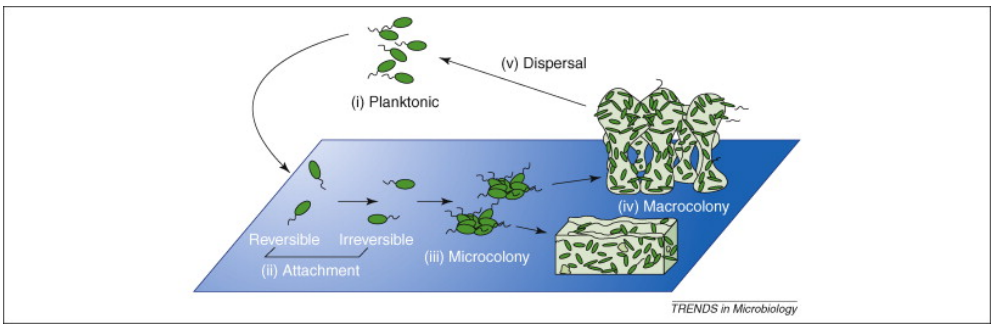

Figure 1.6 *(Reproduced from [73]) Developmental model of biofilm formation. Cells begin as free swimmers, called planktonic, before attaching to a surface. As initial attachment is often weak, they may go through a reversible attachment phase before attaching irreversibly. Discrete cell clusters, known as microcolonies, then form before growing and coalescing into macrocolonies. They are held together by an exopolysaccharide matrix that also contains the debris from dead cells and extracellular DNA. Eventually, the macrocolony may dissolve releasing the cells that may return to their planktonic form.*

of *E. coli*, where experimental results suggest that motility is relevant to biofilm development [79], run-and-tumble dynamics under volume exclusion have been shown in simulations to form clusters [74].

From a fundamental perspective, the propensity for clusters to form in out-of-equilibrium systems finds its origin in the fact that there is no one-to-one relationship between a potential that governs interparticle forces and the probability distribution of configurations. Therefore effective forces between particles can emerge as a consequence of the microscopic breaking of time-reversal symmetry [3]. Previous work has shown that these forces can lead to the clustering of self-propelled particles, such as those interacting via alignment [80–83]. Remarkably, however, the effective attraction can be sufficiently strong that clusters form even if the interaction potential is purely repulsive and there is no alignment interaction. This has been observed in the computational studies of Fily and collaborators [28], Redner and collaborators [29], and a range of theoretical studies [84–86] of systems of active Brownian particles.

Motility-induced phase separation was first described in the context of interacting run-and-tumble particles [87]. Now extended to other types of self-propelled particles [31, 85], this theory derived criteria for motility-induced phase separation to occur using a coarse-grained model. In [87], Tailleur and Cates show that when the mean run speed of the particles decreases as a function of the local density of the particles to a sufficient extent, then clusters form. Their theory

was based on deriving a drift-diffusion equation for the microscopic dynamics of a single particle at large scales, and then extending it to describe the evolution of a system of interacting particles in terms of a coarse-grained, locally smooth density field ρ. I briefly summarise the main results of this work following the review [3].

In one-dimension the evolution of the coarse-grained many-body particle density is given by

$$\dot{\rho} = (-\rho V + D\rho' + (2D\rho)^{1/2}\Lambda) \tag{1.16}$$

where $V([\rho], x)$ is the drift velocity, given by

$$V = -\frac{vv'}{\tilde{\alpha}} \tag{1.17}$$

and $D([\rho], x)$ is the one-body diffusivity

$$D = v^2/\tilde{\alpha}. \tag{1.18}$$

Λ is unit white noise. Note that the dependence on $\tilde{\alpha}$ and v of the persistent random walker model passes to the density dependence of V and D. This many-body equation can be mapped at large scales to a set of Brownian particles if the following functional $F_{\text{ex}}[\rho]$ exists:

$$V/D = -[\delta F_{\text{ex}}/\delta\rho]'. \tag{1.19}$$

The functional exists when v and $\tilde{\alpha}$ depend on ρ in a purely local way. In this case, when v decreases sufficiently rapidly as a function of ρ the system separates into two domains of coexisting densities, where the higher density corresponding to clusters. Thus the work of [87] predicts this clustering phenomenon at the macroscopic scale, which then sets the challenge of understanding how, at the microscopic scale, individual particles interact to induce this effective attraction.

Understanding of the run-and-tumble clustering phenomenon at a more microscopic level has been obtained with reference to lattice-based models [74, 88, 89]. In these models, space is discretised and particles hop between neighbouring sites on a lattice instead of moving continuously. The simplest interaction rule to implement is hard-core exclusion, whereby no two particles can occupy the same site simultaneously (although softer rules that allow multiple occupancy are sometimes implemented [88, 89]). An example of a realisation of motility-

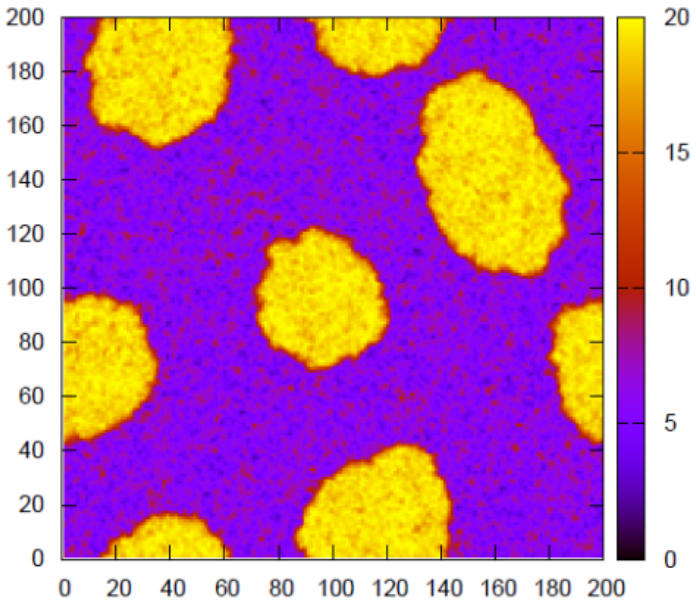

Figure 1.7 *(Reproduced from [3]) A two-dimensional run-and-tumble system undergoing motility-induced phase separation. Hops are allowed to nearest neighbours plus diagonals. There are a maximum number of particles allowed per site implementing a partial exclusion interaction. The local density is colour-coded on the scale at the right.*

induced phase separation is shown in Figure 1.7. These lattice-based works have shown that the coarse-grained many-body theory described above is recovered in the appropriate limit [88] and that dependence of the particle hop rate on the local density that is implied by hard-core exclusion does indeed lead to the formation of particle clusters [74, 88, 89]. However, an analytic understanding of the microscopic mechanisms leading to this cluster formation is still in the early stages of research. We turn to this in the next section.

1.5 Effective interactions of interacting active random walkers

For clusters to form, self-propulsion must mediate an effective attraction between otherwise repulsive particles [90]. Because coarse-grained approaches explicitly leave out the specific details of the microscopic mechanism that breaks the time-reversal symmetry characteristic of equilibrium, they lack the power to quantify the relationship between the effective attraction that arises between

particles and the underlying microscopic dynamics. Initial progress towards an analytic microscopic theory was based on a mean field description of self-propelled repulsive disks [91]. The authors found that the mechanism that resulted in an effective slowing down of the discs came from a force imbalance, which they characterised using the discs' approximate pair distribution function. However, no systematic method for determining the form of this emergent attraction that leads to clustering from the underlying microscopic dynamics yet exists. Such a method would pave the way towards a deeper understanding of the mechanism behind motility-induced phase separation.

A number of approaches [92–94], approximate in nature, quantify emergent interactions by considering a minimal model for an active system composed of overdamped interacting particles driven by persistent noise with a correlation that decays exponentially in time. This is known as *coloured* noise and stands in contrast with white noise, seen in, for example, Eq. (1.3). White noise has no time scale and the associated process is therefore 'memoryless' or *Markovian* [95]. Coloured noise thus allows the description of non-Markovian behaviour. For self-propelled particles this stems from their persistent motion, which has an associated persistence time τ. In the limit of no persistence time, $\tau \to 0$, the noise becomes white, the behaviour Markovian and the probability distribution approaches the Boltzmann measure. The works in [92–94] consider whether an *effective* Markovian description can be given in the case that τ is small but finite.

In [93, 94], the authors apply a generalisation of the *unified coloured noise approximation* [96], which allows an effective Markovian description of two [93] and then many [94] interacting persistent particles with coloured noise. Following [95], I will now briefly outline the unified coloured noise approximation for a one-dimensional flow. Consider the Langevin equation with additive noise

$$\dot{x} = f(x) + \xi(t), \tag{1.20}$$

where $\xi(t)$ is *Ornstein-Uhlenbeck* noise correlated as

$$\langle \xi(t)\xi(s)\rangle = \frac{D}{\tau} e^{-|t-s|/\tau} \ , \tag{1.21}$$

where D is the noise intensity. This may be recast as a two-dimensional Markov

process as follows:

$$\dot{x} = f(x) + \xi \tag{1.22}$$

$$\dot{\xi} = -\frac{1}{\tau}\xi + \frac{D^{1/2}}{\tau}\zeta(t) \tag{1.23}$$

where $\zeta(t)$ has the correlation function $\langle \zeta(t)\zeta(x)\rangle = 2\delta(t-s)$, and so is Gaussian white noise. ξ can be eliminated from Eq. (1.22) by differentiating with respect to time and substituting in Eq. (1.23). This yields

$$\ddot{x} + \dot{x}[\tau^{-1} - f'(x)] - f(x)/\tau = \frac{D^{1/2}}{\tau}\zeta(t). \tag{1.24}$$

Differentiating with respect to $s = t\tau^{-1/2}$ leads to

$$\ddot{x} + \gamma(x,\tau)\dot{x} - f(x) = \frac{D^{1/2}}{\tau^{1/4}}\zeta(s), \tag{1.25}$$

where

$$\gamma(x,\tau) = \tau^{-1/2} + \tau^{1/2}[-f'(x)]. \tag{1.26}$$

When $\gamma(x,\tau) \gg 1$, the positive damping becomes large and we may set $\ddot{x} = 0$. This leaves a Markovian approximation for the process:

$$\dot{x} = \frac{f(x)}{\gamma(x,\tau)} + \frac{D^{1/2}}{\tau^{1/4}\gamma(x,\tau)}\zeta(s) \tag{1.27}$$

with this one-dimensional equation expressed only in terms of Gaussian white noise.

Using the unified coloured noise approximation, Maggi and collaborators find an approximate expression for the steady-state probability distribution P_S for their systems of interacting active particles. In the two particle case they can interpret P_S as an effective pair potential, ϕ_{eff}, using $P_S \propto \exp(-\phi_{\text{eff}}/D)$ [93, 94]. For particles with mutually repulsive interactions, the resulting effective potential is attractive, and captures steady-state phenomena that are clearly due to activity, such as accumulation of particles near the boundaries of their container [93, 94]. Furthermore, the universal coloured noise approximation works not only in the steady-state but also for the dynamics [94, 97].

In [92], a different method, known as *Fox theory* [98, 99], is used to derive an approximated expression for the steady-state probability distribution of the interacting persistent random walker model with coloured noise. Similarly, to the

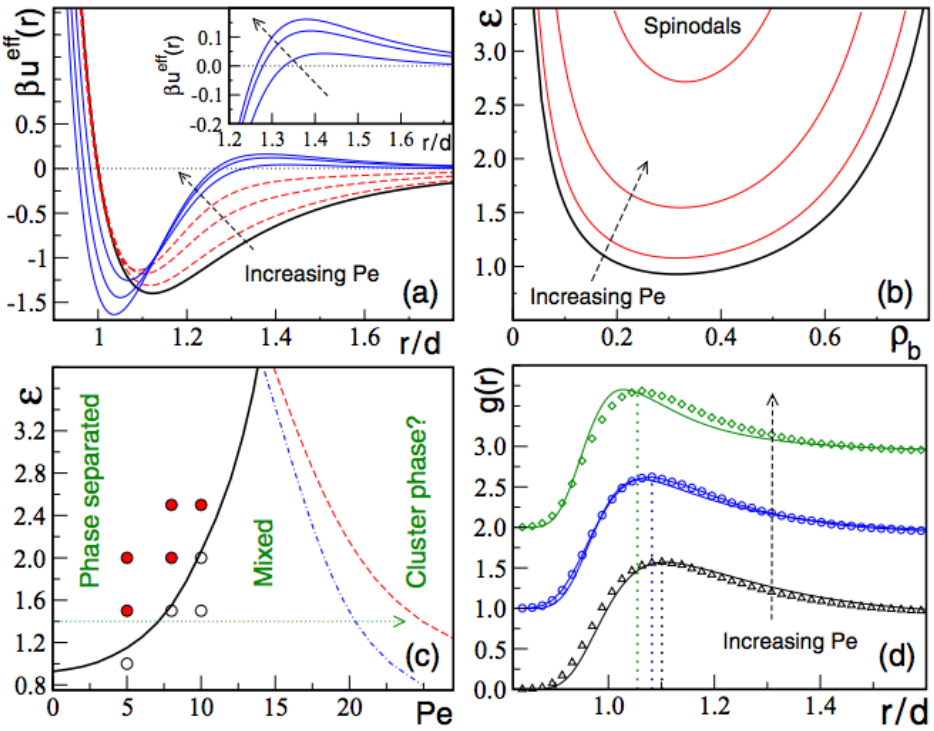

Figure 1.8 *(Reproduced from [92]) The effect of an attractive Lennard-Jones potential* $\beta u = 4\epsilon(r^{-12} - r^{-6})$ *(with* β *inverse temperature, and* ϵ *a parameter controlling the strength of the potential) on phase separation in a persistent random walker model investigated using Fox theory. (a) shows the evolution of the effective potential as a measure of the persistence time, Pe, is increased from zero. Both the depth and range of the effective potential reduce significantly. In (b), increases in Pe lead to higher values of* ϵ *required for phase separation. Thus a passively phase-separated system can go back to a single phase when the activity (measured by Pe) is increased. (c) shows the phase diagram for the system. Open circles indicate points where simulations find a mixed state, and closed circles the phase-separated state. Competition between long-range repulsion and the attractive component of the potential suggests clustering without coarsening to phase separation. (d) presents a comparison of the radial distribution function* $g(r)$ *as calculated by theory (lines) and simulation (symbols).*

unified coloured noise approximation, Fox theory transforms a non-Markovian Langevin equation into an effective Markovian description. However, rather than a Langevin equation that is Markovian in a large damping limit, the result from Fox theory leads to an approximate equation for the time evolution of the configurational probability distribution known as a *Fokker-Planck* equation [92], which is implicitly Markovian. Farage and collaborators extract the pair potential from this approximate Fokker-Planck equation. They find approximate effective

two-body interactions that are attractive in nature, leading to the separation into high and low density phases that is characteristic of motility-induced phase separation [92]. Furthermore, and remarkably, when the interparticle potential is attractive, the effective interactions can be repulsive at large distances, creating a two-body phase diagram with phase separated, mixed and finite-cluster phases [92], which is shown in Figure 1.8.

Both the generalisation of the universal coloured noise approximation, and Fox theory suffer from the same limitation: they are only strictly valid in the limit of small persistence time [96, 99]. In the limit of vanishing persistence time their steady-state distributions approach the Boltzmann equilibrium. Furthermore, because both theories map an active model onto an effective equilibrium one, macroscopic steady-state fluxes are ruled out, so neither approximation could describe a system where such behaviour does arise. Thus despite their success in elucidating some aspects of emergent interactions in nonequilibrium systems, further progress depends on results that do not suffer from these limitations.

In this thesis, using exact methods and an approximate approach valid in the limit of large persistence time, I investigate the relationship between microscopic dynamics and emergent interactions using the run-and-tumble model of bacterial dynamics.

1.6 The structure of this thesis

The remainder of this thesis is divided into four parts: chapters 2—4 describe in detail the methods and results of original analytic investigations into variants of a one-dimensional lattice model of two interacting run-and-tumble random walkers, with the conclusions in chapter 5.

In chapter 2, the minimal model of lattice-based interacting run-and-tumble particles is introduced, which applies periodic boundary conditions, and approximates the tumbling of the walkers as instantaneous. The probability distribution for the separation of the particles in the steady state is found exactly, and interpreted as an effective nonequilibrium pair potential between the particles, attractive in nature. A *scaling* limit is taken where motion in continuous space and time is recovered, showing that the effective interaction persists in this case more realistic continuous run-and-tumble dynamics.

The approximation of instantaneous tumbles is relaxed in chapter 3, where the tumbling duration is instead governed by the exponential distribution. This finite tumbling model is also solved exactly, with a generalisation of the method used in chapter 2. A new interaction, directly related to the finite tumbling duration, is identified, with a different lengthscale to the interaction found in the model with instantaneous tumbling, which is also present in the finite tumbling case. Both interactions survive in the scaling limit of the finite tumbling model.

In chapter 4, I turn back to the instantaneous tumbling approximation, but apply reflecting, rather than periodic, boundary conditions. This reflecting boundaries model is not directly amenable to the exact analysis of chapters 2 and 3 so a different, perturbative approach based in graph theory is adopted allowing a solution in the limit of a low tumbling rate. The resulting expressions for the stationary distribution suggest a new attractive interaction, between the walls and the particles, is present in addition to the interparticle attraction.

The conclusions of these works, as well as the outlook for further investigations of interacting run-and-tumble random walkers, are presented in chapter 5.

Chapter 2

A generating-function approach to a model of interacting run-and-tumble random walkers

In this chapter, we consider an extension of the persistent random walker model described in section 1.3 to include volume exclusion between the particles. A many-body version was introduced in [88], with further computational study of it undertaken in [74]. This two particle, one-dimensional system is a minimal model of interacting run-and-tumble particles. The simplicity of this model makes it appropriate as a starting point for which to study the emergence of effective interactions between run-and-tumble particles and so add to the body of knowledge summarised in section 1.5. We will see that an emergent attraction does indeed manifest, and the dynamical mechanisms that generate it can be pinpointed. This attraction contributes to the understanding of the genesis of the clustering described in section 1.4 from a microscopic perspective.

In order to solve the minimal model studied in this chapter, an approach based in generating functions is used. We find that this standard mathematical tool is particularly appropriate for this run-and-tumble problem, and leads to an exact solution for the steady-state probability distribution. This work therefore adds to the catalogue of exact steady-state solutions of nonequilibrium systems.

This chapter is organised as follows. In section 2.1, the minimal run-and-tumble model is defined. We review time reversibility, known as *detailed balance*, more

formally in section 2.2 and show that it is the interactions between particles that determine the way detailed balance is broken in the run-and-tumble model. In sections 2.3—2.5 the solution to the model is derived and its behaviour analysed. In section 2.6 the limitations of the generating function method are discussed, and simulations of the many-body model are presented. Finally, some concluding remarks are made in section 2.7.

2.1 A microscopic run-and-tumble model

In this section, we review a minimal microscopic model of interacting run-and-tumble particles, which is the focus of this chapter. It is based on the persistent random walker model. We have seen in sections 1.2 and 1.3 that the persistent random walker model is already an approximation to the swimming of real bacteria. Idealisations are, of course, inevitable in constructing analytically manageable systems. The specific motivation behind each of the principal idealisations for the model studied in this chapter are described below.

The first constraint imposed is that the motion of the particles in our model takes place on a one-dimensional lattice. We have seen in section 1.2.2 that the one-dimensional motion of run-and-tumble *E. coli* is of experimental interest. Lattice-based motion, however, does not reflect the continuous dynamics of real run-and-tumble swimmers as seen in section 1.2. This issue is addressed through the derivation a scaling limit of the lattice-based model in section 2.5 for which off-lattice motion is recovered.

A second constraint is that the boundary conditions for the one-dimensional lattice are chosen to be periodic, as they simplify the mathematics considerably. This does imply that any experiments testing the results in this chapter would require a ring geometry. We note that the only experiment confining bacteria to a one-dimensional environment undertaken so far had open boundaries (as described in subsection 1.2.2). Thus, if the results in this chapter are to be testable, experimental innovation to a ring permitting one-dimensional bacterial dynamics is required. We examine the complications that arise in considering reflecting boundaries in section 2.6. These are addressed directly in Chapter 4, where a perturbative approach based in graph theory is used to derive the leading-order steady-state probability weights for the model with reflecting boundaries.

A further idealisation is that we will consider the simplest set-up allowing inter-particle interactions: a two-particle model. The difficulties in generalising the solution of the model to more particles is discussed in section 2.6, where the results of many-body simulations are also presented.

Thus the model of interest in this chapter comprises two particles that occupy sites of a periodic one-dimensional lattice of L sites. Each particle has an orientation $\sigma_i = \pm$ indicating its direction of motion. A right-moving particle ($\sigma_i = +$) hops by one site to the right with Poisson-distributed rate γ; likewise, a left-moving particle ($\sigma_i = -$) hops with rate γ to the left. The exception is when the target site is occupied by another particle, in which case hopping is not allowed: this implements a hard-core exclusion interaction between particles. Due to the translational invariance of the system, a microscopic configuration is fully specified by $1 \leq n < L$, the distance between the two particles in units of the lattice spacing, and the two particle velocities, σ_1 and σ_2.

This lattice-based model with hopping implies that the particles do not move with a constant velocity — the hopping is stochastic. It may be argued that the stochasticity of the hopping, which implies a distribution of run speeds over some time interval, could act as a proxy description of the distribution of run speeds observed in the density-dependent swimming of some run-and-tumble bacteria (as was discussed in the introduction in section 1.4). However, here the principal motivation for such a description is that it is amenable to mathematical analysis, as we will see later. Ultimately, we will derive the off-lattice dynamics, where this stochastic hopping becomes ballistic.

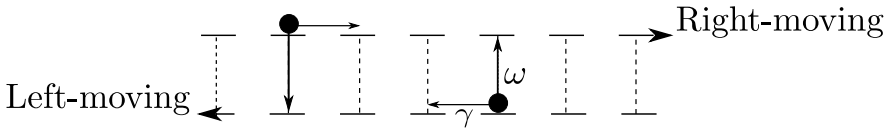

Figure 2.1 *Microscopic update schematic for separated particles: this diagram shows an example configuration of the model, with right-moving particles depicted on the upper row, and left-moving particles on the lower row. Here, one particle is right-moving and one is left-moving. The arrows signify which microscopic dynamical updates are available to the particles. As both particles are separated – not on adjacent lattice sites – they are both able to hop or tumble. Considering the right-moving particle explicitly, this means that it is able to hop to the next lattice site to the right (at rate γ) or tumble (at rate ω), thereby becoming left-moving, where it would be on the same lattice site, but represented on the lower row.*

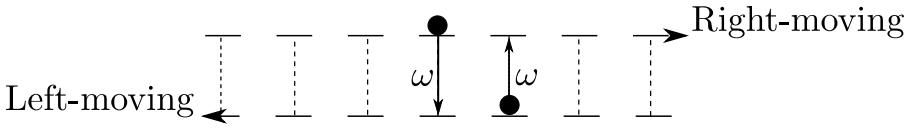

Figure 2.2 *Microscopic update schematic for colliding particles: this diagram represents a collision between the two run-and-tumble random walkers in the model. As they are adjacent but have opposite velocities, they are unable to successfully execute a hop. Therefore the configuration can only change when they tumble.*

In addition to the hopping dynamics, particles also reverse their velocity at Poisson-distributed rate $\tilde{\omega}$ (see [74, 88] for related models). This stochastic modelling of particle tumbles is a reflection of the underlying randomness of tumble times. We have seen in section 1.2 the extent to which such Poisson-distributed run lengths are supported by experimental observations of run-and-tumble swimmers. The instantaneous tumbling is, of course, an approximation, motivated by the fact that run durations are much longer than tumbling durations. In the next chapter, we relax this idealisation by including a finite Poisson-distributed tumble duration in a more general model, with a more complex solution. Returning to this model with instant tumbling, we take $\gamma = 1$, which corresponds to a rescaling of time. A reversal rate rescaled by the hopping rate $\omega = \tilde{\omega}/\gamma$ is also introduced.

Figures 2.1 and 2.2 illustrate the microscopic update dynamics for this model. In the next section we examine how these dynamics take the run-and-tumble model out of equilibrium.

2.2 Breaking detailed balance: comparison to an equilibrium model

In the introduction, we saw that macroscopic phenomena in active matter, such as clustering, differ to those of passive, equilibrium matter. In this section, I elucidate the difference at a microscopic level by comparing the interacting run-and-tumble model defined in the previous section to a related one-particle model, which can be mapped onto equilibrium. Specifically, we will find that the dynamics of this one-particle model satisfy a condition known as *dynamic reversibility* [100]. Its steady-state probability weights can therefore be written

in the Gibbs-Boltzmann form familiar from equilibrium statistical mechanics, without much mathematical work. In contrast, in the interacting run-and-tumble model, we find that we are unable to satisfy this condition in the same way because of the interparticle collisions.

The related one-particle run-and-tumble model, first suggested in [88], has one-dimensional lattice-based model motion. The single particle is located on some site i with velocity σ and has site- and direction-dependent hopping rates, γ_i^σ, and tumbling rates, ω_i^σ. This dynamics is motivated by bacterial movement with a bias, which might be due to external conditions such as gravity, causing an asymmetry in the run speed (in this model, the hopping rates), or the presence of a chemical gradient, in response to which the bacterium might vary its tumble rate [88].

The rates are defined precisely as follows. For a right-moving particle on site i the hopping rate is γ_i^+, and for a left-moving particle on site i the hopping rate is γ_i^-. Similarly, a right- or left-moving particle on site i has reversal rates of ω_i^+ and ω_i^- respectively (see Figures 2.4 and 2.3). Reversals occur instantaneously. To complete the model, we take reflecting boundaries, where if a particle tries to jump outside the lattice at either end the hop fails and it is instead kept where it is at the boundary. In this case, for the system to change configuration, the particle must reverse its velocity as it cannot hop.

Application of what is known as the detailed balance conditions [100] will elucidate how microscopic dynamics with interactions mark a fundamental difference between the physics of the single particle model and interacting run-and-tumble system. First, we review more formally the concept of a stationary distribution, described in the introduction as a probability distribution that does

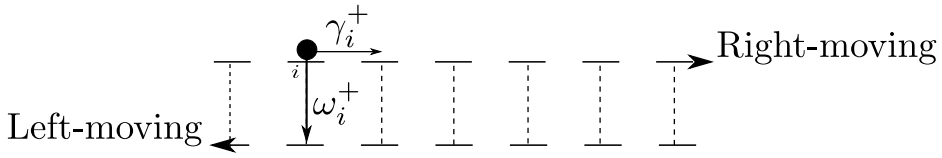

Figure 2.3 *Microscopic update schematic for for the one-particle system with a right-moving particle: this diagram shows an example configuration of the model, with the particle on site i moving to the right and therefore depicted on the upper row. It hops to the right with rate γ_i^+ and tumbles with rate ω_i^+, where it would change direction to become right-moving and then be depicted on the lower row.*

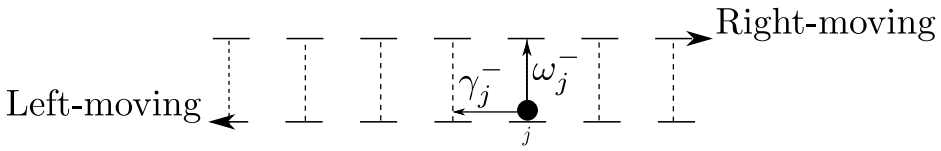

Figure 2.4 *Microscopic update schematic for the one-particle system with a left-moving particle: this diagram shows an example configuration of the model, with the particle on site j moving to the left and therefore depicted on the lower row.*

not change in time, which will provide the necessary context in which to apply these conditions. In the proceeding discussion of stochastic properties of Markov processes we follow the terminology and conceptual development of Chapter 1 of Kelly's book *Reversibility and Stochastic Networks* [100].

2.2.1 Stationary Markov processes

In both the single- and the two-particle models, the next state depends only on the state at the time immediately preceding it. This property means that the models are *Markov* processes. A Markov process can be formally defined as follows. Let $X(t)$ be a stochastic process in a countable statespace $\mathcal{K}$ for time $t \in \mathcal{T}$, $\mathcal{T} \in [0, \infty)$, taking values $X(t_n) = \mathcal{C}_n$, where $\mathcal{C} \in \mathcal{K}$. A Markov process has the property that for any set of n successive times $(t_1 < t_2, ... < t_n)$, the transition probability, W, between states of the system is not dependent on any knowledge of values at earlier times [101, 102]. We now note two conditions satisfied by all the Markov processes considered in this thesis. First, the processes are *time homogeneous*: for each process the probability to move from a state $\mathcal{C}$ at time t to a state $\mathcal{C}'$ at a later time $t + \tau$ does not depend upon t. Second, the processes are *irreducible*: every state in each process can be reached from every other state in the same process.

We first consider the case where both states and time are *discrete*. The *transition probability*, W, from a state $\mathcal{C}$ to a state $\mathcal{C}'$ for a time homogenous discrete time Markov process is formally expressed as [100]

$$W(\mathcal{C} \to \mathcal{C}') = P(X(t+1) = \mathcal{C}' | X(t) = \mathcal{C}). \tag{2.1}$$

For a system that has evolved for $n - 1$ time steps, the Markov condition can

then be expressed as [100]

$$W_{1|n-1}(\mathcal{C}_n|\mathcal{C}_1, \mathcal{C}_2, ..., \mathcal{C}_{n-1}) = W_{1|0}(\mathcal{C}_n|\mathcal{C}_{n-1}). \tag{2.2}$$

A discrete time Markov process can also be referred to as a *Markov chain* [100, 102]. In this thesis, any further discussion of discrete time processes will refer to them as Markov chains, retaining use of Markov processes exclusively for their continuous time counterparts.

In this thesis we are concerned with *continuous time* Markov processes. For such processes the transition probability is defined as [100]

$$W(\mathcal{C} \to \mathcal{C}') = \lim_{\tau \to 0} \frac{P(X(t+\tau) = \mathcal{C}'|X(t) = \mathcal{C})}{\tau} \,. \tag{2.3}$$

A Markov process remains in a state $\mathcal{C}$ for a period that is exponentially distributed according the parameter

$$\bar{W}(\mathcal{C}) = \sum_{\mathcal{C}'} W(\mathcal{C} \to \mathcal{C}'). \tag{2.4}$$

The probability to leave state $\mathcal{C}$ to move into $\mathcal{C}'$ is given by

$$p(\mathcal{C} \to \mathcal{C}') = \frac{W(\mathcal{C} \to \mathcal{C}')}{\bar{W}(\mathcal{C})}. \tag{2.5}$$

A probability distribution, $P(\mathcal{C})$, for the states of a continuous time Markov process is of particular interest if it satisfies the stationarity equations[1]. These are [100]:

$$P(\mathcal{C}) \sum_{\mathcal{C}' \in \mathcal{K}} W(\mathcal{C} \to \mathcal{C}') = \sum_{\mathcal{C}' \in \mathcal{K}} P(\mathcal{C}') W(\mathcal{C}' \to \mathcal{C}). \tag{2.6}$$

Such a distribution will exist if the statespace $\mathcal{K}$ is finite. When such a distribution exists it is unique and it is also the limiting distribution, satisfying [100]

$$\lim_{t \to \infty} \tilde{P}(X(t) = \mathcal{C}|X(0) = \mathcal{C}') = P(\mathcal{C}). \tag{2.7}$$

A Markov process is *stationary* when the distribution, $P(\mathcal{C})$, is the same for all configurations in $\mathcal{K}$ at any time given that the process started with that

[1]Note that in [100] Kelly refers to these as 'equilibrium equations', where they relate to stationarity, reflecting a difference in terminology used in the physics and mathematics literatures. We use stationarity here and keep equilibrium to mean "in thermal equilibrium"

distribution [100]:

$$\tilde{P}(X(0) = \mathcal{C}) = P(\mathcal{C}) = \tilde{P}(X(t) = \mathcal{C}),\ \mathcal{C} \in \mathcal{K},\ \forall t \in \mathcal{T}. \tag{2.8}$$

This provides a complete definition of the concept of a stationary distribution, also known as a *steady-state distribution*.

2.2.2 Time reversibility and detailed balance

We are now in a position to define the detailed balance conditions. I first introduce the *simple detailed balance* condition, which is expressed as [15, 100, 103]:

$$P(\mathcal{C})W(\mathcal{C} \to \mathcal{C}') = P(\mathcal{C}')W(\mathcal{C}' \to \mathcal{C}). \tag{2.9}$$

An important related feature is known as *reversibility*. A process is reversible if a configuration $(X(t_1), X(t_2), ...X(t_n))$ has the same distribution as $(X(\tau - t_1), X(\tau - t_2), ...X(\tau - t_n))$ [100]. A Markov process is reversible if and only if it obeys the detailed balance condition (2.9). Time reversibility and the detailed balance condition in (2.9) are therefore equivalent.

If a system satisfies time reversibility it is possible to write down the stationary weight for each configuration directly in Gibbs-Boltzmann form, $P(\mathcal{C}) \sim e^V$, using only the transition rates of the system. This is because the potential difference, ΔV, is the logarithm of the ratio of the forward and backward transition rates in the detailed balance condition:

$$\Delta V = V(\mathcal{C}) - V(\mathcal{C}') = \log\left[\frac{W(\mathcal{C}' \to \mathcal{C})}{W(\mathcal{C} \to \mathcal{C}')}\right]. \tag{2.10}$$

Therefore, if a system obeys detailed balance we have the ratio of the probabilities of any two configurations immediately.

However, in order to check directly whether a system satisfies detailed balance using (2.9) requires *a priori* knowledge of the distribution $P(\mathcal{C})$. It would be useful to be able to determine whether time reversibility is satisfied purely from the model definition i.e. when only the transition rates are known, as is the case for the run-and-tumble models. To achieve this, the detailed balance condition can be re-expressed as the *Kolmogorov criteria*, which state that a stationary Markov process obeys detailed balance if and only if its transition rates satisfy [15,

100, 103]

$$W(\mathcal{C}_1 \to \mathcal{C}_2)W(\mathcal{C}_2 \to \mathcal{C}_3)....W(\mathcal{C}_n \to \mathcal{C}_1) = W(\mathcal{C}_1 \to \mathcal{C}_n)...W(\mathcal{C}_2 \to \mathcal{C}_1). \quad (2.11)$$

Kolmogorov's criteria re-casts the detailed balance condition in (2.9) as a path independence condition: if the product of all the transition rates in some loop is equal to its time-reversed path, then detailed balance is obeyed. Thus the Kolmogorov criteria encode the uniqueness of each of the potentials, $V(\mathcal{C})$: for any set of transition rates chosen in the loop, V is single-valued.

2.2.3 Reversibility in the run-and-tumble models

We can apply Kolmogorov's criteria (2.11) to the run-and-tumble models directly. The single-particle and interacting models both immediately violate the criteria due to their persistent motion: because the particles remember their velocities, any forwarding hopping transition cannot be time-reversed. For example, for the simple loop in Figure 2.5 for the single-particle model, the time-reversed loop would be zero because hopping from $(i, -)$ to $(i+1, -)$ and from $(i+1, +)$ to $(i, +)$ cannot happen. This is also true for the two-particle model. Indeed persistent random walkers systems by definition trivially break the simple form of detailed balance expressed by (2.11).

However, it may still be possible to make a connection to the Boltzmann weight by considering the time-reversed process, even if it is not statistically the same as the original process. Let us first define the concept of a *reversed process* more formally. If $X(t)$ is a stationary Markov process with transition rates $W(\mathcal{C} \to \mathcal{C}')$ and equilibrium distribution $P(\mathcal{C})$, then the reversed process is a stationary Markov

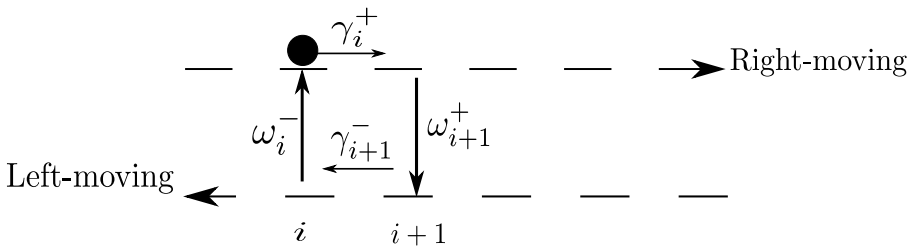

Figure 2.5 *Schematic of a loop in the original process for the one particle run-and-tumble model with site- and direction-dependent hopping and tumbling rates.*

process with transition rates

$$\hat{W}(\mathcal{C} \to \mathcal{C}') = \frac{P(\mathcal{C}')W(\mathcal{C}' \to \mathcal{C})}{P(\mathcal{C})} \tag{2.12}$$

and the same stationary distribution.

For the run-and-tumble model, the transition rates of the process under time reversal do not yield the same stationary distribution as the forward process. The relevant question is: is it possible that the reversed process would have the same stationary distribution if some the configurations were interchanged? More precisely, is there for every configuration $\mathcal{C}$ in the reversed process a conjugate configuration $\hat{\mathcal{C}}$ such that the reversed process $X(\tau - t)$ is statistically indistinguishable from the original process? If there is, the process is said to be *dynamically reversible* [100].

The condition for dynamic reversibility may be stated as follows [100]: a stationary Markov process with configurations $\mathcal{C} \in \mathcal{K}$, transition rates W, and conjugate configurations $\hat{\mathcal{C}} \in \mathcal{K}$ that satisfy

$$\sum_{\mathcal{C}' \in \mathcal{K}} W(\mathcal{C} \to \mathcal{C}') = \sum_{\hat{\mathcal{C}}' \in \mathcal{K}} W(\hat{\mathcal{C}} \to \hat{\mathcal{C}}'), \tag{2.13}$$

is dynamically reversible if and only if there exists a probability distribution, $P(C)$ that satisfies

$$P(\mathcal{C}) = P(\hat{\mathcal{C}}) \text{ and} \tag{2.14}$$

$$P(\mathcal{C})W(\mathcal{C} \to \mathcal{C}') = P(\hat{\mathcal{C}}')W(\hat{\mathcal{C}}' \to \hat{\mathcal{C}}). \tag{2.15}$$

When such a probability distribution exists, it is the stationary distribution of the process.

Conditions (2.13)—(2.15) may be expressed using a generalised form of the Kolmogorov criteria that bypasses the need to identify conjugate configurations. These generalised Kolmogorov criteria state that if for a Markov process with transition probabilities W, it is possible to find a set of transition probabilities, $\hat{W}$, that satisfy [100]

$$W(\mathcal{C}_1 \to \mathcal{C}_2)W(\mathcal{C}_2 \to \mathcal{C}_3)....W(\mathcal{C}_{n-1} \to \mathcal{C}_n)W(\mathcal{C}_n \to \mathcal{C}_1) = \hat{W}(\mathcal{C}_1 \to \mathcal{C}_n)\hat{W}(\mathcal{C}_n \to \mathcal{C}_{n-1})...\hat{W}(\mathcal{C}_2 \to \mathcal{C}_1), \tag{2.16}$$

and

$$\sum_{\mathcal{C}' \in \mathcal{K}} W(\mathcal{C} \to \mathcal{C}') = \sum_{\mathcal{C}' \in \mathcal{K}} \hat{W}(\mathcal{C} \to \mathcal{C}'), \tag{2.17}$$

then these $\hat{W}$ are the transition probabilities of the reversed process $X(\tau - t)$. Weights for dynamically reversible systems may then be written straightforwardly in Gibbs-Boltzmann form using

$$\log\left[\frac{P(\mathcal{C}')}{P(\mathcal{C})}\right] = \log\left[\frac{W(\mathcal{C} \to \mathcal{C}')}{\hat{W}(\mathcal{C}' \to \mathcal{C})}\right]. \tag{2.18}$$

We shall now construct a reversed process for the single particle run-and-tumble model.

Condition (2.17) may be re-expressed as

$$r(\mathcal{C}) = \sum_{\mathcal{C}' \in \mathcal{K}} W(\mathcal{C} \to \mathcal{C}') \tag{2.19}$$

$$\hat{r}(\hat{\mathcal{C}}) = \sum_{\hat{\mathcal{C}}' \in \mathcal{K}} \hat{W}(\hat{\mathcal{C}} \to \hat{\mathcal{C}}') \tag{2.20}$$

$$r(\mathcal{C}) = \hat{r}(\hat{\mathcal{C}}). \tag{2.21}$$

The transition rates for the reversed process are labelled as $\hat{\gamma}_i^\sigma$ and $\hat{\omega}_i^\sigma$. The condition reduces to

$$\hat{\gamma}_i^\sigma + \hat{\omega}_i^\sigma = \gamma_i^\sigma + \omega_i^\sigma. \tag{2.22}$$

Without loss of generality, we can make the following choices for the reversed transition rates:

$$\hat{\gamma}_i^\sigma = \frac{\gamma_i^{\bar{\sigma}}(\gamma_i^\sigma + \omega_i^\sigma)}{(\gamma_i^{\bar{\sigma}} + \omega_i^{\bar{\sigma}})} \quad \text{and} \tag{2.23}$$

$$\hat{\omega}_i^\sigma = \frac{\omega_i^{\bar{\sigma}}(\gamma_i^\sigma + \omega_i^\sigma)}{(\gamma_i^{\bar{\sigma}} + \omega_i^{\bar{\sigma}})}, \tag{2.24}$$

where $\bar{\sigma} = -\sigma$. A loop for the original process and its corresponding reversed processes loop may be found in Figures 2.5 and 2.6. We see that the condition (2.16) is satisfied for these loops:

$$\gamma_i^+ \omega_{i+1}^+ \gamma_{i+1}^- \omega_i^- = \hat{\omega}_i^+ \hat{\gamma}_i^- \hat{\omega}_{i+1}^- \hat{\gamma}_{i+1}^+. \tag{2.25}$$

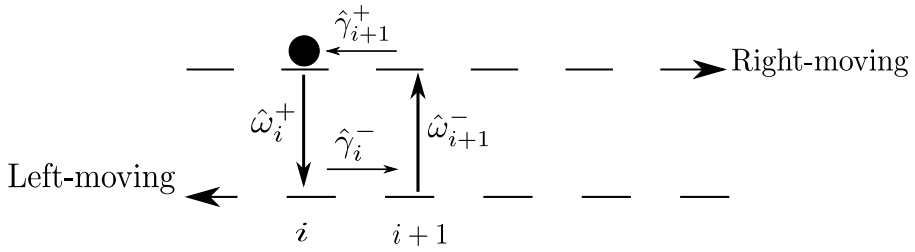

Figure 2.6 *Schematic of a loop in the reversed process for the one particle run-and-tumble model with site- and direction-dependent hopping and tumbling rates.*

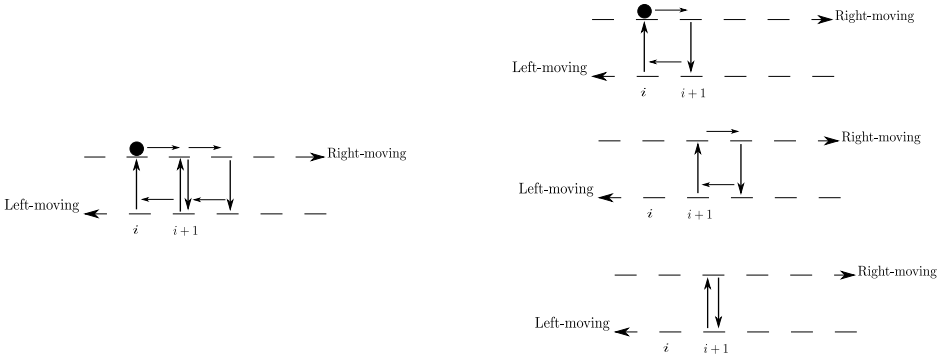

Figure 2.7 *Any loop can be broken down into loops of the type in Figure 2.5 or pure tumbling loops. For the example in this schematic, pictured on the left, it is broken down into two loops of the type in Figure 2.5 and one pure tumbling loop.*

The symmetry of the statespace of the one particle model means that any loop choice satisfies the condition similarly. This can be seen by noting that any loop configuration can be broken down into loops of the type in Figure 2.5 or pure tumbling loops, which are also reversible — see Figure 2.7. Thus dynamic reversibility is satisfied.

We may now find the Boltzmann weight for any configuration using the relation (2.18). For example,

$$\begin{aligned}\frac{W([i,+]\to[i+1,+])}{\hat{W}([i+1,+]\to[i,+])} &= \frac{\gamma^+_i}{\hat{\gamma}^+_{i+1}} \\ &= \frac{\gamma^+_i}{[\gamma^-_{i+1}(\gamma^-_{i+1}+\omega^+_{i+1})]/(\gamma^-_{i+1}+\omega^-_{i+1})}\end{aligned}$$

$$\frac{W([i,+]\to[i+1,+])}{\hat{W}([i+1,+]\to[i,+])}=\frac{\gamma_i^+(\gamma_{i+1}^-+\omega_{i+1}^-)}{\gamma_{i+1}^-(\gamma_{i+1}^++\omega_{i+1}^+)}. \tag{2.26}$$

This agrees with the result for $P(i+1,+)/P(i,+)$ in Eq. (7) in [88], which was derived by alternate means.

We now turn to the interacting run-and-tumble model. It is apparent that satisfying (2.13) is not straightforward. The reason lies in the fact that $r(\mathcal{C})$ is now state dependent in a stronger sense than for the one particle model: certain states do not have a finite hopping exit or entry transition probability. This is due to the interaction between the particles. To show this more explicitly, we attempt use of (2.23) and (2.24) as ansätze for transition rates of the reversed process for the interacting run-and-tumble model.

Example reversed loops of the interacting run-and-tumble process are shown in Figures 2.8 and 2.9. When the particles are separated, as in Figure 2.8, we can see that (2.23) and (2.24) satisfy condition (2.13), as they are both special cases of the loops in the single particle model simplified to no hopping or direction dependence. However, by comparing Figures 2.9 and 2.10 we can immediately see that collisions in the reversed process are not the same as they are in the original process. In the reversed process, a collision will occur in configurations that do not lead to collisions in the original process as exemplified by Figure 2.9. Therefore the sum of escape rates differ, and (2.13) does not hold.

Through this detailed balance analysis, we have seen that run-and-tumble random walkers with interactions defy a treatment where reversed process transition rates can be straightforwardly found, and that it is the collisions specifically that are responsible. To elucidate the physics of these nonequilibrium interactions, as well

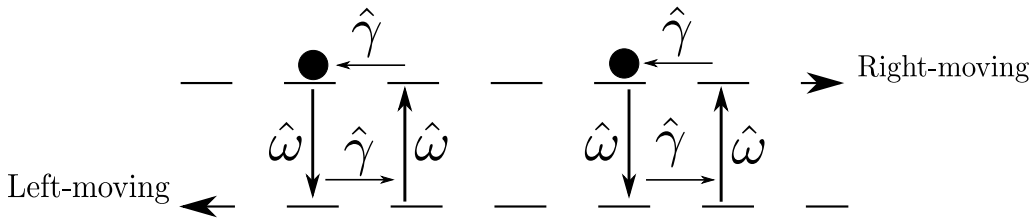

Figure 2.8 *For separated particles in the reversed process of the interacting run-and-tumble model, condition (2.13) is satisfied by the ansätze (2.23) and (2.24).*

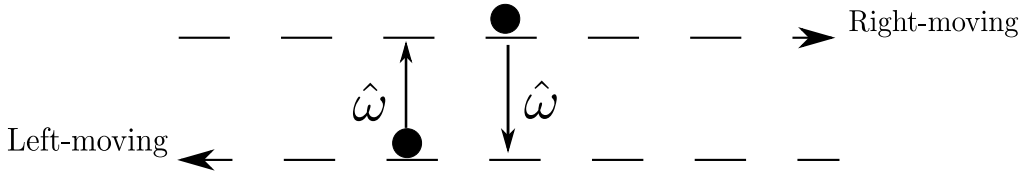

Figure 2.9 *For colliding particles in in the reversed process of the interacting the run-and-tumble model, condition (2.13) is* ***not*** *satisfied by the ansätze (2.23) and (2.24).*

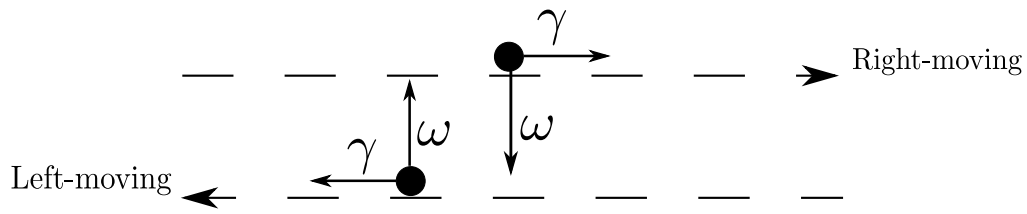

Figure 2.10 *In the original process, the interacting run-and-tumble model does not have the same escape rates for a configuration that represents a collision in the reversed process (see Figure 2.9).*

as to explore the mathematics that can provide understanding of such strongly nonequilibrium models at a microscopic level, we turn to back to a stochastic description as the starting point from which to solve the interacting run-and-tumble model.

2.3 The run-and-tumble master equation

The model of two interacting run-and-tumble random walkers defined in section 2.1 is a continuous time Markov process and thus can be described by a *master equation* [101]. The master equation is a probability gain-loss equation for the states of the system. It is written in terms of the probability, $P(\mathcal{C})$, of the system being in a particular configuration, $\mathcal{C}$ and the transition rates, $W(\mathcal{C} \to \mathcal{C}')$, between $\mathcal{C}$ and another configuration $\mathcal{C}'$. The general form of the master equation is

$$\dot{P}(\mathcal{C},t) = \sum_{C' \neq \mathcal{C}} P(\mathcal{C}',t) W(\mathcal{C}' \to \mathcal{C}) - \sum_{\mathcal{C}' \neq \mathcal{C}} P(\mathcal{C},t) W(\mathcal{C} \to \mathcal{C}'), \tag{2.27}$$

where the first term on the right-hand side represents the ratio of probability gain, and the second term on the right-hand side represents the ratio of probability loss. We now write the master equation for the two-particle run-and-tumble model.

The run-and-tumble master equation may be written as a set of equations, corresponding to probability gain-loss equations for each of the four different pairs of particle velocities: $++$, $+-$, $-+$ and $--$ with particle separation n (see section 2.1 for a definition of the interacting run-and-tumble model). As an example for how to construct these equations, the gain and loss terms for the $++$ equation are explicitly built up below.

Using (2.27) as a template, we first identify positive contributions (the probability gain) to $\dot{P}_{++}(n)$, which come from hopping and tumbling into $P_{++}(n)$ from other configurations. The hopping contributions come from configurations where two right-moving particles are separated by one lattice site more or less than n. In the case where the particles are separated by $n-1$ sites, the particle 'in front' can hop one site away from the particle 'behind', bringing the separation to n. If, on the other hand, the particles are separated by $n+1$ sites, the particle behind can hop one site towards the particle in front, bringing the separation to n. Since the hopping rate has been rescaled to $\gamma = 1$, these processes occur at rate 1. The configurations $P_{+-}(n)$ and $P_{-+}(n)$ each tumble into $P_{++}(n)$ at rate ω. Bringing these positive contributions together gives

$$P_{++}(n-1)I_{n>1} + P_{++}(n+1)I_{L-n>1} + \omega[P_{+-}(n) + P_{-+}(n)], \tag{2.28}$$

where the indicator $I_{k>1} = 1$ if $k > 1$ and is zero otherwise. This indicator variable is introduced to account for the adjacent states where $n = 1, L-1$, where one of the particles is blocked from hopping by the other. There is therefore no contribution from these states.

We now consider the probability loss from $\dot{P}_{++}(n)$. Each particle can always tumble, which will cause a change of configuration and represent a loss to $\dot{P}_{++}(n)$. As long as the particles are separated by more than one site, a particle can also always hop out of the configuration. Therefore the loss terms are given by:

$$P_{++}(n)[2\omega + I_{n>1} + I_{L-n>1}]. \tag{2.29}$$

The same approach may be used to find the probability gain-loss terms for

$P_{+-}(n)$. The master equation for the interacting run-and-tumble model is then:

$$\begin{aligned}\dot{P}_{++}(n) &= P_{++}(n-1)I_{n>1} + P_{++}(n+1)I_{L-n>1} \\ &\quad + \omega[P_{+-}(n) + P_{-+}(n)] \\ &\quad - P_{++}(n)[2\omega + I_{n>1} + I_{L-n>1}] \qquad (2.30) \\ \dot{P}_{+-}(n) &= 2P_{+-}(n+1)I_{L-n>1} + \omega[P_{++}(n) + P_{--}(n)] \\ &\quad - P_{+-}(n)[2\omega + 2I_{n>1}] \qquad (2.31)\end{aligned}$$

along with counterparts for $P_{-+}(n)$ and $P_{--}(n)$, which follow from the symmetries

$$P_{--}(n) = P_{++}(n) \text{ and} \qquad (2.32)$$

$$P_{-+}(n) = P_{+-}(L-n). \qquad (2.33)$$

As noted in the previous section, a stationary distribution will exist for any Markov process that is irreducible and finite. This is the case for the run-and-tumble model: there are no isolated configurations, and the number of lattice sites, L, is finite. The stationary distribution is the limiting distribution and so the system will inevitably evolve into it. Thus the steady state will capture all the physics after relaxation and is therefore of particular interest. It be the focus of the remainder of this chapter.

2.4 Derivation of the stationary distribution

The run-and-tumble master equation may be solved by transforming it into a system of *generating function* equations. A generating function is a formal power series used to study a particular sequence of numbers $\{a_0, a_1, ...\}$, where the coefficients of the power series are the numbers in the sequence. As poetically described by the combinatorialist Herbert Wilf, generating functions can be used as "clotheslines" on which to hang the sequence without requiring any of the properties of the functions that may be represented by the power series (if the functions exist at all) [104]. This allows questions of convergence or other function-theoretic issues to be dismissed without compromising the integrity of a generating function approach.

Here the sequence of numbers we are interested in is the set of steady-state probabilities of the run-and-tumble model. We can associate each probability

with the coefficient of a formal power series by introducing the (terminated) generating function

$$G_{\sigma_1\sigma_2}(x) = \sum_{n=1}^{L-1} x^n P_{\sigma_1\sigma_2}(x). \tag{2.34}$$

The master equation in (2.30) and (2.31) may then be re-packaged in terms of these generating functions.

2.4.1 Transformation of the master equation to a system of generating functions

We consider this transformation explicitly for the equation for $\dot{P}_{++}(n)$ as an example for the other generating function equations that will be written down directly. First, we substitute $\dot{P}_{++}(n)$ into the definition (2.34) yields

$$\dot{G}_{++}(x) = \sum_{n=1}^{L-1} x^n \Big(P_{++}(n-1)I_{n>1} + P_{++}(n+1)I_{L-n>1} + \omega[P_{-+}(n) + P_{+-}(n)] - P_{++}(n)[I_{n>1} + I_{L-n>1} + 2\omega] \Big). \tag{2.35}$$

Transformation of the equation requires it to be independent of any distribution (although the probability for a particular configuration e.g. $P_{++}(1)$ may remain). We first consider $\sum_{n=1}^{L-1} x^n I_{n>1} P_{++}(n-1)$. The only probability distribution present is $P_{++}(n-1)$. Note that each x^n term should be one power higher than the corresponding $P_{++}(n-1)$ term. Therefore we can pre-multiply the generating function by x: $xG_{++}(x)$. However, this contains an $x^L P(L-1)$ term, which needs to be removed as $x^{L-1}P(L-2)$ is the highest order x term:

$$\sum_{n=1}^{L-1} x^n I_{n>1} P_{++}(n-1) = xG_{++}(x) - x^L P_{++}(L-1). \tag{2.36}$$

We now turn to $\sum_{n=1}^{L-1} x^n I_{L-n>1} P_{++}(n+1)$. Here each x^n term is one power lower than the corresponding $P(n+1)$ term. Therefore we pre-multiply the generating function by x^{-1}. However, this now contains a $x^{-1}P(1)$ term, where as the lowest order term should be $xP(2)$. Therefore we remove this extra term by subtraction:

$$\sum_{n=1}^{L-1} x^n I_{L-n>1} P_{++}(n+1) = x^{-1}G_{++}(x) - x^{-1}P_{++}(1). \tag{2.37}$$

Writing the tumbling in terms of generating functions is straightforward as all terms are directly transformable:

$$\sum_{n=1}^{L-1} x^n \omega[P_{-+}(n) + P_{+-}(n)] = \omega[G_{-+}(x) + G_{+-}(x)]. \tag{2.38}$$

Finally, we consider the second line of (2.35). Rewriting $-\sum_{n=1}^{L-1} x^n I_{n>1} P_{++}(n)$ as $-G_{++}(x)$, introduces an extra $-xP_{++}(1)$ that needs to be removed. Similarly, rewriting $-\sum_{n=1}^{L-1} x^n I_{L-n>1} P_{++}(n)$ introduces an extra $-x^{L-1}P_{++}(L-1)$. The remaining $-2\omega \sum_{n=1}^{L-1} x^n P_{++}(n)$ term is directly transformable. This line becomes

$$\sum_{n=1}^{L-1} x^n \left[-P_{++}(n)[I_{n>1} + I_{L-n>1} + 2\omega]\right] = xP_{++}(1) + x^{L-1}P_{++}(L-1) - 2\omega]G_{++}(x). \tag{2.39}$$

Drawing these pieces together gives the full ++ generating function equation:

$$\begin{aligned} \dot{G}_{++}(x) = (x + x^{-1} - 2[1+\omega])G_{++}(x) \\ - (1-x)(1-x^{L-1})P_{++}(1) \\ + \omega[G_{+-}(x) + G_{-+}(x)]. \end{aligned} \tag{2.40}$$

A similar approach to transforming the probability gain-loss equation (2.31) for $\dot{P}_{+-}(n)$ leads to

$$\begin{aligned} \dot{G}_{+-}(x) = 2(x^{-1} - [1+\omega])G_{+-}(x) \\ - 2(1-x)P_{+-}(1) \\ + \omega[G_{++}(x) + G_{--}(x)]. \end{aligned} \tag{2.41}$$

Here we are concerned with the stationary probability distribution: where $\dot{P}_{\sigma_1\sigma_2} = 0$, implying that $\dot{G}_{\sigma_1\sigma_2} = 0$. The symmetries $P_{++}(n) = P_{--}(n) = P_{++}(L-n)$ and $P_{+-}(n) = P_{-+}(L-n)$ from equations (2.32) and (2.33) in the stationary probability distribution translate to the symmetries

$$G_{++}(x) = G_{--}(x) = x^L G_{++}(x^{-1}) \text{ and} \tag{2.42}$$

$$G_{+-}(x) = x^L G_{-+}(x^{-1}) \tag{2.43}$$

in the stationary values of their generating functions. By exploiting these

symmetries, we find from (2.40) and (2.41) that the stationary generating functions must be the solution of the linear system

$$\begin{pmatrix} \mu(x)+\nu(x) & \omega & \omega \\ \omega & \nu(x) & 0 \\ \omega & 0 & \mu(x) \end{pmatrix} \begin{pmatrix} G_{++}(x) \\ G_{+-}(x) \\ G_{--}(x) \end{pmatrix} = (1-x) \begin{pmatrix} (1-x^{L-1})P_{++}(1) \\ P_{+-}(1) \\ -x^{L-1}P_{+-}(1) \end{pmatrix} \quad (2.44)$$

where

$$\mu(x) = x - (1+\omega) \text{ and} \quad (2.45)$$

$$\nu(x) = x^{-1} - (1+\omega) = \mu(1/x). \quad (2.46)$$

The inverse of the matrix appearing on the left-hand side of this expression is

$$\frac{x^2}{(1+\omega)(x-z)(x-\frac{1}{z})(1-x)(x-1)} \times \begin{pmatrix} \mu\nu & -\mu\omega & -\nu\omega \\ -\mu\omega & \mu(\mu+\nu)-\omega^2 & \omega^2 \\ -\nu\omega & \omega^2 & \nu(\mu+\nu)-\omega^2 \end{pmatrix}, \quad (2.47)$$

where z and $1/z$ are the two roots of $x^2 - 2(1+\omega)x + 1$ and recalling that μ and ν are defined as in Eqs. (2.45) and (2.46).

We seek a solution of the generating functions $G_{\sigma_1\sigma_2}(x)$ in a form where I can read off the probabilities $P_{\sigma_1\sigma_2}(n)$. This means writing the generating functions in this matrix equation in the form of the power series in (2.34), but where every probability $P_{\sigma_1\sigma_2}(n)$ is only a function of the model parameters. These probabilities were first derived in [75]. We follow the same method here.

2.4.2 Pole cancellation in the generating function equations

The approach we will use to solve this generating function system of equations is a variant of what is known as the *kernel method* [105, 106]. The exact procedure for using the kernel method will depend on the problem at hand. It first appeared in the form of an exercise in a book on computer programming [106, 107], but

more recently was formalised by Bousquet-Mélou and co-workers in [105]. It has appeared in several mathematical works, including in the enumeration of combinatorial problems such as the classes of column-convex polygons [108] and two-stack sorting problems [109]. Many of the applications have been to random walks [106]. We will see that it is key to the solution of the interacting persistent random walk in this chapter.

We have already undertaken the first step in the kernel method, which is to use generating functions to describe the random walk. In broad terms, the next steps use the fact that the generating function equations in Eq. (2.44) cannot diverge as they have a power series expansion by definition. Therefore if there are any poles in these expressions (i.e. if the denominator vanishes) then at the corresponding values of x the numerator must also vanish. Ultimately, this indentification will allow inversion of the matrix equation (2.44).

We first consider the expression for G_{++} from the inverse matrix in Eq. (2.47). Expanding the top line of equation (2.47) yields

$$G_{++}(x) = \frac{x^2}{(1+\omega)(x-1)(x-z)(x-\frac{1}{z})} \times \\ \left\{\mu(x)\nu(x)[1-x^{L-1}]P_{++}(1) + \right. \\ \left. \omega[\nu(x)x^{L-1} - \mu(x)]P_{+-}(1)\right\} . \quad (2.48)$$

For general values of $P_{++}(1)$ and $P_{+-}(1)$, this gives an infinite series in x. However, due to the original definition of the generating function (2.34), it must terminate at order x^{L-1}. We now examine the nature of the poles of the denominator. We known that the equation must not diverge in the limits $x \to 1$, $x \to z$ or $x \to 1/z$. Since $\nu(1) = \mu(1)$, the $x = 1$ pole is already canceled by a zero in the numerator. For this also to be the case at $x = z$, the numerator

$$\left\{\mu(x)\nu(x)[1-x^{L-1}]P_{++}(1) + \omega[\nu(x)x^{L-1} - \mu(x)]P_{+-}(1)\right\} \quad (2.49)$$

must also vanish. In the context of the kernel method, the numerator in Eq. (2.49) is known as the *kernel*. The condition that the kernel must vanish is equivalent to:

$$\mu(z)\nu(z)P_{++}(1) - \omega\mu(z)P_{+-}(1) = \\ z^{L-1}\left[\mu(z)\nu(z)P_{++}(1) - \omega\nu(z)P_{+-}(1)\right] . \quad (2.50)$$

As $\mu(x) = \nu(1/x)$, the pole at $x = 1/z$ is also canceled if this relation holds. Furthermore, by making the substitutions $\mu(z) = -\nu(z) = \frac{1}{2}(z - 1/z)$ and $\omega = (z-1)^2/2z$, the following relation holds:

$$\frac{P_{++}(1)}{P_{+-}(1)} = \frac{1 + z^{L-1}}{1 - z^{L-1}} \frac{(1-z)^2}{1-z^2} \, . \tag{2.51}$$

The relationship (2.51) leaves $P_{+-}(1)$ as the only remaining undetermined constant. $P_{+-}(1)$ will be set by normalisation at the end of the derivation.

2.4.3 Inversion of the generating functions

We may now proceed to invert the generating function G_{++} so that it is in the form expressed in Eq. (2.34), from which the probabilities can be read off immediately. Recalling that by definition G_{++} must terminate at order x^{L-1}, we now separate the numerator into terms with order x^{L-1} or less from higher order terms. This yields

$$G_{++}(x) = \frac{x}{1+\omega} \frac{xJ(x)}{(x-1)(x-z)(x-\frac{1}{z})} + x^L H_{++}(x), \tag{2.52}$$

where

$$J(x) = \mu(x)\nu(x)P_{++}(1) - \omega\mu(x)P_{+-}(1) \tag{2.53}$$

is quadratic in x and $H_{++}(x)$ is some power series in x that absorbs the remaining terms in $G_{++}(x)$. Since $P_{++}(n)$ is given by the coefficient of the x^n and $n < L$, it follows that none of the terms in $H_{++}(x)$ contribute to the $P_{++}(n)$ of interest. In fact, all terms of order $n > L$ in $H_{++}(x)$ will necessarily cancel with terms of order greater than L from the denominator of the first term in G_{++}.

In order to access $P_{++}(n)$, we need to be able to read off the coefficient of x^n in the first term of (2.52) (we can ignore $H_{++}(x)$ as it does not contribute). Since $J(x)$ is quadratic, and the denominator is cubic, we can perform partial fraction decomposition, which yields

$$G_{++}(x) = \frac{x}{1+\omega}\left[\frac{J(1)}{(1-z)(\frac{1}{z}-1)(1-x)} + \frac{1}{(z-1)(\frac{1}{z}-z)}\left(\frac{zJ(1/z)}{1-zx} + \frac{J(z)}{1-x/z}\right)\right] + x^L H_{++}(x). \tag{2.54}$$

From (2.50) and the relation $\mu(x) = \nu(1/x)$, it follows that

$$J(z) = z^{L-1} J(1/z). \tag{2.55}$$

This symmetry allows us to re-write Eq. (2.54) as

$$G_{++}(x) = \frac{x}{1+\omega}\left[\frac{J(1)}{(1-z)(\frac{1}{z}-1)(1-x)} + \frac{J(1/z)}{(z-1)(\frac{1}{z}-z)}\left(\frac{z}{1-zx} + \frac{z^{L-1}}{1-x/z}\right)\right] + x^L H_{++}(x), \tag{2.56}$$

which has the structure

$$G_{++}(x) = x\left[\frac{a(z)}{1-x} + \frac{b(z)z}{1-zx} + \frac{b(z)z^{L-1}}{1-x/z}\right] + x^L H_{++}(x) \tag{2.57}$$

where

$$a(z) = \frac{J(1)}{(1+\omega)(\frac{1}{z}-1)(1-z)} \tag{2.58}$$

$$= \frac{(1-z)^2(1-z^L)}{(1+z)(1+z^2)(1-z^{L-1})} P_{+-}(1) \tag{2.59}$$

and

$$b(z) = \frac{J(1/z)}{(1+\omega)(z-1)(\frac{1}{z}-z)} \tag{2.60}$$

$$= \frac{1-z}{(1+z^2)(1-z^{L-1})} P_{+-}(1)\ . \tag{2.61}$$

Here the ratio in Eq. (2.51) was used to express everything in terms of a single unknown constant $P_{+-}(1)$ that will be fixed by normalisation. We can write $P_{+-}(1)$ as

$$P_{+-}(1) = \frac{(1+z)(1+z^2)(1-z^{L-1})}{Z}, \tag{2.62}$$

and reading off the coefficient of x^n in (2.57) yields

$$P_{++}(n) = \frac{1}{Z}\left[q(z) + p(z)(z^n + z^{L-n})\right], \tag{2.63}$$

where the functions $p(z) = Zb(z)$ and $q(z) = Za(z)$ have the functional forms

$$z = 1 + \omega - \sqrt{\omega(2+\omega)} \tag{2.64}$$

$$p(z) = 1 - z^2 \tag{2.65}$$

$$q(z) = (1-z)^2(1-z^L) \tag{2.66}$$

$$Z = 4[\Delta(z) + (L-1)q(z)] \, . \tag{2.67}$$

The inversion of $G_{+-}(x)$ proceeds similarly, with a subtlety arising from the jamming occurring in this sector. Here

$$G_{+-}(x) = -\frac{x}{1+\omega}\frac{xK(x)}{(x-1)(x-z)(x-\frac{1}{z})} + \frac{x\mu(x)P_{+-}(1)}{(1+\omega)(x-1)} + x^L H_{+-}(x) \tag{2.68}$$

where

$$K(x) = \omega[\mu(x)P_{++}(1) + \omega P_{+-}(1)] \, , \tag{2.69}$$

which is again quadratic in x. The term $\frac{x\mu(x)P_{+-}(1)}{(1+\omega)(x-1)}$ that appears in the generating function would be cubic in x if it were brought over a common denominator: this would not then be amenable to partial fraction decomposition. The significance of this term is that it can ascribe an anomalously large weight to the jammed configuration.

Performing partial fraction decomposition on Eq. (2.68) gives

$$G_{+-}(x) = \frac{x}{1+\omega}\Bigg[\left((1+\omega)P_{+-}(1) - \frac{K(1)}{(1-z)(\frac{1}{z}-1)} - xP_{+-}(1)\right)\frac{1}{1-x} + \frac{1}{(1-z)(\frac{1}{z}-z)}\left(\frac{zK(1/z)}{1-zx} + \frac{K(z)}{1-x/z}\right)\Bigg] + x^L H_{+-}(x) \, . \tag{2.70}$$

An analogous symmetry to $J(z)$ in Eq. (2.55) holds for $K(z)$,

$$K(z) = -z^{L-1}K(1/z), \tag{2.71}$$

which can be established using (2.50), along with the relations $\mu(x) = \nu(1/x)$ and $\mu(z) = -\nu(z)$. $G_{+-}(x)$ therefore has the form

$$G_{+-}(x) = x\left[\frac{a'(z) + c'(z) - xc'(z)}{1-x} + \frac{b'(z)z}{1-zx} - \frac{b'(z)z^{L-1}}{1-x/z}\right] + x^L H_{++}(x), \tag{2.72}$$

where

$$a'(z) = P_{+-}(1) - \frac{K(1)}{(1+\omega)(1-z)(\frac{1}{z}-1)} - \frac{P_{+-}(1)}{1+\omega} \tag{2.73}$$

$$= a(z)$$

$$b'(z) = \frac{1}{1+\omega}\frac{K(1/z)}{(1-z)(\frac{1}{z}-z)} \tag{2.74}$$

$$= \frac{(1-z)^2}{(1+z)(1+z^2)(1-z^{L-1})}P_{+-}(1)$$

$$c'(z) = \frac{P_{+-}(1)}{1+\omega} = \frac{2z}{1+z^2}P_{+-}(1)\ . \tag{2.75}$$

Substituting in (2.62) and reading off the coefficient of x^n in (2.72) finally yields

$$P_{+-}(n) = \frac{1}{Z}\left[p'(z)(z^n - z^{L-n}) + q(z) + \delta_{n,1}\Delta(z)\right], \tag{2.76}$$

where $p'(z) = Zb'(z)$ and $\Delta(z) = Zc'(z)$ have the functional forms

$$p'(z) = \frac{1-z}{1+z}p(z) = (1-z)^2 \tag{2.77}$$

$$\Delta(z) = 2(1+z)(z-z^L). \tag{2.78}$$

Note that the parameter z lies in the range $0 < z < 1$, hence $p(z)$, $p'(z)$, $q(z)$ and $\Delta(z)$ are all positive. Expressions for $P_{--}(n)$ and $P_{-+}(n)$ follow from the symmetries $P_{--}(n) = P_{++}(n)$ and $P_{-+}(n) = P_{+-}(L-n)$ stated in equations (2.32) and (2.33).

2.4.4 Emergent interactions

Equations (2.63) and (2.76) reveal that the stationary distribution is a sum of three distinct components, which we explicitly identify now. When the separation between the particles is large, n, $L-n \gg 1$, the particle distribution is uniform and proportional to $q(z)$, independent of n as for regular diffusion. This part of the distribution fills the whole of phase space, and so can be referred to as an *extended* component [75]. At intermediate separations, the probability distribution for the separation between particles decays exponentially as z^n with a characteristic lengthscale

$$\xi = 1/|\ln(z)| \tag{2.79}$$

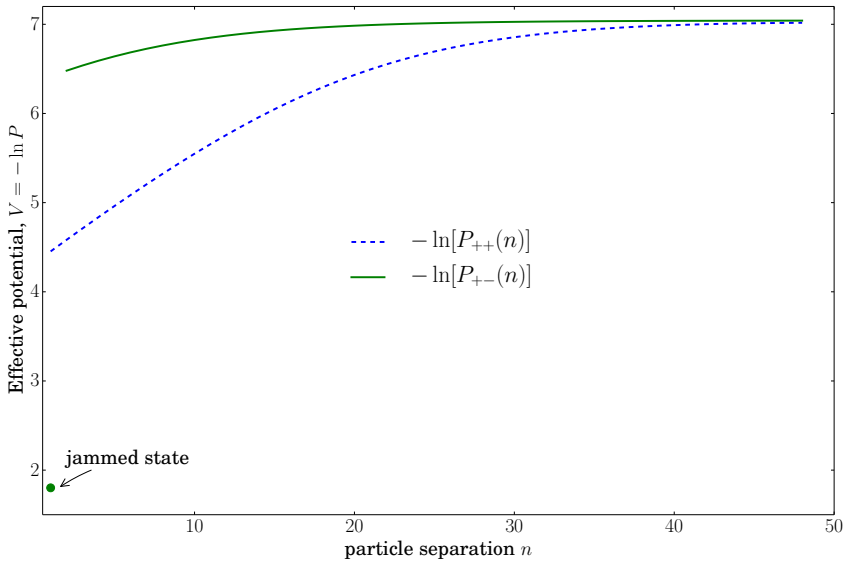

Figure 2.11 *(Partly reproduced from [75]) Effective pair potentials, defined by the logarithms of the probability distributions, $P_{++}(n)$ and $P_{+-}(n)$, for the case of $L = 100$ lattice sites and velocity reversal rate $\omega = 0.01$. These distributions have three components: jammed (indicated), attractive (linear piece at intermediate separations) and extended (constant piece at large separations).*

Note that γ does not appear in this lengthscale because it was scaled to 1 when the master equations were written down in section 2.3. However, the hop rate, γ enters through the scaled reversal rate $\omega = \tilde{\omega}/\gamma$, where $\tilde{\omega}$ is the bare reversal rate, in $z = 1 + \omega - \sqrt{\omega(2+\omega)}$ (see Eq. (2.64)). Note that the ratio $\gamma/\tilde{\omega}$ determines the run length. The origin of the lengthscale ξ is due to the stochastic hopping dynamics. When particles hop together in the same direction, the stochasticity of the hopping causes some broadening of the separation between the particles to occur, which generates this lengthscale. The physics of this lengthscale for limiting values of ω is considered in more detail in the next section. The final component concerns the jammed configurations that have particles facing each other on adjacent sites ($n = 1$), and hence the smallest possible separation, add their anomalous weight to the distribution.

Although the steady state is inherently nonequilibrium, equations (2.63) and (2.76) may be recast in the form of effective pair potentials $V_{\sigma_1\sigma_2}(n) = -\ln P_{\sigma_1\sigma_2}(n)$ by analogy with the Boltzmann distribution $P \propto \mathrm{e}^{-\beta V}$ (where we measure V in terms of $k_{\mathrm{B}}T$). The analogy to equilibrium systems holds to the extent that a passive system with this potential would have the same stationary distribution as the run-and-tumble one. However, the dynamics

would be different. Therefore here we use *effective interactions* to mean that the stationary probability distribution is the same for the system of interacting run-and-tumble particles as a passive system with a corresponding interaction potential.

The effective pair potentials are plotted for a specific choice of parameter values in Figure 2.11. Three distinct pieces of the potentials corresponding to the three components of the particle distribution are evident. At large separations, n, $L - n \gg 1$, the effective potentials are constant. At intermediate separations, the potentials are linear and attractive. Finally, there is a nearest-neighbour ($n = 1$) delta function attractive potential. This attraction is very strong when the reversal rate ω is small.

The work described in section 1.5 found effective potentials emerge from systems of interacting active particles, and we have seen that such interactions may be derived exactly for the minimal interacting run-and-tumble model in one dimension. As other work has found, the effective potential is very different to the bare exclusion potential that served as an input to the model, and gives indications as to the system's collective behaviour. In the case of the interacting run-and-tumble model, we may postulate that the emergent attraction between the two particles indicates the genesis of the clustering phenomenon that leads to motility-induced phase separation as described in section 1.4.

We may also compare this relationship to the Boltzmann weight with that of the single run-and-tumble random walker model in section 2.2, which broke the time reversibility condition but satisfied dynamic reversibility allowing the Boltzmann weight to be calculated directly from the transition rates. The interactions of this model rendered it inaccessible to a detailed balance analysis but the effective interaction that emerges still fits into our intuition of attractive potentials familiar from equilibrium problems. However, as we shall see in the next section, this potential is generated by a very different mechanism: the interactions between the particles.

2.5 Limiting behaviour of the stationary distribution

The origin and physics of the different components of the stationary distribution, and hence also the emergence of the effective interactions, can be understood from limiting cases. When velocity reversal is rapid, $\omega \to \infty$, standard diffusion should be recovered, as memory of a particle's velocity is erased between each hop. This is the limit of zero persistence time. To express this limit, we sum over all four velocity states to obtain the total probability that the two particles are a distance n apart. In the limit $\omega \gg 1$ becomes

$$P(n) \sim \frac{1}{L-1}\left[1 + \frac{1}{2\omega}\left(\delta_{n,1} + \delta_{n,L-1} - \tfrac{2}{L-1}\right) + O\left(\tfrac{1}{\omega^2}\right)\right]. \tag{2.80}$$

At leading order in $1/\omega$, only the extended component survives, and we therefore identify repeated velocity reversal as the physical origin of this contribution to the stationary distribution. The jammed component provides the leading correction, whilst the attractive component does not enter at order $O(1/\omega)$.

For the opposite limit, $\omega \to 0$, the limiting forms of equations (2.63) and (2.76)

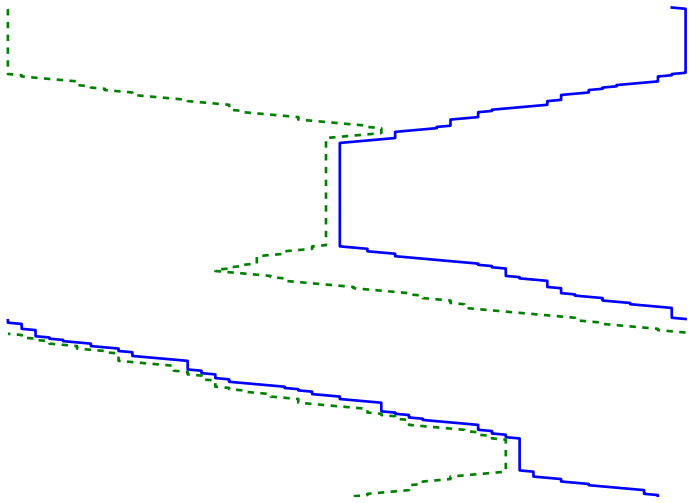

Figure 2.12 *(This plot appears in [75].) Simulation of Model System: A space-time plot (time in the vertical direction) of a simulation of two run-and-tumble random particles on a one-dimensional ring of* 100 *sites in the low tumble-rate regime with particles reversing their direction after traversing* 100 *lattice sites on average. The full and dotted trajectories each represent an individual particle.*

are

$$P_{++}(n) = \frac{1}{4(L-1)} \quad \text{and} \quad P_{+-}(n) = \frac{1}{4}\delta_{n,1} \ , \tag{2.81}$$

with corrections of order $L\omega$, implying that expressions in (2.81) are valid when $\omega \ll 1/L$. In this regime, particles hop many times between velocity reversals, and so in this limit the stationary distribution in each velocity sector should approximate that which would be reached in the absence of any tumbling. For the case where particles are approaching $(+-)$, the particles quickly reach the jammed configuration, $n = 1$, compared to the timescale of tumbling. When they exit this configuration into one where both particles have the same velocity (e.g., $++$), fluctuations in the distance traveled by each particle, generated by the stochastic particle hopping dynamics, cause the distribution of the relative distance coordinate, n, to broaden. When this tumble rate is low, the distribution broadens to fill the entire system, thereby generating a uniform distribution, but one that is crucially distinct from the extended component that arises from velocity reversals.

In Figure 2.12, we see the dynamics of the two run-and-tumble particles following a collision where the tumble rate is small compared to the hop rate. We can see that this snapshot does not represent the steady-state distribution because it captures dynamics only when the particles are close together even when they both have $+$ or $-$ velocities. In the steady state on average there is a equal probability of any separation in these velocity sectors in the low tumble limit, which is seen in the long-time limit.

At higher tumble rates, the broadening of the distribution is curtailed on the timescale of tumbling, and is later restarted from the jammed configuration $n = 1$. This process is similar to that of diffusion (here, of the particle separation) with stochastic resetting (to the jammed configuration), which generates the exponentially-decaying attractive component of the distribution [110].

We now turn to the scaling limit $\omega \to 0$, $L \to \infty$ with ωL held fixed, in which run-and-tumble dynamics in continuous space and time is recovered. This limit is of significance because it might more closely reflect the continuous dynamics of real run-and-tumble swimmers. To make the connection with a physical set-up, we introduce the physical system size ℓ and reinstate the run rate γ which had previously set the unit of time. Then, the mean run velocity is

$$v = \gamma\ell/L, \tag{2.82}$$

and the velocity reversal rate

$$\omega = \tilde{\alpha}/2\gamma = \tilde{\alpha}\ell/2Lv, \tag{2.83}$$

where $\tilde{\alpha}$ is the physical tumble rate. This describes the general tumble events where a velocity v or $-v$ is immediately adopted with equal probability, rather than just the reversal rate as described by ω, which was also rescaled by γ. This rate was introduced in Eq. (1.9) in section 1.3 of the introduction. Substituting these expressions (2.82) and (2.83) into equations (2.63) and (2.76), and introducing the continuous spatial separation $x = n\ell/L$, yields

$$P_{++}(x) = \frac{\tilde{\alpha} + 2v\delta(x) + 2v\delta(\ell - x)}{4(\tilde{\alpha}\ell + 4v)} \tag{2.84}$$

$$P_{+-}(x) = \frac{\tilde{\alpha} + 4v\delta(x)}{4(\tilde{\alpha}\ell + 4v)} \tag{2.85}$$

in the limit $L \to \infty$. Here, the delta functions are to be thought of as slightly displaced into the interior region from the boundaries at $x = 0, \ell$, so that the integral $\int_0^\ell \mathrm{d}x\delta(x) = 1$.

In contrast to the other two limits considered so far, all three components of the stationary distribution survive in the scaling limit. The extended and attractive components are present in the $++$ and $--$ sectors. In particular, the lengthscale

$$\xi \simeq 1/(2\omega)^{1/2} \tag{2.86}$$

of the exponential decay corresponds to a microscopically large number of lattice sites of order $\sqrt{L}$. This is, however, small on the macroscopic scale, where each unit of length comprises $\sim L$ lattice sites: thus the attraction is confined to a fraction $\sim 1/\sqrt{L}$ of the total system. At the same time, the amplitude of this exponential decay diverges as $\sqrt{L}$, and hence this component is manifested as the delta function appearing in Eq. (2.84) — this delta function thus represents an attractive state in which particles move together with zero separation.

Turning to Eq. (2.85), we see that the extended and jammed components appear, where here the delta function has its origins in the Kronecker delta that appears in Eq. (2.76) and represents a jammed configuration. Eq. (2.85) shows that the particles spend a fraction $v/(\tilde{\alpha}\ell + 4v)$ of time in each of the two symmetrically-related jammed configurations and from (2.84) that a fraction $v/(2(\tilde{\alpha}\ell + 4v))$ is spent in each of the four attractive states with zero separation. Thus the total

fraction of time spent in a state in which particles are adjacent ($x = 0$ or ℓ) is $4v/(\tilde{\alpha}\ell + 4v)$. In addition, a first passage time calculation undertaken in [75] showed the mean time between entering and leaving a nonadjacent state is ℓ/v. Intriguingly, this result is independent of the tumble rate α, despite the fact that particles must typically tumble over this lifetime: otherwise, the time spent in this state would be close to its minimum value $\ell/2v$. We can compare this with the total fraction of time spent in an adjacent state, $\frac{4/\tilde{\alpha}}{(\ell/v+4/\tilde{\alpha})}$, and see the mean time spent in an adjacent state is $4/\tilde{\alpha}$.

2.6 Reflecting boundaries, two-dimensional and many-body models

In section 2.1 it was noted that various idealisations in the interacting run-and-tumble model were made in order to make it analytically tractable. These included periodic rather than reflecting boundaries; motion restricted to one dimension; and only two particles. The difficulties in relaxing these assumptions, within the context of the generating function method that has been used, are all related. They lie in increasing the number of variables in the generating functions from one to two or more.

As the derivation of the probability distribution of the run-and-tumble model above shows, the number of variables in the generating function equations (2.40), (2.41) and their symmetric counterparts, equals the number of random variables required to describe the system. In the case of a periodic one-dimensional lattice with only two particles, the only variable required is the separation between the particles, n. In contrast, in the case of reflecting boundaries, the periodic symmetry is broken and each of the particle positions relative to the boundaries is required. Therefore the generating functions required to describe the system are of the form $G_{\sigma_1,\sigma_2}(x, y)$. In turn, the requisite pole cancellation of the equivalent of (2.48) is achieved not through identifying linear equations, as for the single-variable case, but quadratic equations. In this way, the problem becomes one of an *obstinate kernel* [108], for which a solution for this run-and-tumble model has not been found. Instead, an approximate approach using graph-theoretic techniques is used to tackle the model with reflecting boundaries in Chapter 4.

The number of generating function variables required also increases in more

dimensions. In two dimensions, two random variables are required to define a general configuration. For example, these could be the distance between the particles, and their angle. It is worth noting that should it prove possible to generalise the exact calculation of the pair potential to two or more dimensions, by analogy with the one-dimensional problem here we might expect the jammed state to be present for a finite fraction of the time, and for particles at intermediate separations to experience an attraction. This appears likely as in two dimensions a pair of diffusing particles (of finite size) will eventually collide with each other [111]. However, we would anticipate that the strength of the attraction between the particles to be significantly weaker compared to one dimension. In two dimensions, when tumbling after a collision, there are three (out of four) directions for a particle to become unbound from the other, compared to only one (out of two) in the one dimensional case.

A model with more than two particles also requires at least two random variables to define a configuration. For example, in a three-body model with periodic boundaries, two position variables are required in order to describe the relative distances between the particles. Many-body systems are, of course, of great interest and have formed the principal focus of the mesoscopic work on run-and-tumble dynamics described in the introduction. In addition to the clustering they present as a phenomenon of active matter, many-body run-and-tumble models are of interest as a way to elucidate the difference between equilibrium and non-equilibrium behaviours. We examine this aspect briefly now.

2.6.1 Simulation of the many-body system

Figure 2.13 shows a comparison of simulations of hard-core particles in one dimension that hop with equal probability to the left or the right in each timestep (left panel) with the run-and-tumble dynamics that is the focus of this work (right panel). The former dynamics is a diffusion process satisfying detailed balance, which relaxes to a homogeneous steady state where all configurations are equally likely.

The algorithm for the Monte Carlo simulation of the many-body interacting run-and-tumble dynamics proceeds as follows. Initially, each particle is labelled with a unique position from 1 to L so that they are uniformly distributed and have a randomly allocated velocity of either -1 or 1 (although how the particles are initially assigned does not affect the steady state). A hop rate γ and reversal rate

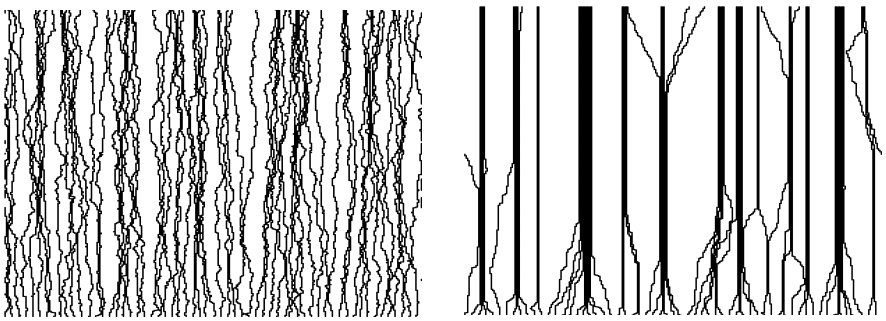

Figure 2.13 *(This plot appears in [75].)Space-time plots (time in the vertical direction) of 60 hard-core particles undergoing symmetric random walks (left) and run-and-tumble motion (right) on a lattice of* 300 *sites. The initial condition and the particle hop rate is the same in both cases. In the run-and-tumble dynamics,* $\omega = 0.01$*. The clustering of particles induced by the nonequilibrium run-and-tumble dynamics is clearly evident (see also [74, 88]).*

$\tilde{\omega}$ is set.

At each time step, a single particle is chosen at random. A random number generator is then used to assign whether the particle should attempt a hop or a tumble, with probability $\gamma/(\gamma+\tilde{\omega})$ for a hop and $\tilde{\omega}/(\gamma+\tilde{\omega})$ for a velocity reversal.

If a tumble is selected, the chosen particle changes its velocity (note that if a tumble is selected no time elapses as the tumbles are instantaneous, therefore the number of time steps equals the number of hops attempted). After a particle tumbles, the new configuration is recorded. This then marks the end of one iteration. A new iteration begins when a particle is randomly selected (it may be the same particle chosen previously) and its action chosen as before.

If a hop is selected, the chosen particle attempts a hop in the direction of its velocity according to the exclusion boundary conditions. If the exclusion interaction is triggered (another particle occupies the target site according to periodic boundary conditions), the hop fails and the particle stays on its current site. Whether the hop was successfully executed or not, the configuration is recorded and a new time step then begins. The simulation is iterated until a steady-state is reached.

Finally, we note that although the model is in continuous time this simulation is in discrete time. In a continuous time model, the joint probability that two events, such as hopping, occur simultaneously is zero. This is required due to the exclusion dynamics: if two particles are approaching one another one site apart and hopped simultaneously there would be an ambiguity in which executed

the hop successfully as they are not allowed to occupy the same site. In this simulation, the ambiguity is avoided by only picking one particle at each iteration with the time defined by the total number of hops attempted. This corresponds to hop and reversal rates that are exponentially distributed in time for each particle as they occur at a fixed rate with an interval defined by the number of hops between the last time that action (hop or reversal) was taken by that particle.

The results in Figure 2.13 are striking: breaking detailed balance by introducing run-and-tumble dynamics causes an inhomogeneous steady state with multiple clusters to appear. We see that the clusters reach a self-limiting size, but note that this is a one-dimensional phenomenon as clusters tend to coarsen in higher dimensions [88]. Similar simulation results have been found in [74] for the same interacting interacting run-and-tumble model with many particles. They also observed clustering behaviour in an extension to the model to two dimensions [74]. The findings in this chapter suggest that, at least in one dimension, the jamming and attraction of pairs of particles may be responsible for this clustering effect.

2.7 Concluding remarks

Generating function methods were used to find an exact expression for the steady-state probability distribution of this pair of run-and-tumble particles, which can then be interpreted as an effective pair potential: an emergent interaction deriving directly from the nonequilibrium dynamics. This interaction comprises a jammed component in which the particles are facing each other on neighbouring lattice sites, an attractive component characterised by an exponential decay over a finite separation length and an extended component in which all microscopic configurations are equally likely. The attraction between the particles is sufficiently strong that even in the scaling limit where continuous space is recovered, the two walkers spend a finite fraction of time in a jammed configuration.

We can conclude that the interacting nonequilibrium dynamics generate emergent interactions between run-and-tumble random walkers, and propose that this is the genesis of the clustering behaviour observed in many-particle systems. Furthermore, the exact solution of the probability distribution allows us to identify that the emergent attraction relates directly to the collisions between

the particles that break detailed balance.

The significance of the emergent attractions identified in this simple model can be partly determined by investigating the effect, if any, of adding more realistic features of bacterial dynamics on the effective interactions. In the next chapter, we extend the model by explicitly incorporating such an additional feature: finite tumble duration.

Chapter 3

Extending the generating-function approach to incorporate finite tumbling duration

In the previous chapter, the persistent random walker model was extended to include inter-particle exclusion, and we found that an effective attraction emerges between these otherwise repulsive particles. However, several idealisations were made, detailed in section 2.1. An approximation that may seem particularly severe is the modelling of tumbling as instantaneous. Clearly this is unphysical: the duration of tumbling must be finite. The instant tumbling idealisation was motivated by the fact that on average *E. coli* spend much less time tumbling ($\sim$0.1s) than they spend running ($\sim$1s), as we saw in section 1.2. Therefore it is not immediately clear that the inclusion of finite tumbling duration would make the behaviour of the model meaningfully closer to that of real run-and-tumble *E. coli*. In this chapter we will examine whether the instantaneous tumbling simplification is warranted by addressing the question: does the inclusion of a finite tumbling duration change the physics of the model?

We shall see that the inclusion of a Poisson-distributed tumble duration in the model of chapter 2 leads to a new interaction manifesting as an extra term the steady-state distribution of the interacting run-and-tumble system. As in chapter 2, we find the steady-state distribution exactly, which enables elucidation of the mechanisms behind this new emergent interaction.

This chapter is structured as follows. I define the model in section 3.1, and then summarise the exact solution in sections 3.2 and 3.3. I set out the derivation of these results in detail in sections 3.4–3.7, beginning with a master equation approach, similar to that of the previous chapter. After transformation to a system of generating functions, this leads to a matrix equation for the steady-state generating functions. I show how to solve this matrix equation and invert the generating functions using a generalisation of the method in Chapter 2. Finally, I determine the exact off-lattice steady state distribution in the limit where continuous space and time is recovered.

3.1 Definition of the interacting run-and-tumble model with finite tumbling duration

As in chapter 2, we consider two particles moving under stochastic dynamics on a periodic one-dimensional lattice of L sites. However, now each particle has one of three internal velocity states, $\sigma_i = 0, +1, -1$. A value $\sigma = \pm 1$ (hereafter denoted simply $+$ or $-$) indicates a direction of motion to right or left respectively; a value $\sigma_i = 0$ indicates that the particle is in a tumbling state and remains stationary on its site.

As for the model with instant tumbling, translational invariance means a microscopic configuration is fully specified by $1 \leq n < L$, the distance between the two particles in units of the lattice spacing, and the two particle velocities, σ_1 and

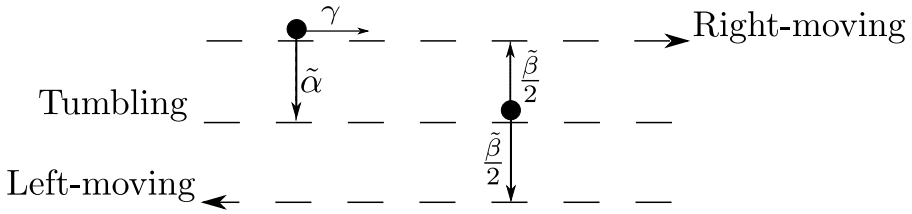

Figure 3.1 *Microscopic update schematic for the finite tumbling model: this diagram shows an example configuration of the model, with the particle moving to the right depicted on the upper row, and the particle tumbling shown on the middle row. The right-moving particle hops to the right with rate γ^- and tumbles with rate $\tilde{\alpha}$, where it would then remain stationary on its site and be depicted on the middle row. The tumbling particle can exit tumbling to have either orientation, with rate $\beta/2$ for each one.*

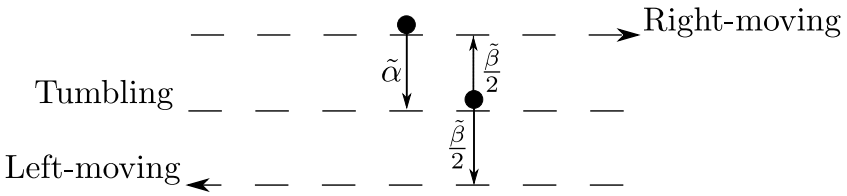

Figure 3.2 *Microscopic update schematic for a blocked tumbling configuration: this diagram shows an example configuration of the model, with one particle moving to the right depicted on the upper row, and an adjacent particle tumbling, depicted on the middle row. The right-moving particle tries to hop to the right with rate γ^-, but is unable to do so while the tumbling particle is adjacent, The right-moving particle can tumble, however, with rate $\tilde{\alpha}$.*

σ_2. A right-moving particle hops one site to the right with rate γ; likewise, a left-moving particle hops with rate γ to the left. When the target site is occupied by another particle, hopping is not allowed: this implements the hard-core exclusion interaction.

When a particle enters a tumbling state $\sigma_i = 0$, the particle stops hopping and remains stationary on its site. The run lengths and tumble durations are both Poisson-distributed, with rate parameters $\tilde{\alpha}$ and $\tilde{\beta}$ respectively: the particle enters the tumbling state from a running state with rate $\tilde{\alpha}$ and re-enters a running state from the tumbling state with rate $\tilde{\beta}$. As section 1.2 details, this is a current best-guess of the real distributions for *E. coli*. In the following we shall consider scaled tumbling rates defined as $\alpha = \tilde{\alpha}/\gamma$ and $\beta = \tilde{\beta}/\gamma$, i.e., the bare rates rescaled by the particle hopping rate γ. Figures 3.1 and 3.2 show the model dynamics.

3.2 Jamming and unjamming dynamics in the steady state

The steady-state probability distribution of this model will be derived in the sections 3.4—3.7 using the kernel method familiar from the derivation in section 2.4. However, given the inclusion of finite tumbling duration in the model in this chapter, the derivation is significantly more involved. Therefore, following [112], I outline the results first here, where I will also describe the physical mechanism that generates the stationary probability distribution.

The interacting run-and-tumble system with finite tumbling duration has the

stationary probability distribution

$$P_{\sigma_1\sigma_2}(n) = a_{\sigma_1\sigma_2}(1) + a_{\sigma_1\sigma_2}(z_+)z_+^{-n+1} + a_{\sigma_1\sigma_2}(1/z_+)z_+^{n-1} + a_{\sigma_1\sigma_2}(z_-)z_-^{-n+1} + a_{\sigma_1\sigma_2}(1/z_-)z_-^{n-1} + w^{(0)}_{\sigma_1\sigma_2}\delta_{n,1} + w^{(1)}_{\sigma_1\sigma_2}\delta_{n,L-1}\ , \quad (3.1)$$

where the amplitudes $a_{\sigma_1\sigma_2}(z)$, $w^{(0)}_{\sigma_1\sigma_2}$ and $w^{(1)}_{\sigma_1\sigma_2}$, the factors z_+ and z_- are functions of the model parameters α, β and L and $\delta_{n,m}$ is the Kronecker delta symbol. We note that z_+ and z_- are implicitly defined in (3.44) and (3.45). In stark contrast with the single parameter z in Eq. (2.64) for the instant tumbling model, the full expressions for z_+ and z_- are cumbersome, and are handled using a computational algebra engine in the derivation later in this chapter. Therefore we leave their full written to Appendix A.

The distribution in Eq. (3.1) comprises a constant part and terms that vary exponentially with the particle separation n with further contributions in states where the two particles are next to each other ($n = 1$ or $n = L - 1$). Thus it already presents strong similarities to the distribution in chapter 2, although we have noted that there are two parameters, z_+ and z_-, each with associated the exponential terms, as opposed to the single parameter z in the instant tumbling model. Of course, there are also many more configurations than in the previous chapter due to the tumbling state 0. Nevertheless, the similarities suggest that we may draw on the insight of the limiting cases for the probability distribution of the instant tumbling model in section 2.5, where we found that the behaviour of the model was principally determined by the dynamics of jamming and unjamming of the particles.

We first consider how particles jam. In the following description it may be of use to refer to Figure 3.3, which shows a realisation of the model dynamics with examples of the major dynamical events, including jamming. Jamming occurs where neither particle can hop freely until one of them changes orientation. This occurs when two particles with equal and opposite velocities collide so that the two particles are on neighbouring sites in either the $(+-, n = 1)$ configuration or its symmetrically related counterpart $(-+, n = L - 1)$. Furthermore, the system cannot change its configuration until one particle starts tumbling. This waiting time is reflected by a delta symbol in the probability of these jammed configurations i.e. $w^{(0)}_{+-}$ is nonzero in $P_{+-}(1)$, and $w^{(1)}_{-+}$ is nonzero in $P_{-+}(L-1)$. Thus this δ-function appears for the same reason as the δ-function in Eq. (2.76) in subsection 2.4.3 for the model with instant tumbling.

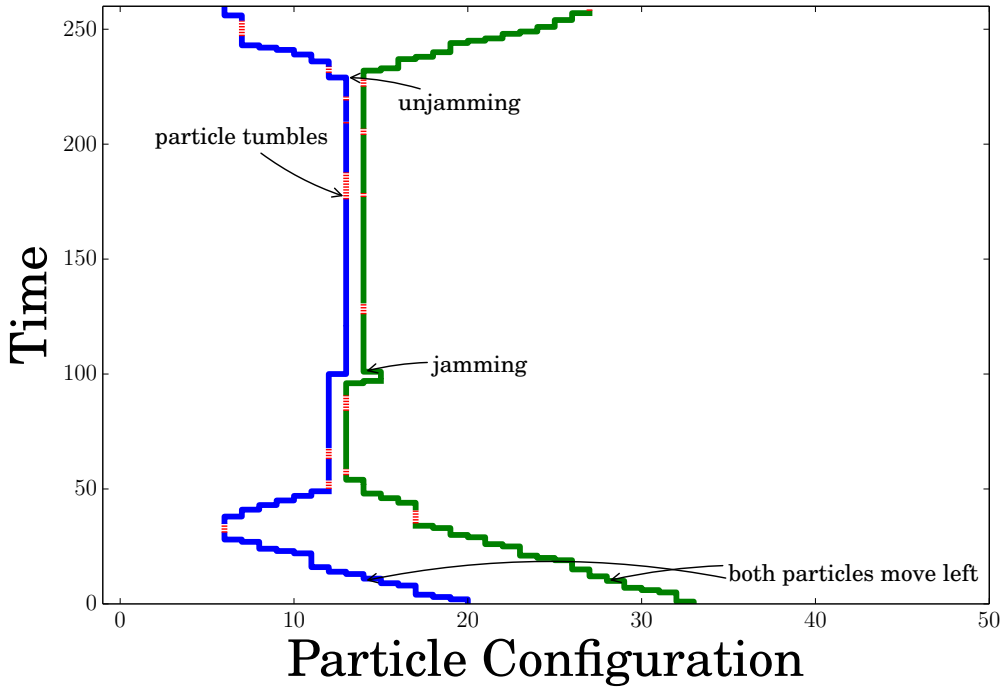

Figure 3.3 *Spatiotemporal plot, with time on the y axis, of a simulation of the lattice-based model with $\alpha = 0.1$, $\beta = 0.9$ and $L = 50$. Each line represents a trajectory of the particle, where particles in the tumbling state are represented by dashed lines.*

Eventually the system enters a jammed configuration of type $(+0, n = 1)$ or one of the symmetric counterparts, in which one of the two particles involved in the collision has begun tumbling. These configurations therefore also each contain a delta symbol in their probabilities. In addition, there is an enhanced probability of entering the $(00, n = 1)$ state in which both adjacent particles are tumbling from these jammed tumbling configurations, which in turn generates delta symbols in $P_{00}(1)$, so that $w_{00}^{(0)}$ and $w_{00}^{(1)}$ are non zero. As these tumbling configurations have no counterpart in the instant tumbling model, these features are completely new. We note that $w_{++}^{(0,1)}$ and $w_{--}^{(0,1)}$ are each zero, as there are no delta-symbol contributions to the probabilities in these velocity sectors.

The second part of the interaction involves unjamming. Particles unjam by leaving a jammed tumbling configuration; that is when the tumbling particle exits tumbling with an orientation different from the one it had on collision. At this point both particles move in the same direction. Due to the stochasticity of the hopping between lattice sites, some broadening of the separation between the two particles will occur, even though they started off next to each other. This broadening generates a spatially decaying component in the probability with

exponential decay length scale $\xi_+ = 1/\ln z_+(\alpha, \beta)$ (analogous to ξ in Eq. (2.79) in subsection 2.4.4), that is a function of the tumbling rates α and β, and is apparent in *all* the velocity sectors.

Finally, we consider what happens when one of the particles enters a tumbling state now that the particles are separated and freely moving in the same direction. The result is a configuration where one particle is stationary and tumbling and the other is hopping freely. The freely moving particle either hops towards or away from the tumbling particle. This contribution to the stationary probability distribution is characterised by an exponential decay, but with a new emergent length scale $\xi_- = 1/\ln z_-(\alpha, \beta)$ for which there is no equivalent in the instant tumbling model. Thus, by considering the dynamics of jamming and unjamming, we have built a heuristic picture of the different microscopic mechanisms that lead to the emergent interactions manifest in the distribution Eq. (3.1).

3.3 Lengthscales in the steady-state scaling limit

We noted in the introduction and in chapter 2 that a lattice-based model is an approximation to the real-world swimming in continuous space and time of run-and-tumble *E. coli*. In section 2.5 we took a scaling limit of the probability distribution that recovered the continuum dynamics for the instant tumbling model. Here we do the same for the finite tumbling model. It is of particular interest as we already know that the crucial parameter z from the previous chapter now has two counterparts, z_+ and z_-. Whether they behave differently to z in the scaling limit will reflect on whether finite tumbling is likely to be significant to the dynamics of real run-and-tumble bacteria, or whether the instant tumbling approximation is sufficient to capture the physics.

In order to recover continuum dynamics, we take the lattice spacing as ℓ/L where ℓ is the physical system size and let $L \to \infty$. In order to keep the physical velocity

$$v = \gamma \frac{\ell}{L} \tag{3.2}$$

invariant we also scale the hopping rate γ with system size

$$\gamma = L/\ell \, . \tag{3.3}$$

Then $v = 1$ and the scaled tumbling rates (ratio of bare tumbling rates to hopping

rates) scale as $1/L$:

$$\alpha = \frac{\tilde{\alpha}}{\gamma} = \frac{\phi}{L} \qquad \beta = \frac{\tilde{\beta}}{\gamma} = \frac{\theta}{L} \tag{3.4}$$

where $\phi = \ell\tilde{\alpha}$ and $\theta = \ell\tilde{\beta}$ are dimensionless constants. Thus in this scaling limit the particles undergo ballistic motion with velocity $v = 1$ interrupted by collision events and stochastic tumbles.

In the scaling limit, the steady-state probabilities of walkers at a separation y have the following form:

$$P_{++}(y) = a_{++} + b_{++}[\delta(y) + \delta(\ell - y)] + c_{++}[e^{-y/\kappa} + e^{-(\ell-y)/\kappa}] \tag{3.5}$$
$$P_{+-}(y) = a_{+-} + c_{+-}^{(0)} e^{-y/\kappa} + c_{+-}^{(1)} e^{-(\ell-y)/\kappa} + w_{+-}\delta(y) \tag{3.6}$$
$$P_{+0}(y) = a_{+0} + c_{+0}^{(0)} e^{-y/\kappa} + c_{+0}^{(1)} e^{-(\ell-y)/\kappa} + w_{+0}\delta(y) \tag{3.7}$$
$$P_{00}(y) = a_{00} + c_{00}[e^{-y/\kappa} + e^{-(\ell-y)/\kappa}] + w_{00}[\delta(y) + \delta(\ell - y)] \tag{3.8}$$

where the length scale κ is given by

$$\kappa = \ell \left(\frac{2}{(\theta + \phi)(\theta + 2\phi)} \right)^{1/2} . \tag{3.9}$$

The amplitudes $a_{\sigma_1\sigma_2}$, $b_{\sigma_1\sigma_2}$ and $c_{\sigma_1\sigma_2}$ derive from the amplitudes $a_{\sigma_1\sigma_2}(z)$ that appear in (3.1). They are functions of the dimensionless parameters θ and ϕ, and are specified explicitly in section 3.7. Superscripts appear where these amplitudes are different at separation $y = 0$ and $y = \ell$. Note that due to the decision to set $v = 1$, the magnitude of the velocity does not appear in this equation.

In equations (3.5)—(3.8) the terms containing z_+ to some power have become delta functions. This behaviour is familiar from equations (2.84) and (2.85) in section 2.5 for the instant tumbling model. We saw that the origin of this vanishing lengthscale lies in the fact that the runs are no longer described by stochastic hops, which in the lattice model leads to broadening of the particle separation in turn generating an exponential decay. The same reasoning holds for the vanishing of the lengthscale in the finite tumbling case here.

The second length scale $1/\ln z_-$ is of particular interest because it is completely new and we now see that it remains finite and present in all velocity sectors in

the scaling limit. This results in a decay length given by

$$\kappa = \frac{\ell}{L}\frac{1}{\ln z_-}. \tag{3.10}$$

To understand the persistence of this lengthscale in the scaling limit, we recall the fact that the tumble duration—and hence, distance travelled by a moving particle when the other particle is tumbling—remains finite in this limit compared to other diffusive lengthscale that disappears in the scaling limit.

We now derive the results of sections 3.2 and 3.3.

3.4 Master equations and generating function matrix equation

The derivation of the stationary probability distribution of the finite tumbling model requires transformation of the master equation into a system of generating function equations followed by inversion. The transformation into generating function equations uses exactly the same procedure as in subsection 2.4.1. However, as there are more velocity sectors this model, we will review the additional symmetries present compared to those in equations (2.32) and (2.33) for the instant tumbling model. We shall then see explicitly how to construct the master equation for the ++ sector in the finite tumbling model.

The configurations of the finite tumbling model are specified in terms of the two particle velocities, $\sigma_1\sigma_2$, where $\sigma_i = \{+1, 0, -1\}$, and the particle separation n. There are nine velocity sectors: $P_{++}(n)$, $P_{+-}(n)$, $P_{-+}(n)$, $P_{--}(n)$, $P_{0+}(n)$, $P_{+0}(n)$, $P_{0-}(n)$, $P_{-0}(n)$, and $P_{00}(n)$. The symmetry relations between the states due to the periodic boundary conditions and direction-inversion symmetry are as follows:

$$P_{++}(n) = P_{--}(n), \tag{3.11}$$
$$P_{+0}(n) = P_{0-}(n), \tag{3.12}$$
$$P_{0+}(n) = P_{-0}(n), \tag{3.13}$$
$$P_{+-}(n) = P_{-+}(L-n), \tag{3.14}$$
$$P_{+0}(n) = P_{0+}(L-n), \tag{3.15}$$
$$P_{-0}(n) = P_{0-}(L-n). \tag{3.16}$$

As can be seen from these symmetry relations, only the $(++)$, $(+-)$, $(-+)$, $(0+)$, $(+0)$, and (00) sectors are independent.

We now explicitly construct the master equation for $\dot{P}_{++}(n)$. The positive contributions to $\dot{P}_{++}(n)$ come from those configurations that can hop, at rate γ, into $P_{++}(n)$ or leave a tumbling configuration (at rate $\tilde{\beta}$) with a + orientation into P_{++}—this will occur on average half of the time, with the other half going into P_{+-} or P_{-+}. Together these contribute the terms

$$\gamma[P_{++}(n-1)I_{n>1} + P_{++}(n+1)I_{L-n>1}] + \frac{\tilde{\beta}}{2}[P_{0+}(n) + P_{+0}(n)] \tag{3.17}$$

where, as for the instant tumbling master equation, the indicator $I_{k>1} = 1$ if $k > 1$ and is zero otherwise. This reflects the fact that the configuration $(++, n = 1)$ cannot have its distance reduced. Turning to the loss terms, these are made up of hopping out of $P_{++}(n)$ at rate γ, or entering a tumbling configuration at rate α for each particle. The loss terms come to

$$P_{++}(n)[\gamma I_{n>1} + \gamma I_{L-n>1} + 2\tilde{\alpha}] \tag{3.18}$$

where $I_{k>1} = 1$ stops extra terms from being counted where hopping out of the configuration is blocked by the exclusion interaction. This completes the construction of the probability gain-loss terms for $\dot{P}_{++}(n)$, which is

$$\begin{aligned}\gamma^{-1}\dot{P}_{++}(n) = {} & P_{++}(n-1)I_{n>1} + P_{++}(n+1)I_{L-n>1} + \frac{\beta}{2}[P_{0+}(n) + P_{+0}(n)] \\ & - P_{++}(n)[I_{n>1} + I_{L-n>1} + 2\alpha]\end{aligned} \tag{3.19}$$

The remaining equations for this system, which can be constructed in the same way as $\dot{P}_{++}(n)$ (recalling that $\alpha = \tilde{\alpha}/\gamma$ and $\beta = \tilde{\beta}/\gamma$ are scaled rates), are

$$\begin{aligned}\gamma^{-1}\dot{P}_{+-}(n) = {} & 2P_{+-}(n+1)I_{L-n>1} + \frac{\beta}{2}[P_{0-}(n) + P_{+0}(n)] \\ & - P_{+-}(n)[2I_{n>1} + 2\alpha]\end{aligned} \tag{3.20}$$

$$\begin{aligned}\gamma^{-1}\dot{P}_{-+}(n) = {} & 2P_{-+}(n-1)I_{n>1} + \frac{\beta}{2}[P_{0+}(n) + P_{-0}(n)] \\ & - P_{-+}(n)[2I_{L-n>1} + 2\alpha]\end{aligned} \tag{3.21}$$

$$\begin{aligned}\gamma^{-1}\dot{P}_{0+}(n) = {} & P_{0+}(n-1)I_{n>1} + \alpha[P_{++}(n) + P_{-+}(n)] + (\beta/2)P_{00}(n) \\ & - P_{0+}(n)\left[I_{L-n>1} + \alpha + \beta\right]\end{aligned} \tag{3.22}$$

$$\gamma^{-1}\dot{P}_{+0}(n) = P_{+0}(n+1)I_{L-n>1} + \alpha[P_{++}(n) + P_{+-}(n)] + (\beta/2)P_{00}(n) - P_{+0}(n)\left[I_{n>1} + \alpha + \beta\right] \tag{3.23}$$

$$\gamma^{-1}\dot{P}_{00}(n) = \alpha[P_{+0}(n) + P_{0+}(n) + P_{-0}(n) + P_{0-}(n)] - 2\beta P_{00}(n). \tag{3.24}$$

Following an analogous approach to the method in the previous chapter, we introduce the generating functions

$$G_{\sigma_1\sigma_2}(x) = \sum_{n=1}^{L-1} x^n P_{\sigma_1\sigma_2}(n) \tag{3.25}$$

and transform the master equations (3.19)—(3.24) into a system of equations for $G_{\sigma_1\sigma_2}(x)$. The aim is exactly as it was in the previous chapter: to remove from the generating function equation for $G_{++}(x)$ all explicit dependence on any $P_{\sigma_1\sigma_2}(n)$.

The generating function equations are as follows:

$$\gamma^{-1}\dot{G}_{++}(x) = [x + x^{-1} - 2(1+\alpha)]G_{++}(x) + \frac{\beta}{2}[G_{0+}(x) + G_{+0}(x)] + (x-1)(1-x^{L-1})P_{++}(1) \tag{3.26}$$

$$\gamma^{-1}\dot{G}_{+-}(x) = [2x^{-1} - (2+2\alpha)]G_{+-}(x) - [2P_{+-}(1) - 2xP_{+-}(1)] + \frac{\beta}{2}[G_{0-}(x) + G_{+0}(x)] \tag{3.27}$$

$$\gamma^{-1}\dot{G}_{-+}(x) = [2x - (2+2\alpha)]G_{-+}(x) - 2[x^L P_{-+}(L-1) - x^{L-1}P_{-+}(L-1)] + \frac{\beta}{2}[G_{0+}(x) + G_{-0}(x)] \tag{3.28}$$

$$\gamma^{-1}\dot{G}_{0+}(x) = [x - (1+\alpha+\beta)]G_{0+}(x) - [x^L P_{0_+}(L-1) - x^{L-1}P_{0_+}(L-1)] + \alpha[G_{++}(x) + G_{-+}(x)] + (\beta/2)G_{00}(x) \tag{3.29}$$

$$\gamma^{-1}\dot{G}_{+0}(x) = [x^{-1} - (1+\alpha+\beta)]G_{+0}(x) - (1-x)P_{+0}(1) + \alpha[G_{++}(x) + G_{+-}(x)] + (\beta/2)G_{00}(x) \tag{3.30}$$

$$\gamma^{-1}\dot{G}_{00}(x) = \alpha[G_{+0}(x) + G_{0+}(x) + G_{-0}(x) + G_{0-}(x)] - 2\beta G_{00}(x). \tag{3.31}$$

We can close the system by making use of the symmetries $G_{0+}(x) = G_{-0}(x)$ and $G_{+0}(x) = G_{0-}(x)$. Similarly, the number of undetermined constants, such as $P_{+-}(1)$ and $P_{-+}(L-1)$, that appear on the right-hand side can be reduced to

just three, namely $P_{++}(1)$, $P_{+-}(1)$ and $P_{+0}(1)$, by using the symmetries

$$P_{++}(L-1) = P_{++}(1), \tag{3.32}$$

$$P_{-+}(L-1) = P_{+-}(1) \text{ and} \tag{3.33}$$

$$P_{0+}(L-1) = P_{+0}(1). \tag{3.34}$$

As before, we can write this system of equations as a matrix equation in which all the generating functions appear on one side, and all the boundary conditions on the other side. This reads

$$A(x)\underline{G}(x) = (1-x)\underline{b}(x) \tag{3.35}$$

where

$$A(x) = \begin{pmatrix} \mu(x)+\nu(x) & 0 & 0 & \beta/2 & \beta/2 & 0 \\ 0 & \nu(x) & 0 & 0 & \beta/2 & 0 \\ 0 & 0 & \mu(x) & \beta/2 & 0 & 0 \\ \alpha & 0 & \alpha & \mu(x)-\beta & 0 & \beta/2 \\ \alpha & \alpha & 0 & 0 & \nu(x)-\beta & \beta/2 \\ 0 & 0 & 0 & \alpha & \alpha & -\beta \end{pmatrix}, \tag{3.36}$$

$$\underline{G}(x) = \begin{pmatrix} G_{++}(x) \\ G_{+-}(x) \\ G_{-+}(x) \\ G_{0+}(x) \\ G_{+0}(x) \\ G_{00}(x) \end{pmatrix}, \qquad \underline{b}(x) = \begin{pmatrix} (1-x^{L-1})P_{++}(1) \\ P_{+-}(1) \\ -x^{L-1}P_{+-}(1) \\ -x^{L-1}P_{+0}(1) \\ P_{+0}(1) \\ 0 \end{pmatrix}, \tag{3.37}$$

where, restating equations (2.45) and (2.46), μ and ν are given by

$$\mu(x) = x - (1+\alpha) \quad \text{and} \quad \nu(x) = x^{-1} - (1+\alpha) = \mu(x^{-1}). \tag{3.38}$$

3.5 Inversion: a power counting strategy

In section 2.4 we inverted the generating functions by explicitly using the inverse matrix describing the system of generating functions in the sense:

$$\underline{G}(x) = (1-x)A^{-1}(x)\underline{b}(x). \tag{3.39}$$

However, the inverse of matrix (3.36) is rather unwieldy due to the extra terms involving β. Therefore we will not pursue the same approach used in chapter 2 here. Instead we will work directly with matrix (3.36), and, using linear algebra to determine features of its inverse, solve Eq. (3.35) to find Eq. (3.1) without explicitly introducing $A^{-1}(x)$. However, explicit versions of elements of $A^{-1}(x)$ will be required to recover the results for the scaling limit in section 3.3. These are detailed in Appendix B.

As before, the aim is to write the generating functions $G_{\sigma_1\sigma_2}(x)$ in a form which allows the probabilities to be read off as coefficients of a power series in x. Using the results in subsection 2.4.1 as a guide, we expect the final form of these generating functions to be

$$G_{\sigma_1\sigma_2}(x) = \sum_{\rho}\left[\frac{xM_{\sigma_1\sigma_2,\rho}}{(1-x/z_\rho)}\right] + w^{(0)}_{\sigma_1\sigma_2}x + w^{(1)}_{\sigma_1\sigma_2}x^{L-1} + H_{\sigma_1\sigma_2}(x), \tag{3.40}$$

where $M_{\sigma_1\sigma_2,\rho}$ and $w_{\sigma_1\sigma_2}$ are functions of the model parameters α, β and L (but independent of x), $H_{\sigma_1\sigma_2}(x)$ are polynomials of order greater than x^{L-1}, and ρ labels the roots z_ρ of the determinant of the matrix A.

The stationary probabilities can be read off immediately as the coefficients of x^n by rewriting each fraction $\frac{xM_{\sigma_1\sigma_2,\rho}}{(1-x/z_\rho)}$ in (3.40) as a geometric series $\sum_{n=1}^{L-1}[\sum_\rho M_{\sigma_1\sigma_2,\rho}z_\rho^{-n+1}x^n] + O(x^L)$. This leaves a probability distribution of the form in (3.1):

$$P_{\sigma_1\sigma_2}(n) = \sum_{\rho} M_{\sigma_1\sigma_2,\rho}z_\rho^{-n+1} + w^{(0)}_{\sigma_1\sigma_2}\delta_{n,1} + w^{(1)}_{\sigma_1\sigma_2}\delta_{L-1,1}\ , \tag{3.41}$$

since terms of order greater than x^{L-1} in (3.40) do not contribute to the probability distribution: the separation n only goes up to $L-1$. In fact, all terms of degree greater than x^{L-1} will cancel out as the generating functions (3.25) do not contain terms beyond that order.

In order to obtain the form (3.40) for $G_{\sigma_1\sigma_2}(x)$, we first re-write (3.39) in terms of the adjugate of A (which is defined as the transpose of the cofactor matrix), the determinant of A and the vector $\underline{b}$ as follows

$$G_{\sigma_1\sigma_2}(x) = (1-x)\sum_{j=1}^{6} A^{-1}_{\sigma_1\sigma_2,j}(x)b_j(x) = (1-x)\frac{\sum_j \mathrm{adj}A_{\sigma_1\sigma_2,j}(x)b_j(x)}{\det A(x)}, \quad (3.42)$$

where the $\sigma_1\sigma_2$ subscript of A^{-1} indicates the row of A^{-1} that corresponds to that generating function, e.g. $++$ corresponds to the first row of A^{-1}; j is the column number of A^{-1}, and adj$A$ is the adjugate of A. We shall see that the introduction of the adjugate matrix into Eq. (3.42) will allow us to write the generating function in the form (3.40) without explicitly finding the inverse matrix A^{-1}. This is because the numerator in Eq. (3.42) plays the role of the kernel in the derivation here, where as in the equivalent equation (2.48) in section 2.4 the kernel was taken directly from the inverse matrix.

3.5.1 The determinant as a rational function

We recall that in the kernel method, the numerator must cancel poles in the denominator. Therefore we now turn to the denominator of Eq. (3.42), which is the determinant of the matrix A, $\det A(x)$. Although this is not easily found by hand, it is nevertheless readily derived using a computational algebra engine such as *Mathematica*. Explicitly, an expression for $\det A(x)$ is

$$\begin{aligned}
\det A(x) = \; & - \frac{\beta(2+\alpha)(x-1)^2}{4x^3}\Big\{ \\
& \quad 2(1+\alpha+\beta) \\
& + \left[\alpha\beta - 2(\alpha+\beta)(3\alpha+\beta) - 4(3\alpha+2\beta+2)\right]x \\
& + 2\left[(\alpha+\beta)\left(2\alpha^2+\alpha\beta+6\alpha+2\beta\right) + (\alpha-6)(10-\beta) + 66\right]x^2 \\
& + \left[\alpha\beta - 2(\alpha+\beta)(3\alpha+\beta) - 4(3\alpha+2\beta+2)\right]x^3 \\
& + 2(1+\alpha+\beta)x^4\Big\}\,.
\end{aligned} \quad (3.43)$$

To find the poles of the determinant, we note that (3.43), can be written as the following polynomial fraction

$$\frac{\det A(x)}{1-x} = \frac{k}{x^3}q(x) \quad (3.44)$$

where

$$q(x) \equiv (x-1)(x-z_+)(x-1/z_+)(x-z_-)(x-1/z_-), \tag{3.45}$$

and

$$k = \frac{\beta}{2}(2+\alpha)(1+\alpha+\beta) \tag{3.46}$$

is a constant. In expression (3.45), z_+ and z_- are independent roots of the determinant, and $1/z_+$ and $1/z_-$ are their inverses (note that they are written out explicitly in Appendix A). There is also a root at $z = 1$. These roots are the poles we are looking for. We can now see how this derivation is leading to the result in Eq. (3.1): these are the five roots z_ρ that appear in (3.40). Explicitly: $z_0 = 1$, $z_1 = z_+$, $z_2 = 1/z_+$, $z_3 = z_-$ and $z_4 = 1/z_-$.

That this factorisation of the determinant holds can be seen from (3.43), where the term in braces is a symmetric quartic polynomial in which the coefficient of the leading term is $2(1+\alpha+\beta)$. The roots come in these reciprocal pairs due to the symmetry of this polynomial.

3.5.2 The generating function as a sum of rational functions

In subsection 2.4.3 we applied pole cancellation at this stage of the calculation, imposing that the kernel (the numerator of the generating function) in Eq. (2.49) vanished at the poles, yielding Eq. (2.50). Here, we change the order of the derivation slightly, and first separate out those terms that are greater than order x^{L-1}, which must ultimately vanish as the generating functions are only defined up to this order. These terms vanish because they are cancelled by other terms that will come from the inversion of the denominator after partial fraction decomposition has taken place. This is the same in principle to the procedure undertaken at the start of subsection 2.4.3.

We first substitute $\det A$ as a polynomial fraction (3.44, 3.45), into (3.42), which gives

$$\begin{aligned} G_{\sigma_1\sigma_2} &= \frac{-x^3(1-x)\sum_j \mathrm{adj}A_{\sigma_1\sigma_2,j}(x)b_j(x)}{k(x-1)^2(x-z_+)(x-1/z_+)(x-z_-)(x-1/z_-)} \\ &= \frac{x^3\sum_j \mathrm{adj}A_{\sigma_1\sigma_2,j}(x)b_j(x)}{kq(x)}. \end{aligned} \tag{3.47}$$

We may then separate terms in $G_{\sigma_1\sigma_2}(x)$ as follows

$$G_{\sigma_1\sigma_2} = \frac{x^3 \sum_j \mathrm{adj} A_{\sigma_1\sigma_2,j}(x) b_j(x)}{kq(x)} = \frac{xp_{\sigma_1\sigma_2}(x)}{q(x)} + \frac{\tilde{H}_{\sigma_1\sigma_2}(x)}{q(x)}, \tag{3.48}$$

where each combination $xp_{\sigma_1\sigma_2}(x)$ is a polynomial of degree less than x^L and $\tilde{H}_{\sigma_1\sigma_2}(x)$ is a polynomial with a lowest order term x^L. Thus $xp_{\sigma_1\sigma_2}(x)$ contains all the terms of $x^3 \sum_j \mathrm{adj} A_{\sigma_1\sigma_2,j}(x) b_j(x)$ with degree less than L.

Now that we have separated out those terms that do not contribute to the generating function, we seek to re-write the contributing terms in the form in Eq. (3.40). This requires individual terms to be over a linear expression $1 - x/z_\rho$. In subsection 2.4.3 this was achieved through partial fraction decomposition. We shall do the same in this chapter. However, we must first convince ourselves that the terms in Eq. (3.48), excepting H, are indeed amenable to partial fraction decomposition. This will be the case if $p_{\sigma_1\sigma_2}(x)$ is of lower degree than $q(x)$; that is if $p_{\sigma_1\sigma_2}(x)$ lower order than x^5.

We shall now see that is not quite the case, but that the only terms in $xp_{\sigma_1\sigma_2}$ of order greater than x^5 are of order x^6 and x^{L-1}. This is the *power counting* part of the derivation strategy, and distinguishes it from the derivation in section 2.4. To do this, we consider those terms in $x^3 \mathrm{adj} A_{\sigma_1\sigma_2,j}(x) b_j(x)$ that are $O(x^m)$ where $5 < m < L - 1$. Cramer's rule [113] leads to the relation

$$\mathrm{adj} A_{i,j}(x) b_j(x) = \det A_i \ , \tag{3.49}$$

where A_i is the matrix formed by replacing the i-th column of A with $\underline{b}$. Then we see that $O(x^6)$ terms in $x^3 \det A_i$ must come from μ^3 terms in $\det A_i$. Likewise, the $O(x^{L-1})$ terms in $x^3 \det A_i$ must come from multiplying x^{L-1} terms in $\underline{b}$ by $\nu(x)^3$ terms in $\det A_i$. Since $\underline{b}$ only contains terms of order $O(1)$ and $O(x^{L-1})$ one can check that all other terms in $x^3 \det A_i$ are $O(x^m)$ where either $m > L - 1$ or $m < 6$.

If $p_{\sigma_1\sigma_2}(x)$ is of lower degree than $q(x)$ (i.e. lower order than x^5), then $p_{\sigma_1\sigma_2}(x)/q(x)$ will be amenable to partial fraction decomposition, but we have seen that this is not the case in general. We therefore separate each $p_{\sigma_1\sigma_2}(x)$ into those terms that will allow partial fraction decomposition, and those that will not:

$$\frac{xp_{\sigma_1\sigma_2}(x)}{q(x)} + \frac{\tilde{H}_{\sigma_1\sigma_2}(x)}{q(x)} = x\frac{J_{\sigma_1\sigma_2}(x)}{q(x)} + \frac{K_{\sigma_1\sigma_2}(x)}{q(x)} + \frac{\tilde{H}'_{\sigma_1\sigma_2}(x)}{q(x)}, \tag{3.50}$$

where $J_{\sigma_1\sigma_2}(x)$ takes terms from $p_{\sigma_1\sigma_2}(x)$ amenable to partial fraction decomposition (ie. those of order less than $q(x)$) and is therefore a polynomial of order x^4 or less, and $K_{\sigma_1\sigma_2}(x)$ takes the higher order terms from $p_{\sigma_1\sigma_2}(x)$. However, at the same time, we want an expression $K_{\sigma_1\sigma_2}(x)/q(x)$ that can be cast as a polynomial rather than a rational function so that we can read off its contribution to the probability.

We therefore define

$$K_{\sigma_1\sigma_2}(x)/q(x) \equiv w^{(0)}_{\sigma_1\sigma_2} x + w^{(1)}_{\sigma_1\sigma_2} x^{L-1}, \tag{3.51}$$

where $w^{(0)}_{\sigma_1\sigma_2}$ is equal to the ratio of the coefficient of the x^6 term in $xp_{\sigma_1\sigma_2}(x)$ with the coefficient of the x^0 term in $q(x)$ and $w^{(1)}_{\sigma_1\sigma_2}$ is equal to the ratio of the coefficient of the x^{L-1} term in $xp_{\sigma_1\sigma_2}(x)$ with the coefficient of the x^5 term in $q(x)$. In order to factorise $K_{\sigma_1\sigma_2}(x)$ by $q(x)$, we add to $K_{\sigma_1\sigma_2}(x)$ any terms required, in addition to the x^6 and x^{L-1} terms in $xp_{\sigma_1\sigma_2}(x)$ already present. If these added terms are of degree less than 5, then we subtract them from $p_{\sigma_1\sigma_2}(x)$. On the other hand, if the added terms are of degree greater than $L-1$ (recall, we have already shown that there are no further terms between x^5 and x^L), we subtract them from $\tilde{H}_{\sigma_1\sigma_2}(x)$, which in turn becomes $\tilde{H}'_{\sigma_1\sigma_2}(x)$.

We are now analogously at the point of Eq. (2.52) in subsection 2.4.3. The next stage is to implement partial fraction decomposition of Eq. (3.50).

3.5.3 Partial fraction decomposition using the 'cover up' method

We now know that the expressions $J_{\sigma_1\sigma_2}(x)$ in Eq. (3.50) are amenable to partial fraction decomposition. We find that we can immediately recover the form where expressions (in terms of only the model parameters) are over linear terms of the form $(1 - x/z_\rho)$ by using *Heaviside's cover-up* method for the partial-fraction expansion of a rational function [114] on the fraction $\frac{J_{\sigma_1\sigma_2}(x)}{q(x)}$.

The cover-up method may be used whenever the denominator of a rational fraction can be factorised into distinct linear factors. We have already seen that $q(x)$ can be written in this form, and that each $J_{\sigma_1\sigma_2}(x)$ is a polynomial, and

therefore the method can be applied to the fraction of interest, which yields

$$\begin{aligned}\frac{J_{\sigma_1\sigma_2}(x)}{q(x)} &= \frac{J_{\sigma_1\sigma_2}(x)}{(x-z_1)(x-z_2)...(x-z_n)} \\ &= \frac{J_{\sigma_1\sigma_2}(z_1)}{(z_1-z_2)...(z_1-z_n)}\cdot\frac{1}{x-z_1}+...+\frac{J_{\sigma_1\sigma_2}(z_n)}{(z_n-z_1)...(z_n-z_{n-1})}\cdot\frac{1}{x-z_n}\end{aligned} \tag{3.52}$$

where $z_1, ..., z_n$ are the roots of $q(x)$. The denominators of each fraction in the resulting decomposition are just the linear factors, as is familiar from normal partial fraction decomposition. The corresponding numerators, $J_{\sigma_1\sigma_2}(z_i)$, are found by covering up the factor $x - z_i$ in $\frac{J_{\sigma_1\sigma_2}(x)}{q(x)}$, and setting $x = z_i$ in the rest of the expression. The terms involving $J_{\sigma_1\sigma_2}$ are now in the form of $\frac{xM_{\sigma_1\sigma_2}(z_\rho)}{(1-z_\rho x)}$ of (3.40) and so straightforwardly invertible. We can ignore the expressions within $\tilde{H}'_{\sigma_1\sigma_2}(x)$ entirely as they do not contribute. We may therefore write the generating function in general as

$$G_{\sigma_1\sigma_2} = \sum_\rho \left[\frac{xJ_{\sigma_1\sigma_2}(z_\rho)}{[q(x)/(x-z_\rho)]_{|x=z_\rho}}\frac{1}{(x-z_\rho)}\right] + w^{(0)}_{\sigma_1\sigma_2}x + w^{(1)}_{\sigma_1\sigma_2}x^{L-1} + x^L\tilde{H}'_{\sigma_1\sigma_2}. \tag{3.53}$$

We then write an expression for the steady-state probabilities of the form in Eq. (3.41)

$$P_{\sigma_1\sigma_2}(n) = \sum_\rho a_{\sigma_1\sigma_2}(z_\rho)z_\rho^{-n+1} + w^{(0)}_{\sigma_1\sigma_2}\delta_{n,1} + w^{(1)}_{\sigma_1\sigma_2}\delta_{L-1,1}. \tag{3.54}$$

where

$$a_{\sigma_1\sigma_2}(z_\rho) = \frac{-J_{\sigma_1\sigma_2}(z_\rho)}{[q(x)/(x-z_\rho)]_{|x=z_{j=\rho}}}. \tag{3.55}$$

We complete the derivation of the general form of the stationary probabilities in Eq. (3.1) by briefly describing how to determine the weights $w^{(i)}_{\sigma_1\sigma_2}$ that are non-zero in their corresponding velocity sectors $\sigma_1\sigma_2$. We proceed column-by-column in A, replacing each with $\underline{b}$ (see Eq. (3.49)). Thanks to the symmetries $G_{+-}(x) = G_{-+}(L-x)$ and $G_{+0}(x) = G_{0+}(L-x)$, we are only required to solve for four generating functions $G_{++}(x), G_{+-}(x), G_{+0}(x)$ and $G_{00}(x)$.

For G_{++}, as a μ is eliminated (replaced by b_1), it is not possible to get a $O(x^6)$ term, nor a $O(x^{L-1})$ term as a ν is also eliminated. Hence all the w_{++} are zero. For $G_{+-}(x)$, we have sufficient factors of μ to get an $O(x^6)$ term but no diagonal x^{L-1} terms for $O(x^{L-1})$ terms. Therefore we have a single nonzero weight, $w^{(0)}_{+-}$.

For $G_{+0}(x)$, we get an $O(x^6)$ term only, for similar reasons and thus a single nonzero weight, $w_{+0}^{(0)}$. For G_{00} both μ^3 and ν^3 terms are possible, and so $G_{00}(x)$ can possess both $O(x^6)$ and $O(x^{L-1})$ terms and so $w_{00}^{(0)}$ and $w_{00}^{(1)}$ are nonzero.

Thus we have derived the general form of the steady-state probability of the interacting run-and-tumble system with finite tumble duration. Note that we did not require the explicit inverse matrix A^{-1}, nor did we even implement the condition that the kernel must vanish at the poles. This pole cancellation is required, however, to determine the constants in Eq. (3.37).

3.5.4 Determination of the constants

We now consider how to determine these constants $P_{++}(1), P_{+-}(1)$ and $P_{+0}(1)$. We may find two of these as yet undetermined constants by imposing the condition that the generating functions must not diverge at any x. As G_i has poles at each of the roots this condition is simply the kernel condition that implies that the numerator, $\mathrm{adj}A_{i,j}(x)\tilde{b}_j(x)$, has to cancel the determinant poles and thus must equal zero at all of the roots.

Here we must turn to the explicit expressions for $\mathrm{adj}A_{i,j}(x)$ (written out in Appendix B), which we have hitherto avoided because they are unwieldy to manipulate by hand. Instead, inputing them into a computational algebra engine, we readily find that at $x = 1$, the numerator is automatically zero. It remains to impose pole cancellation for the roots $z = z_+, 1/z_+, z_-, 1/z_-$. Although there are 24 simultaneous equations following from this condition, manipulation with a computational algebra engine leads to only two that are linearly independent. From these two simultaneous equations we can find any two of $P_{++}(1), P_{+-}(1)$ and $P_{+0}(1)$. The remaining constant is found by imposing normalisation: $\sum_{\sigma_1\sigma_2}\sum_{n=1}^{L-1} P_{\sigma_1\sigma_2}(n) = 1$.

3.6 Plot of the probability distribution and comparison with simulation

Although we have derived the general form of the steady-state probability distribution, (3.54) and (3.55), there remain a number of expressions that have not been presented explicitly in terms of the model parameters α and

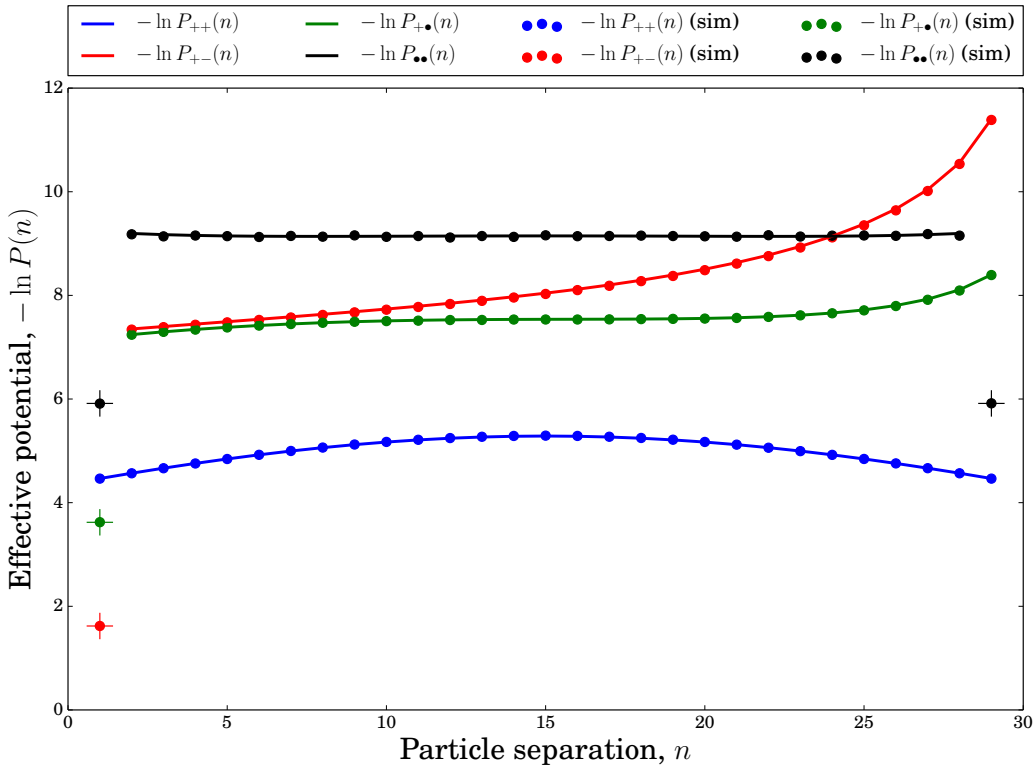

Figure 3.4 *(Reproduced from [112]) Comparison of analytic calculation of probability and simulation results for $L = 30$, $\alpha = 0.01$, $\beta = 0.1$. The crosses mark the analytic results that contain delta symbols.*

β. These are the roots $z_\rho = z_\rho[\alpha, \beta]$, the weights $w_{\sigma_1\sigma_2} = w_{\sigma_1\sigma_2}[\alpha, \beta]$, the amplitudes $a_{\sigma_1\sigma_2}(z_\rho) = a_{\sigma_1\sigma_2}(z_\rho)[\alpha, \beta]$, and the constants $P_{++}(1) = P_{++}(1)[\alpha, \beta]$, $P_{+-}(1) = P_{+-}(1)[\alpha, \beta]$ and $P_{+0}(1) = P_{+0}(1)[\alpha, \beta]$.

It is possible to find these expressions explicitly, but due to their unwieldy form the details are consigned to a *Mathematica* notebook in Appendix C. The notebook performs an exact analytic calculation of the probability distribution up to the normalisation of the distributions $P_{\sigma_1\sigma_2}(n)$. Normalisation for a specific set of model parameters is achieved numerically, calculated to arbitrary precision limited only by machine capability.

A comparison of a simulation with the analytic solution for particular values of the model parameters is shown in Figure 3.4, showing complete agreement. The simulation is similar to that of the instant tumbling model described in section 2.6, but the inclusion of the tumbling configurations, mediated by rates $\tilde{\alpha}$ and $\tilde{\beta}$, slightly changes the update procedure.

As before each particle is assigned a position and a velocity, but now this velocity

can be $-1, 0$ or 1. Again, at each time step a particle is chosen at random. An action is then determined for this chosen particle. However, this process will depend on the velocity of the particle.

If the chosen particle has a velocity of -1 or 1, then a tumble or hop action is designated according to the ratio of the respective rates: $\tilde{\alpha}/(\gamma + \tilde{\alpha})$. If a tumble is chosen, the particle enters a tumbling state with new velocity 0. Note that a particle enters the tumbling state instantaneously, although it will take a finite time to finish tumbling. A new particle is then chosen in the same time step. If, instead, a hop is chosen, then the particle hops in the direction of its velocity according to the exclusion and periodic boundary conditions. After a hop attempt, successful or not, a new time step begins.

If the chosen particle has a velocity of 0, then the particle can only choose to remain tumbling or exit the tumbling state according to the ratio of the respective rates: $\tilde{\beta}/(\gamma + \tilde{\beta})$. After this action (continued tumbling, or leaving the tumbling state) is executed, a new time step begins. The simulation is iterated until a steady state is reached.

As in chapter 2, the results are presented in the form of effective potentials, $V(x) = -\ln P(x)$. Recall that for equilibrium systems, we would obtain a Boltzmann distribution $P \propto \mathrm{e}^{-V(x)}$. The effective potential for a nonequilibrium tells us what kind of potential an equilibrium system, without internal propulsion, would have to have in order to see the same macroscopic physics. For simplicity, only the four sectors that do not have symmetry relations with each other are plotted. These sectors are where the particles are approaching ($+-$ and $+0$ sectors) or maintain a constant (average) separation ($++$ and 00 sectors). We see there is an attraction towards low separations, $n \ll L$, in the sectors where the particles are approaching, and that the characteristic lengthscales differ between these two approaching sectors.

3.7 Scaling limit of the probability distribution

In deriving the stationary probability distribution of the lattice-based model with finite tumbling duration, we left the final results in equations (3.54) and (3.55) in schematic form due to the unwieldy parameters z_+ and z_-. The exact expressions in terms of the model parameters was left to a computational algebra engine as

described in the previous section, 3.5.4. Here, however, for the scaling limit defined by Eqs. (3.2)—(3.4), we may find tractable closed-form expressions for the probability distributions.

The stationary probability in the scaling limit has already been presented in equations (3.5)—(3.8) in section 3.3. In this section, the derivation of the exact expressions for the various amplitudes $a_{\sigma_1\sigma_2}$, $b_{\sigma_1\sigma_2}$, $c_{\sigma_1\sigma_2}$, $w_{\sigma_1\sigma_2}$ is presented. These exact expressions are written out explicitly in subsection 3.7.3.

The derivation of equations (3.5)—(3.8) proceeds in three parts. We first find the roots z_ρ and the constants $P_{++}(1)$ and $P_{+-}(1)$ in the scaling limit in terms of $P_{+0}(1)$, ϕ and θ by cancelling poles in the generating functions (cf. subsection 3.5.4). Next, using these expressions, we write the amplitudes in terms of $P_{+0}(1)$, ϕ and θ only. Finally, we impose normalisation, which gives $P_{+0}(1)$ in terms of ϕ and θ only. At the end of this process we arrive at the normalised probability distribution, $P_{\sigma_1\sigma_2}(y)$ in terms of the parameters ϕ, θ and ℓ only. This derivation has similarities to that of the scaling limit for the instant tumbling model presented in section 2.5, which was found directly from the exact solution in equations (2.63) and (2.76). However, here we start from expressions (3.54) and (3.55) where normalisation has not formally been implemented and so the normalisation step forms a distinct step in the derivation.

3.7.1 Constants from pole cancellation

In order to implement the pole cancellation condition on equations (3.54) and (3.55), each pole corresponding to a root z_ρ of $\det A$ must be cancelled by a zero in the numerator. As described in subsection 3.5.4, each such condition leads to a linear equation in $P_{++}(1)$, $P_{+-}(1)$ and $P_{+0}(1)$. We noted that it turns out that there are only two linearly independent equations in these quantities. This means that a further condition (namely, normalisation) is required to determine them all.

One of the roots is $z_\rho = 1$. Through the use of a computational algebra engine, we readily find that the numerator of (3.47) is always zero at $x = 1$, which does not provide any information about $P_{++}(1), P_{+-}(1)$ and $P_{+0}(1)$. However, at the other roots $x = z_+, 1/z_+, z_-, 1/z_-$, the numerator is not automatically zero.

Consequently, we impose the condition

$$\sum_j \mathrm{adj}A_{\sigma_1\sigma_2,j}(z_\rho)\, b_j(z_\rho) = 0, \tag{3.56}$$

at each of the roots $z_\rho = z_+, z_-, 1/z_+$ and $1/z_-$. We find the two desired linearly independent conditions by taking $z = z_+$ and $z = z_-$ in (3.56) with $\sigma_1\sigma_2 = ++$. Using the expression (3.37) for $b_j(x)$, each of these conditions takes the form

$$\begin{aligned}&\tilde{A}_{++,1}(z_\rho)P_{++}(1) + \tilde{A}_{++,2}(z_\rho)P_{+-}(1) + \tilde{A}_{++,5}(z_\rho)P_{+0}(1)\\ &\quad = z_\rho^{L-1}\left[\tilde{A}_{++,1}(z_\rho)P_{++}(1) + \tilde{A}_{++,3}(z_\rho)P_{+-}(1) + \tilde{A}_{++,4}(z_\rho)P_{+0}(1)\right]\end{aligned} \tag{3.57}$$

where, for convenience, we introduce the notation $\tilde{A}_{\sigma_1\sigma_2,j}(x) \equiv \mathrm{adj}A_{\sigma_1\sigma_2,j}$.

To apply these two conditions, we need to know the location of the roots z_+ and z_- of $\det A$, as defined by (3.44). By expanding $z_\pm$ about 1 in powers of $1/\sqrt{L}$ in the explicit expression (3.43) for the determinant, we find that

$$z_+ \sim 1 + \frac{\sqrt{2\phi}}{\sqrt{L}} + \frac{\phi}{L} + O\left(L^{-3/2}\right) \tag{3.58}$$

$$z_- \sim 1 + \sqrt{\frac{(\theta+\phi)(\theta+2\phi)}{2}}\frac{1}{L} + O\left(L^{-3/2}\right)\ . \tag{3.59}$$

A straightforward way to recover the results in Eqs. (3.58) and (3.59) is to make the ansatz

$$z = 1 + \epsilon_{1/2}^{(1)} L^{-1/2}, \tag{3.60}$$

and substitute it into the determinant (3.44) using a computational algebra engine. The result is a series of terms in powers of $L^{-1/2}$:

$$\frac{2(\epsilon_{1/2}^{(1)})^4 - 4(\epsilon_{1/2}^{(1)})^2\phi}{L^2} - \frac{4(\epsilon_{1/2}^{(1)})^3\phi}{L^{5/2}} + O(L^{-3}). \tag{3.61}$$

The condition that highest-order term is zero is equivalent to

$$2(\epsilon_{1/2}^{(1)})^4 - 4(\epsilon_{1/2}^{(1)})^2\phi = 0. \tag{3.62}$$

We see that a solution to this equation is $\epsilon_{1/2}^{(1,+)} = \sqrt{2\phi}$, which gives the coefficient of $L^{-1/2}$ in Eq. (3.58). The conjugate solution $-\sqrt{2\phi}$ gives the scaling of the reciprocal root to z_+, $1/z_+$. The second term in Eq. (3.58) may be derived by

again using an ansatz, but this time of the form

$$z = 1 + \frac{\sqrt{2\phi}}{\sqrt{L}} + \epsilon_1^{(1)} L^{-1}. \tag{3.63}$$

We now find the condition

$$8\sqrt{2}\epsilon_1^{(1)}\phi^{3/2} - 8\sqrt{2}\phi^{5/2} = 0, \tag{3.64}$$

where the solution is $\epsilon_1^{(1)} = \phi$. Thus we have derived the scaling in Eq. (3.58).

The Eq. (3.62) is also solved by zero, in addition to $\epsilon_{1/2}^{(1,+)}$ and its conjugate. This implies that there is a second set of of roots solving Eq. (3.44), which we can now deduce are z_- and its reciprocal. We follow the same procedure as for z_+ above, but now make the initial ansatz

$$z = 1 + \frac{\sqrt{2\phi}}{\sqrt{L}} + \epsilon_1^{(2)} L^{-1}. \tag{3.65}$$

We find $\epsilon_1^{(2,+)} = \sqrt{\frac{(\theta+\phi)(\theta+2\phi)}{2}}$, and thus the scaling of z_- described by Eq. (3.59). We now also note the scaling of the reciprocal roots

$$1/z_+ \sim 1 - \frac{\sqrt{2\phi}}{\sqrt{L}} + \frac{\phi}{L} + O\left(L^{-3/2}\right) \tag{3.66}$$

$$1/z_- \sim 1 - \sqrt{\frac{(\theta+\phi)(\theta+2\phi)}{2}}\frac{1}{L} + O\left(L^{-3/2}\right) \ . \tag{3.67}$$

Substituting these roots into (3.57), we find that $z_+^{L-1} \to \infty$, and so the terms in square brackets on the right-hand side of (3.57) need to cancel at this root. At z_-, the factor z_-^{L-1} approaches e^{λ} where $\lambda = \lim_{L\to\infty} L[z_- - 1]$ is given by

$$\lambda = \left(\frac{(\theta+\phi)(\theta+2\phi)}{2}\right)^{1/2} \ . \tag{3.68}$$

The next step is to determine the leading large-L forms of the adjugate elements $\tilde{A}_{\sigma_1\sigma_2,j}(x)$ appearing in (3.57) at each of the roots. All subleading terms will vanish in the scaling limit. To identify these leading terms, we require explicit expressions for $\tilde{A}_{\sigma_1\sigma_2,j}(x)$ in the constants α, β and the functions $\mu(x) = x-(1+\alpha)$ and $\nu(x) = x^{-1} - (1+\alpha) = \mu(x^{-1})$. These can be obtained straightforwardly using a computational algebra package, and are detailed in Appendix B.

Table 3.1 *Adjugate elements in the scaling limit required to evaluate* $P_{++}(1)$ *and* $P_{+-}(1)$ *and* J_{++}.

	$x=1$	$x=z_+$	$x=1/z_-$
$\tilde{A}_{++,1}$	$-\frac{\theta^2\phi^2\zeta}{4L^5}$	$-\frac{4\theta\phi^2}{L^3}$	$\frac{\theta^3\zeta^2}{4L^5}$
$\tilde{A}_{++,2}$	$-\frac{\theta^2\phi^2\zeta}{4L^5}$	$-\frac{\theta^2\phi^2}{L^4}$	$-\frac{\theta^2\phi\zeta\,(2\lambda+\zeta)}{4L^5}$
$\tilde{A}_{++,3}$	$-\frac{\theta^2\phi^2\zeta}{4L^5}$	$-\frac{\theta^2\phi^2}{L^4}$	$-\frac{\theta^2\phi\zeta\,(-2\lambda+\zeta)}{4L^5}$
$\tilde{A}_{++,4}$	$-\frac{\theta^2\phi^2\zeta}{4L^5}$	$\frac{\sqrt{2}\theta^2\phi^{3/2}}{L^{7/2}}$	$-\frac{\theta^3\zeta\,(2\lambda-2\zeta)}{8L^5}$
$\tilde{A}_{++,5}$	$-\frac{\theta^2\phi^2\zeta}{4L^5}$	$-\frac{\sqrt{2}\theta^2\phi^{3/2}}{L^{7/2}}$	$\frac{\theta^3\zeta\,(2\lambda+2\zeta)}{8L^5}$

We will work through $A_{++,1}$ as an explicit example. In full, $A_{++,1}$ is given by

$$\tilde{A}_{++,1}(x) = -\frac{1}{4}\beta\Big(\beta^2(\alpha+2\mu)(\alpha+2\nu) - \beta(\alpha+2\mu)(\mu+\nu)(\alpha+2\nu) + 2\mu\nu(\alpha(\mu+\nu)+2\mu\nu)\Big) \tag{3.69}$$

where μ and ν, defined in (3.38), are functions of x. Substituting the L-dependent expressions for α and β, (3.4), along with the large L form of z_+, (3.59), into the above expression yields the large-L result

$$\tilde{A}_{++,1}(z_+) \sim -\frac{4\theta\phi^2}{L^3} + O\left(L^{-7/2}\right) \ . \tag{3.70}$$

Using the same method, we can find the leading terms of each of the adjugate elements in (3.57) at each of the roots z_ρ. The results are summarised in Table 3.1.

Now, solving the two equations arising from substituting $x = z_+$ and $x = 1/z_-$ into (3.57) we find for large L

$$P_{++}(1) \sim \frac{\theta}{2\sqrt{2L\phi}} P_{+0}(1) \tag{3.71}$$

$$P_{+-}(1) \sim \frac{\theta\left(e^\lambda(\zeta+\lambda)-\zeta+\lambda\right)}{\phi\left(\zeta\left(e^\lambda-1\right)+2\left(e^\lambda+1\right)\lambda\right)} P_{+0}(1) \ , \tag{3.72}$$

where

$$\zeta \equiv \theta + 2\phi \tag{3.73}$$

$$\eta \equiv \theta + \phi \, . \tag{3.74}$$

The remaining constant $P_{+0}(1)$ will be found by normalisation (see section 3.7.4 below).

3.7.2 Decay lengths and amplitudes

In the scaling limit, we wish to move from a discrete separation of n lattice sites to a continuous separation y that lies between 0 and ℓ, in which terms the scaling limit is expressed in equations (3.2)–(3.4). This is achieved with the transformation

$$n = \frac{Ly}{\ell} \, , \tag{3.75}$$

under which $P_{\sigma_1\sigma_2}(y) = \frac{L}{\ell} P_{\sigma_1\sigma_2}(n)$. The discrete distribution (3.53) contains a set of terms of the form

$$a_{\sigma_1\sigma_2}(z_\rho) z_\rho^{-n+1} \quad \text{where} \quad a_{\sigma_1\sigma_2}(z_\rho) = \frac{-J_{\sigma_1\sigma_2}(z_\rho)}{[q(x)/(x - z_\rho)]_{|x=z_{j=\rho}}} \tag{3.76}$$

and z_ρ is one of the five roots, $z_\rho \in \{1, z_+, 1/z_+, z_-, 1/z_-\}$. We now establish their behaviour in the scaling limit.

We first consider $z_\rho = 1$, where the amplitude $a_{\sigma_1\sigma_2}$ that appears in the result for the scaling limit, (3.5)–(3.8), is equal to $\lim_{L\to\infty} \frac{L}{\ell} a_{\sigma_1\sigma_2}(1)$.

At $z_\rho = z_+$ the amplitude is given by the combination

$$\lim_{L\to\infty} \frac{L}{\ell} a_{\sigma_1\sigma_2}(z_+) \left(1 + \frac{\sqrt{2\phi}}{\sqrt{L}}\right)^{-n+1} \, , \tag{3.77}$$

which, in terms of the continuous coordinate y, becomes

$$\lim_{L\to\infty} \frac{L}{\ell} a_{\sigma_1\sigma_2}(z_+) \exp\left(-\frac{\sqrt{2\phi L}}{\ell} y\right) = \left[\lim_{L\to\infty} a_{\sigma_1\sigma_2}(z_+) \sqrt{\frac{L}{2\phi}}\right] \delta(y) \, . \tag{3.78}$$

Note that the delta function should be thought of as being slightly displaced from the boundary at $y = 0$, so that the integral $\int_0^\ell \mathrm{d}y \, \delta(y) = 1$. The scaling of $a_{\sigma_1\sigma_2}(z_+)$ in the large L limit determines whether the delta function actually

appears in the $\sigma_1\sigma_2$ sector. In particular, if $a_{\sigma_1\sigma_2}(z_+)$ decays faster than $1/\sqrt{L}$, we will not get a delta function contribution. The quantity in the square bracket can be identified as $b^{(0)}_{\sigma_1\sigma_2}$ that appears in the probability distribution in the scaling limit. Note that in Equations (3.5)–(3.8) the superscripts on the amplitudes in the scaling limit were dropped where this was unambiguous.

At $z_\rho = 1/z_+$, we find

$$\left[\lim_{L\to\infty} a_{\sigma_1\sigma_2}(1/z_+)\sqrt{\frac{L}{2\phi}}\right]\delta(\ell - y)\ . \tag{3.79}$$

Here, the term in square brackets defines the amplitude $b^{(1)}_{\sigma_1\sigma_2}$.

Turning now to the root $z_\rho = z_-$, we have

$$\lim_{L\to\infty}\frac{L}{\ell}a_{\sigma_1\sigma_2}(z_-)\left(1+\frac{\lambda}{L}\right)^{-n+1} = \left[\lim_{L\to\infty}\frac{L}{\ell}a_{\sigma_1\sigma_2}(z_-)\right]\exp\left(-\frac{y}{\kappa}\right) \tag{3.80}$$

in which we have introduced the lengthscale

$$\kappa = \frac{\ell}{\lambda} = \frac{\sqrt{2}\ell}{\sqrt{(\phi+\theta)(2\phi+\theta)}}\ . \tag{3.81}$$

The square-bracketed term defines the amplitude $c^{(0)}_{\sigma_1\sigma_2}$.

Finally, at $z_\rho = 1/z_-$, we find

$$\lim_{L\to\infty} a_{\sigma_1\sigma_2}(1/z_-)\left(1-\frac{\lambda}{L}\right)^{-n+1} = \left[\lim_{L\to\infty} a_{\sigma_1\sigma_2}(1/z_-)e^{\lambda}\right]\exp\left(-\frac{\ell-y}{\kappa}\right)\ , \tag{3.82}$$

which furnishes an expression for the amplitude $c^{(1)}_{\sigma_1\sigma_2}$.

It now remains to evaluate the amplitudes. Recall that $J_{\sigma_1\sigma_2}(x)$, defined by (3.50), is by construction a polynomial of degree ≤ 4. Specifically,

$$J_{\sigma_1\sigma_2}(x) = \hat{T}_4\sum_j x^2 \mathrm{adj}A_{\sigma_1\sigma_2,j}(x)b_j(x) \tag{3.83}$$

where the operator $\hat{T}_4$ discards terms of order x^5 and higher in a power series in x. This we may write as

$$J_{\sigma_1\sigma_2}(x) = \tilde{A}'_{\sigma_1\sigma_2,1}P_{++}(1) + \tilde{A}'_{\sigma_1\sigma_2,2}P_{+-}(1) + \tilde{A}'_{\sigma_1\sigma_2,5}P_{+0}(1)\ , \tag{3.84}$$

where $\tilde{A}'_{\sigma_1\sigma_2,j}(x) = \hat{T}_4 x^2 \mathrm{adj} A_{\sigma_1\sigma_2,j}(x)$.

In the ++ sector, the adjugate elements exhibit the symmetries

$$\tilde{A}_{++,1}(x) = \tilde{A}_{++,1}(1/x) \tag{3.85}$$
$$\tilde{A}_{++,2}(x) = \tilde{A}_{++,3}(1/x) \tag{3.86}$$
$$\tilde{A}_{++,5}(x) = \tilde{A}_{++,4}(1/x) \tag{3.87}$$

as can be verified by inspection of the explicit expressions presented in Appendix B. Using these symmetries in (3.57), one can show that

$$J_{++}(1/z_\rho) = z_\rho^{1-L} J_{++}(z_\rho) \tag{3.88}$$

at each of the roots z_ρ. The same symmetry also applies in the 00 sector, namely $J_{00}(1/z_\rho) = z_\rho^{1-L} J_{00}(z_\rho)$.

Meanwhile, the denominator $[q(x)/(x - z_\rho)]_{|x=z_\rho}$ that appears in (3.76), has limiting expressions that are symmetric in $z_\rho \to 1/z_\rho$. These expressions are

$$[q(x)/(x-1)]|_{x=1} \sim \frac{\phi(\theta+\phi)(\theta+2\phi)}{L^3} \tag{3.89}$$
$$[q(x)/(x-z_+)]|_{x=z_+} \sim [q(x)/(x-1/z_+)]|_{x=1/z_+} \sim \frac{8\phi^2}{L^2} \tag{3.90}$$
$$[q(x)/(x-z_-)]|_{x=z_-} \sim [q(x)/(x-1/z_-)]|_{x=1/z_-} \sim \frac{2\phi(\theta+\phi)(\theta+2\phi)}{L^3}\,. \tag{3.91}$$

The consequence of these symmetries is that the amplitudes $b^{(0)}_{++} = b^{(1)}_{++} \equiv b_{++}$, $c^{(0)}_{++} = c^{(1)}_{++} \equiv c_{++}$, and similarly $b^{(0)}_{00} = b^{(1)}_{00} \equiv b_{00}$, $c^{(0)}_{00} = c^{(1)}_{00} \equiv c_{00}$.

The remaining ingredient in the amplitudes is the leading large-L behaviour of the truncated adjugate elements $\tilde{A}'_{\sigma_1\sigma_2,j}(x)$ in the scaling limit. In the ++ sector, these coincide with the expressions set out in Table 3.1. The expressions that are required in the $+-$, $+0$ and 00 sectors are provided in Tables 3.2—3.4.

Table 3.2 *Adjugate elements in the scaling limit for J_{+-}.*

	$x=1$	$x=z_+$	$x=1/z_-$	$x=z_-$
$\tilde{A}_{+-,1}$	$-\frac{\theta^2\phi^2\zeta}{4L^5}$	$-\frac{\theta^2\phi^2}{L^4}$	$-\frac{\theta^2\phi\zeta\,(2\lambda+\zeta)}{4L^5}$	$-\frac{\theta^2\phi\zeta(\zeta-2\lambda)}{4L^5}$
$\tilde{A}'_{+-,2}$	$-\frac{\theta^2\phi^2\zeta}{4L^5}$	$\frac{\theta^3\phi^{3/2}}{L^{9/2}}$	$\frac{\theta\phi^2\zeta\,(4\lambda+\zeta+2\eta)}{4L^5}$	$\frac{\theta\phi^2\zeta\,(-4\lambda+\zeta+2\eta)}{4L^5}$
$\tilde{A}'_{+-,5}$	$-\frac{\theta^2\phi^2\zeta}{4L^5}$	$\frac{-\sqrt{2}\theta^3\phi^{3/2}}{4L^{9/2}}$	$-\frac{\theta^2\phi\zeta\,(6\lambda+2\zeta+2\eta)}{8L^5}$	$-\frac{\theta^2\phi\zeta\,(-6\lambda+2\zeta+2\eta)}{8L^5}$

Table 3.3 *Adjugate elements in the scaling limit in J_{+0} .*

	$x=1$	$x=1/z_-$	$x=z_-$
$\tilde{A}_{+0,1}$	$-\frac{\theta\phi^3\zeta}{2L^5}$	$\frac{\theta^2\phi\zeta\,(2\lambda+2\zeta)}{4L^5}$	$\frac{\theta^2\phi\zeta\,(-2\lambda+2\zeta)}{4L^5}$
$\tilde{A}'_{+0,2}$	$-\frac{\theta\phi^3\zeta}{2L^5}$	$-\frac{\theta\phi^2\zeta\,(6\lambda+2\zeta+2\eta)}{4L^5}$	$-\frac{\theta\phi^2\zeta\,(-6\lambda+2\zeta+2\eta)}{4L^5}$
$\tilde{A}'_{+0,5}$	$-\frac{\theta\phi^3\zeta}{2L^5}$	$\frac{\theta^2\phi\zeta\,(4\lambda+2\zeta+\eta)}{4L^5}$	$\frac{\theta^2\phi\zeta\,(-4\lambda+2\zeta+\eta)}{4L^5}$

Table 3.4 *Adjugate elements in the scaling limit for J_{00}.*

	$x=1$	$x=1/z_-$
$\tilde{A}'_{00,1}$	$-\frac{\phi^4\zeta}{L^5}$	$\frac{\theta\phi^2\eta(\zeta+2\phi)}{2L^5}$
$\tilde{A}'_{00,2}$	$-\frac{\phi^4\zeta}{L^5}$	$-\frac{\phi^3\zeta\,(2\lambda+\zeta)}{L^5}$
$\tilde{A}'_{00,5}$	$-\frac{\phi^4\zeta}{L^5}$	$\frac{\theta\phi^2\zeta\,(2\lambda+2\zeta)}{2L^5}$

3.7.3 Explicit expressions for the amplitudes in the scaling limit

Putting this all together, we obtain explicit expressions for the amplitudes that appear in the scaling limit of the stationary probability distribution, Eqs. (3.5)–(3.8). The amplitudes that remain finite in the $L \to \infty$ limit are

$$a_{++} = \frac{\zeta\theta^2 P_{+0}(1)\left(e^{\lambda}(\eta+\lambda)-\eta+\lambda\right)}{4\eta\ell L\left(\zeta\left(e^{\lambda}-1\right)+2\left(e^{\lambda}+1\right)\lambda\right)} \tag{3.92}$$

$$b_{++} = \frac{\theta^2 P_{+0}(1)}{4L\phi} \tag{3.93}$$

$$c_{++} = \frac{\zeta\theta^3 e^{\lambda} P_{+0}(1)}{8\ell L\phi\left(e^{\lambda}(\eta+\lambda)+\eta-\lambda\right)} \tag{3.94}$$

$$a_{+-} = \frac{\zeta\theta^2 P_{+0}(1)\left(e^{\lambda}(\eta+\lambda)-\eta+\lambda\right)}{4\eta\ell L\left(\zeta\left(e^{\lambda}-1\right)+2\left(e^{\lambda}+1\right)\lambda\right)} \tag{3.95}$$

$$c^{(0)}_{+-} = \frac{\zeta\theta^3 e^{\lambda} P_{+0}(1)}{8\ell L\left(e^{\lambda}\left(2\theta^2+3\theta(\lambda+2\phi)+4\phi(\lambda+\phi)\right)+\theta\lambda\right)} \tag{3.96}$$

$$c^{(1)}_{+-} = -\frac{\zeta\theta^2 e^{\lambda} P_{+0}(1)(\eta+\lambda)}{4\eta\ell L\left(\zeta\left(e^{\lambda}-1\right)+2\left(e^{\lambda}+1\right)\lambda\right)} \tag{3.97}$$

$$a_{+0} = \frac{\zeta\theta P_{+0}(1)\phi\left(e^{\lambda}(\eta+\lambda)-\eta+\lambda\right)}{2\eta\ell L\left(\zeta\left(e^{\lambda}-1\right)+2\left(e^{\lambda}+1\right)\lambda\right)} \tag{3.98}$$

$$c^{(0)}_{+0} = \frac{\zeta\theta^2 e^{\lambda} P_{+0}(1)(2\lambda-\eta)}{4\eta\ell L\left(\zeta\left(e^{\lambda}-1\right)+2\left(e^{\lambda}+1\right)\lambda\right)} \tag{3.99}$$

$$c^{(1)}_{+0} = \frac{\zeta\theta^2 e^{\lambda} P_{+0}(1)(\eta+2\lambda)}{4\eta lL\left(\zeta\left(e^{\lambda}-1\right)+2\left(e^{\lambda}+1\right)\lambda\right)} \tag{3.100}$$

$$a_{00} = \frac{\zeta P_{+0}(1)\phi^2\left(e^{\lambda}(\eta+\lambda)-\eta+\lambda\right)}{\eta\ell L\left(\zeta\left(e^{\lambda}-1\right)+2\left(e^{\lambda}+1\right)\lambda\right)} \tag{3.101}$$

$$c_{00} = \frac{\zeta\theta e^{\lambda} P_{+0}(1)\phi}{2\ell L\left(e^{\lambda}(\eta+\lambda)+\eta-\lambda\right)}\,. \tag{3.102}$$

All other amplitudes are zero.

The w coefficients are more straightforward to obtain, since the Kronecker delta symbols $\delta_{n,1}$ and $\delta_{n,L-1}$ in (3.41) turn into Dirac delta functions $\delta(y)$ and $\delta(\ell-y)$, respectively, with their amplitudes unchanged. These amplitudes, $w^{(0)}_{\sigma_1\sigma_2}$ and $w^{(1)}_{\sigma_1\sigma_2}$

are found to be

$$w_{+-}^{(0)} = \frac{1}{2}(\alpha+2)\beta P_{+-}(1) + \beta^2 P_{+-}(1) + \beta^2 P_{+0}(1)/2 \tag{3.103}$$

$$\sim \frac{P_{+-}(1)\theta}{L} = \frac{\theta^2 P_{+0}(1)\left(e^{\lambda}(\zeta+\lambda)-\zeta+\lambda\right)}{L\phi\left(\zeta\left(e^{\lambda}-1\right)+2\left(e^{\lambda}+1\right)\lambda\right)} \tag{3.104}$$

$$w_{+0}^{(0)} = \alpha\beta P_{+-}(1) + \alpha\beta P_{+0}(1) + \beta P_{+0}(1) \sim \frac{P_{+0}(0)\theta}{L} \tag{3.105}$$

$$w_{00}^{(0)} = \alpha^2 P_{+-}(1) + (\alpha+\alpha^2) P_{+0}(1) \sim \frac{P_{+0}(1)\phi}{L} \tag{3.106}$$

$$w_{00}^{(1)} = w_{00}^{(0)} \ . \tag{3.107}$$

Again the other w amplitudes are all zero.

Note that although all the amplitudes have the superficial appearance of a $1/L$ decay, this is in fact cancelled by the remaining constant, $P_{+0}(1)$, which scales as L as will be determined by normalising the distribution. We now turn to normalisation, from which we find this final remaining constant.

3.7.4 Normalisation

Rather than impose normalisation on the whole probability distribution, it is sufficient (and more straightforward) to impose it on a single velocity sector in order to determine $P_{+0}(1)$. The relative weight of each sector can be calculated straightforwardly because transitions between sectors occur at rates that are decoupled from the hopping dynamics i.e. the transitions between sectors are independent of the particle separation n. Moreover, each particle enters a velocity state independently of the other. Consequently, if we define the marginal probability distribution

$$P_{\sigma_1} = \sum_{\sigma_2} \int_0^{\ell} \mathrm{d}y \, P_{\sigma_1\sigma_2}(y) \tag{3.108}$$

then I have for the probability of being in the velocity sector $\sigma_1\sigma_2$ that

$$P_{\sigma_1\sigma_2} = \int_0^{\ell} \mathrm{d}y \, P_{\sigma_1\sigma_2}(y) = P_{\sigma_1} P_{\sigma_2} \ . \tag{3.109}$$

The master equation for the single particle velocity distribution reads

$$\frac{\partial P_+}{\partial t} = -\alpha P_+ + \frac{\beta}{2} P_0 \tag{3.110}$$

$$\frac{\partial P_-}{\partial t} = -\alpha P_- + \frac{\beta}{2} P_0 \tag{3.111}$$

$$\frac{\partial P_0}{\partial t} = \alpha[P_+ + P_-] - \beta P_0 \; . \tag{3.112}$$

In the steady state, I have $P_+ = P_-$ by symmetry and consequently

$$P_0 = \frac{2\alpha}{\beta} P_+ \; . \tag{3.113}$$

Using this result and the fact that $P_+ + P_0 + P_- = 1$, I find

$$P_+ = P_- = \frac{1}{2(1 + \alpha/\beta)} \; . \tag{3.114}$$

Insisting now that $\int_0^\ell \mathrm{d}\ell P_{++}(y) = P_+^2$, I find that

$$P_{+0}(1) = L\Bigg[(\theta+\phi)^2\Bigg(\zeta\Bigg(\frac{\sqrt{2}\theta\left(e^\lambda - 1\right)}{\phi\sqrt{\zeta\eta}\left(\eta + e^\lambda(\theta+\lambda+\phi) - \lambda\right)} \tag{3.115}$$

$$+ \frac{e^\lambda(\eta+\lambda) - \theta + \lambda - \phi}{\eta\left(\zeta\left(e^\lambda - 1\right) + 2\left(e^\lambda + 1\right)\lambda\right)}\Bigg) + \frac{2}{\phi}\Bigg)\Bigg]^{-1}, \tag{3.116}$$

which completes our derivation of eqs (3.5)—(3.8).

3.7.5 Plots of the scaling limit distribution

We can directly simulate the scaling limit by having particles move ballistically at speed v and undergo tumbling and untumbling events at times drawn from an exponential distribution with means $1/\alpha$ and $1/\beta$ respectively. In Figures 3.5 and 3.6 the distributions (in the form of effective potentials) obtained from this simulation with the analytical calculation are compared. Once again, we find complete agreement.

As discussed in section 3.3, and as seen explicitly above, one of the two exponential decays collapses to a delta function in this limit. This presents the same behaviour as the lengthscale ξ, Eq. (2.86) in section 2.5. However, the second lengthscale, $\xi_- = 1/\ln z_-(\alpha,\beta)$, which is induced by the finite tumbling time, remains physically relevant in the scaling limit, expressed by κ in Eq. (3.81). We may

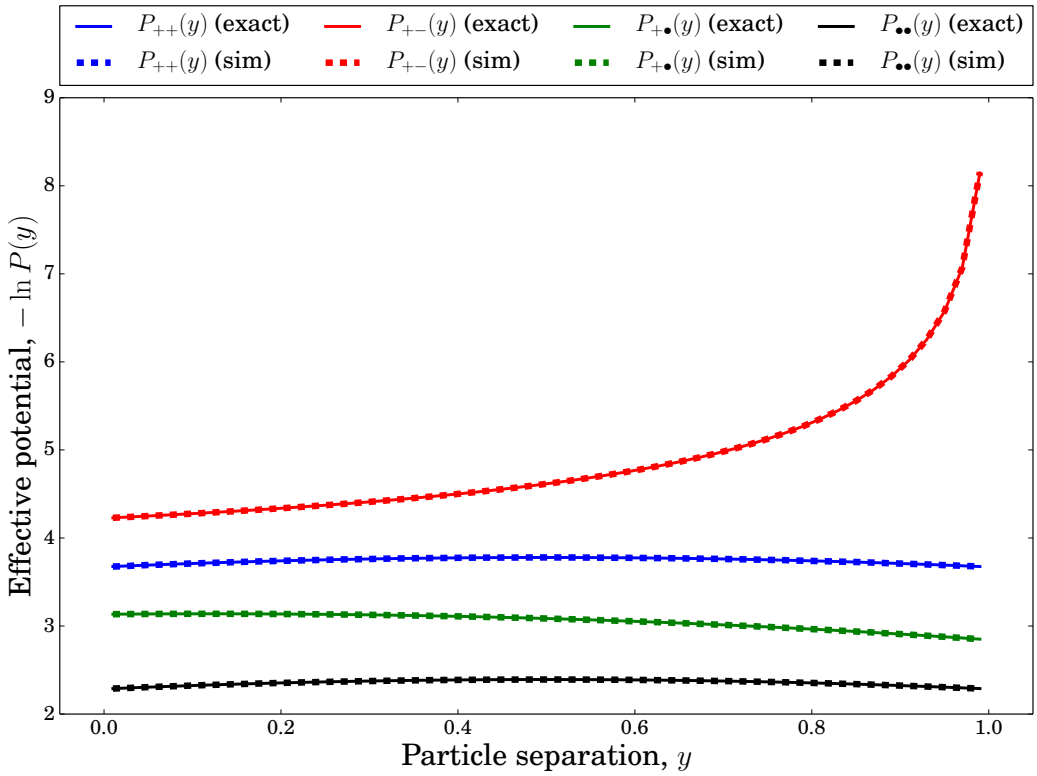

Figure 3.5 *(Reproduced from [112]) Comparison of exact analytic results (solid lines) with simulation results (dotted lines) for scaling limit. Model with $\phi = \theta = 1$ and $\ell = 1$.*

make a formal connection to the work in chapter 2 by considering the limit where the exit rate from tumbling $\beta \to \infty$. In this limit tumbling is instantaneous, and we recover the probability distribution in the scaling limit of Eqs. (2.84) and (2.85) in section 2.5:

$$P_{++}(y) = \frac{\phi}{4\ell(4+\phi)} + \frac{\delta(y)+\delta(\ell-y)}{2(4+\phi)} = \frac{\tilde{\alpha}+2v[\delta(y)+\delta(\ell-y)]}{4(4v+\tilde{\alpha}\ell)} \tag{3.117}$$

$$P_{+-}(y) = \frac{\phi}{4\ell(4+\phi)} + \frac{\delta(y)}{(4+\phi)} = \frac{\tilde{\alpha}+4v\delta(y)}{4(4v+\tilde{\alpha}\ell)} \tag{3.118}$$

$$P_{+0}(y) = P_{00}(y) = 0. \tag{3.119}$$

We now note exactly how this limit is recovered, which shows how the terms from the scaling limit in equations (3.5)–(3.8) contribute to the $\beta \to \infty$ limit.

As expected, all contributions from states with a tumbling particle vanish in this limit. There are no contributions from $c_{+-}^{(0)} e^{-y/\kappa}$ and $c_{+-}^{(1)} e^{-(\ell-y)/\kappa}$ as the

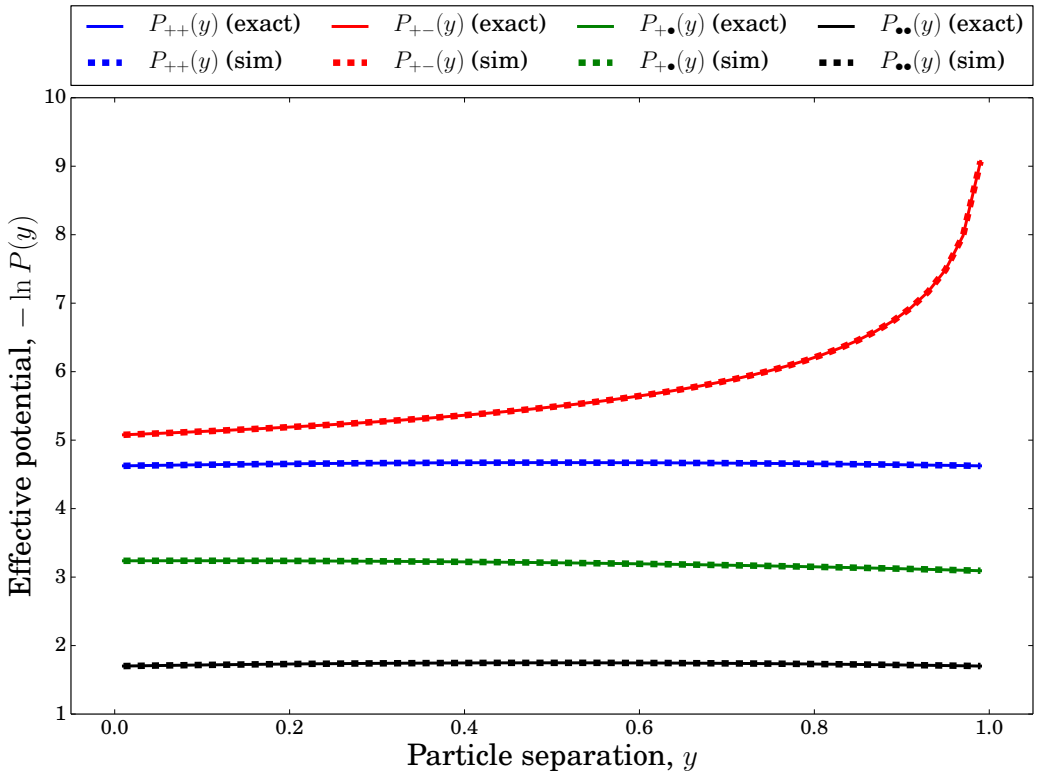

Figure 3.6 *(Reproduced from [112]) Comparison of exact analytic results (solid lines) with simulation results (dotted lines) for scaling limit. Model with* $\phi = 1.1$, $\theta = 0.51$ *and* $\ell = 1$.

exponentials vanish. Therefore the only terms that contribute from $(+-)$ are

$$a_{+-} \sim \frac{\phi}{4\ell(4+\phi)} \quad \text{and,} \tag{3.120}$$

$$w^{(0)}_{+-} \sim \frac{1}{4(4+\phi)} \,. \tag{3.121}$$

However, all of the terms in $(++)$ (and, equivalently, its symmetric counterpart $(--)$) do contribute to the probability in this limit. Specifically, the constant

$$a_{++} \sim \frac{\phi}{4\ell(4+\phi)}, \tag{3.122}$$

and

$$b_{++}[\delta(y) + \delta(\ell - y)] \sim \frac{\sqrt{2}}{4(4+\phi)}[\delta(y) + \delta(\ell - y)] \quad \text{and} \tag{3.123}$$

$$c_{++}[e^{-y/\kappa} + e^{-(\ell-y)/\kappa}] \sim \left(\frac{1}{2(4+\phi)} - \frac{\sqrt{2}}{4(4+\phi)} \right) [\delta(y) + \delta(\ell - y)]. \tag{3.124}$$

Thus we see that not all of the probability in the delta functions in (3.117) comes from the delta-function term b_{++}, but that there is also a contribution from the originally finite exponential piece multiplying c_{++}. This may be understood as follows. After a collision, one particle may tumble and change its orientation such that the particles are no longer jammed but instead moving in the same direction. We are interested in the case where the particle 'behind' then begins tumbling. When the average tumbling time is short (but not zero), very small inter-particle separations are generated with a high probability. The effect of this is seen in simulations: when β is set very large but not strictly infinite there is a significant fraction of the probability for configurations at very marginal but non-zero separations. Only when β is set strictly infinite does this probability moves into the delta-function terms.

3.8 Concluding remarks

In this chapter, we have built on the study of the interacting run-and-tumble model in chapter 2, in which particle tumbled instantaneously, by including a finite tumbling duration. This was initially motivated by the fact that modelling tumbling as instantaneous is intrinsically unphysical but widely used in the literature. Thus it is of interest to determine the extent to which a more physical, finite tumbling duration has an effect on the physics of the run-and-tumble system.

To enable a comparison of the instantaneous and finite duration tumbling models the exact stationary distribution of the finite tumbling duration model was found by using a generalisation of the generating function method in chapter 2. The results, visualised in Figs. 3.4 and 3.5 in the form of effective potentials, show that as in the case of instantaneous tumbling, effective attractions emerge due to particle collisions in the finite tumbling model. On collision, the particles jam until one of them tumbles, changes direction and moves away, which causes probability to accumulate in configurations where particles are jammed on neighbouring sites. Mathematically, this is represented by the delta symbol contributions in Eq. (3.1), as it was in the previous chapter. However, this type of delta symbol contribution also appears where particles are on adjacent sites and are both tumbling. This is due to the high probability of entering this configuration from jamming collisions. This was our first encounter with new physics in the model with finite tumbling duration.

The most significant new feature was the emergence of a lengthscale, ξ_-, that remained finite in the scaling limit, where the more realistic continuum dynamics of the run-and-tumble random walkers is recovered. This may contribute to the long-range attractive effects observed through the coarse-grained many-body models that present motility-induced phase separation. This lengthscale may therefore be relevant to macroscopic behaviours of run-and-tumble systems. Furthermore, should the model be testable in the sense described in section 2.1, the results in this chapter and chapter 2 present an opportunity to test the difference in the predictions between a model with instantaneous tumbling and a finite tumbling duration.

More generally in the context of nonequilibrium statistical mechanics, the work of this chapter has shown that changes in the microscopic dynamics can lead to additional structure entering the stationary distribution in a variety of ways. We now consider this with specific reference to the generating function method. A crucial step is the inversion of the matrix A in Eq. (3.36) that relates the generating functions in each velocity sector to one another. The elements of this matrix contain terms proportional to the generating function variable x or to its reciprocal, $1/x$. This is due to particles hopping one site at a time (if they could hop two sites, one would obtain x^2 and $1/x^2$, and so on). The consequence of this is that the elements of the inverse matrix A^{-1} can be written as the ratio of two polynomials, each related to the determinant of A or one of its submatrices. If the numerator polynomial is of lower degree than the denominator polynomial, the generating function has simple poles which, on inversion, translate to exponential decays in the stationary probability distribution. On the other hand, if the numerator polynomial has the same or higher degree than the denominator polynomial, there are additional contributions corresponding to particle separations that are determined by the difference in the degree of the two polynomials. In the case of the run-and-tumble models, these additional contributions have been of δ-function form for jammed configurations.

It is not obvious that the addition of stochastic switching between a running and a tumbling state without changing its position, which is internal to the particle dynamics, should be of the type that generates an extra lengthscale rather than a δ-function contribution to the probability distribution. It would be interesting to understand more deeply the structure of the A matrix and thereby what physical processes tend to create effective inter-particle interactions of different types.

Chapter 4

A graph-theoretic approach to the run-and-tumble model with reflecting boundaries

In section 2.6, I described how modifications to the run-and-tumble model, such as higher dimensions, more particles and reflecting boundaries introduce more variables into the generating function equations. Such multiple variable generating function equations are not amenable the simple kernel method of chapters 2 and 3 (although may be in general soluble by other kernel methods). To make progress in the analysis of the interacting run-and-tumble system with more variables we therefore look to other tools, which do not suffer from the one-variable limitation.

In this chapter, we consider a brute force method based in graph theory to finding the stationary probability of a Markov process, known as the matrix tree theorem. We find that in the limit where the tumbling rate is low compared to the hopping rate—the relevant limit for run-and-tumble swimmers—it is possible to evaluate the leading order terms in the steady-state probability distribution of the instantaneous tumbling run-and-tumble model with reflecting boundaries. We can think of the reflecting boundaries as walls, and so the results are relevant to studies of active particle interactions under confinement. By comparison with limiting behaviour from the periodic boundaries model in chapter 2, we find evidence in the reflecting boundaries model not only of an effective attraction between the particles, but between the particles and the walls as well.

4.1 The matrix tree theorem

The matrix tree theorem, also known as Kirchhoff's matrix tree theorem or the Markov tree theorem, allows a brute force solution to the steady-state master equation [115]. It is based on the construction and enumeration of a certain type of graph, known as a spanning in-tree, where the graph vertices represent the configurations of the Markov process, and the edges represent transitions between the configurations, weighted by their corresponding rates.

Before stating the matrix tree theorem, I first review a formulation of the master equation different to that found in Eq. (2.27) in section 2.3, following the exposition in [116]. This will allow a precise connection to be made between the approach from linear algebra used in the previous chapters to solve the master equation, and the graph-theoretic method adopted in this chapter.

The master equation for configurations $\mathcal{C} \in \mathcal{K}$ in a Markov process with transition probabilities W may be written as a set of probability gain-loss equations for each configuration $\mathcal{C}$ as

$$\dot{P}(C,t) = \sum_{C' \neq C} P(C',t)W(C' \to C) - \sum_{C' \neq C} P(C,t)W(C \to C')$$

(as written in Eq. (2.27) in section 2.3). In the steady state, these equations can be drawn together into a vector equation as

$$\frac{\mathrm{d}}{\mathrm{d}t}\mathbf{P} = \Omega\mathbf{P} = 0, \tag{4.1}$$

where Ω is the transition rate matrix

$$\begin{aligned}[\Omega]_{ij} &= W(\mathcal{C}_i \to \mathcal{C}_j), \quad i \neq j \\ &= -\sum_k W(\mathcal{C}_i \to \mathcal{C}_k), \quad i = j\end{aligned} \tag{4.2}$$

and $\mathbf{P}$ is the stationary probability vector, where the i^{th} component of $\mathbf{P}$, P_i, is the stationary probability for the configuration $\mathcal{C}_i$. Eq (4.1) is undetermined as one of the eigenvalues of Ω is zero. However, the sum of the distributions $\mathbf{P}$ must be unity. By incorporating this condition, the following equation holds:

$$\widetilde{\Omega}^i\mathbf{P} = \mathbf{e}_i \tag{4.3}$$

where $\widetilde{\Omega}^i$ is the matrix obtained from $\widetilde{\Omega} = -\Omega$ by replacing the i^{th} row with the vector $(1, 1, ..., 1)$ [117]. This multiplies each probability in $\mathbf{P}$ by 1 in row i, and therefore the sum resulting from the matrix multiplication must be unity. The other elements in Ω^i correspond to the steady-state equation, and therefore the results of the matrix multiplication must cancel.

Replacing column j of $\widetilde{\Omega}^i$ with $\mathbf{e}_j$ leads to $\widetilde{\Omega}^{i;j}$. The quantity $f_j = \det \widetilde{\Omega}^{j;j}$ (i.e. taking $i = j$) is a cofactor of $\widetilde{\Omega}$. Using Cramer's rule [116] on this set of equations (4.3) gives

$$P_j = \frac{\det \widetilde{\Omega}^{i;j}}{\det \widetilde{\Omega}^i} = \frac{f_j}{\sum_{k=1}^{N} f_k}. \tag{4.4}$$

We can make the identification that $\det \widetilde{\Omega}^i = \sum_{k=1}^{N} f_k$, where N is the number of states of the system. The cofactor f_j may therefore be identified as the weight of the steady state of configuration $\mathcal{C}_j$. The weights f may be obtained through the enumeration of graphs using the matrix tree theorem.

The elements of graph theory needed to express the matrix tree theorem are defined below following [118].

Directed graph $G = (V, E)$: A collection of points called vertices, V, and directed lines called edges, E, which connect some subset of the vertices.

Path in graph G: A sequence of distinct vertices $(\mathcal{C}_1, \mathcal{C}_2, ..., \mathcal{C}_m)$ where each $\mathcal{C}_{k+1}$ is related to $\mathcal{C}_k$ such that the edge $(\mathcal{C}_k, \mathcal{C}_{k+1}) \in E$.

Spanning in-tree, A**, of** G **with a sink** $\mathcal{C}$: A subgraph of G, which contains exactly one directed path from every vertex $\mathcal{C}' \neq \mathcal{C}$ to $\mathcal{C}$.

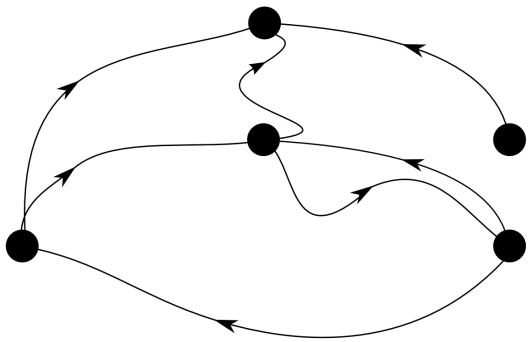

Figure 4.1 *An example directed graph. The vertices are the black circles, and the edges are the connecting lines with arrows.*

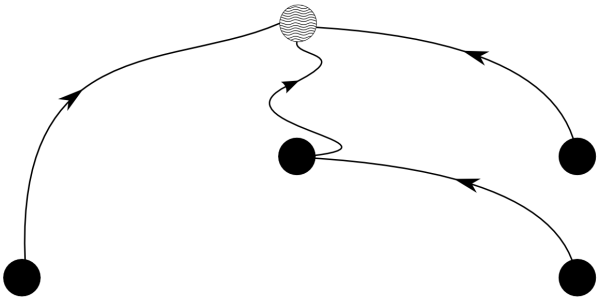

Figure 4.2 *A spanning in-tree of the example directed graph in Figure 4.1. The sink is the circle filled with wavy lines.*

Let every distinct configuration, $\mathcal{C}$, correspond to a unique vertex on a graph G. Every possible transition between any two configurations, $\mathcal{C} \to \mathcal{C}'$, is represented by directed edges from the vertex corresponding to $\mathcal{C}$ to the vertex corresponding to $\mathcal{C}'$.

Following [119], the matrix tree theorem may be stated as follows

Let S be the set of all spanning in-trees of G rooted at $\mathcal{C}_i$. For each spanning in-tree $A \in S$ let w_A be the product of $[\Omega^{j;j}]_{ij}$ over all directed edges $(j \to i)$ in A. Then the identity $\sum_{A \in S} w_A = f_i$ holds.

The matrix tree theorem states that the stationary weight of a configuration is determined by counting all of the possible transition graphs that end up at that configuration (i.e. where it is the sink of the spanning in-tree), weighted by the particular transition rates of the edges in each of those spanning in-trees. Normalisation to a probability is given by dividing each weight by the sum of all the weights in the usual way.

A number of proofs have been given for this theorem, or variants of it. Kirchhoff's original proof appeared in German [120], and is available in translation [121]. More recent proofs appear in [119], and in the context of solving stationary Markov systems in [122] and [123].

In summary, the stationary probability distribution of a system may be calculated by enumerating the (weighted) spanning in-trees of its transition graph. In systems of even a modest size, the set of such trees becomes very large, and so this is normally an intractable computation. However, in certain systems where the transition rates have a sufficient separation of scales, their graph structures can be amenable to a perturbative solution [124–126]. Given that, as we saw in the introduction, in the run-and-tumble system the run rate is higher than the

reversal rate, there may be an opportunity to apply the matrix tree theorem. We will examine the conditions for such an approach in the next section.

4.2 Timescale separation in the transition rates

The contribution of the spanning in-trees to the stationary probability depends on two features: the number of spanning in-trees and the weights associated with each of the spanning in-trees (the product of the weights of the edges in the spanning in-tree). If there are edges with much greater weights (corresponding to larger transition rates) than others, then the spanning in-trees with more of those edges will individually contribute more to the probability than those with fewer large-weight edges. Intuitively, if there is a set of spanning in-trees containing each tree that has the joint-greatest number of edges with the largest weight W_{B} then, in the limit of W_{B} *large enough*, that set of spanning in-trees will dominate the stationary probability. This limit of W_{B} large enough would amount to a separation in the timescale of the transition rates of the system: the transitions occurring at rate W_{B} would have to be sufficiently faster than any others.

Alternatively, there may be a set of trees with the same edge weights that make up the largest number of spanning in-trees. In this case, if all the transition rates are small enough, then this set of spanning in-trees would dominate the stationary probability distribution. For either of these cases, only a subset of the spanning in-trees of the whole system would need to be enumerated to find the stationary solution.

Several researchers have independently refined this intuition in order to find approximate solutions to the master equation [124–128]. In [125], Basile and collaborators find a perturbative solution to the chemical master equation, which is a stochastic description of the reaction kinetics in mesoscopic systems, by expanding the eigenvalues of the transition matrix and calculating approximations for their corresponding eigenvectors using a tree-based method. Szavits-Nossan takes a different approach in [126], where he shows that in the low-current regime of the totally asymmetric simple exclusion process, the current is determined solely by the current-minimising subset of equal hopping rates, regardless of other hopping rates. Work that brings together both a tree-based method and scale separation in the transition rates may be found in a series of papers by Maes and co-workers [124, 127, 128]. This approach is closely related to the work in this

chapter, and I outline it briefly in the following subsection 4.2.1. In subsection 4.2.2, I adapt this formulation so that it may be applied to our run-and-tumble problem as formulated in chapter 2.

4.2.1 A low temperature expansion

In [124], the authors consider a Markov jump process on a finite set of states $x, y, ... \in K$ with associated energy levels $E(x), E(y)...$, and transition rates $W(x \to y) = W(x, y)$ that depend on a parameter β, interpreted as inverse temperature. Dynamic reversibility is then imposed, such that if $W(x, y) > 0$, then $W(y, x) > 0$. Their goal is to find the stationary probability.

The authors assume the existence of the limit

$$\lim_{\beta\to\infty} \frac{1}{\beta} \log W(x, y) =: \phi(x, y), \tag{4.5}$$

where $\beta \geq 0$ is the inverse temperature of the environment. They prove that as $\beta \to \infty$ the occupation of a state x, $P^*(x)_{\text{low T}}$, can be expressed as

$$P^*(x)_{\text{low T}} = \frac{1}{Z} A(x) e^{\beta[\Gamma(x)-\Theta(x)]}(1 + O(e^{-\beta\epsilon})),\ \epsilon > 0 \tag{4.6}$$

where $Z = \sum_y P^*(y)_{\text{low T}}$ and $A(x)$ is the reactivity in the Arrhenius sense. We now consider each of the terms in Eq. (4.6) and relate them to the model definition.

We first define the quantity

$$\Gamma(x) = -\max_y \phi(x, y), \tag{4.7}$$

which is a measure of the lifetime of the state x. The log-asymptotic transition probability between states x and y is given by

$$U(x, y) := -\max_y \phi(x, y) - \phi(x, y) = -\Gamma(x) - \phi(x, y). \tag{4.8}$$

The accessibility, $\Theta(x)$, is the probability of other states transitioning into x. By orientating all the edges towards x and forming a spanning in-tree rooted at x, T_x, we have

$$U(T_x) = \sum_{y,y' \in T_x} U(y, y'). \tag{4.9}$$

There may be many spanning in-trees for a state. However, as the maximum transition rates dominate, the accessibility of a state is determined by picking only the spanning in-trees which minimise $U(T_x)$. The measure for the accessibility is then

$$\Theta(x) := \min_{T} U(T_x). \tag{4.10}$$

The set of trees which minimise $U(T_x)$ is denoted $M(x)$. We now define reactivities a, which will form part of the expression for $A(x)$:

$$a(x, y) = W(x, y)e^{-\beta\phi(x,y)}, \tag{4.11}$$

which are the sub-exponential part of the transition rates. Then

$$A(x) := \sum_{T \in M(x)} \prod_{(y,y') \in T} a(y, y') = e^{o(\beta)} \tag{4.12}$$

Maes and collaborators apply this formula to a number of toy systems including a flashing potential ratchet, and a model of an equalising process in lasers [124]. They also find the dominant states of the boundary driven Kawasaki process in the low temperature regime [128].

The key advantage of this low temperature regime is that evaluation of the stationary probabilities only requires enumeration of the U-minimising set of spanning in-trees rather than the all the possible spanning in-trees. This method also includes the dynamics by counting the number of spanning in-trees, rather than just evaluating the product of the edges in the U-minimising spanning in-trees. This profound reduction in computation occurs because the maximum transition rates dominate in the low temperature regime. In the next subsection, we show that this is not restricted to dynamically reversible systems that obey all the conditions above, but can be extended to any Markov system exhibiting a sufficient separation of scales.

4.2.2 A general scale-separated expansion

The run-and-tumble model does not satisfy the dynamic reversibility of the formulation considered in [124] and so the work of Maes and collaborators cannot be directly applied. However, their approach of finding a much smaller subset of trees to enumerate that yields leading-order steady-state weights can serve as

inspiration for a more general perturbative method, which is the focus of this subsection.

I now assume that scale-separation exists between the transition rates in a Markov process and show that a perturbative stationary probability solution emerges. This solution follows directly from the matrix tree theorem, and holds in the limit that the contributions to the probability weights from the spanning in-trees containing the greatest number of edges with the largest transition rate dominate all other contributions from other spanning in-trees.

Consider a Markov process on a finite set of N states $\mathcal{C}_1, \mathcal{C}_2, ..., \mathcal{C}_N$ with M transition rates $W_1, W_2, ..., W_M$. We label the transition rates of the Markov process according to their size, such that $W_1 > W_2 > ... > W_M$. The matrix tree theorem gives the stationary probability weights as a sum of products of these transition rates, or edge weights, with prefactors corresponding to the number of spanning in-trees associated with each set of the same transition-rate edge weights. This may be written explicitly as

$$f(\mathcal{C}_i) = \sum_{\phi_{l,i} \in \Phi_i} \prod_{j=1}^{M} W_j^{p_{j,l}}, \tag{4.13}$$

where Φ_i is the set of all spanning in-trees of the state $\mathcal{C}_i$, $\phi_{l,i}$ is an element of Φ_i, where each $\phi_{l,i}$ corresponds to one spanning in-tree of $\mathcal{C}_i$ with a particular set of edges, j labels each of the transition rates (or edge weights) W_j, $p_{j,l}$ is the number of edges with weight W_j in the spanning in-tree $\phi_{l,i}$. We work in the regime where the transition rates imply that the hierarchy of stationary probability weights is determined only by the spanning in-trees which have the most edges corresponding to the largest transition rate W_B: the 'leading-order' spanning in-trees.

We may now factorise by collecting all the terms with the same powers of the biggest edge weights in their respective spanning in-trees. Let the largest power of the biggest edge weight W_{B_i} for any of the spanning in-trees of $\mathcal{C}_i$ be $a_{1,i}$ and the next highest be $a_{2,i}$, and so on. The stationary probability weights factorised in this way have the form

$$f(\mathcal{C}_i) = \sum_{k} W_{B_i}^{a_{k,i}} \sum_{\psi_{l,i} \in \Phi_{W_{k,i}}} \prod_{j > B_i}^{M} W_j^{q_{j,l}} \tag{4.14}$$

where $\Phi_{W_{k,i}}$ is the set of all spanning in-trees of the state $\mathcal{C}_i$ that have $a_{k,i}$ edges of weight W_{B_i}, $\psi_{l,i}$ labels each spanning in-tree in $\Phi_{W_{k,i}}$ (that is, a spanning in-tree of $\mathcal{C}_i$ with $a_{k,i}$ edges of transition rate W_{B_i}), and $q_{j,l}$ is the number of edges with weight W_j in the spanning in-tree labelled by $\psi_{l,i}$. In this way we have built up an expansion for the stationary probability weights in terms of the leading-order spanning in-trees.

The leading-order spanning in-trees for a state $\mathcal{C}_i$ are defined as the spanning in-trees of that state with the greatest number of edges with the greatest transition rate W_{B_i}. We now impose a condition on the transition rates such that only the leading-order set of spanning in-trees is needed in order to establish the hierarchy of stationary probabilities. We require that W_{B_i} be sufficiently larger than any other transition rates such that all sub-leading order contributions (combined) are smaller than the leading-order contribution. We may then re-write (4.14) as

$$f(\mathcal{C}_i) = W_{B_i}^{a_{1,i}} \sum_{\psi_{l,i} \in \Phi_{W_{B_i}}} \prod_{j>B_i}^{M} W_j^{q_{j,l}} + O(W_{B_i}^{a_{2,i}}) \tag{4.15}$$

The precise scale separation of the transition rates required for this expansion to hold will depend on the contributions from sum for $k > B_i$ in (4.14). We note that this leading-order approximation does not capture any difference between the sub-leading orders of these configurations

Despite this significant simplification compared with the original incarnation of the matrix tree theorem, the resulting calculations are not necessarily straightforward. Specifically, for the hierarchy of the stationary probabilities to be tractable will require the structure of the leading order spanning in-trees to be amenable to enumeration. The run-and-tumble model of bacterial dynamics provides a natural opportunity to investigate this method as it exhibits timescale separation in its transition rates.

4.3 Application of the matrix tree theorem to the instant tumbling run-and-tumble model with periodic boundaries

We saw previously in section 2.5 for the interacting run-and-tumble model with instantaneous tumbling that in the limit where the reversal rate, ω, goes to infinity, the equilibrium simple exclusion process is recovered and the emergent attraction, apparent in the full solution, disappears (see Eq. (2.80)). However, in the opposite limit in Eq. (2.81), where the hopping rate, γ, is high, the combined effects of mutual exclusion between the particles and persistent dynamics left the emergent interactions intact. The limit $\gamma \gg \omega$ is therefore of particular interest in this thesis.

Furthermore, the $\gamma \gg \omega$ limit is an expression of scale separation in the transition rates of the model of interacting run-and-tumble random walkers. Thus it presents an opportunity to apply Eq. (4.15) in a case where there are only two edge weights: γ and ω. In this section I will show the leading-order probability weight can be exactly calculated for every configuration by explicitly finding every term in Eq. (4.15) explicitly. Of course, the physics of this limit is already understood as it was derived from the exact solution in equations (2.63) and (2.76). However, later in this chapter we will see that this graph-theoretic approach is also able to provide an analytic expression for the $\gamma \gg \omega$ limit of the run-and-tumble model with reflecting boundaries, which was not accessible with the previous generating function approaches. Application to the model with periodic boundaries is therefore not only a proof of principle, it will also prepare us for the more involved work required to solve the reflecting boundaries case.

I now derive the limit Eq. (2.81) using the graph theory approach outlined by Eq. (4.15). The leading-order stationary probability of a configuration will consist of all the contributions of the spanning in-trees (with that configuration as the sink) that have the most hopping edges. Equivalently, these are the spanning in-trees with the fewest tumbles. The leading-order stationary probability weight of a configuration will therefore have the form

$$f_{\text{lead}}(\mathcal{C}_i) = \gamma^{h_i}\omega^{t_i} \sum_{\phi_l \in \Phi_\gamma} 1, \tag{4.16}$$

where h_i is the number of hopping edges in the leading-order spanning in-trees for a particular state, t_i is the number of velocity reversal edges, and the sum counts the number of spanning in-trees at this order. Furthermore, for any configuration $\mathcal{C}_i$,

$$h_i + t_i = \Omega - 1, \tag{4.17}$$

where Ω is the total number of states in the two particle system. $\Omega - 1$ may be understood as the number of edges needed to join all the configurations in a spanning in-tree.

In the following subsection, we will see that it is straightforward to identify the value of h and t for each of the configurations in this system.

4.3.1 Hopping-only graphs

To identify the value of h_i, which then automatically gives t_i through Eq. (4.17), it is only necessary to find the number of hopping edges in the spanning in-tree or trees with the most hopping edges. As the spanning in-trees must connect all the configurations in the system, some tumbling edges will be necessary. For example, there is no way to connect configurations in $++$ to $+-$ without a tumble edge.

Intuitively, the structure of the spanning in-tree(s) with the most hopping edges will be related to the graphs containing all possible hopping edges within each velocity sector. Graphs with all the possible hopping edges in each velocity sector are termed *hopping-only graphs*. By connecting up modifications of the hopping-only graphs with tumbling edges, it should be possible to construct the spanning in-trees with the most hopping edges.

In Figures 4.3 and 4.4 the hopping-only graphs are drawn for the $++$ and $+-$ velocity sectors. We can take advantage of the symmetries with $--$ and $-+$, and therefore do not need to draw their hopping-only graphs explicitly.

The hopping-only graphs have a straightforward structure. In order to draw full spanning in-trees a number of observations are useful. First, in the $++$ sector every configuration is accessible from any other through hopping edges only, as is shown in Figure 4.3. It follows that it is possible to connect a sink $\mathcal{C}$ in $++$ to all other $++$ configurations in a spanning in-tree with only hopping edges. This is depicted in Figure 4.5. The sink, coloured in cyan, could equivalently be

moved to any other configuration $(n, ++)$ and still be accessible from every other $++$ configuration using only hopping edges. Therefore for $\mathcal{C}$ in $++$ the task of constructing the spanning in-trees is reduced to connecting all the configurations in the other velocity sectors to some configuration (not necessarily $\mathcal{C}$) in $++$. By symmetry, it is the same for sinks in $--$.

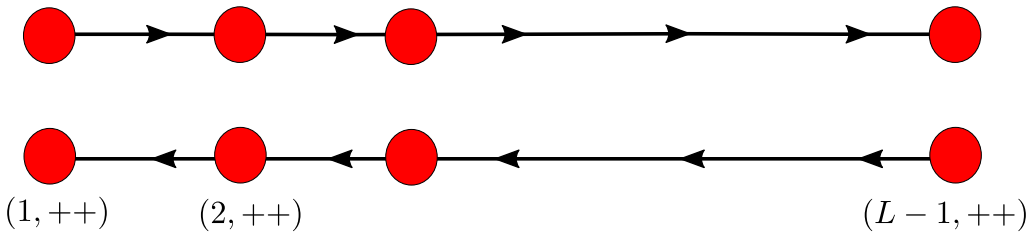

Figure 4.3 *Graphs for the $++$ sector with only hopping edges with configurations denoted by circles and hopping edges in and out of configurations by arrows.*

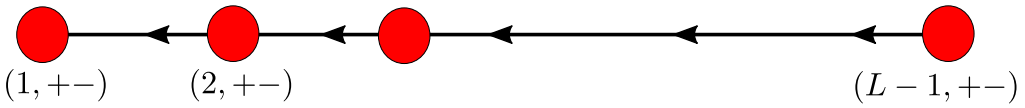

Figure 4.4 *A graph of the $+-$ sector with only hopping edges*

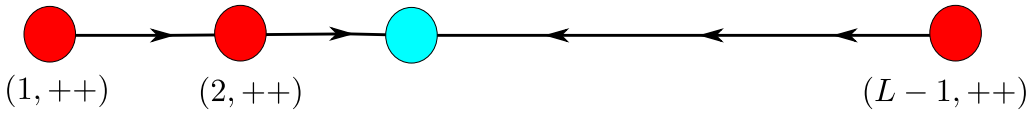

Figure 4.5 *A graph with all edges in $++$ leading to a configuration coloured in cyan.*

The hopping-only graphs for the $+-$ sector are different. The configurations $(1, +-)$ and $(L-1, +-)$ are special. All configurations in $+-$ can be reached only via hopping edges from $(L-1, +-)$, and all configurations can be connected to $(1, +-)$ only along hopping edges. For $-+$, the symmetric configuration to

$(1, +-)$ is $(L-1, -+)$ and has the same feature. Similarly, for $(L-1, +-)$ the symmetric configuration in $-+$ is $(1, -+)$. These will play a key role in constructing spanning in-trees with the fewest tumbling edges.

4.3.2 Connecting the hopping-only graphs

The fact that all configurations in $+-$ can be connected to $(1, +-)$ only by hopping edges provides a way to connect all configurations in $+-$ to a sink in a different velocity sector without introducing many tumbling edges. They can be first routed through $(1, +-)$, which can then be connected by a tumbling edge to a different velocity sector.

Similarly, $(L-1, +-)$ provides a way to connect configurations from other velocity sectors to a sink in $+-$. Both $(1, +-)$ and $(L-1, +-)$ can work together to provide access to sinks in $+-$. These special states are shown in Figure 4.6. Analysis of Figure 4.6 permits evaluation of h_i for every configuration $\mathcal{C}_i$. We consider each velocity sector in turn.

Calculation of h for the $++$ configurations proceeds in four steps. The first step is to consider $(1, ++)$ as a sink and connect all configurations in $++$ to $(1, ++)$, which can be achieved with only hopping edges. This is shown in Figure 4.7. The following three steps are shown in Figure 4.8. They involve connecting the remaining configurations in the system, which are all in other velocity sectors, to some configuration in $++$. As all $++$ configurations are already connected to the sink, once this is done, we will have a spanning in-tree.

In steps 2 and 3, all configurations in $+-$ and $-+$ are connected to the sink. In step 2, $+-$ configurations are connected by hopping edges to $(1, +-)$. $(1, +-)$ is then connected by one tumbling edge to $(1, ++)$. In step 3, all configurations in $-+$ can be connected by hopping only edges to $(L-1, -+)$. $(L-1, -+)$ can be connected by one tumbling edge to $(L-1, ++)$, which in turn is connected by hopping only edges to $(1, ++)$.

In the final step, we consider the $--$ configurations. As any configuration in $--$ can be connected to any other by only hopping edges, we can pick any configurations to act as a 'sub-sink' for all the configurations in $--$. Then we require only one tumbling edge to connect to any configuration in either $+-$ or $-+$, which from steps 2 and 3 will already be connected to $(1, ++)$.

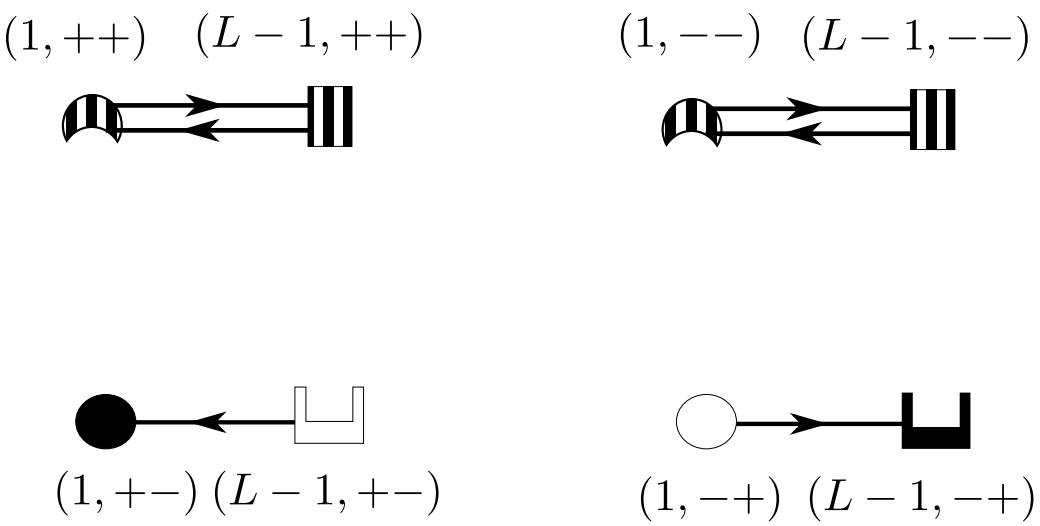

Figure 4.6 *A schematic of the key configurations in the model with periodic boundaries. Configurations that can be reached by hopping edges only from any other configuration in their velocity sector are coloured in black. Configurations that can reach any other configuration in their velocity sector are coloured in white. The configurations in* $++$ *and* $--$ *are both, so are striped black/white. Those configurations that can be linked by a tumbling edge to configurations in other velocity sectors have complementary shapes. For example, the crescent* $(1, ++)$ *configuration can be linked by a tumbling edge to the circular* $(1, +-)$ *configuration.*

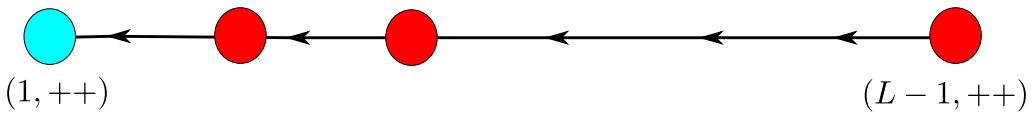

Figure 4.7 *All configurations in* $++$ *are connected to* $(1, ++)$ *by hopping edges only.*

This completes a spanning in-tree for $(1, ++)$, which has three tumbling edges. We know that this is the minimum number possible, as at least one tumbling edge is required to connect configurations in one velocity sector to a sink in a different velocity sector. There are always three velocity sectors apart from the one housing the sink. There are, of course, further spanning in-trees that can be formed for $(1, ++)$, which we will address in the next subsection. Turning to the number of tumbling edges for the other configurations in $++$, we can use the

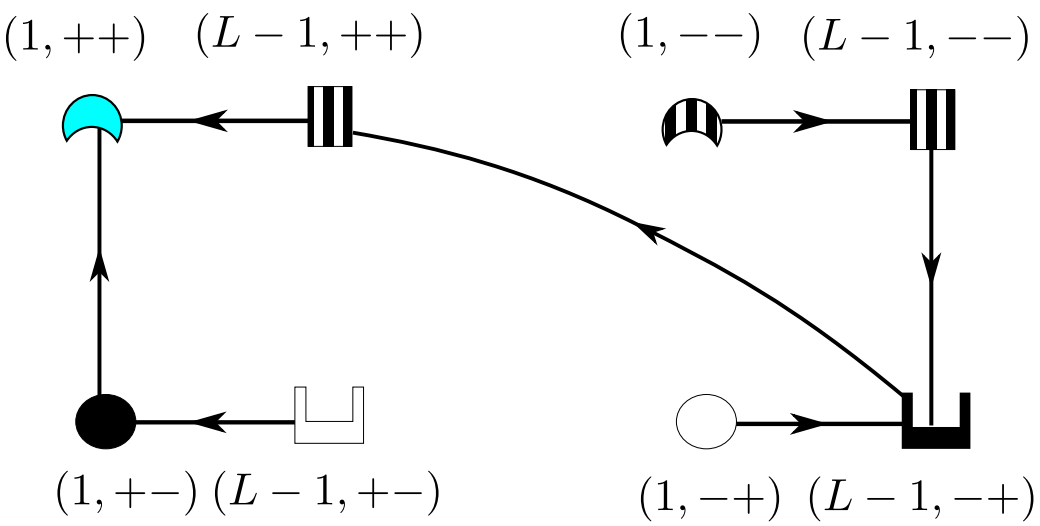

Figure 4.8 *All configurations are connected to the sink* $(1,++)$ *in a spanning in-tree.*

fact than any configuration in $++$ can be connected to any other without the need for further tumbling edges. Thus all $++$ sinks required the same number of tumbling edges as $(1,++)$. By symmetry this analysis also holds for $--$. Thus a spanning in-tree for any configuration in $++$ (or $--$) can be constructed with only three tumbling edges.

The construction of spanning in-trees for the $(1,+-)$ and $(L-1,-+)$ configurations is similar to the above for $++$. This is because every configuration in their respective sectors can be connected to them via only hopping edges. However, when other $+-$ and $-+$ configurations are the sinks, this is not possible and will necessitate further tumbling edges out of $+-$ or $-+$.

Therefore we can determine that only $(1,+-)$ and $(L-1,-+)$ will contribute at the same order as the $++$ and $--$ configurations. To recover Eq. (2.81), we can then safely ignore the other configurations in $+-$ or $-+$. Using the symmetry between $(1,+-)$ and $(L-1,-+)$, t for $(1,+-)$ will be the same as $(L-1,-+)$. We therefore now find t for $(1,+-)$.

A spanning in-tree with the minimum tumbling edges for $(1,+-)$ is shown in Figure 4.9. It may be constructed as follows. All configurations in $+-$ may be connected by only hopping edges to $(1,+-)$. Then all configurations in $++$ and

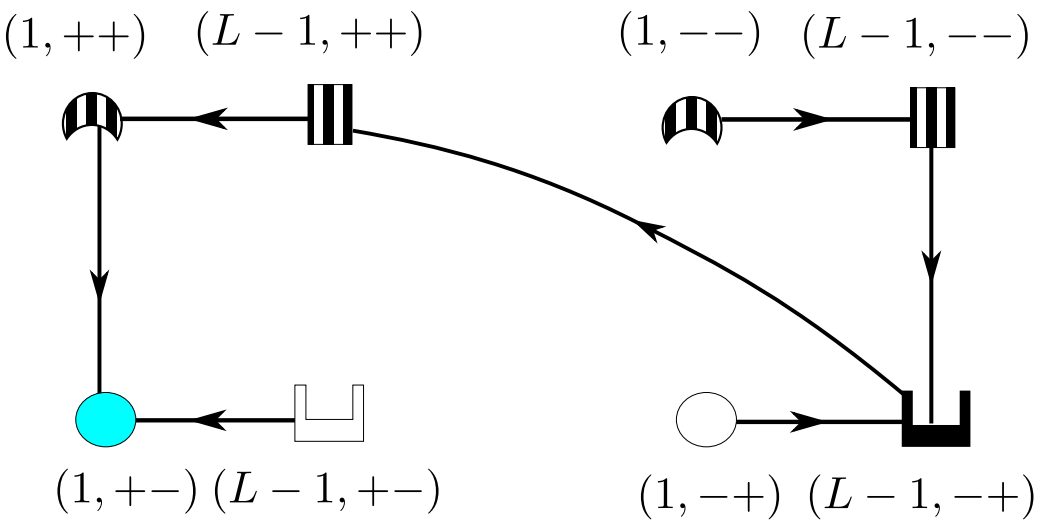

Figure 4.9 *All configurations are connected to the sink* $(1,+-)$ *in a spanning in-tree.*

$--$ may be connected by only hopping edges to $(1,++)$ and $(1,--)$ respectively. $(1,++)$ and $(1,--)$ may be connected to $(1,+-)$ by a tumbling edge each. Lastly, all configurations in $-+$ may be connected to $(L-1,+-)$, which may be connected to any configuration in $++$ or $--$ as these configurations are already connected to $(1,+-)$.

4.3.3 Recovery of the low-tumble limit

It remains to determine how many spanning in-trees there are for each $++$ (and $--$) configuration, and for $(1,+-)$ and $(L-1,-+)$. Here symmetry can be used to shorten the calculation. Every configuration in $++$ is equivalent in terms of the construction of spanning in-trees because they are all mutually accessible. Therefore they have the same number of spanning in-trees at this leading order. Secondly, as each velocity sector must have $1/4$ of the probability and there are $L-1$ configurations in $++$, the leading order probability is

$$P_{++}(n) = \frac{1}{4(L-1)}, \tag{4.18}$$

which recovers the result in Eq. (2.81). The calculation is even easier for $(1, +-)$ as it is the only contribution at this order. Therefore

$$P_{+-}(n) = \frac{1}{4}\delta_{n,1}, \tag{4.19}$$

recovering the second part of the result in Eq. (2.81).

4.4 A run-and-tumble model with reflecting boundaries

I now define a new run-and-tumble model, with the same bulk dynamics as the instant tumbling model but different boundary conditions: reflecting boundaries. As before, we have lattice-based run-and-tumble random walkers under mutual exclusion that hop at rate γ on a lattice of N sites (distinguishing this model from the L-site lattice with periodic boundaries). A state is uniquely described by $(a\delta, b\epsilon)$, where $a, b = 1, ..., N$ are the occupied sites, and $\delta, \epsilon = \pm$ are the directions. For example, a configuration $(1+, 2+)$ means the first particle is right-moving and on site 1, and the second particle is also right-moving and on site 2. Velocity reversal occurs for each particle at rate ω as for the instant tumbling model in chapter 2. The model is depicted in Figures 4.10 and 4.11.

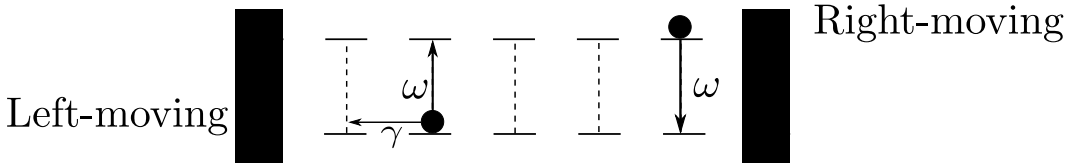

Figure 4.10 *Microscopic update schematic for separated particles, with one at a boundary: this diagram shows an example configuration of the model, with a right-moving particle depicted on the upper row, and a left-moving particle on the lower row. The arrows signify which microscopic dynamical updates are available to the particles. The right-hand particle is blocked by the boundary, so velocity reversal is the only option available to it. The left-hand particle is freely moving.*

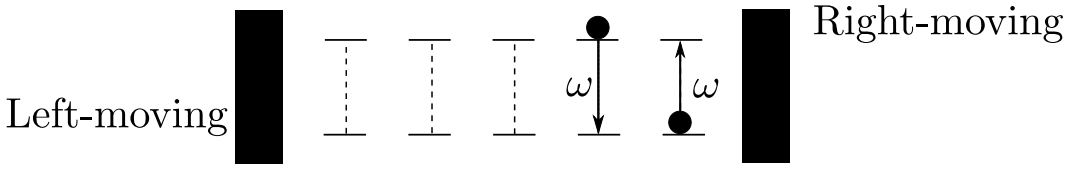

Figure 4.11 *Microscopic update schematic for particles colliding at a boundary: this diagram shows an example configuration of the model, with a right-moving particle depicted on the upper row, and left-moving particle on the lower row. The arrows signify which microscopic dynamical updates are available to the particles. The right-hand particle is left-moving, and so it is not blocked by the boundary, but as it is in a collision with the left-hand particle velocity reversal is the only option available to it.*

I now apply the scale-separated steady-state formula in (4.15) to the run-and-tumble model with reflecting boundaries.

4.5 Leading-order exponents

As for the run-and-tumble model with periodic boundaries, the leading-order probability weights for configurations in the model with reflecting boundaries will be of the form of Eq. (4.16). Calculation of the weights also proceeds along the same principles as the periodic boundaries case, although enumeration of the spanning in-trees is significantly more involved. In this section, I elucidate the structure of the hopping-only graphs of the reflecting boundaries model, which enables identification of the leading-order exponents, h and t, for every configuration. In the next section, I shall enumerate the corresponding spanning in-trees for each configuration using lattice path enumeration methods.

4.5.1 Hopping-only graphs

In Figures 4.12—4.15 the hopping-only graphs of the four velocity sectors for the run-and-tumble model with reflecting boundaries are drawn. Note that the symmetry in $+-$ and $-+$ is broken by the walls. The symmetry between $++$ and $--$, however, remains.

The following features of the hopping-only graphs, which formalise the role of the

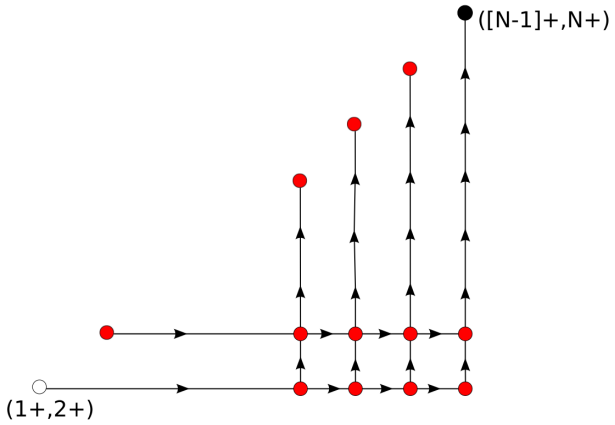

Figure 4.12 *A schematic of the hopping-only graph for ++ sector. As this is a schematic for an arbitrary system with N lattice sites only some of the configurations are drawn, and are indicated with circles. Similarly, only some edges are included. The hopping subsource $(1+, 2+)$, denoted by a white circle, can reach any configuration in ++. Similarly, all configuration can be connected to the hopping subsink $([N-1]+, N+)$, which is denoted by a black circle.*

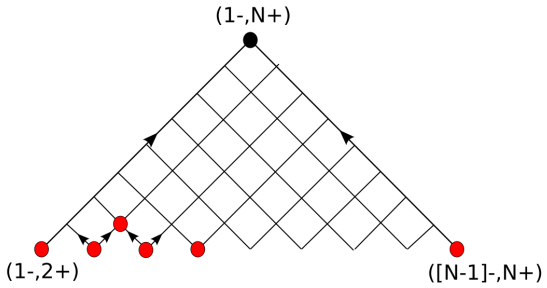

Figure 4.13 *A schematic of the hopping-only graph for −+ sector. As this is a schematic for an arbitrary system with N lattice sites only some of the configurations are drawn, and are indicated with circles. Similarly, only some edges are included. All configurations can be connected to the hopping subsink $(1+, N-)$, which is denoted by a black circle.*

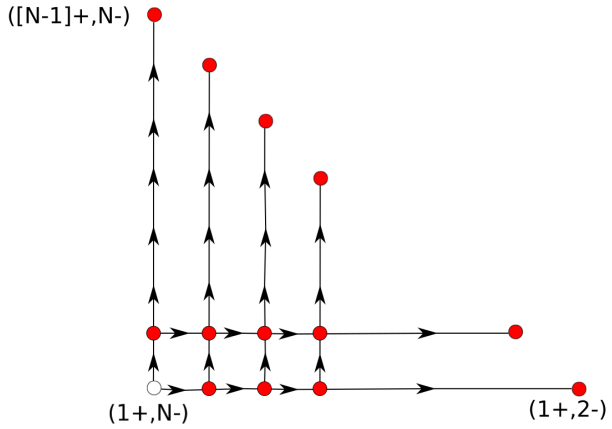

Figure 4.14 *A schematic of the hopping-only graph for $+-$ sector. As this is a schematic for an arbitrary system with N lattice sites only some of the configurations are drawn, and are indicated with circles. Similarly, only some edges are included. The hopping subsource $(1-, N+)$, denoted by a white circle, can reach any configuration in $+-$.*

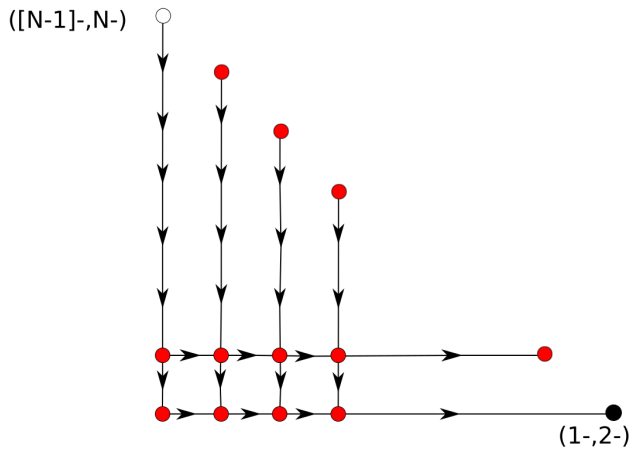

Figure 4.15 *A schematic of the hopping-only graph for $--$ sector. As this is a schematic for an arbitrary system with N lattice sites only some of the configurations are drawn, and are indicated with circles. Similarly, only some edges are included. The hopping subsource $([N-1]-, N-)$, denoted by a white circle, can reach any configuration in $++$. Similarly, all configuration can be connected to the hopping subsink $(1-, 2-)$, which is denoted by a black circle.*

key configurations familiar from the periodic boundaries case, will be of use in finding the exponents of the leading order spanning in-trees:

1. The $++$, $--$ and $+-$ graphs have *hopping subsources* (white circles): vertices from which any other vertex within the hopping-only graph can be reached only along hopping edges.

2. The $++$, $--$ and $-+$ graphs have *hopping subsinks* (black circles): vertices to which any other vertex within the hopping-only graph can reach only along hopping edges.

As argued before for the model with periodic boundaries, the leading-order spanning in-trees will be determined by connecting the hopping-only graphs with the fewest tumbles. We will see how to do this using an analogous formulation to the key configurations depicted in Figure 4.6 for the periodic boundaries model.

4.5.2 Connecting the hopping-only graphs

A schematic of the key configurations is shown in Figure 4.16. This reduced description of the hopping-only graphs will be used to find the leading-order exponents and, in the next section, to explicitly enumerate the leading-order spanning in-trees. It is these key configurations, analogous to those in Figure 4.6 for the periodic boundaries model, on which all tumbling edges are dependent to leading order regardless of the actual sink of any one spanning in-tree.

To summarise the goal briefly: a leading-order spanning in-tree connects all the configurations in the system to the sink, either by direct tumbling/hopping to the sink or indirectly through other configuration(s) connected directly by hopping to the sink, with the minimum number of tumbles. In practice, this means connecting some of the key configurations identified in Figure 4.16 with tumbling edges. Note that each of the jammed configurations $(a+, [a+1]-)$, unless acting as the sink of the in-tree, *must* tumble because they cannot hop to any other configuration. Similarly, all the hopping subsinks must tumble. Given these constraints, and that spanning in-trees must contain no loops, the minimum number of tumbles for in-trees of a particular state can be counted.

There are fourteen separate calculations required to find the leading-order exponents for all the configurations. However, these can be reduced to four

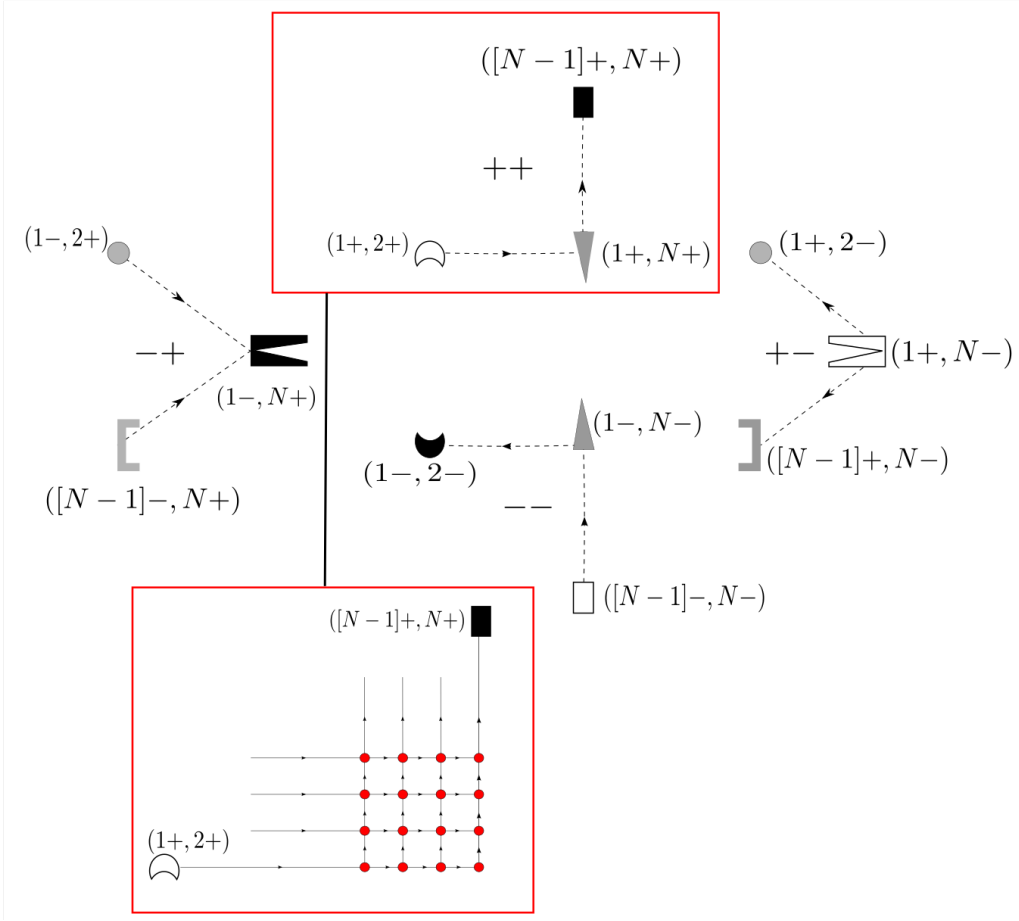

Figure 4.16 *A schematic of the key configurations. The dotted lines with arrows indicate the direction of hopping within the sectors. Hopping subsources are coloured in white. Hopping subsinks are depicted in black. The configurations which can tumble directly to each other have complementary shapes. For example, the crescent* $(1-, 2-)$ *may tumble directly to the circular* $(1+, 2-)$*.* $(1-, 2-)$ *may not tumble directly to* $(1+, 2+)$ *- it would require two tumbles - and therefore these states do not have a complementary shapes.*

cases, which are shown in detail below. The full set of leading-order exponents may be found in Table 4.1. All expressions have been checked explicitly using a computational algebra engine up to $N = 10$.

Case 1: $([N-1]+, N+)$

We first consider the hopping subsink $([N-1]+, N+)$ as the sink of the whole spanning in-tree. An example of a leading-order tumbling diagram is shown in Figure 4.17.

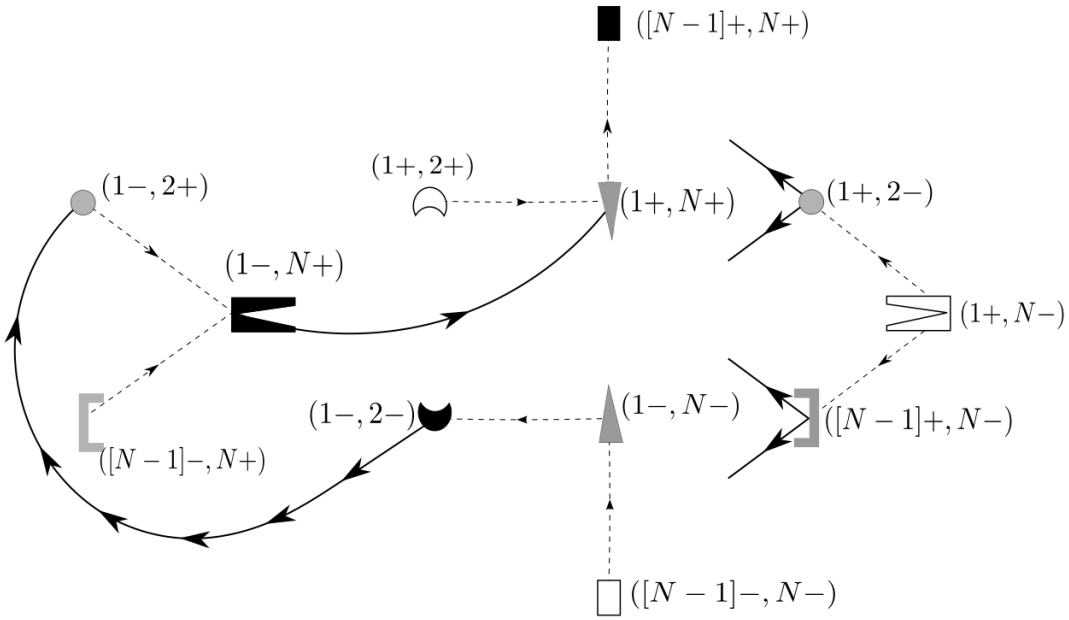

Figure 4.17 *A leading order tumbling diagram for* $([N-1]+, N+)$ *as the sink of the spanning in-tree. This schematic only shows the key configurations as detailed in Figure 4.16 and the corresponding edges in to them and out of them. The unconnected arrows from* $(1+, 2-)$ *and* $([N-1]+, N-)$ *indicate that they may tumble to either the* $++$ *or* $--$ *sectors. This is the case for all the remaining further* $N-3$ *jammed configurations, which are not explicitly shown in this diagram. As* $([N-1]+, N+)$ *is a hopping sink for the* $++$ *sector, it is sufficient for all states to be connected to the* $++$ *sector as wherever they are connected to by tumbling in the* $++$ *sector, they will then be connected to* $([N-1]+, N+)$ *by hopping within the* $++$ *sector.*

As long as every configuration in the other sectors is connected to some state in the $++$ sector, which will necessarily involve tumbling, and there are no loops, then we have an in-tree for $([N-1]+, N+)$. No further tumbling edges are required, as all $++$ sector states may be connected by hopping to $([N-1]+, N+)$.

The $--$ and $-+$ sectors have hopping subsinks. We exploit these to minimise the number of tumbles: all states in these sectors will be connected to $([N-1+], N+)$ via their respective hopping subsinks. Only one tumble is then required from each of the $--$ and $-+$ sectors. We are left to consider the $+-$ sector. Together, all the states in the $+-$ sector can hop to one of the $N-1$ jammed configurations $(a+, [a+1]-)$. We therefore require all the jammed configurations to tumble, but

no others in the $+-$ sector. In total, we require $2+(N-1)=N+1$ tumbles for each of the leading order spanning in-trees of $([N-1+],N+)$. We now have the exponent for $([N-1+],N+)$: $\gamma^{2(N-1)N-N-2}\omega^{N+1}$.

A similar analysis holds for the other hopping subsinks $(1-,2-)$ and $(1-,N+)$, where states in $++$ are connected to them via a tumbling edge from $([N-1+],N+)$. $(1-,2-)$ and $(1-,N+)$ therefore have the same leading-order exponents.

Case 2: $(a+,b+)$

We now consider the other configurations in the $++$ sector, namely $(a+,b+)$. Again, we take advantage of the hopping subsources and subsinks in each of the sectors. We note that the spanning in-trees will be very similar to those for $([N-1]+,N+)$ with one added complication: configurations of the form $(a+,b+)$ are not hopping subsinks. Therefore a number of configurations within the $++$ sector cannot be connected by hopping to $(a+,b+)$ and the paths within the $++$ sector will split into two.

In order to address this complication, we note that $(1+,2+)$, as a hopping subsource, can always be connected by hopping to any $(a+,b+)$. Let us impose this condition, i.e. $(1+,2+)$ is connected by hopping edges to $(a+,b+)$. A schematic for this *backbone* can be found in Figure 4.18. We then note that as long as $([N-1]+,N+)$ is connected via tumbling to a configuration in another velocity sector to $(1+,2+)$ we can recycle much of the analysis in Case 1. This will produce leading-order spanning in-trees because it maximises hopping by

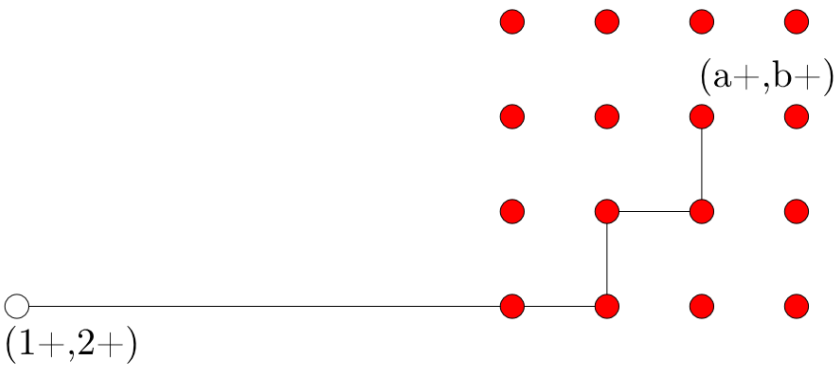

Figure 4.18 *A path from the $++$ hopping subsource to a configuration in $++$.*

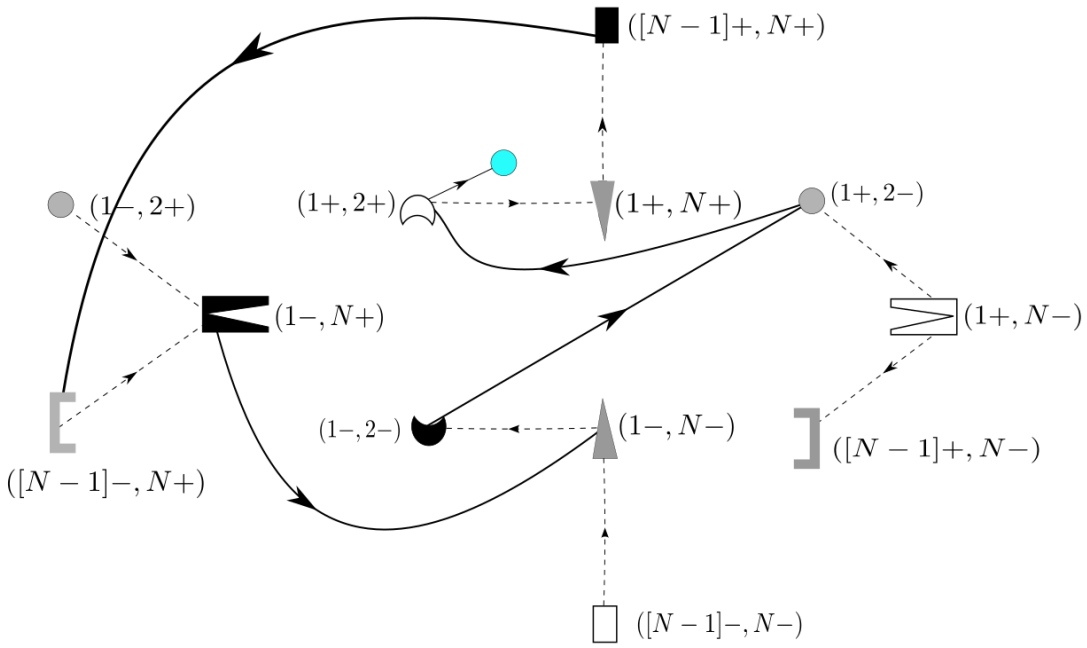

Figure 4.19 *A tumbling diagram for a sink $(a+, b+)$, $b \neq N$. The sink is coloured in cyan. Note that all the hopping sinks tumble.*

making use of the hopping subsink $([N-1]+, N+)$.

Thus the leading-order spanning in-trees for $(a+, b+)$ have one more tumble than for $([N-1+], N+)$, as the configuration $([N-1+], N+)$ must tumble to some other velocity sector, before being connected to the sink in $++$ through that other velocity sector configuration. Hence, the exponent is given by $\gamma^{2(N-1)N-N-3}\omega^{N+2}$. An example tumbling diagram is shown in Figure 4.19.

By symmetry, $(a-, b-)$ spanning in-trees have the same leading-order exponents as $(a+, b+)$ configurations. Furthermore, this same backbone argument, where the backbone is made by imposing the condition that the sink is connected to the hopping subsource in same hopping-only graph, can be made for the other configurations to derive their leading-order exponents, as well shall see with the next example.

Case 3: $(a+, b-)$

For the $+-$ sector, we first consider the configurations $(a+, b-)$, $|b-a| > 1$. As was the case for $(a+, b+)$, $(a+, b-)$, $|b-a| > 1$ is not a hopping subsink. Therefore at least one extra tumbling edge is required compared to the configurations with spanning in-trees with the fewest tumbles, such as $([N-1]+, N+)$.

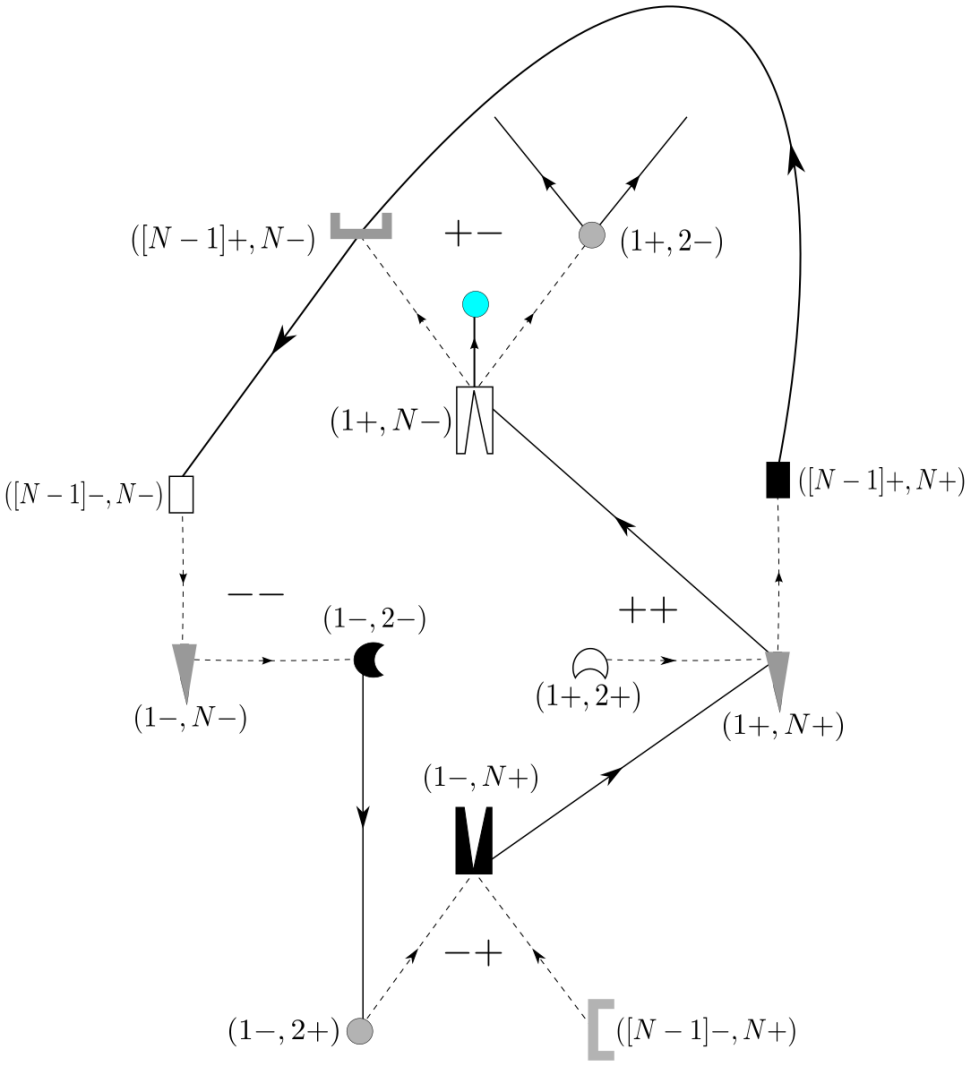

Figure 4.20 *A tumbling scheme for leading-order spanning in-tree with a sink* $(a+, b-)$, $|b-a|>1$. *All* $--$ *configurations are routed through* $(1-, 2+)$ *first, and then* $(1+, N+)$, *which tumbles directly to* $(1+, N-)$. $(1+, N-)$ *is connected by hopping edges to the sink.*

When building a spanning in-tree with $(a+, b-)$, $|b-a|>1$ as the sink, we can make use of the hopping subsource $(1+, N-)$ and impose the condition that it is connected by hopping edges to $(a+, b-)$, $|b-a|>1$. Thus a backbone is formed in much the same way as was done in the previous example where $(1+, 2+)$ was connected by hopping edges to $(a+, b+)$.

It remains to ensure that all the other configurations in the system are somehow connected to this backbone. Here we can make further use of the hopping subsinks in $++$, $--$ and $-+$ so the problem reduces to ensuring the key configurations

$([N-1+], N+)$, $(1-, 2-)$ and $(1-, N+)$, as well as the remaining configurations in $+-$, are connected to the backbone.

$(1-, N+)$, through which all $-+$ configurations can be connected by hopping edges, cannot be connected by a tumbling edge directly to $(1+, N-)$. Therefore configurations in $-+$ have to be routed through $++$ or $--$ in order to be connected to $+-$. This restriction will mean that an extra tumbling edge is required for spanning in-trees of $(a+, b-)$, $|b-a| > 1$ configurations compared to $(a+, b+)$ above.

Let us show this explicitly with an example of a leading-order spanning in-tree. $(1-, 2-)$, though which all $--$ configurations are connected, may be connected via a tumbling edge to $(1-, 2+)$. $(1-, N+)$, through which all $-+$ configurations, and now all $--$ configurations, are linked may be connected to $(1+, N+)$. $(1+, N+)$ may then be connected via a tumbling edge to $(1+, N-)$, and thus to the sink $(a+, b-)$, $|b-a| > 1$. The remaining $++$ configurations not connected to $(1+, N-)$ via $(1+, N+)$, can hop to $([N-1]+, N+)$, which can then tumble to $-+$ to be connected to the sink via $(1+, N-)$. Lastly, all configurations in $+-$ not connected to the sink via the backbone can hop to one of the jammed configurations in $+-$, which necessarily tumble to either $++$ or $--$, where all configurations have already been connected to the sink. A diagram for this tumbling scheme is shown in Figure 4.20. The resulting leading-order exponent is $\gamma^{2(N-1)N-N-4}\omega^{N+3}$.

It might be expected that this analysis would also hold for the jammed configurations $(a+, [a+1]-)$. However, in the above scheme for $(a+, b-)$, $|b-a| > 1$ all jammed configurations tumble, but should not when they are sinks. Therefore for the jammed configurations one less tumbling edge is required, and they have leading-order exponents of $\gamma^{2(N-1)N-N-3}\omega^{N+2}$.

Case 4: $(a-, b+)$

It remains to derive the leading-order exponents for $(a-, b+)$. Let us consider $(a-, b+)$, $a, b \neq 1, N$ first. For $-+$ there is no hopping subsource within the hopping-only graph to use as the origin for the backbone, as we did for the previous two examples. Therefore the backbone, rather than being in the sink's hopping-only graph, will be in either $++$ or $--$. The backbone will end at either $(a+, b+)$ or $(a-, b-)$. One of these configurations can collect all the other configurations in the in-tree and then tumble directly to the sink $(a-, b+)$. Depending on whether $(a+, b+)$ or $(a-, b-)$ is chosen as the configuration to

tumble directly to the sink, the hopping subsource in $++$, $(1+, 2+)$, or $--$, $([N-1]-, N-)$, respectively will be the origin of the backbone.

Let us consider an example explicitly where $(a+, b+)$ is chosen as the configuration at the end of the backbone, exactly as in Figure 4.18. We want all the configurations in the system, except the sink $(a-, b+),\ a, b \neq 1, N$, to be connected to $(a+, b+)$ via $(1+, 2+)$. All configurations in $--$ can be connected via the hopping subsink $(1-, 2-)$ to $(1+, 2-)$ with a tumbling edge and then $(1+, 2+)$ through a further tumbling edge. If all $+-$ jammed configurations tumble to $--$ then they will also be connected to the sink. $([N-1]+, N+)$ can collect all those configurations in $++$ not part of the backbone, and, via a tumbling edge to $+-$, be connected to the sink.

We can then make use of the fact that all the configurations in $-+$ can be connected via hopping edges to $(1-, N+)$. $(1-, N+)$ can be connected via a tumbling edge to $(1-, N-)$, which in turn we know is connected to the sink, as all $--$ configurations have already been connected to the sink. Thus the leading order exponent for the configurations $(a-, b+),\ a, b \neq 1, N$ is $\gamma^{2(N-1)N-N-4}\omega^{N+3}$.

For $(a-, N+),\ a > 1$, and its symmetric counterpart $(1-, b+),\ b < N$, one less tumbling edge is required. This is because it is possible to construct a backbone within $-+$ for such configurations. Let us consider an example explicitly.

For a sink on the $N+$ branch in $-+$, $(a-, N+),\ a > 1$, the configuration $([N-1]-, N+)$ can be connected by hopping edges to it to form the backbone. We can then make use of the hopping subsink in $++$, $([N-1]+, N+)$, which can be connected by a tumbling edge to $([N-1]-, N+)$, and thus connected to the sink. By routing all the other configurations in the spanning in-tree through $([N-1]+, N+)$ we eliminate the need for the tumble directly to the sink from its conjugate configuration in $++$ or $--$, as required above.

4.5.3 Table of leading-order exponents

The leading-order exponents for all the configurations are brought together in the table below. These have been checked up to $N = 10$ using by explicitly solving Eq. (4.4) for this system using a computational algebra package.

From Table 4.1, a hierarchy in the weights is immediately apparent. We see that jammed configurations by the walls are of the highest order. In contrast

State(s)	Exponent
$([N-1+], N+)$	$\gamma^{2(N-1)N-N-2}\omega^{N+1}$
$(a+, b+), \quad a \neq N-1$	$\gamma^{2(N-1)N-N-3}\omega^{N+2}$
$(1-, 2-)$	$\gamma^{2(N-1)N-N-2}\omega^{N+1}$
$(a-, b-), \quad b \neq 2$	$\gamma^{2(N-1)N-N-3}\omega^{N+2}$
$(1+, 2-)$	$\gamma^{2(N-1)N-N-2}\omega^{N+1}$
$([N-1]+, N-)$	$\gamma^{2(N-1)N-N-2}\omega^{N+1}$
$(a+, [a+1]-)$, $a, \neq 1, N-1$	$\gamma^{2(N-1)N-N-3}\omega^{N+2}$
$(a+, b-),\ \lvert b-a\rvert > 1,$	$\gamma^{2(N-1)N-N-4}\omega^{N+3}$
$(1-, N+)$	$\gamma^{2(N-1)N-N-2}\omega^{N+1}$
$(1-, b+),\ b < N$	$\gamma^{2(N-1)N-N-3}\omega^{N+2}$
$(a-, N+),\ a > 1$	$\gamma^{2(N-1)N-N-3}\omega^{N+2}$
$(a-, b+),\ a, b \neq 1, N$	$\gamma^{2(N-1)N-N-4}\omega^{N+3}$

Table 4.1 *Table of leading order exponents of the weights of the run-and-tumble model with reflecting boundaries.*

to the run-and-tumble model with periodic boundaries, jammed configurations are not only those of type $(a+, [a+1]-)$ but also include several configurations jammed by the walls: $([N-1]+, N+)$ and its symmetric counterpart $(1-, 2-)$, $(1+, 2-)$, $([N-1]+, N-)$ and $(1-, N+)$. These exponents demonstrate that not only is there an emergent attraction between the particles, but there is also an emergent attraction between the particles and the walls, at least in the low-tumble limit. We note that this leading-order approximation does not capture any difference between the sub-leading orders of these configurations. In this limit, the particle interaction with the walls dominates the inter-particle attraction: jammed configurations that are not jammed by the walls, of type $(a+, [a+1]-)$ where $a \neq 1, N-1$, are one order lower than the highest order. However, the jammed configuration where the particles are separated, $(1-, N+)$, is of the highest order.

We can understand this hierarchy of interactions by considering how the particles preferentially explore statespace in this low-tumble limit. That configurations $([N-1]+, N+)$, $(1-, 2-)$ and $(1-, N+)$ have the highest order exponents is most easily explained. When the two particles have the same velocity, $++$ or $--$, one of the particles will quickly hit one of the walls, and, as this particle jammed by the wall will take a long time to reverse its velocity in the low-tumble limit, the second particle will, on average, join it quickly. Thus the system will

be in one of the configurations $([N-1]+, N+)$ or $(1-, 2-)$ depending on which velocities the particles started with.

Once the particles are in one of these two configurations, after a velocity reversal of the outer particle ($a = N-1$ and $b = 2$ for $++$ and $--$ respectively), the outer particle will quickly hop to the other wall leading to the configuration $(1-, N+)$. Then a velocity reversal from either particle will lead back to $([N-1]+, N+)$ or $(1-, 2-)$, and so the cycle continues. $(1+, 2-)$ and $([N-1]+, N-)$ are of the highest order because they are jammed and are also likely to be tumbled into by the other highest-order configurations $(1-, 2-)$ and $([N-1]+, N+)$ respectively.

We can gain an understanding of the next-highest order by considering what happens inbetween the jamming with walls. When the outer particle tumbles out of $([N-1]+, N+)$ or $(1-, 2-)$, then either the left hand particle originally at $a = N-1$ for $++$ or right-hand particle originally at $b = 2$ for $--$ will begin the journey to the other wall, leaving the jammed particle behind. Hence, configurations of type $(a-, N+)$ or $(1-, b+)$ are of the next highest order.

In the case where both particle are moving in the same direction, but neither is at the walls, there is some small probability that the particle 'in front', i.e. nearer to wall in the direction of travel, will tumble. The particles will then quickly jam to the configurations $(a+, [a+1])$. These configurations will take a long time to unjam and hence they are of the next-highest order. When they do unjam it will be because one of the particles has changed its velocity, and so will return to configurations where the particles have the same velocity. Thanks to the necessity of going into configurations with $\sigma_1 = \sigma_2$ from the jammed configurations $(a+, [a+1]-)$, configurations of type $(a+, b+)$ and $(a-, b-)$ are, like the collisional configurations $(a+, [a+1])$ $a \neq 1, N-1$, of next-highest order.

The remaining configurations are of the lowest order in the leading-order exponents because they do not benefit from the jamming either of collisions between the particles or with the walls.

By analogy with the results for the run-and-tumble model with periodic boundaries, I can suggest some potential features of the full solution to the model with reflecting boundaries. The highest-order configurations in this low-tumble limit, which are all jammed by the walls, are likely to present δ-functions in the full solution, by analogy the jammed configuration $P_{+-}(1)$ in the periodic boundaries model Eq. (2.76). By analogy with the exponential decay in the distance between the particles generated by the stochastic hopping with resetting,

we might anticipate similar behaviour the configurations in this model. This would be due to the jamming from particle collisions, which acts as the reset, still present in this model. However, there could also be a second lengthscale, with associated exponential decay, due to the resetting caused by the walls.

In the scaling limit, again by analogy to the periodic boundaries model, we might expect the δ-functions from jamming to be preserved, but the lengthscale due to resetting from interparticle collisions to vanish and be replaced by a δ-function, as in equations (2.84) and (2.85) in section 2.5. However, by analogy with the lengthscale in the model with finite tumbling duration associated with one particle on its site tumbling and the other running that remains finite in the scaling limit, it is possible that a lengthscale due to the walls, should it exist in the lattice model, would present similar behaviour in the scaling limit.

4.6 Enumeration of the leading-order spanning in-trees

In order to find the leading-order expressions (4.16), it remains to evaluate the sum $\sum_{\phi_l \in \Phi_\gamma} 1$ for each configuration: to actually count all of the leading-order spanning in-trees associated with each configuration. These are of interest for two reasons. First, these *prefactors* may shed further light on the behaviour of the run-and-tumble system with reflecting boundaries in the low-tumble limit, complementing the picture established by the leading-order exponents. We have already seen from the corresponding limit for the periodic boundaries case in equations (4.18) and (4.19) that these prefactors are significant. Second, they will enable us to establish the range of validity of the leading-order weights by comparing the analytic results to simulations of the system for different values of the parameter combination γ/ω. In this section, we find these prefactors for the run-and-tumble model with reflecting boundaries.

Enumeration of the spanning in-trees requires more involved calculations than were needed for the leading-order exponents in the previous section; no shortcuts of the type in subsection 4.3.3 are available to us here. Following the exponents approach in the previous section, we can calculate examples explicitly that demonstrate all the methods necessary to enumerate the prefactors for all the configurations. First, I present the full list of prefactors, which may be found in

Table 4.2.

4.6.1 Table of prefactors

The number of spanning in-trees at the leading order for each configuration is shown in Table 4.2 below. As for the leading-order exponents, the expressions in this table have been checked explicitly using an computational algebra engine up to $N = 10$.

Table 4.2 complements Table 4.1 to give us more precise information about the relative stationary probability weights of the system's configurations in the low-tumble limit. We can see that the three hopping subsinks, $(1-, 2-)$, $([N-1]+, N+)$ and $(1-, N+)$ each have the same weight in this limit. Interestingly, the other configurations jammed at the wall $(1+, 2-)$ and $([N-1]+, N-)$ have half the weight of the hopping subsinks. This might be understood as deriving from the fact that they do not benefit from having a high probability of being hopped to: for example, if the left-hand particle is at the left boundary, $a = 1$, and the right-hand particle is separated from it at $b \gg 2$, it is unlikely that the right-hand particle would hop all the way to $b = 2$ before the left-hand particle moves. Thus these configurations only occur when the appropriate particle tumbles in $(1-, 2-)$ or $([N-1]+, N+)$. The other expressions in Table 4.2 capture even greater variation in the leading-order weights in this limit.

The sums over binomial coefficients reflect the interplay of the interactions between the particles and between the particles and the walls. In the following subsections I elucidate how they arise from the enumeration of the leading-order spanning in-trees for each of the configurations. These calculations do not form an exhaustive list of every step required to find the prefactors in 4.2, but they are representative of all the types of calculations needed. Details of the remaining steps are outlined at the end of this section.

State(s)	Prefactor
$([N-1+], N+)$	$2^{2(N-1)N-6N+10}$
$(a+, b+), \quad b < N$	$2^{2(N-1)N-6N+12-a-b}\binom{a+b-3}{a-1}$
$(a+, N+), \quad a \neq N-1$ if $a > 1$ add term:	$2^{2(N-1)N-7N+12} + 2^{2(N-1)N-6N+10}$ $+2^{2(N-1)N-7N+13}\sum_{i=2}^{a} 2^{-i}\binom{i+N-4}{i-1}$
$(1-, 2-)$	$2^{2(N-1)N-6N+10}$
$(a-, b-), \quad a > 1$	$2^{2(N-1)N-8N+10+a+b}\binom{-a-b+2N-1}{-a+N-1}$
$(1-, b-), \quad b \neq 2$ if $b < N$ add term:	$2^{2(N-1)N-7N+12} + 2^{2(N-1)N-6N+10}$ $+2^{2(N-1)N-8N+12}\sum_{j=b}^{(N-1)} 2^{j}\binom{-j+2N-3}{N-3}$
$(1+, 2-)$	$2^{2(N-1)N-6N+9}$
$([N-1]+, N-)$	$2^{2(N-1)N-6N+9}$
$(1+, N-)$	$2^{2(N-1)N-7N+12} + 2^{2(N-1)N-6N+10}$
$(a+, [a+1]-)$, $a, \neq 1, N-1$	$2^{2(N-1)N-8N+14}\binom{N-2}{a-1} + 2^{2(N-1)N-7N+12}\binom{N-2}{a-1}$ $+2^{2(N-1)N-6N+12}\sum_{i=1}^{i=a}\sum_{j=a+1}^{j=N-1} 2^{-2j}\binom{-i+j-1}{a-i}\binom{i+j-3}{i-1}$ $+(2^{2(N-1)N-8N+12} + 2^{2(N-1)N-7N+10})\sum_{i=2}^{i=a} 2^{i}\binom{-i+N-1}{a-i}$ $+2^{2(N-1)N-8N+13}\sum_{i=2}^{a} 2^{i}\sum_{j=2}^{j=i} 2^{-j}\binom{-1-i+N}{a-i}\binom{-4+N+j}{j-1}$ $+2^{2(N-1)N-8N+10}\sum_{i=2}^{i=a+1}\sum_{j=a+1}^{j=N} 2^{2i}\binom{-i+j-1}{a-i}\binom{-i-j+2N-1}{-i+N-1}$ $+(2^{2(N-1)N-7N+13} + 2^{2(N-1)N-6N+11})\sum_{i=a+1}^{N-1} 2^{-i}\binom{i-2}{a-1}$ $+2^{2(N-1)N-8N+13}\sum_{i=a+1}^{i=N-1} 2^{-i}\binom{i-2}{a-1}\sum_{j=i}^{N-1} 2^{j}\binom{-j+2N-3}{N-3}$
$(a+, b-), \ \lvert b-a\rvert > 1,$ $a, b \neq 1, N$	$(2^{-a+b+2(N-1)N-8N+13} + 2^{-a+b+2(N-1)N-7N+11})\binom{a-b+N-1}{a-1}$ $+2^{2(N-1)N-6N+11-a+b}\sum_{i=1}^{a}\sum_{j=b}^{N-1} 2^{-2j}\binom{a-b-i+j}{a-i}\binom{i+j-3}{i-1}$ $+(2^{2(N-1)N-8N+13-a+b} + 2^{2(N-1)N-7N+9-a+b})\sum_{i=2}^{a} 2^{i}\binom{a-b-i+N}{a-i}$ $+2^{2(N-1)N-8N+12-a+b}\sum_{i=2}^{a} 2^{i}\binom{a-b-i+N}{a-i}\sum_{j=2}^{i} 2^{-j}\binom{j+N-4}{j-1}$ $+2^{2(N-1)N-8N+9-a+b}\sum_{i=2}^{a}\sum_{j=b}^{N} 2^{2i}\binom{a-b-i+j}{a-i}\binom{-i-j+2N-1}{-i+N-1}$ $+\left(2^{2(N-1)N-7N+12-a+b} + 2^{2(N-1)N-6N+10-a+b}\right)\sum_{i=b}^{N-1} 2^{-i}\binom{a-b+i-1}{a-1}$ $+2^{2(N-1)N-8N+12-a+b}\sum_{i=b}^{N-1} 2^{-i}\binom{a-b+i-1}{a-1}\sum_{j=i}^{N-1} 2^{j}\binom{-j+2N-3}{N-3}$
$(1-, N+)$	$2^{2(N-1)N-6N+10}$
$(1-, b+), \ b < N$	$2^{2(N-1)N-6N+10}$
$(a-, N+), \ a > 1$	$2^{2(N-1)N-6N+10}$
$(a-, [a+1]+)$	$2^{-2a+2(N-1)N-6N+10}\binom{2a-2}{a-1} + 2^{2(a+1)+2(N-1)N-8N+8}\binom{-2a+2N-2}{-a+N-1}$
$(a-, b+), \ b-a > 1$ $a, b \neq 1, N$	$2^{2(N-1)N-6N+11+a-b}\sum_{j=a+1}^{b}\sum_{i=a}^{i=j-1} 2^{-2i}\binom{-a+b+i-j}{-a+i}\binom{i+j-3}{i-1}$ $+2^{(2(N-1)N-8N+9+a-b}\sum_{j=a+1}^{b}\sum_{i=a}^{i=j-1} 2^{2j}\binom{-a+b+i-j}{-a+i}\binom{-i-j+2N-1}{-i+N-1}$

Table 4.2 *Table of leading order prefactors of the weights of the run-and-tumble model with reflecting boundaries.*

4.6.2 Example 1: $([N-1]+, N+)$

Enumeration of all the spanning in-trees for a particular sink requires generating all the possible tumbling diagrams corresponding to them. There are three such diagrams for $([N-1]+, N+)$. They are explicitly drawn in Figures 4.21—4.23.

Let us consider Figure 4.21. From finding the leading-order exponents in section 4.5.2, we known that each jammed $+-$ configuration must have a tumbling edge from it to connect it to other configurations. There are, in general, two options for each edge: one in $++$ and one in $--$. There are therefore 2^{N-1} spanning in-trees described by the tumbling diagram in Figure 4.21. In order to show that there are two options for the jammed configurations, I leave edges pointing out of $(1+, 2-)$ and $([N-1]+, N-)$ unattached. Turning to Figures 4.22 and

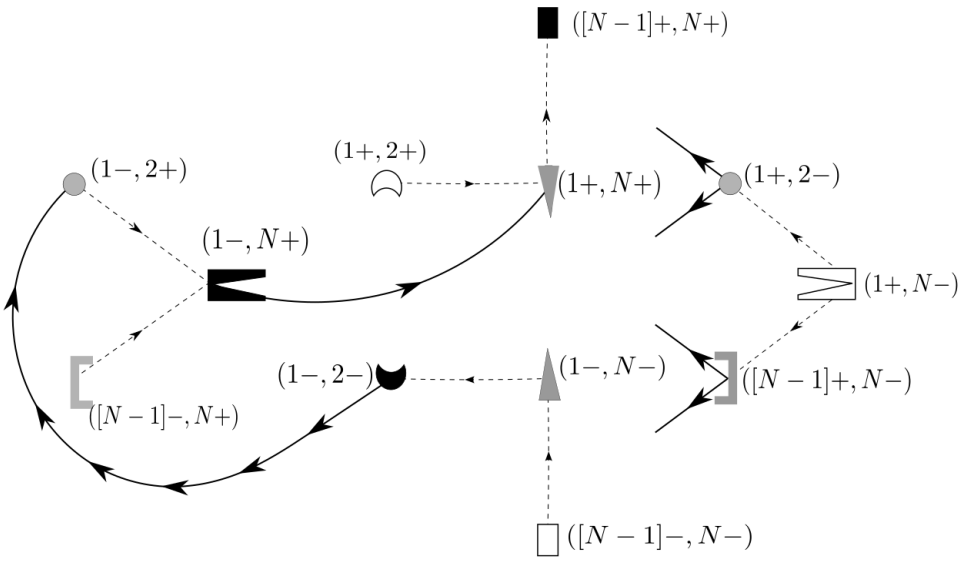

Figure 4.21 *The $i = 1$ leading order tumbling diagrams for $([N-1]+, N+)$ as the sink of the spanning in-tree. The unconnected arrows from $(1+, 2-)$ and $([N-1]+, N-)$ indicate that they may tumble to either the $++$ or $--$ sectors. This is the case for all the $N-1$ jammed configurations. As $([N-1]+, N+)$ is a hopping sink for the $++$ sector, it is sufficient for all states to be connected to the $++$ sector as wherever they are connected to by tumbling in the $++$ sector, they will then be connected to $([N-1]+, N+)$ by hopping within the $++$ sector. This tumbling diagram therefore contributes $2^{(N-1)}$ to the prefactor of the leading order probability of $([N-1]+, N+)$.*

4.23, we see that in these schemes the tumbling edges from one of the jammed configurations is fixed, and so they each only have multiplicities of 2^{N-2}.

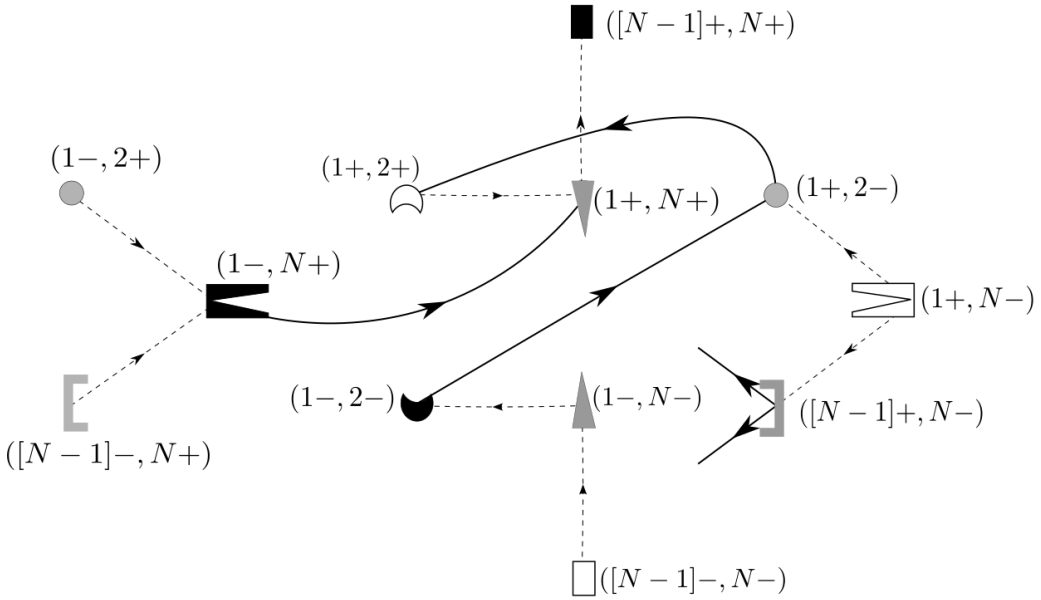

Figure 4.22 *The $i = 2$ leading order tumbling diagrams for $([N-1]+, N+)$ as the sink of the spanning in-tree.*

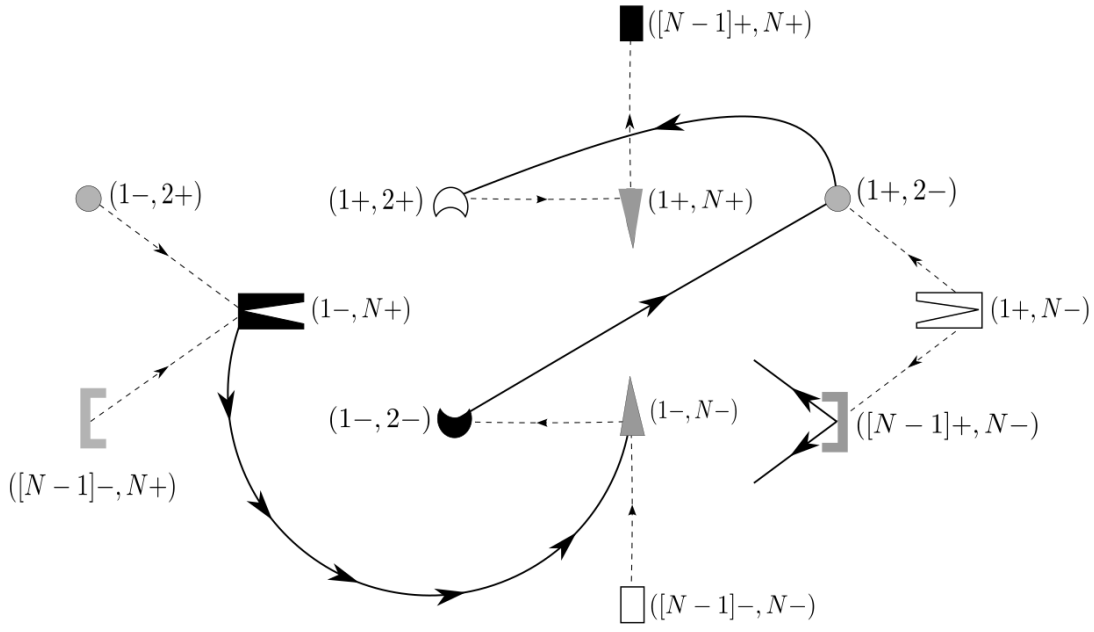

Figure 4.23 *The $i = 3$ leading order tumbling diagrams for $([N-1]+, N+)$ as the sink of the spanning in-tree.*

We now consider the paths within sectors, i.e. the number of paths in each of the hopping-only graphs corresponding to each tumbling diagram. We can term these *intrasector* paths. Each separate path will correspond to a different spanning in-tree.

Consider the ++ sector. We require the number of ways there are of connecting all the configurations in the ++ sector to $([N-1]+, N+)$ by hopping only. Fortunately, this is straightforward. It amounts to finding the ways of connecting up Figure 4.12 with only one edge into and one edge out of each configuration. Configurations which have one particle stuck at the boundary and/or have neighbouring sites occupied can only hop in one way or not at all. These configurations do not add to the multiplicity of the number of paths. The other configurations have two options for hopping. As all configurations in the ++ sector are guaranteed to eventually end up hopping to $([N-1]+, N+)$, the number of paths in ++ corresponds to the number of configurations with two hopping options.

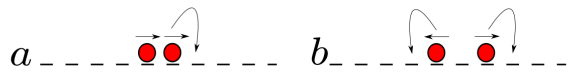

Figure 4.24 *(a) A configuration with only one hopping option. (b) A configuration with two hopping options.*

We evaluate these by counting the configurations without two options for hopping in the ++ sector and subtracting them from the total number of configurations $\binom{N}{2}$. Configurations with less than two hopping options are (i) the $N-1$ configurations with one particle on stuck at site N; and (ii) the $N-2$ distinct configurations with neighbouring particles, where $([N-1]+, N+)$ is already included by (i). Therefore the number of configurations with two hopping options in the ++ sector is

$$L_{(+,+)} = 2^{\left(\binom{N}{2} - [(N-1)+(N-2)]\right)} = 2^{\left(\binom{N}{2} - (2N-3)\right)} \tag{4.20}$$

Following a similar procedure for the other sectors gives

- for $(+,-)$: $L_{(+,-)} = 2^{\left(\binom{N}{2} - (N-1)\right)}$
- for $(-,+)$: $L_{(-,+)} = 2^{\left(\binom{N}{2} - (2N-3)\right)}$
- for $(-,-)$: $L_{(-,-)} = 2^{\left(\binom{N}{2} - (2N-3)\right)}$

We let

$$L_{\text{all}} = L_{(+,+)} \times L_{(+,-)} \times L_{(-,+)} \times L_{(-.-)}. \tag{4.21}$$

$K_{\sigma_1\sigma_2}$ is chosen to be the power of 2 appearing in each $L_{\sigma_1\sigma_2}$ and so,

$$K_{\text{all}} = K_{(+,+)} + K_{(+,-)} + K_{(-,+)} + K_{(-.-)}, \tag{4.22}$$

where

$$K_{\text{all}} = 2(N-1)N - 7N + 10, \tag{4.23}$$

and

$$2^{K_{\text{all}}} = L_{\text{all}}. \tag{4.24}$$

We now refer back to our tumbling diagrams, given in Figures 4.21—4.23. These give us the constraints on the allowed paths. We can see that in the case of these tumbling diagrams there are no constraints on the allowed paths within each sector. This is because all configurations will inevitably end up hopping to one of the tumbling states. Therefore each tumbling diagram has $2^{K_{\text{all}}}$ intrasector paths. We now draw this all together into Table 4.3.

State	Exponent	i	$p_{t,i}$	$p_{w,i}$
$([N-1]+, N+)$	$\gamma^{2(N-1)N-N-2}\omega^{N+1}$	1	2^{N-1}	$2^{K_{\text{all}}}$
	$\gamma^{2(N-1)N-N-2}\omega^{N+1}$	2	2^{N-2}	$2^{K_{\text{all}}}$
	$\gamma^{2(N-1)N-N-2}\omega^{N+1}$	3	2^{N-2}	$2^{K_{\text{all}}}$

Table 4.3 *Leading order weights of* $([N-1]+, N+)$*. Each* $p_{t,i}$ *corresponds to the number of paths due to the multiplicity of the* i^{th} *tumbling diagram in Figures 4.21—4.23. Each* $p_{w,i}$ *corresponds to the total of the sum of all the paths within the hopping-only graphs associated with the tumbling diagram* i*.*

By symmetry this result holds for $(1-, 2-)$. The enumeration of the spanning in-trees for other configurations with the highest-order exponents is similar. For $(1-, N+)$ instead of a tumbling edge leading out of $(1-, N+)$, there are choices for where to connect a tumbling edge out of $([N-1]+, N+)$. Thanks to the similarities between the tumbling diagrams of $(1-, N+)$ and $(1-, b+)$ and $(a-, N+)$, these configurations share the same number of spanning in-trees. Counting the spanning in-trees for $(1+, 2-)$ and $([N-1]+, N-)$ also proceeds along these lines, but there is a reduction in the multiplicity of the tumbling diagrams by a factor of 2, as the sink in $+-$, which would normally have a choice to tumble to $++$ or $--$, does not tumble at all.

4.6.3 Example 2: $(a+, b+),\ b \neq N$

Enumeration of the spanning in-trees for $(a+, b+),\ b \neq N$ is similar to $([N-1]+, N+)$. Here, the backbone approach, familiar from calculating the leading-order exponents, is used again. There are three tumbling diagrams. They are presented in Figures 4.25—4.27.

Let us now consider the paths within the hopping-only graphs. For clarity, the backbone of the spanning in-tree is presented again in Figure 4.28. The number of paths that are allowed, given this backbone constraint, consists of two quantities:

1. the number of ways to connect $(1+, 2+)$ to $(a+, b+)$
2. the number of other paths that do not conflict with 1.

The paths within the velocity sectors are calculated using lattice path enumeration [129]. Specifically, the reflection method is used to evaluate the number of

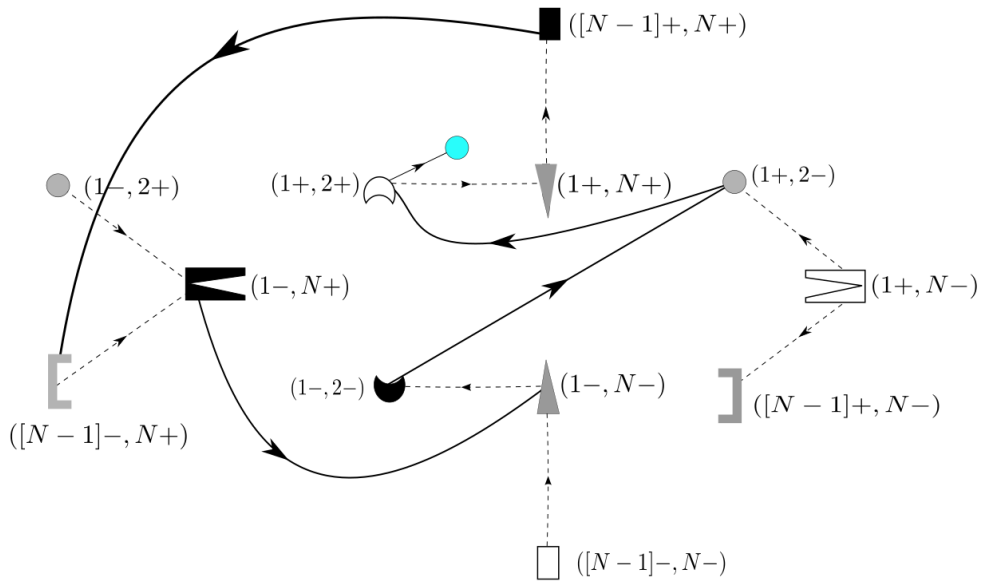

Figure 4.25 *The $i = 1$ tumbling diagram for a sink $(a+, b+),\ b \neq N$. The sink is coloured in cyan. Note that all the hopping sinks tumble. This diagram has a multiplicity of 2^{N-2} because there are $N-2$ jammed configurations that have a choice of whether to tumble to $++$ or $--$, $N-3$ of which are not explicitly included in this diagram.*

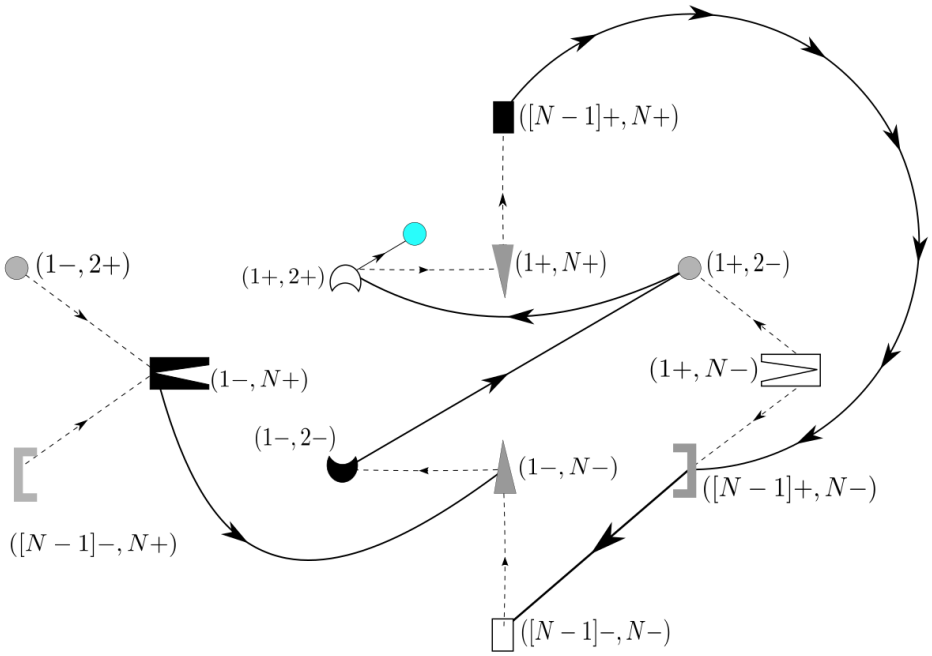

Figure 4.26 *The $i = 2$ tumbling diagram for a sink $(a+, b+)$, $b \neq N$. The sink is coloured in cyan. This diagram has a multiplicity of 2^{N-3} because there are $N-3$ jammed configurations not explicitly included in this diagram that must tumble.*

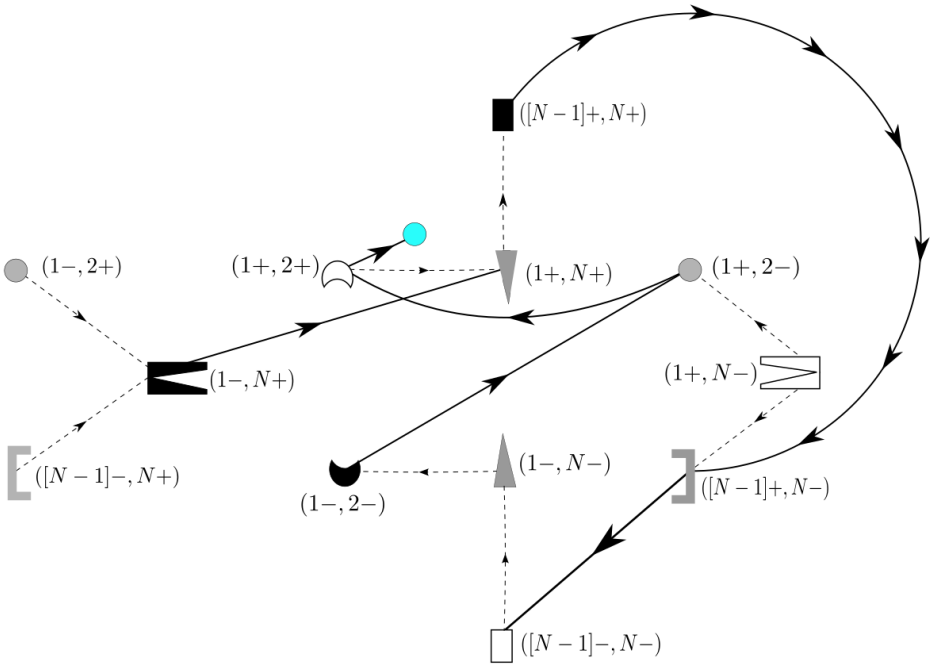

Figure 4.27 *The $i = 3$ tumbling diagram for a sink $(a+, b+)$, $b \neq N$. The sink is coloured in cyan.*

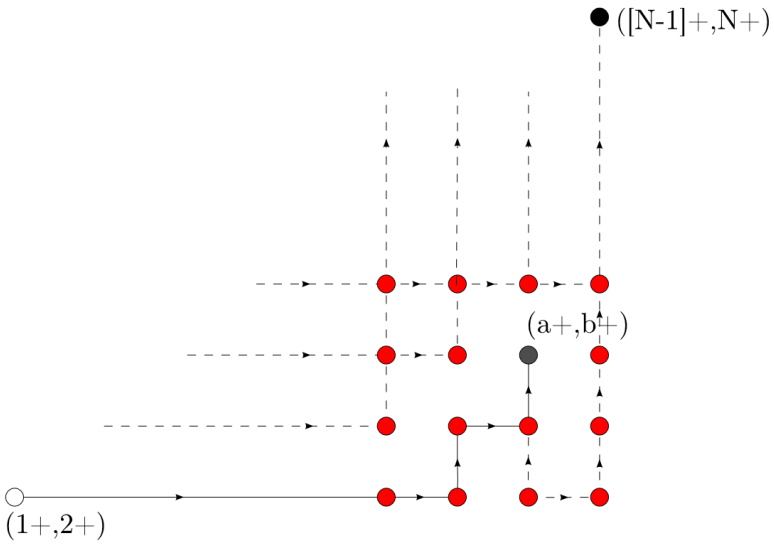

Figure 4.28 *Schematic for the backbone of the spanning in-tree connecting* $(1+, 2+)$ *to* $(a+, b+)$*, which is depicted with solid a solid line. The other possible edges are drawn with dashed lines*

paths if $(1+, 2+)$ must be connected to $(a+, b+)$. This is given by

$$g_{(1+,2+),(a+,b+)} = \binom{a+b-3}{a-1} \tag{4.25}$$

where $a + b - 3$ is the total number of steps necessary to move from $(1+, 2+)$ to $(a+, b+)$. The total number of paths in the $++$ sector for a sink $(a+, b+)$ is then given by

$$2^{K_{++}-(a+b-2)} \times 2 \times \binom{a+b-3}{a-1}, \tag{4.26}$$

where the factor $(a + b - 2)$ removes the states involved in connecting $(1+, 2+)$ to $(a+, b+)$ from being counted twice.

In a similar manner to Table 4.3, we bring together the various calculations for a $++$ sector state $(a+, b+)$, $b \neq N$ in Table 4.4.

State	Exponent	i	$p_{t,i}$	$p_{w,i}$
$(a+, b+), b \neq N$	$\gamma^{2(N-1)N-N-3}\omega^{N+2}$	1	2^{N-2}	$2^{K_{all}-(a+b-2)} \times 2 \times \binom{a+b-3}{a-1}$
	$\gamma^{2(N-1)N-N-3}\omega^{N+2}$	2	2^{N-3}	$2^{K_{all}-(a+b-2)} \times 2 \times \binom{a+b-3}{a-1}$
	$\gamma^{2(N-1)N-N-3}\omega^{N+2}$	3	2^{N-3}	$2^{K_{all}-(a+b-2)} \times 2 \times \binom{a+b-3}{a-1}$

Table 4.4 *Leading order steady-state weights for configurations* $(a+, b+), b \neq N$*.*

There are a couple of complications with states on the $N+$ branch. First, there are more tumbling diagrams. Second, $g_{(1+,2+),(a+,b+)}$ does not hold for $b = N$. The number of paths in the $++$ sector must therefore be calculated recursively. Such recursive calculations are explored in the next example.

4.6.4 Example 3: $(a+, b-),\ |b-a| > 1$

We begin with a consideration of the tumbling diagrams for $(a+, b-),\ |b-a| > 1$. Three such tumbling diagrams are shown in Figures 4.29—4.31.

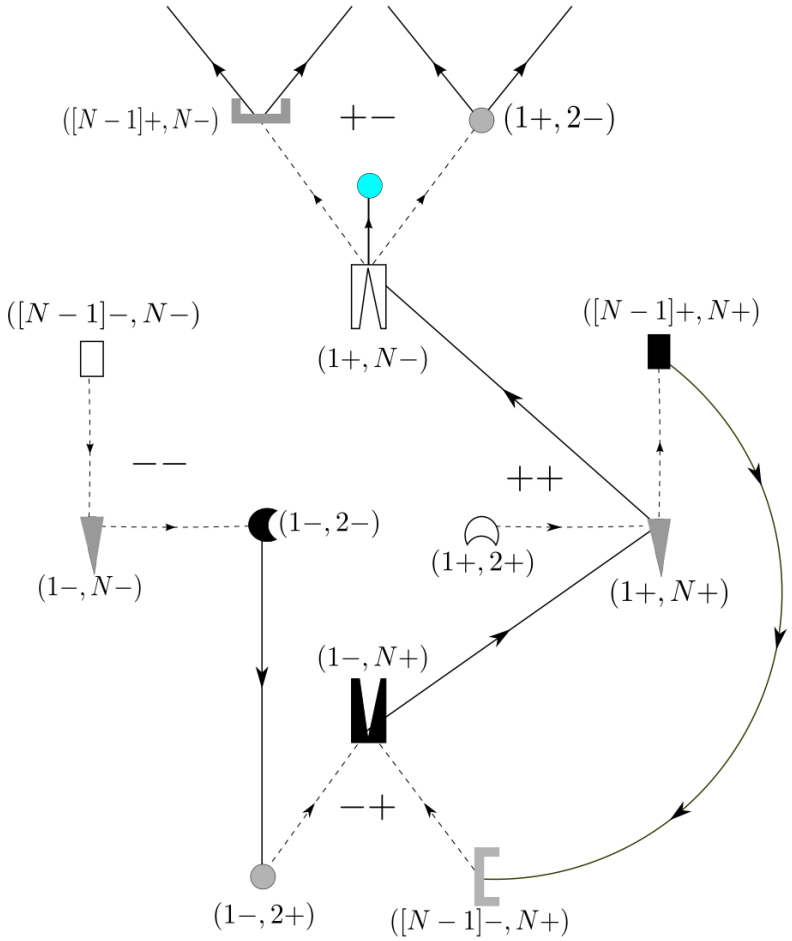

Figure 4.29 *The $i = 1$ tumbling diagram for a sink $(a+, b-)$. The sink is coloured in cyan.*

These figures were constructed by assuming some general backbone in $+-$ with an origin that can be connected by hopping edges only to the sink. A configuration in $++$ is then used to collect all the remaining configurations outside $+-$. This configuration in $++$ is then connected to the origin of the $+-$ backbone directly

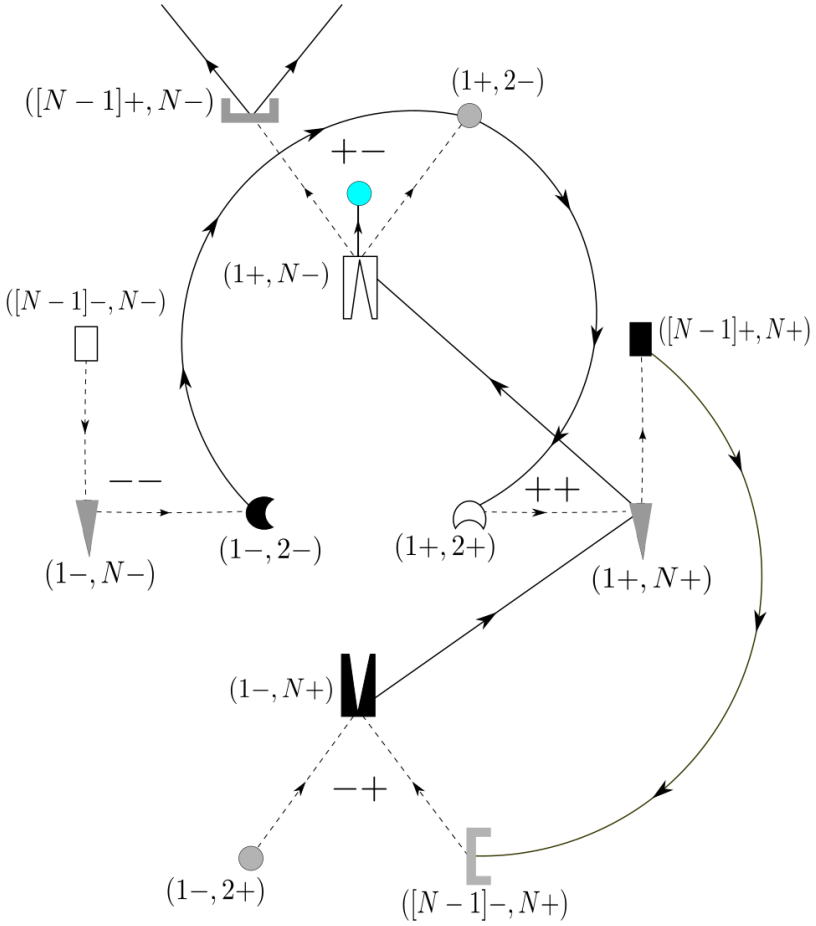

Figure 4.30 *The $i = 2$ tumbling diagram for a sink $(a+, b-)$. The sink is coloured in cyan.*

via a tumbling edge. There are a complementary set of tumbling diagrams that can be generated by using a configuration in $--$ rather than $++$ to collect the remaining configurations outside $+-$.

I now discuss how to enumerate the spanning in-trees associated with these tumbling diagrams, and hence how to derive the expressions for configurations in $+-$ in Table 4.2.

We first consider the expression $2^{-a+b+2(N-1)N-7N+11}\binom{a-1+N-b}{a-1}$. A backbone is imposed in $+-$, connecting the hopping subsource $(1+, N-)$ to the sink $(a+, b-)$. The paths within $+-$ have the multiplicity

$$2^{K_{+-}-(a-1+N-b)} \times g_{(1+,N-),(a+,b-)} = 2^{\binom{N}{2}-2N+2+b-a}\binom{a-1+N-b}{a-1}, \qquad (4.27)$$

using the path enumeration method from the previous section. There are no

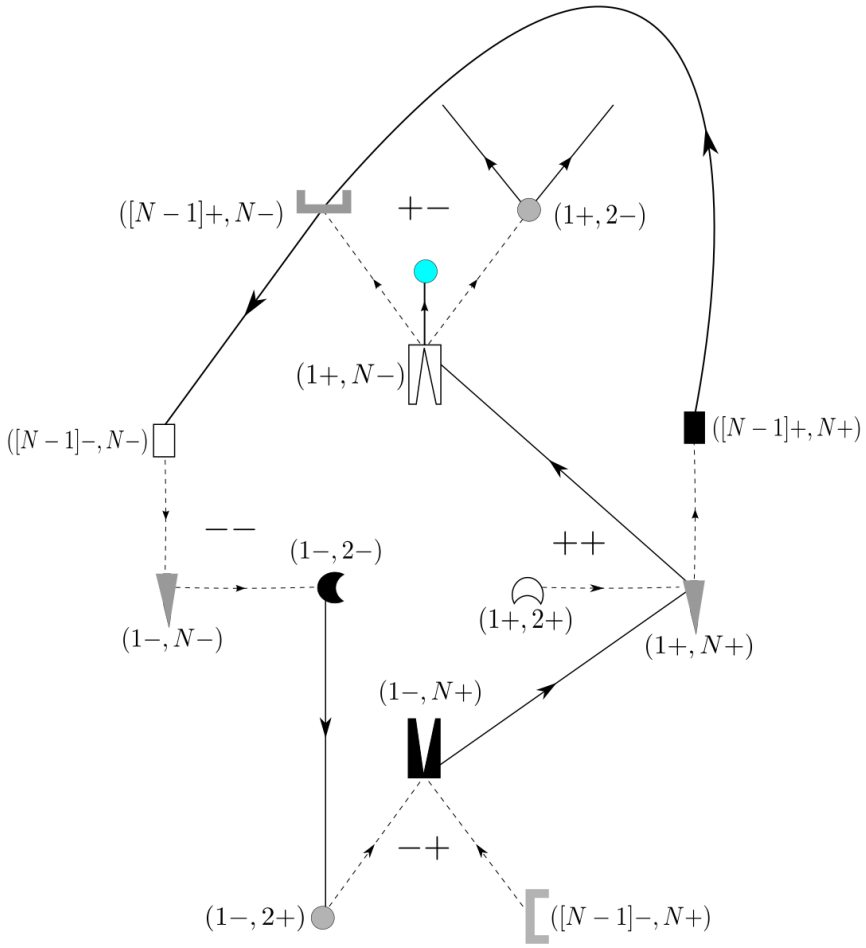

Figure 4.31 *The $i = 3$ tumbling diagram for a sink $(a+, b-)$. The sink is coloured in cyan.*

restrictions on the paths allowed within the other velocity sectors, except that $(1+, N+)$ cannot have a hopping edge leading outwards, as it already has a tumbling edge to $(1+, N-)$. Therefore the paths within those sectors are the full L_{++}, L_{-+} and L_{--}. This leads to

$$2^{-a+b+2(N-1)N-8N+11}\binom{a-1+N-b}{a-1}. \tag{4.28}$$

It remains to consider the multiplicity of the tumbling diagrams. Figure 4.29 has a multiplicity of 2^{N-1} as all the jammed configurations in $+-$ can tumble to either $++$ or $--$. Then we should multiply by a factor of two for the complementary $--$ spanning in-trees. Thus Figure 4.29 is associated with $2^{-a+b+2(N-1)N-7N+11}\binom{a-1+N-b}{a-1}$ spanning in-trees.

We now consider Figures 4.30 and 4.31. $([N-1]+, N-)$ is constrained to have a tumbling edge so to $([N-1]-, N-)$ the multiplicity of each diagram is 2^{N-2}. As each diagram has a complementary $--$ mirror, there are four in total, with total multiplicity 2^N. There are no further constraints on these diagrams and so the total number of spanning in-trees is

$$2^N \times 2^{K_{\text{all}}-(a-1+N-b)} \times g_{(1+,N-),(a+,b-)} = 2^{2(N-1)N-7N+11+b-a} \binom{a-1+N-b}{a-1}, \tag{4.29}$$

recovering the second expression for the prefactor for $(a+, b-)$, $|b-a| > 1$ in Table 4.2.

Now that we have seen a number of explicit examples for constructing the spanning in-trees, we turn to a description that provides an outline of the rest of the enumeration of the spanning in-trees.

We have seen that the prefactor for a given configuration is calculated in 2 steps:

1. Intersector paths $p_{t,i}$: Counting the ways of allowed minimum tumbling edges between sectors (the multiplicity will come from the tumbling of the jammed configurations in $+-$), with each diagram labelled $i = 1, 2, ...$
2. Intrasector paths $p_{w,i}$: Counting the sum of all paths within each sector corresponding to each intersector path $p_{t,i}$.

There are three types of intersector sector paths for sinks in the $+-$ sector:

- Type 1 paths connected through the hopping subsource of the approaching sector $(1+, N-)$—we have seen examples of these already in Figures 4.29—4.31.
- Type 2 paths: a backbone in the $++$ or $--$ sectors ends in a configuration with a tumbling edge directly to the sink in $+-$.
- Type 3 paths: a backbone in the $++$ or $--$ sectors ends in a configuration with a tumbling edge to a configuration in $+-$ that is the origin of another backbone connected by hopping edges to the sink.

Type 2 and 3 paths: connecting through the $++/--$ sectors

In Type 2 paths, a $++/--$ backbone ending in the configurations $(a+, b+)$ or $(a-, b-)$ respectively is connected by a tumbling edge directly to the sink

$(a+, b-)$. As before, to keep the number of tumbling edges to a minimum, many of the configurations in the spanning in-trees are connected, via their sectors' hopping subsinks to the hopping subsource in the sector where the backbone is imposed, i.e. $(1+, 2+)$ or $([N-1]-, N-)$. The hopping subsource becomes the origin of the backbone and, in turn, is connected to $(a+, b+)$ or $(a-, b-)$.

In Type 3 paths, the first step is to identify all the configurations in the $+-$ sector that are connected only by hopping edges to the sink $(a+, b-)$. Let such configurations be denoted $(i+, j-)$ where $i = 1, ..., a$ and $j = b, ..., N$. The leading-order intersector paths connect all other configurations in the system through either $(i+, j+)$ or $(i-, j-)$ to $(i+, j-)$ with a tumbling edge. Type 2 paths may be viewed then as a subset of Type 3 paths.

Given the structure of the $+-$ sector, configurations $(i+, j-)$ have $i \leq a$ and $j \geq b$. Note that this includes the sink itself. For each tumbling diagram where $(i+, j+)$ or $(i-, j-)$ has a tumbling edge to $(i+, j-)$, $(i+, j-)$ must be connected to the sink $(a+, b-)$. For such a tumbling diagram, the number of paths *within* the approaching sector associated to it is

$$g_{(i+,j-),(a+,b-)} = 2^{K_{+-}-([i-1]-[a-1])+([N-b]-[N-j])} \times \binom{([i-1]-[a-1])+([N-b]-[N-j])}{[i-1]-[a-1]} \tag{4.30}$$

Let us first consider Type 3 paths where a backbone in $++$ connects to a backbone $+-$, and the configuration that tumbles from $++$ is on the $N+$ branch i.e. $(i+, N+)$. All sinks in $+-$ can be connected by hopping edges to any configuration with $(i+, N-)$, as long as $i < a$. Imposing this as a backbone in $+-$ means that the configuration connected to $+-$ from $++$ can be any $(i+, N+)$ with $i < a$. In $++$, we know that $(1+, N+)$ is connected by hopping edges to any $(i+, N+)$ with $i < a$, so there is no need to impose a further constraint connecting these. Thus spanning in-trees where $(1+, N+)$ collects those configurations not connected to the sink by the backbone in $+-$ can be connected through $(1+, N+)$ to $(i+, N+)$ $i < a$. A schematic for the tumbling diagram for these spanning in-trees is shown in 4.32. Summing over all the allowed is, and pursuing this same process for connecting through $--$, gives the term

$$(2^{2(N-1)N-8N+13-a+b} + 2^{2(N-1)N-7N+9-a+b}) \sum_{i=2}^{a} 2^i \binom{a-b-i+N}{a-i} \tag{4.31}$$

in Table 4.2.

Note that this same method can be used to enumerate the spanning in-trees for

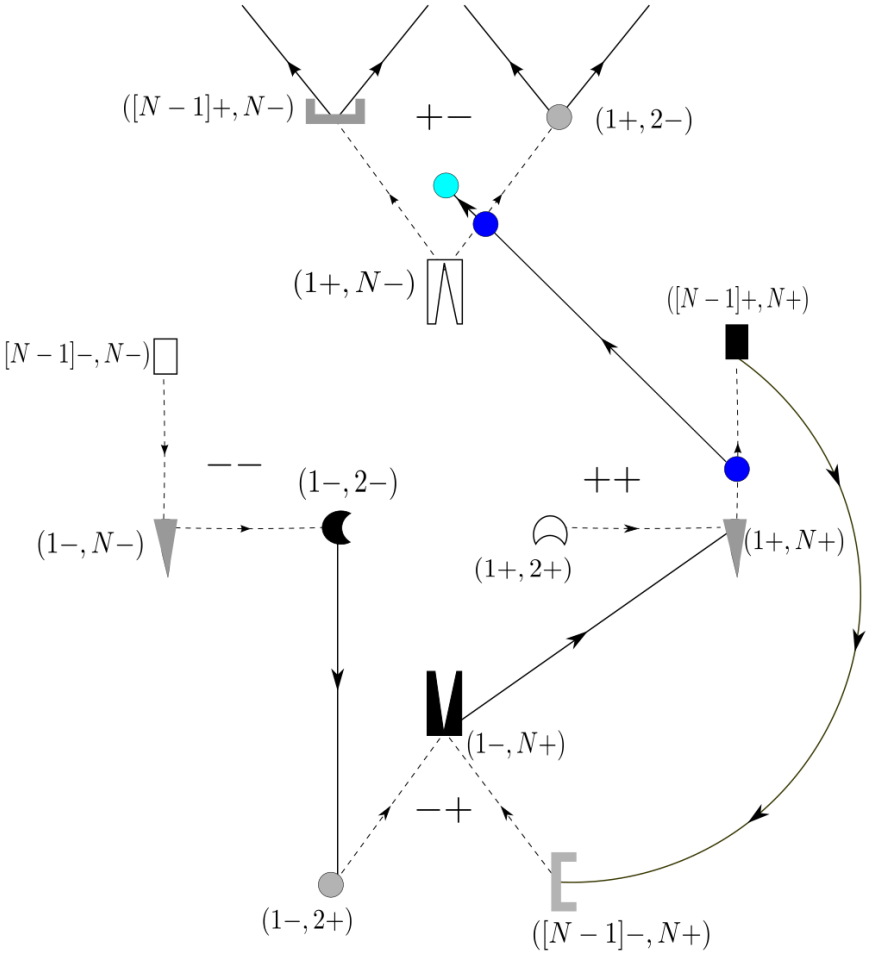

Figure 4.32 *Type 3 paths where* $(a+, N+)$ *has a tumbling edge out of it.*

$(a+, N+)$, and their symmetric counterparts $(1-, b-)$. Consider, for example, Figure 4.26. If the sink is on the $N+$ branch, i.e. it is $(a+, N+)$, it is only necessary to connect the hopping subsource $(1+, 2+)$ to some $(i+, N+)$ $i < a$, as $(i+, N+)$ will necessarily be connected by hopping edges to $(a+, N+)$. Therefore there are $i = 1, ..., a$ options for the backbone. Thus to enumerate the spanning in-trees requires a sum of over the possible backbones. This is the origin of the sum in the expressions for $(a+, N+)$, and $(1-, b-)$.

In some tumbling diagrams for $(a+, b-)$, such as the one shown in Figure 4.33, the hopping subsource in $++$, $(1+, 2+)$, must be connected by hopping edges to the configuration on the N branch in $++$ that has a tumbling edge out, $(i+, N+)$. This means that we need to another sum over the options that $(1+, 2+)$ must be connected to: $j = 2, ..., i$. For each of those there is a corresponding sum over

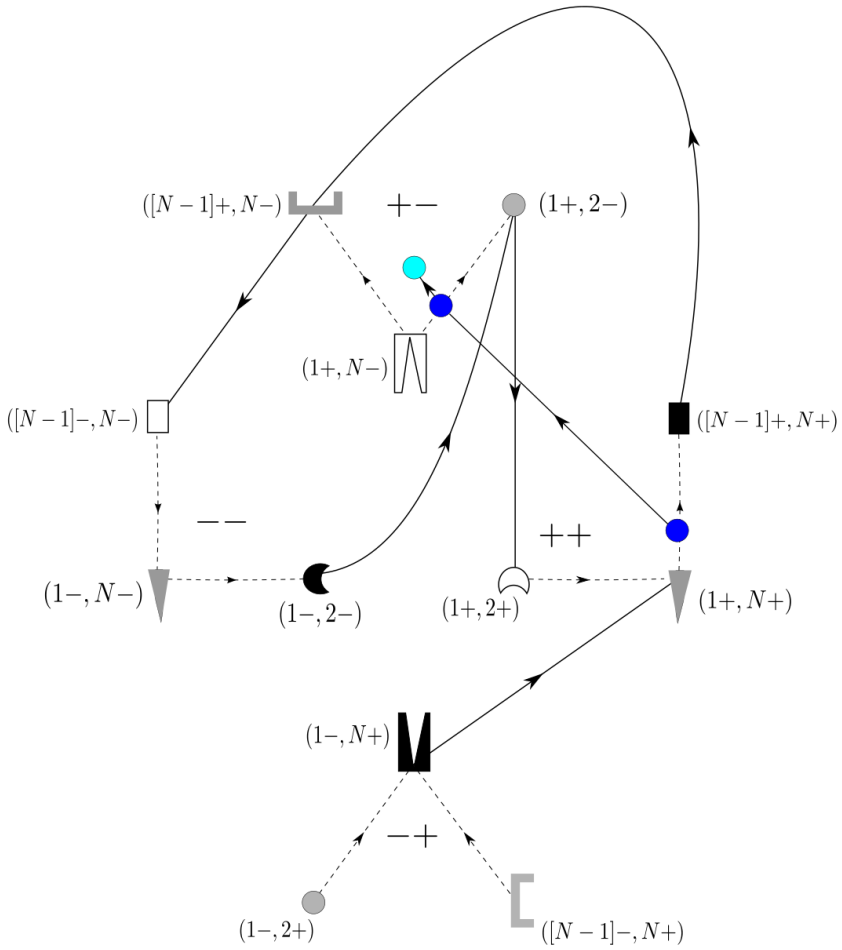

Figure 4.33 *Type 3 paths where $(i+,N+)$ has a tumbling edge out, and $(1+,2+)$ must be connected to $(i+,N+)$ by hopping edges only.*

the configurations $i = 2, ..., a$. This provides the term

$$2^{2(N-1)N-8N+12-a+b} \sum_{i=2}^{a} 2^i \binom{a-b-i+N}{a-i} \sum_{j=2}^{i} 2^{-j} \binom{j+N-4}{j-1} \tag{4.32}$$

and its symmetric counterpart

$$2^{2(N-1)N-8N+12-a+b} \sum_{i=b}^{N-1} 2^{-i} \binom{a-b+i-1}{a-1} \sum_{j=i}^{N-1} 2^j \binom{-j+2N-3}{N-3}. \tag{4.33}$$

Lastly, we consider the case where the configuration that has a tumbling edge from $++$ to $+-$ is not on the $N+$ branch, and as such it is labelled $(i+,j+)$. A schematic for this is shown Figure 4.34. Here we must sum over the possible

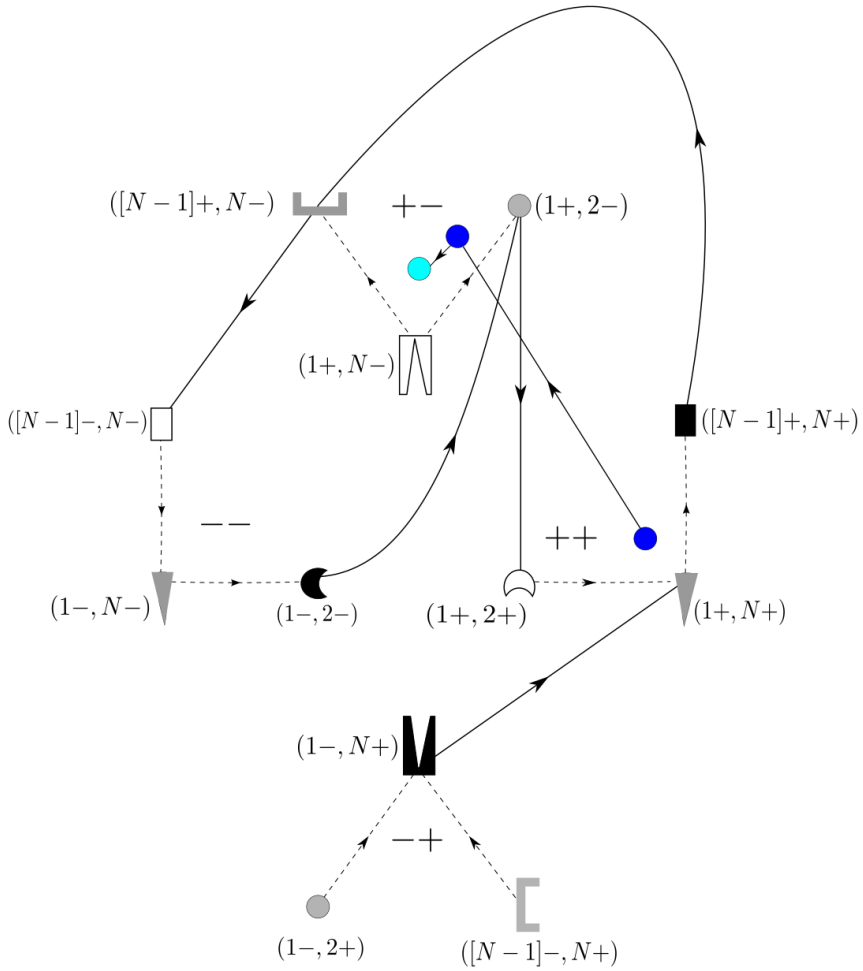

Figure 4.34 *The configuration that has a tumbling edge from ++ to +− is not on the $N+$ branch.*

configurations that are connected to $(i+, j+)$ by hopping only. This leads to the terms

$$2^{2(N-1)N-6N+11-a+b} \sum_{i=1}^{a} \sum_{j=b}^{N-1} 2^{-2j} \binom{a-b-i+j}{a-i} \binom{i+j-3}{i-1} \tag{4.34}$$

and its symmetric counterpart

$$2^{2(N-1)N-6N+11+a-b} \sum_{j=a+1}^{b} \sum_{i=a}^{i=j-1} 2^{-2i} \binom{-a+b+i-j}{-a+i} \binom{i+j-3}{i-1}. \tag{4.35}$$

This completes our outline of the derivation of the prefactors for $(a+, b-)$, $|b-a| > 1$. The prefactors for $(a+, [a+1-])$ proceed along the same lines.

Lastly, we consider the $-+$ sector. For $-+$ configurations, there are no intersector paths of Type 1, as there is no hopping subsource in this sector. However, there are Type 2 and 3 paths that can enumerated in the same way as for the example above, although the tumbling diagrams are different. A list of the number of tumbling diagrams, along with their associated multiplicities, $p_{t,i}$, for configurations in $+-$ and $-+$ are shown in Tables 4.5 and 4.6 respectively.

Configuration(s)	i	$p_{t,i}$
$(1+, N-)$	1	2^{N-1}
	2	2^{N-2}
	3	2^{N-2}
	4	2^{N-2}
	5	2^{N-3}
	6	2^{N-3}
	7-12	As 1-6
$(a+, b-), \lvert a-b\rvert > 1$	1-6	As $(1+, N-)$ 1-6
	7-12	As 1-6
	13-18	As 1-6
	19-24	As 7-12
$(a+, [a+1]-)$	As for $(a+, b-), \lvert a-b\rvert > 1$	

Table 4.5 *List of tumbling diagrams for configurations in the $+-$ sector.*

Configuration(s)	i	$p_{t,i}$
$(1-, b+), b < N$	1	2^{N-2}
	2	2^{N-2}
	3	2^{N-2}
	4	2^{N-2}
$(a-, N+), a > 1$	1-4	As $(1-, b+), b < N$ 1-4
$(a-, [a+1]+), a \neq 1, N$	1	2^{N-2}
	2	2^{N-3}
	3	2^{N-3}
	4-6	As 1-3
$(a-, b+), a, b \neq 1, N$	1-3	As $(a-, [a+1]+), a \neq 1, N$ 1-3
	4-6	As $(a-, [a+1]+), a \neq 1, N$ 4-6

Table 4.6 *List of tumbling diagrams for configurations in the $-+$ sector.*

4.7 Validity of the leading-order approximation

It is not *a priori* possible to know the range of validity of the limit from Eq. (4.16). Figures 4.35—4.37 compare the probabilities calculated from the leading-order expressions in Tables 4.2 and 4.1 and the results of simulations.

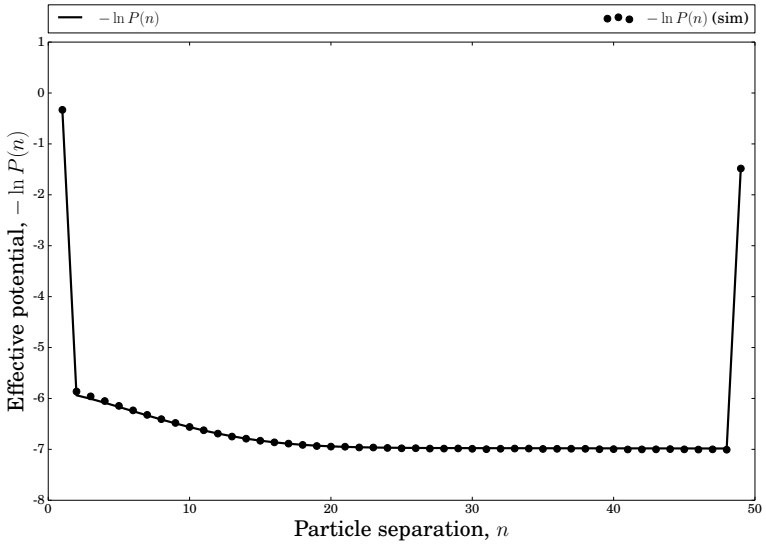

Figure 4.35 *Comparison of the analytic probability calculated numerically using the weights in Tables 4.1 (solid line) and 4.2 and simulation results for $\gamma/\omega = 999$ and $N = 50$ (dots). The simulation results are in close agreement with the leading-order probabilities as calculated using the matrix tree theorem. For this ratio, the leading-order approximation is therefore valid.*

In these figures some coarse-graining of the expressions in Tables 4.1 and 4.2 occurs. Specifically, instead of plotting the probability as a function of the particle position and velocity $(a\delta, b\epsilon)$, instead the probability is plotted as a function of particle separation. Thus, for each n we sum over all the configurations with $b - a = n$.

Figures 4.35—4.37 provide insight into the range of validity of the approximation. We note that the configurations within the sectors do not have all the same exponents. This may introduce errors for those separations that include leading-order weights with the largest exponents, for which sub-leading terms have not been calculated. Namely, they may be undervalued compared to separations that have exponents smaller than the largest order and thus have their sub-leading correction specified. However, in Figure 4.35, where the ratio $\gamma/\omega = 999$, the close agreement with the results of simulations shows that the ratio $\gamma/\omega = 999$

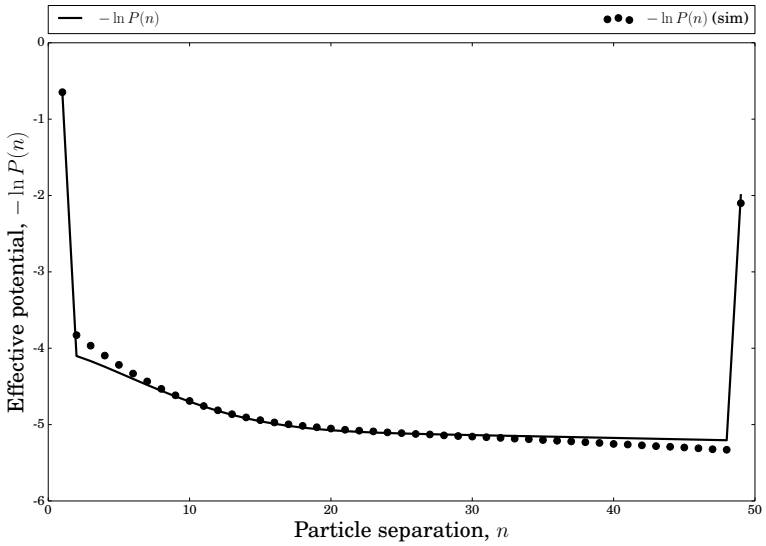

Figure 4.36 *Comparison of the analytic probability calculated numerically using the weights in Tables 4.1 and 4.2 and simulation results for $\gamma/\omega = 99$ and $N = 50$. For this γ/ω there is still good quantitative agreement between the simulation results and the leading-order probabilities, but there are some signs that the approximation is breaking down.*

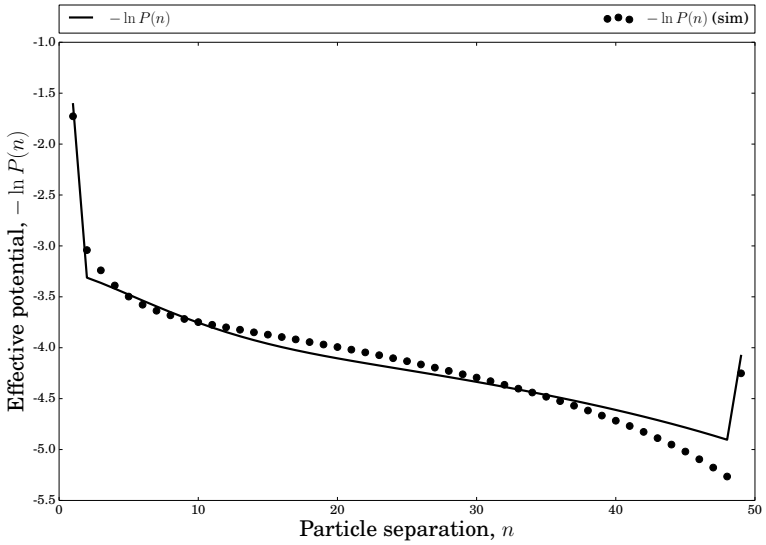

Figure 4.37 *Comparison of the analytic probability calculated numerically using the weights in Tables 4.1 and 4.2 and simulation results for $\gamma/\omega = 9$ and $N = 50$. Although the leading-order approximation captures the qualitative trends of the distribution from simulations, there is quantitative disagreement for many of the configurations.*

is within the range of validity of the limit.

In Figures 4.38 and 4.39, however, we can see that this close agreement for the coarse-grained probability hides some differences on the level of individual

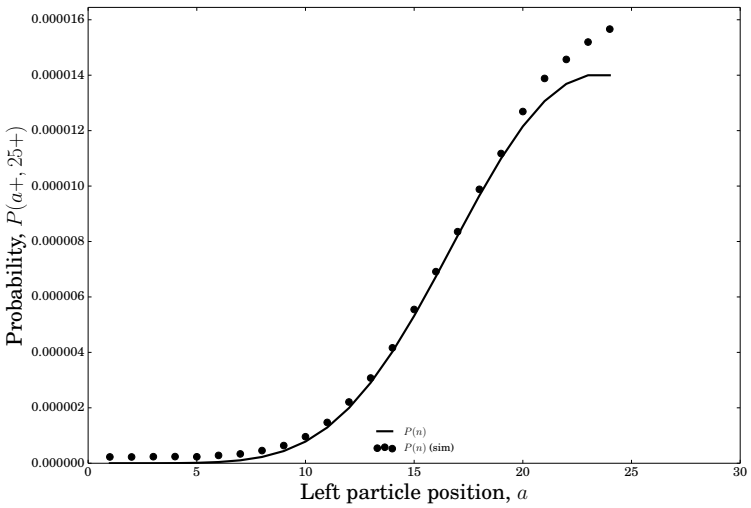

Figure 4.38 *Comparison of the analytic probability calculated numerically using the weights in Tables 4.1 and 4.2 and simulation results for* $\gamma/\omega = 999$ *and* $N = 30$.

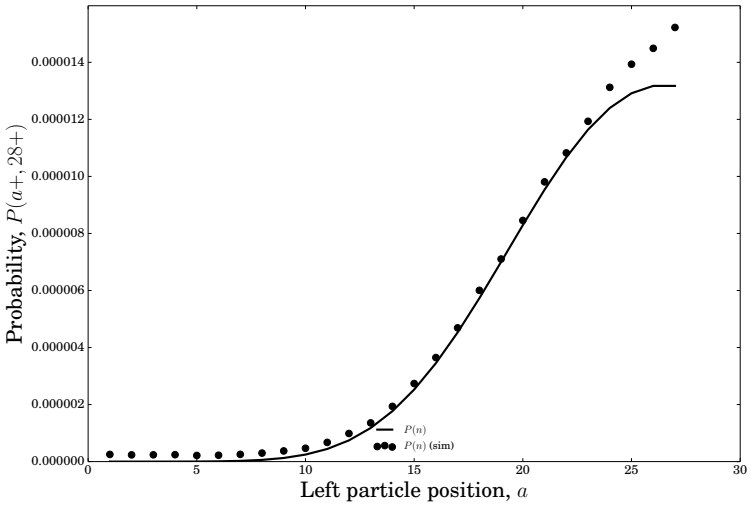

Figure 4.39 *Comparison of the analytic probability calculated numerically using the weights in Tables 4.1 and 4.2 and simulation results for* $\gamma/\omega = 999$ *and* $N = 30$.

configurations. Figures 4.38 and 4.39 compare the results of simulations with the leading-order expressions for a range of configurations in ++. For configurations where the left particle position approaches the right particle position, the leading-order expressions give values for the probabilities under those of simulations.

This could be for two reasons. One is related to the difference between simulation and leading-order probabilities when the particles are separated by a large distance. Here simulations could undervalue the probability compared to the leading-order expressions. These configurations have a very low probability

anyway, so it is possible that simulations were not run for long enough to capture their occupancy. In turn, this could lead to simulations overvaluing the more likely configurations when the particles are near. However, simulations undertaken both using smaller lattice sizes and more iterative steps showed no appreciable improvement in the correspondence between the leading-order approximation and the simulations.

Disagreement may also come from the leading-order expressions not properly taking into account the interactions between adjacent particles going in the same direction. Recall, that for the periodic boundaries case in this limit—cf. Eq. (4.18)—there was no interaction elevated probability between adjacent particles moving in the same direction, but in the full solution in equations (2.84) and (2.85) there was. The discrepancy seen in Figures 4.38 and 4.39 could therefore be due to this missing interaction. In order to capture this effect it may be necessary to have further orders in the expansion. This corresponds to the point made earlier in subsection 4.5.3: the leading-order weights of those configurations with the exponents with the largest weights do not have their subleading corrections calculated, which may be the source of the disagreement between the analytic approximation and the simulations.

Turning to Figures 4.36 and 4.37, as the γ/ω ratio decreases, the agreement between the leading-order expressions and simulations worsens compared to Figure 4.35. Nevertheless some quantitative agreement persists in the ratio $\gamma/\omega = 99$, and the leading-order expressions still capture some of the more qualitative trends present when the ratio $\gamma/\omega = 9$. We might expect a ratio of 9 to be far outside of the validity of the leading-order expressions, so this is a remarkable result.

4.8 Concluding remarks

In the previous two chapters, we considered the effect of interparticle interactions on the behaviour of run-and-tumble random walkers. However, the environment may also play an important role in generating nonequilibrium phenomena in active systems. In particular, experiments have observed the accumulation of self-propelled particles at boundaries [130–132] and several theoretical studies have been undertaken considering the effect of walls [62, 130, 133–135], including the relationship between the pressure exerted on walls and accumulation near

them [136].

In this chapter, we have seen that a graph-theoretic approach applied to the run-and-tumble model with reflecting boundaries does enable us to understand the effects of walls on a run-and-tumble system with interparticle interactions in the low-tumble limit and, by comparison with the exact solution for periodic boundaries, even suggest how the scaling limit might look. Attractive interactions in addition to those seen with a ring geometry emerge, and so this limit is quantitatively and qualitatively different from the corresponding limit in the system with periodic boundaries. However, this perturbative method does not give us rigorous access to higher tumble rate behaviour, and, considering the complexity of the calculation here, it presents little opportunity to scale to more particles or higher dimensions.

Nevertheless, as we have seen when comparing the analytic results to those from simulations, the leading-order weights do give relatively strong quantitative predictions for an intermediate ratio of run to tumble rate, and even capture some the qualitative trends when the run and tumble rates are similar. This suggests our analysis for the mechanism that generate the behaviour in the low tumble limit may largely hold as the tumble rate increases compared to the run rate.

Chapter 5

Conclusions

In this thesis, we have seen that nonequilibrium interactions emerge from the interparticle collisions of a simple model of run-and-tumble bacterial dynamics. These interactions manifest as an effective attraction between otherwise purely repulsive particles. We performed a detailed balance analysis of the minimal run-and-tumble model with instantaneous tumbling, which showed that the breaking of detailed balance was due to inter-particle collisions. Using the exact expressions for the stationary probability distribution for two variants of the model with periodic boundary conditions we saw how an emergent attraction was generated by the dynamics of these collisions. Thus the precise relationship between the breaking of detailed balance and the emergent interactions in the model of run-and-tumble particles lies in their jamming and unjamming dynamics.

We have also seen calculations for the leading-order stationary weights for a third variant of the model with reflecting boundary conditions. They gave insight into the principal mechanisms determining the behaviour of the system when it was confined by walls in the low-tumble limit, and suggested that effective attractions can emerge not only between run-and-tumble particles, but also between the particles and walls. These could be understood with reference to the exact results for periodic boundaries, where the interaction when reflecting boundaries are present is determined not just by interparticle collisions, but also by collisions with the walls.

These results are of interest in three complementary ways. First, they add to the body of work on effective potentials of systems of persistent random walkers by Maggi, Farage and others [92–94, 97]. In particular, the methods used here

are strictly valid in the regime of large persistence time, which was not the case for previous theories. As such, the findings in this thesis, and especially the exact results, provide a benchmark for which to compare perturbative theories for the emergent interactions of nonequilibrium systems. Secondly, the steady-state expressions are sufficiently simple that they provide precise insight into the mechanisms that lead to the effective attraction between particles. The results therefore provide a pathway to understanding the macroscopic clustering characteristic of motility-induced phase separation in this canonical model of self-propelled particles that is already well-described by coarse-grained theories. Thirdly, the methods used to derive the probability distributions and weights are well-understood and easily incorporated into a theorist's toolkit. The opportunities they present, as well as their limitations, have been elucidated here and thus these techniques of generating functions and tree counting are ripe for further exploitation in other nonequilibrium contexts quite apart from run-and-tumble dynamics.

I now turn to the results in each chapter and evaluate them in the broader context of bacterial dynamics and nonequilibrium statistical mechanics.

In chapter 2, we considered the minimal model for a microscopic interacting run-and-tumble system: two particles acting under mutual exclusion on a one dimensional lattice with periodic boundaries. The particles each hop at the same Poisson rate, and reverse their direction instantaneously according to an exponential distribution with rate ω, representing tumbling events. The simplicity of the model yielded dividends, where a generating function method allowed an exact solution to the steady-state probability distribution. Furthermore, it was easily expressed in terms of a simple parameter $z = 1 + \omega + \sqrt{\omega(2+\omega)}$. Each piece of the probability distribution was related to the underlying microscopic dynamics, which generates an effective attraction between the particles that is not just the δ-function expected from jammed particle configurations but longer range in nature, governed by an exponential decay with characteristic length $\xi = [\ln z]^{-1}$.

The behaviour in a scaling limit, where motion in continuous space and time is recovered, applies more directly to the dynamics of real run-and-tumble particles, which occur off-lattice. Here, the finite-range lengthscale ξ collapses to a δ-function. Thus, in the model with instantaneous tumbling, although an effective attraction is present in the scaling limit, it is only short-range in nature. This raises the question of whether the clustering observed in macroscopic theories [87]

derives purely from this short-range attraction between pairs of particles or whether many-body effects lead to further emergent interactions. Given that real swimmers, such as *E. coli*, must spend some finite duration tumbling, it was important to determine whether this made any difference to the findings for the case of instantaneous tumbling.

The system studied in chapter 3 modelled tumbling with finite duration, where particle runs and tumbles were individually governed by a Poisson process. A generalisation of the generating function method from chapter 2 allowed an exact solution to this model with finite tumbling duration. The stationary probability distribution is characterised by two lengthscales ($[\ln z_+]^{-1}$ and $[\ln z_-]^{-1}$ in comparison to the single $\ln z$ of the model with instantaneous tumbling. However, the z_+ and z_- of the model in chapter 3 are not straightforwardly expressed in terms of the model parameters as for z, but are cumbersome and long expressions.

The first of the lengthscales ($[\ln z_+]^{-1}$) is analogous to ξ in the chapter 2 model. The second lengthscale ($[\ln z_-]^{-1}$) is unique to the finite tumbling system. This lengthscale depends on a combination of both the tumbling entry and tumbling exit rates, as together they determine how far the moving particle may separate itself from the stationary particle. It furthermore appears in all the velocity sectors. In the scaling limit for the finite tumbling model, the difference between the two lengthscales is emphasised. As for ξ in chapter 2, $[\ln z_+]^{-1}$ vanishes because the decay length is small on the scale of the system. In contrast, the second lengthscale $[\ln z_-]^{-1}$ remains finite in this limit. Thus, even in a model with only two interacting particles, finite-range interactions can be generated in off-lattice dynamics. This may contribute to the finite-range attractive effects observed through the coarse-grained many-body models that present motility-induced phase separation.

The results of chapters 2 and 3 add to the body of work in exact results in nonequilibrium interacting systems [137, 138], where the catalogue of exact steady-states remains limited [139]. They also making a connection to emerging investigations of effective potentials in active matter [92–94, 97]. The advantage of this approach is that the mechanisms that generate these interactions can be pinpointed thanks to the exact solutions. The drawback is that the mathematics is challenging, and the method is not easily extended to more particles, higher dimensions or even slightly different geometries such as reflecting boundaries.

These limitations led to the consideration of a different approach to solve the

instant tumbling model with reflecting boundaries in chapter 4. A graph-theoretic method known as the matrix tree theorem was used to find the leading-order steady-state weights in the low-tumble limit. Their form suggested the mechanisms generating these weights, and hence the stationary behaviour, had their origin in the jamming-unjamming dynamics of the particles. In contrast with the periodic boundaries case, however, jamming occurred not just between the particles but also between particles and the walls. The expressions for leading-order stationary weights suggests that an attraction emerges from these wall-particle interactions, in addition to the effective attraction from interparticle interactions. These findings add to the body of work on the interaction of bacterial swimmers with walls [130–136], and suggest that one manifestation of the importance of geometry could be emergent interactions due to run-and-tumble collisions with confining walls.

Despite rendering the reflecting-boundaries case accessible to analytic investigation, the matrix tree theorem is in essence a brute force tool, which was reflected in the length and difficulty of the calculation for the stationary weights. This presents a significant drawback to this method as a widely applicable approach to systems with some natural scale separation in their transition rates. However, as we have seen in chapter 4, when used in concert with exact results for related systems, the matrix tree theorem can yield significant quantitative insights in the appropriate limit, that is also the limit not accessible to previous studies of nonequilibrium effective potentials [92–94, 97].

I now consider the prospects for further work, both on further investigating the model of interacting run-and-tumble random walkers and applying the methods used in this thesis to other nonequilibrium systems.

The most obvious direction for further study would be in increasing the number of particles and the dimensionality of the run-and-tumble system. In the former case, it would be interesting to determine whether an effective interaction between three (or more) particles can be decomposed into two-body interactions. A recent work using generating function methods and overcoming the obstinate kernel may offer a pathway towards solving the three-body problem [140]. In higher dimensions it is not obvious how the short range attraction mediated by jamming would be modified, or whether it will be of any significance at all, especially in the limit of continuous space and time. Progress in either, and particularly both, of these directions would allow a more direct relation to be drawn between the coarse-grained theories of motility-induced phase separation and the results of

simulations [84, 87, 88].

The first steps towards increased particle number need not be exact. One avenue for the study of more particles would be to use the effective pair potential from chapter 2 in the many-body case. For example, a many-body potential could be obtained by treating a summation of the pair potentials as an ansatz and see what predictions result for the physics of the many-body case. These predictions could then be compared with the results of simulations described in subsection 2.6.1.

Turning to the graph-theoretic approach in chapter 4, we saw that enumeration of the leading-order prefactors required long and complex calculations. Furthermore, they were only tractable because the intersector paths could be mapped to two-dimensional lattice path enumeration problems. Extending this approach to more particles, or higher dimensions, would change the structure of the spanning in-trees so that they are no longer planar. The path enumeration problem would then be in three-dimensions, and correspondingly even more challenging. However, we saw that finding the leading-order exponents was not so involved but still yielded much of the physics of the system with reflecting boundaries. Therefore this method might be applicable to completely different systems that exhibit the scale separation in their transition rates described in subsection 4.2.2. Lastly, if the graph-theoretic method could be computerised by formulating an appropriate algorithm using the key configurations of systems as elucidated here, it may offer a more efficient path to solving problems with scale-separation in their transition rates.

In this thesis, we have focused on the steady-state dynamics of the models because they dominate its long-time behaviour. Nevertheless, it would also be of interest to consider the dynamics: the approach to stationarity. In particular, the relaxation time of the lattice-based systems are not necessarily of order L^2 as would be expected of diffusion. For example, a single persistent random walker which changes direction with probability $1/L$ at each step has relaxation time $O(L)$ [141]. The transient times for the interacting run-and-tumble models presented in the preceding chapters are open problems.

Perhaps the most important question for the critical scientist is: are the results in this thesis relevant to experiment? The micro-channel work of Mannik and collaborators [54] does suggest that experimental realisation of the variants of the interacting run-and-tumble model studied here could be possible. This would require two principal modifications to the set-up described in [54]. First, the

geometry of the effective one-dimensional channel would have to be changed. The case of periodic and reflecting boundaries would require a ring and a channel with closed ends respectively. These geometric constraints mean that the bacterial sources in the experiment, namely chambers connected to the channel through its open ends would either need to be fitted with valves (should such a component be feasible), or the bacteria would need to be injected into the channel using an alternative method. Should these practical obstacles be overcome, the work in this thesis provides quantitative predictions that could be directly tested in experiments.

Appendix A

Exact expressions for parameters in chapter 3

In Eq. 3.1 in section 3.2, the parameters z_+ and z_- are used. In this appendix they are written out explicitly. First, we define $z_{+++} = 1/z_{--+} \equiv z_+$ and $z_{-+-} = 1/z_{---} \equiv 1/z_-$

The exact expressions for z_+ and z_- (and their symmetry roots) are then

$$z_{\sigma_1\sigma_2\sigma_3}(\alpha,\beta) = \frac{1}{8}\left[\zeta(\alpha,\beta) + \sigma_1\kappa(\alpha,\beta) + \sigma_2\sqrt{\eta(\alpha,\beta) + \sigma_3\rho(\alpha,\beta)}\right], \tag{A.1}$$

where

$$\zeta(\alpha,\beta) = \frac{\beta^2+\beta+2}{\alpha+\beta+1} + 6\alpha + \beta + 6 \tag{A.2}$$

$$\kappa(\alpha,\beta) = \sqrt{\frac{4\alpha^4 + 4\alpha^3(\beta+4) + \alpha^2(\beta(9\beta+8)+16) + 12\alpha\beta^3 + 4\beta^4}{(\alpha+\beta+1)^2}}, \tag{A.3}$$

$$\eta(\alpha,\beta) = 2\Bigg[\frac{\left(6\alpha^2 + \alpha(7\beta+12) + 2(\beta+2)^2\right)^2}{(\alpha+\beta+1)^2} - 8(\alpha+2)\beta - \frac{16(\alpha+1)}{\alpha+\beta+1} - 16(\alpha(\alpha+2)+2) - 16\Bigg], \tag{A.4}$$

$$\rho(\alpha,\beta) = 2\left[\frac{(6\alpha^2+\alpha(7\beta+12)+2(\beta+2)^2)\sqrt{\frac{4\alpha^4+4\alpha^3(\beta+4)+\alpha^2(\beta(9\beta+8)+16)+12\alpha\beta^3+4\beta^4}{(\alpha+\beta+1)^2}}}{\alpha+\beta+1}\right]. \tag{A.5}$$

Appendix B

Inverse matrix in chapter 3

Here the terms $\sum_j \text{adj}\, A_{\sigma_1\sigma_2,j}(x)b_j(x)$ are written out explicitly. We will use the notation $\tilde{A}_{\sigma_1\sigma_2,i}(x) \equiv \text{adj}\, A_{\sigma_1\sigma_2,i}(x)$. We first consider $\tilde{A}_{++,\{i\}}\underline{b}(x)$.

$$\tilde{A}_{++,\{i\}}\underline{b}(x) = \begin{pmatrix} -\frac{1}{4}\beta\left(\beta^2(\alpha+2\mu)(\alpha+2\nu) - \beta(\alpha+2\mu)(\mu+\nu)(\alpha+2\nu) + 2\mu\nu(\alpha(\mu+\nu)+2\mu\nu)\right) \\ \frac{1}{4}\alpha\beta^2\left(\alpha\beta - 2\mu^2 + 2\beta\mu\right) \\ \frac{1}{4}\alpha\beta^2\left(\alpha\beta - 2\nu^2 + 2\beta\nu\right) \\ -\frac{1}{4}\beta^2\mu\left(\alpha\beta - 2\nu^2 + 2\beta\nu\right) \\ -\frac{1}{4}\beta^2\nu\left(\alpha\beta - 2\mu^2 + 2\beta\mu\right) \\ -\frac{1}{8}\beta^2(\beta(\alpha(\mu+\nu)+4\mu\nu) - 2\mu\nu(\mu+\nu)) \end{pmatrix} \cdot \begin{pmatrix} P_{++}(1)\left(1-x^{L-1}\right) \\ P_{+-}(1) \\ -P_{+-}(1)x^{L-1} \\ -P_{+0}(1)x^{L-1} \\ P_{+0}(1) \\ 0 \end{pmatrix} \tag{B.1}$$

We define

$$J_{++}(x) \equiv \tilde{A}_{++,1}(x)P_{++}(1) + \tilde{A}_{++,2}(x)P_{+-}(1) + \tilde{A}_{++,5}(x)P_{+0}(1). \tag{B.2}$$

It then falls to find the symmetries of $\tilde{A}_{++,i}$. The relevant symmetry relations of

$\mu(x)$ and $\nu(x)$ are

$$\mu(x)\nu(x) = \mu(1/x)\nu(1/x), \text{ and} \tag{B.3}$$
$$\nu(x) + \mu(x) = \mu(1/x) + \nu(1/x) = 2[1 + \alpha + \kappa(\alpha, \beta)]. \tag{B.4}$$

The symmetries of $\tilde{A}_{++,i}$ are as follows

$$\tilde{A}_{++,1}(z) = \tilde{A}_{++,1}(1/z), \tag{B.5}$$
$$\tilde{A}_{++,2}(z) = \tilde{A}_{++,3}(1/z), \text{ and} \tag{B.6}$$
$$\tilde{A}_{++,4}(z) = \tilde{A}_{++,5}(1/z). \tag{B.7}$$

We are now in a position to find the symmetries in $J_{++}(x)$:

$$\begin{aligned} J_{++}(1/z) &= \tilde{A}_{++,1}(1/z)P_{++}(1) + \tilde{A}_{++,2}(1/z)P_{+-}(1) + \tilde{A}_{++,5}(1/z)P_{+0}(1) \\ &= \tilde{A}_{++,1}(z)P_{++}(1) + \tilde{A}_{++,3}(z)P_{+-}(1) + \tilde{A}_{++,4}(z)P_{+0}(1) \\ &= z^{1-L}[\tilde{A}_{++,1}(z)P_{++}(1) + \tilde{A}_{++,2}(z)P_{+-}(1) + \tilde{A}_{++,5}(z)P_{+0}(1)] \\ &= z^{1-L}J_{++}(z). \end{aligned} \tag{B.8}$$

We now turn to $\tilde{A}_{+-,\{i\}}\underline{b}(x)$. The equation is

$$\tilde{A}_{+-,\{i\}}\underline{b}(x) = \begin{pmatrix} \frac{1}{4}\alpha\beta^2\left(\alpha\beta - 2\mu^2 + 2\beta\mu\right) \\ -\frac{1}{4}\beta[\beta^2\left\{\alpha^2 + 2\alpha(3\mu+\nu) + 4\mu(\mu+\nu)\right\} - // \\ // - \beta(\mu+\nu)\left\{\alpha^2 + 2\alpha(3\mu+\nu) + 4\mu(\mu+\nu)\right\} + 2\mu(\mu+\nu)\left\{\alpha(\mu+\nu) + 2\mu\nu\right\}] \\ \frac{1}{4}\alpha^2\beta^2(-\beta+\mu+\nu) \\ -\frac{1}{4}\alpha\beta^2\mu(-\beta+\mu+\nu) \\ \frac{1}{4}\beta^2(\mu(\alpha+2\mu)(\mu+\nu) - \beta(\alpha(2\mu+\nu) + 2\mu(\mu+\nu))) \\ \frac{1}{8}\beta^2(\mu+\nu)\left(2\mu^2 - \beta(\alpha+2\mu)\right) \end{pmatrix} \bullet \begin{pmatrix} P_{++}(1)\left(1 - x^{L-1}\right) \\ P_{+-}(1) \\ -P_{+-}(1)x^{L-1} \\ -P_{+0}(1)x^{L-1} \\ P_{+0}(1) \\ 0 \end{pmatrix}. \tag{B.9}$$

We now turn to $\tilde{A}_{+0,\{i\}}\underline{b}(x)$. The equation is

$$\tilde{A}_{+0,\{i\}}\underline{b}(x) = \begin{pmatrix} -\frac{1}{2}\alpha\beta\nu\left(\alpha\beta - 2\mu^2 + 2\beta\mu\right) \\ \frac{1}{2}\alpha\beta(\mu(\alpha+2\mu)(\mu+\nu) - \beta(\alpha(2\mu+\nu) + 2\mu(\mu+\nu))) \\ -\frac{1}{2}\alpha^2\beta\nu(-\beta+\mu+\nu) \\ \frac{1}{2}\alpha\beta\mu\nu(-\beta+\mu+\nu) \\ \frac{1}{2}\beta\nu(\beta(\alpha(2\mu+\nu) + 2\mu(\mu+\nu)) - \mu(\alpha+2\mu)(\mu+\nu)) \\ -\frac{1}{4}\beta\nu(\mu+\nu)\left(2\mu^2 - \beta(\alpha+2\mu)\right) \end{pmatrix} \bullet \begin{pmatrix} P_{++}(1)\left(1-x^{L-1}\right) \\ P_{+-}(1) \\ -P_{+-}(1)x^{L-1} \\ -P_{+0}(1)x^{L-1} \\ P_{+0}(1) \\ 0 \end{pmatrix} \tag{B.10}$$

Finally, we turn to $\tilde{A}_{00,\{i\}}\underline{b}(x)$. The equation is

$$\tilde{A}_{00,\{i\}}\underline{b}(x) = \begin{pmatrix} -\frac{1}{2}\alpha^2(\beta(\alpha(\mu+\nu)+4\mu\nu) - 2\mu\nu(\mu+\nu)) \\ \frac{1}{2}\alpha^2(\mu+\nu)\left(2\mu^2 - \beta(\alpha+2\mu)\right) \\ \frac{1}{2}\alpha^2(\mu+\nu)\left(2\nu^2 - \beta(\alpha+2\nu)\right) \\ -\frac{1}{2}\alpha\mu(\mu+\nu)\left(2\nu^2 - \beta(\alpha+2\nu)\right) \\ -\frac{1}{2}\alpha\nu(\mu+\nu)\left(2\mu^2 - \beta(\alpha+2\mu)\right) \\ \frac{1}{4}\left(-2\beta(\mu+\nu)\left(\alpha\left(\mu^2+\mu\nu+\nu^2\right) + 2\mu\nu(\mu+\nu)\right) + 4\mu^2\nu^2(\mu+\nu) + 2\beta^2(\alpha+\mu+\nu)(\alpha(\mu+\nu)+2\mu\nu)\right) \end{pmatrix} \bullet \begin{pmatrix} P_{++}(1)\left(1-x^{L-1}\right) \\ P_{+-}(1) \\ -P_{+-}(1)x^{L-1} \\ -P_{+0}(1)x^{L-1} \\ P_{+0}(1) \\ 0 \end{pmatrix} \tag{B.11}$$

Appendix C

Mathematica notebook used for chapter 3

The *Mathematica* notebook over the page performs an exact analytic calculation of the probability distribution up to the normalisation of the distributions $P_{\sigma_1\sigma_2}(n)$. Normalisation for a specific set of model parameters is achieved numerically, calculated to arbitrary precision limited only by machine capability.

```
ClearAll["Global`*"]

(*************************************************************************
************)
(*************************************************************************
************)
(*************************************************************************
************)
(* NOTEBOOK TO SOLVE LATTICE MODEL OF 2-
 BODY RUN-AND-TUMBLE WITH FINITE TUMBLE DURATION *)
(*************************************************************************
************)
(*************************************************************************
************)
(*************************************************************************
************)


(*************************************************************************
************)
(***************** UN-
 NORMALISED EXACT PROBABILITY DISTRIBUTION FUNCTION ****************)
(*************************************************************************
************)

(* Functions for matrix A eq(3.38) *)
μ[x_] := x - (1 + α)
ν[x_] := (x^(-1)) - (1 + α)

(* Matrix A eq(3.36) *)
a[x_, α_, β_] := {{ μ[x] + ν[x], 0, 0, β / 2, β / 2, 0},
    {0, ν[x], 0, 0, β / 2, 0},
    {0, 0, μ[x], β / 2, 0, 0},
    {α, 0, α, μ[x] - β, 0, β / 2},
    {α, α, 0, 0, ν[x] - β, β / 2},
    {0, 0, 0, α, α, -β}} ;

(* det(A) *)
detA[x_, α_, β_] := Evaluate[FullSimplify[Det[a[x, α, β]]]]

inverseA[x_, α_, β_] := Evaluate[FullSimplify[Inverse[a[x, α, β]]]]

(* Vector b(x) in eq(3.37) *)
bVec[x_, pp1_, pm1_, pTum1_, L_] :=
  (1 - x) * {(1 - x^(L - 1)) * pp1, pm1, -x^(L - 1) * pm1, -x^(L - 1) * pTum1, pTum1, 0}

(* NUMERATOR OF INVERSE MATRIX A^(-1)(x) *)
inverseANumer[x_, α_, β_] :=
 Evaluate[FullSimplify[inverseA[x, α, β] * detA[x, α, β]]]

(* NUMERATORS of Gs eq(3.47)*)
gppNum[x_, α_, β_, pp1_, pm1_, pTum1_, L_] := Evaluate[FullSimplify[Sum[
     inverseANumer[x, α, β][[1, i]] * bVec[x, pp1, pm1, pTum1, L][[i]], {i, 1, 6}]]]
```

```
(* ROOTS OF THE DETERMINANT 1/z_{-} and z_{+} *)
zMiR[x_, α_, β_] := 1/8 (6 + 6 α + β + (2 + β + β^2)/(1 + α + β) -
    Sqrt[(1/(1 + α + β)^2) (4 α^4 + 12 α β^3 + 4 β^4 + 4 α^3 (4 + β) + α^2 (16 + β (8 + 9 β)))] -
    Sqrt[2] Sqrt[-16 - 16 (2 + α (2 + α)) - 8 (2 + α) β - 16 (1 + α)/(1 + α + β) +
      (6 α^2 + 2 (2 + β)^2 + α (12 + 7 β))^2/(1 + α + β)^2 - 1/(1 + α + β) (6 α^2 + 2 (2 + β)^2 + α (12 + 7 β))
        Sqrt[(1/(1 + α + β)^2) (4 α^4 + 12 α β^3 + 4 β^4 + 4 α^3 (4 + β) + α^2 (16 + β (8 + 9 β)))]]);

zPl[x_, α_, β_] := 1/8 (6 + 6 α + β + (2 + β + β^2)/(1 + α + β) +
    Sqrt[(1/(1 + α + β)^2) (4 α^4 + 12 α β^3 + 4 β^4 + 4 α^3 (4 + β) + α^2 (16 + β (8 + 9 β)))] +
    Sqrt[2] Sqrt[-16 - 16 (2 + α (2 + α)) - 8 (2 + α) β - 16 (1 + α)/(1 + α + β) +
      (6 α^2 + 2 (2 + β)^2 + α (12 + 7 β))^2/(1 + α + β)^2 + 1/(1 + α + β) (6 α^2 + 2 (2 + β)^2 + α (12 + 7 β))
        Sqrt[(1/(1 + α + β)^2) (4 α^4 + 12 α β^3 + 4 β^4 + 4 α^3 (4 + β) + α^2 (16 + β (8 + 9 β)))]]);

(**** ++ PROBABILITY AND CONSTANTS P_{++}(1) and P_{+-}(1) ****)

(* J_{++} - see eq(3.50) *)
jppPhys[x_, α_, β_, pp1_, pm1_, pTum1_] :=
 Evaluate[(1 / x) * (inverseANumer[x, α, β][[1, 1]] * pp1 +
     inverseANumer[x, α, β][[1, 2]] * pm1 + inverseANumer[x, α, β][[1, 5]] * pTum1)]

(* q(x) eq(3.45) *)
q[x_, α_, β_] := (x - 1) * (x - zPl[x, α, β]) *
   (x - zMiR[x, α, β]) * (x - (1 / zPl[1, α, β])) * (x - (1 / zMiR[1, α, β]))

(* Find P_{++}(1) and P_{+-}(1) - subsubsection 3.5.4 *)
pp1pm1Sols = Solve[
    gppNum[zPl[x, α, β], α, β, pp1, pm1, pTum1, L] == 0 &&
     gppNum[zMiR[x, α, β], α, β, pp1, pm1, pTum1, L] == 0,
    {pp1, pm1}
  ];

ppOne[x_, α_, β_, pTum1_, L_] := Evaluate[pp1 /. Flatten[pp1pm1Sols]]

pmOne[x_, α_, β_, pTum1_, L_] := Evaluate[pm1 /. Flatten[pp1pm1Sols]]

jpp[x_, α_, β_, pTum1_, L_] := Evaluate[
  jppPhys[x, α, β, pp1, pm1, pTum1] /. pp1 → ppOne[zPl[1, α, β], α, β, pTum1, L] /.
   pm1 → pmOne[zPl[1, α, β], α, β, pTum1, L] ]

(* ++ amplitudes *)

qZOne[x_, α_, β_] := Evaluate[q[x, α, β] / (x - 1)]
```

```
appOne[x_, α_, β_, pTum1_, L_] := Evaluate[jpp[x, α, β, pTum1, L] / qZOne[x, α, β]]

qZPP[x_, α_, β_] := Evaluate[q[x, α, β] / (x - zPl[x, α, β])]

appZPl[x_, α_, β_, pTum1_, L_] := Evaluate[jpp[x, α, β, pTum1, L] / qZPP[x, α, β]]

appZPlR[x_, α_, β_, pTum1_, L_] :=
 Evaluate[jpp[x, α, β, pTum1, L] / qZPPInverse[x, α, β]]

qZPPInverse[x_, α_, β_] := Evaluate[q[x, α, β] / (x - (1 / zPl[x, α, β]))]

qZMM[x_, α_, β_] := Evaluate[q[x, α, β] / (x - zMiR[x, α, β])]

appZMiR[x_, α_, β_, pTum1_, L_] := Evaluate[jpp[x, α, β, pTum1, L] / qZMM[x, α, β]]

qZMMInverse[x_, α_, β_] := Evaluate[q[x, α, β] / (x - (1 / zMiR[x, α, β]))]

appZMi[x_, α_, β_, pTum1_, L_] :=
 Evaluate[jpp[x, α, β, pTum1, L] / qZMMInverse[x, α, β]]

(* Un-normalised P_{++}(n)  *)

ppProb[n_, α_, β_, pTum1_, L_] := Evaluate[(-appOne[1, α, β, pTum1, L] +
     (-appZPl[zPl[1, α, β], α, β, pTum1, L] * (zPl[1, α, β] ^ (3 - n))) +
     (-appZPlR[1 / zPl[1, α, β], α, β, pTum1, L] * zPl[1, α, β] ^ (n - 3)) +
     (-appZMiR[zMiR[1, α, β], α, β, pTum1, L] * (zMiR[1, α, β] ^ (3 - n))) +
     (-appZMi[1 / zMiR[1, α, β], α, β, pTum1, L] * zMiR[1, α, β] ^ (n - 3)))]

(******* +- PROBABILITY *******)

gpmPhys[x_, α_, β_, pp1_, pm1_, pTum1_] :=
 Evaluate[x^(2) * (inverseANumer[x, α, β][[2, 1]] * pp1 +
     inverseANumer[x, α, β][[2, 2]] * pm1 + inverseANumer[x, α, β][[2, 5]] * pTum1 )]

(* Power counting for G_{+-} *)
λPmZero[α_, β_, pp1_, pm1_, pTum1_] :=
 Evaluate[CoefficientList[gpmPhys[x, α, β, pp1, pm1, pTum1], x][[1]]]

λPmOne[α_, β_, pp1_, pm1_, pTum1_] :=
 Evaluate[CoefficientList[gpmPhys[x, α, β, pp1, pm1, pTum1], x][[2]]]

λPmTwo[α_, β_, pp1_, pm1_, pTum1_] :=
 Evaluate[CoefficientList[gpmPhys[x, α, β, pp1, pm1, pTum1], x][[3]]]

λPmThree[α_, β_, pp1_, pm1_, pTum1_] :=
 Evaluate[CoefficientList[gpmPhys[x, α, β, pp1, pm1, pTum1], x][[4]]]

λPmFour[α_, β_, pp1_, pm1_, pTum1_] :=
 Evaluate[CoefficientList[gpmPhys[x, α, β, pp1, pm1, pTum1], x][[5]]]

λPmFive[α_, β_, pp1_, pm1_, pTum1_] :=
 Evaluate[CoefficientList[gpmPhys[x, α, β, pp1, pm1, pTum1], x][[6]]]

qZero[α_, β_] := Evaluate[CoefficientList[q[x, α, β], x][[1]]]

qOne[α_, β_] := Evaluate[CoefficientList[q[x, α, β], x][[2]]]

qTwo[α_, β_] := Evaluate[CoefficientList[q[x, α, β], x][[3]]]

qThree[α_, β_] := Evaluate[CoefficientList[q[x, α, β], x][[4]]]

qFour[α_, β_] := Evaluate[CoefficientList[q[x, α, β], x][[5]]]

qFive[α_, β_] := Evaluate[CoefficientList[q[x, α, β], x][[6]]]
```

```
wPm[α_, β_, pp1_, pm1_, pTum1_] :=
 Evaluate[λPmFive[α, β, pp1, pm1, pTum1] / qFive[α, β]]

dPmFour[α_, β_, pp1_, pm1_, pTum1_] :=
 Evaluate[λPmFour[α, β, pp1, pm1, pTum1] - wPm[α, β, pp1, pm1, pTum1] * qFour[α, β]]
dPmThree[α_, β_, pp1_, pm1_, pTum1_] := Evaluate[
  λPmThree[α, β, pp1, pm1, pTum1] - wPm[α, β, pp1, pm1, pTum1] * qThree[α, β]]
dPmTwo[α_, β_, pp1_, pm1_, pTum1_] :=
 Evaluate[λPmTwo[α, β, pp1, pm1, pTum1] - wPm[α, β, pp1, pm1, pTum1] * qTwo[α, β]]
dPmOne[α_, β_, pp1_, pm1_, pTum1_] :=
 Evaluate[λPmOne[α, β, pp1, pm1, pTum1] - wPm[α, β, pp1, pm1, pTum1] * qOne[α, β]]
dPmZero[α_, β_, pp1_, pm1_, pTum1_] :=
 Evaluate[λPmZero[α, β, pp1, pm1, pTum1] - wPm[α, β, pp1, pm1, pTum1] * qZero[α, β]]

jPmPhys[x_, α_, β_, pp1_, pm1_, pTum1_] :=
 Evaluate[(dPmZero[α, β, pp1, pm1, pTum1]) +
   (dPmOne[α, β, pp1, pm1, pTum1] * x) + (dPmTwo[α, β, pp1, pm1, pTum1] * x^(2)) +
   (dPmThree[α, β, pp1, pm1, pTum1] * x^(3)) +
   (dPmFour[α, β, pp1, pm1, pTum1] * x^(4))]

jPM[x_, α_, β_, pTum1_, L_] :=
 Evaluate[jPmPhys[x, α, β, pp1, pm1, pTum1] /. pp1 → ppOne[0, α, β, pTum1, L] /.
   pm1 → pmOne[0, α, β, pTum1, L] ]

(* +- amplitudes *)
qZPPInv[x_, α_, β_] := Evaluate[q[x, α, β] / (x - (1 / zPl[x, α, β]))]
qZMMInv[x_, α_, β_] := Evaluate[q[x, α, β] / (x - (1 / zMiR[x, α, β]))]

apmOne[x_, α_, β_, pTum1_, L_] := Evaluate[jPM[x, α, β, pTum1, L] / qZOne[x, α, β]]

apmZPl[x_, α_, β_, pTum1_, L_] := Evaluate[jPM[x, α, β, pTum1, L] / qZPP[x, α, β]]

apmZPlR[x_, α_, β_, pTum1_, L_] := Evaluate[jPM[x, α, β, pTum1, L] / qZPPInv[x, α, β]]

apmZMiR[x_, α_, β_, pTum1_, L_] := Evaluate[jPM[x, α, β, pTum1, L] / qZMM[x, α, β]]

apmZMi[x_, α_, β_, pTum1_, L_] := Evaluate[jPM[x, α, β, pTum1, L] / qZMMInv[x, α, β]]

wPMwPm[α_, β_, pTum1_, L_] :=
 Evaluate[wPm[α, β, pp1, pm1, pTum1] /. pp1 → ppOne[zPl[1, α, β], α, β, pTum1, L] /.
   pm1 → pmOne[zPl[1, α, β], α, β, pTum1, L] ]

(* Un-normalised P_{+-}(n)  *)
pmProb[n_, α_, β_, pTum1_, L_] :=
 Evaluate[(-apmOne[1, α, β, pTum1, L]
    - (apmZPl[zPl[1, α, β], α, β, pTum1, L] * zPl[1, α, β]^(-n))
    - ((apmZPlR[1 / zPl[1, α, β], α, β, pTum1, L]) * zPl[1, α, β]^(n))
    - ((apmZMiR[zMiR[1, α, β], α, β, pTum1, L]) * zMiR[1, α, β]^(-n))
    - ((apmZMi[1 / zMiR[1, α, β], α, β, pTum1, L]) * zMiR[1, α, β]^(n))
    + KroneckerDelta[n, 1] * wPMwPm[α, β, pTum1, L])]

(***** +0 PROBABILITY *****)
gpTumNum[x_, α_, β_, pp1_, pm1_, pTum1_, L_] := Evaluate[FullSimplify[Sum[
    inverseANumer[x, α, β][[5, i]] * bVec[x, pp1, pm1, pTum1, L][[i]], {i, 1, 6}]]]

gpTumPhys[x_, α_, β_, pp1_, pm1_, pTum1_] :=
 Evaluate[x^(2) * (inverseANumer[x, α, β][[5, 1]] * pp1 +
     inverseANumer[x, α, β][[5, 2]] * pm1 + inverseANumer[x, α, β][[5, 5]] * pTum1 )]

(* Power counting for G_{+0} *)
λPTumZero[α_, β_, pp1_, pm1_, pTum1_] :=
 Evaluate[CoefficientList[gpTumPhys[x, α, β, pp1, pm1, pTum1], x][[1]]]
```

```
λPTumOne[α_, β_, pp1_, pm1_, pTum1_] :=
 Evaluate[CoefficientList[gpTumPhys[x, α, β, pp1, pm1, pTum1], x][[2]]]

λPTumTwo[α_, β_, pp1_, pm1_, pTum1_] :=
 Evaluate[CoefficientList[gpTumPhys[x, α, β, pp1, pm1, pTum1], x][[3]]]

λPTumThree[α_, β_, pp1_, pm1_, pTum1_] :=
 Evaluate[CoefficientList[gpTumPhys[x, α, β, pp1, pm1, pTum1], x][[4]]]

λPTumFour[α_, β_, pp1_, pm1_, pTum1_] :=
 Evaluate[CoefficientList[gpTumPhys[x, α, β, pp1, pm1, pTum1], x][[5]]]

λPTumFive[α_, β_, pp1_, pm1_, pTum1_] :=
 Evaluate[CoefficientList[gpTumPhys[x, α, β, pp1, pm1, pTum1], x][[6]]]

wPTum[α_, β_, pp1_, pm1_, pTum1_] :=
 Evaluate[λPTumFive[α, β, pp1, pm1, pTum1] / qFive[α, β]]

dPTumFour[α_, β_, pp1_, pm1_, pTum1_] := Evaluate[
  λPTumFour[α, β, pp1, pm1, pTum1] - wPTum[α, β, pp1, pm1, pTum1] * qFour[α, β]]
dPTumThree[α_, β_, pp1_, pm1_, pTum1_] := Evaluate[
  λPTumThree[α, β, pp1, pm1, pTum1] - wPTum[α, β, pp1, pm1, pTum1] * qThree[α, β]]
dPTumTwo[α_, β_, pp1_, pm1_, pTum1_] := Evaluate[
  λPTumTwo[α, β, pp1, pm1, pTum1] - wPTum[α, β, pp1, pm1, pTum1] * qTwo[α, β]]
dPTumOne[α_, β_, pp1_, pm1_, pTum1_] := Evaluate[
  λPTumOne[α, β, pp1, pm1, pTum1] - wPTum[α, β, pp1, pm1, pTum1] * qOne[α, β]]
dPTumZero[α_, β_, pp1_, pm1_, pTum1_] := Evaluate[
  λPTumZero[α, β, pp1, pm1, pTum1] - wPTum[α, β, pp1, pm1, pTum1] * qZero[α, β]]

jPTumPhys[x_, α_, β_, pp1_, pm1_, pTum1_] :=
 Evaluate[(dPTumZero[α, β, pp1, pm1, pTum1]) +
    (dPTumOne[α, β, pp1, pm1, pTum1] * x) + (dPTumTwo[α, β, pp1, pm1, pTum1] * x^(2)) +
    (dPTumThree[α, β, pp1, pm1, pTum1] * x^(3)) +
    (dPTumFour[α, β, pp1, pm1, pTum1] * x^(4))]

jPTum[x_, α_, β_, pTum1_, L_] :=
 Evaluate[jPTumPhys[x, α, β, pp1, pm1, pTum1] /. pp1 → ppOne[0, α, β, pTum1, L] /.
   pm1 → pmOne[0, α, β, pTum1, L] ]

(* +0 amplitudes *)
apTumOne[x_, α_, β_, pTum1_, L_] :=
 Evaluate[jPTum[x, α, β, pTum1, L] / qZOne[x, α, β]]

apTumZpl[x_, α_, β_, pTum1_, L_] := Evaluate[jPTum[x, α, β, pTum1, L] / qZPP[x, α, β]]

apTumZPlR[x_, α_, β_, pTum1_, L_] :=
 Evaluate[jPTum[x, α, β, pTum1, L] / qZPPInv[x, α, β]]

apTumZMiR[x_, α_, β_, pTum1_, L_] :=
 Evaluate[jPTum[x, α, β, pTum1, L] / qZMM[x, α, β]]

apTumZMi[x_, α_, β_, pTum1_, L_] :=
 Evaluate[jPTum[x, α, β, pTum1, L] / qZMMInv[x, α, β]]

wPTumwPTum[α_, β_, pTum1_, L_] := Evaluate[
  wPTum[α, β, pp1, pm1, pTum1] /. pp1 → ppOne[zPl[1, α, β], α, β, pTum1, L] /.
   pm1 → pmOne[zPl[1, α, β], α, β, pTum1, L] ]
```

```
pTumProb[n_, α_, β_, pTum1_, L_] :=
 Evaluate[(-apTumOne[1, α, β, pTum1, L]
    - (apTumZpl[zPl[1, α, β], α, β, pTum1, L] * zPl[1, α, β]^(-n))
    - ((apTumZPlR[1 / zPl[1, α, β], α, β, pTum1, L]) * zPl[1, α, β]^(n))
    - ((apTumZMiR[zMiR[1, α, β], α, β, pTum1, L]) * zMiR[1, α, β]^(-n))
    - ((apTumZMi[1 / zMiR[1, α, β], α, β, pTum1, L]) * zMiR[1, α, β]^(n))
    + KroneckerDelta[n, 1] * wPTumwPTum[α, β, pTum1, L])]

(* 00 PROBABILITY *)
gTumTumNum[x_, α_, β_, pp1_, pm1_, pTum1_, L_] := Evaluate[FullSimplify[Sum[
    inverseANumer[x, α, β][[6, i]] * bVec[x, pp1, pm1, pTum1, L][[i]], {i, 1, 6}]]]

gTumTumPhys[x_, α_, β_, pp1_, pm1_, pTum1_] :=
 Evaluate[x^(2) * (inverseANumer[x, α, β][[6, 1]] * pp1 +
     inverseANumer[x, α, β][[6, 2]] * pm1 + inverseANumer[x, α, β][[6, 5]] * pTum1 )]

gTumTumPhysExtra[x_, α_, β_, pp1_, pm1_, pTum1_, L_] :=
 x^(L - 2) * (-pm1 α^2 - pTum1 α (1 + α))

(* Power counting for G_{00} *)
λTumTumZero[α_, β_, pp1_, pm1_, pTum1_] :=
 Evaluate[CoefficientList[gTumTumPhys[x, α, β, pp1, pm1, pTum1], x][[1]]]

λTumTumOne[α_, β_, pp1_, pm1_, pTum1_] :=
 Evaluate[CoefficientList[gTumTumPhys[x, α, β, pp1, pm1, pTum1], x][[2]]]

λTumTumTwo[α_, β_, pp1_, pm1_, pTum1_] :=
 Evaluate[CoefficientList[gTumTumPhys[x, α, β, pp1, pm1, pTum1], x][[3]]]

λTumTumThree[α_, β_, pp1_, pm1_, pTum1_] :=
 Evaluate[CoefficientList[gTumTumPhys[x, α, β, pp1, pm1, pTum1], x][[4]]]

λTumTumFour[α_, β_, pp1_, pm1_, pTum1_] :=
 Evaluate[CoefficientList[gTumTumPhys[x, α, β, pp1, pm1, pTum1], x][[5]]]

λTumTumFive[α_, β_, pp1_, pm1_, pTum1_] :=
 Evaluate[CoefficientList[gTumTumPhys[x, α, β, pp1, pm1, pTum1], x][[6]]]

wTumTum[α_, β_, pp1_, pm1_, pTum1_] :=
 Evaluate[λTumTumFive[α, β, pp1, pm1, pTum1] / qFive[α, β]]

dTumTumFour[α_, β_, pp1_, pm1_, pTum1_] := Evaluate[
  λTumTumFour[α, β, pp1, pm1, pTum1] - wTumTum[α, β, pp1, pm1, pTum1] * qFour[α, β]]
dTumTumThree[α_, β_, pp1_, pm1_, pTum1_] :=
 Evaluate[λTumTumThree[α, β, pp1, pm1, pTum1] -
   wTumTum[α, β, pp1, pm1, pTum1] * qThree[α, β]]
dTumTumTwo[α_, β_, pp1_, pm1_, pTum1_] := Evaluate[
  λTumTumTwo[α, β, pp1, pm1, pTum1] - wTumTum[α, β, pp1, pm1, pTum1] * qTwo[α, β]]
dTumTumOne[α_, β_, pp1_, pm1_, pTum1_] := Evaluate[
  λTumTumOne[α, β, pp1, pm1, pTum1] - wTumTum[α, β, pp1, pm1, pTum1] * qOne[α, β]]
dTumTumZero[α_, β_, pp1_, pm1_, pTum1_] := Evaluate[
  λTumTumZero[α, β, pp1, pm1, pTum1] - wTumTum[α, β, pp1, pm1, pTum1] * qZero[α, β]]

jTumTumPhys[x_, α_, β_, pp1_, pm1_, pTum1_] := Evaluate[
  (dTumTumZero[α, β, pp1, pm1, pTum1]) + (dTumTumOne[α, β, pp1, pm1, pTum1] * x) +
   (dTumTumTwo[α, β, pp1, pm1, pTum1] * x^(2)) +
   (dTumTumThree[α, β, pp1, pm1, pTum1] * x^(3)) +
   (dTumTumFour[α, β, pp1, pm1, pTum1] * x^(4))]

jTumTum[x_, α_, β_, pTum1_, L_] :=
 Evaluate[jTumTumPhys[x, α, β, pp1, pm1, pTum1] /. pp1 → ppOne[0, α, β, pTum1, L] /.
   pm1 → pmOne[0, α, β, pTum1, L] ]
```

```
(* +0 amplitudes *)
aTumTumOne[x_, α_, β_, pTum1_, L_] :=
 Evaluate[jTumTum[x, α, β, pTum1, L] / qZOne[x, α, β]]

aTumTumZPl[x_, α_, β_, pTum1_, L_] :=
 Evaluate[jTumTum[x, α, β, pTum1, L] / qZPP[x, α, β]]

aTumTumZPlR[x_, α_, β_, pTum1_, L_] :=
 Evaluate[jTumTum[x, α, β, pTum1, L] / qZPPInv[x, α, β]]

aTumTumZMiR[x_, α_, β_, pTum1_, L_] :=
 Evaluate[jTumTum[x, α, β, pTum1, L] / qZMM[x, α, β]]

aTumTumZMi[x_, α_, β_, pTum1_, L_] :=
 Evaluate[jTumTum[x, α, β, pTum1, L] / qZMMInv[x, α, β]]

wTumTumwTumTum[α_, β_, pTum1_, L_] := Evaluate[
  wTumTum[α, β, pp1, pm1, pTum1] /. pp1 → ppOne[zPl[1, α, β], α, β, pTum1, L] /.
   pm1 → pmOne[zPl[1, α, β], α, β, pTum1, L] ]


(* Un-normalised P_{00}(n)  *)
TumTumProb[n_, α_, β_, pTum1_, L_] :=
 Evaluate[ (-aTumTumOne[1, α, β, pTum1, L]
    - (aTumTumZPl[zPl[1, α, β], α, β, pTum1, L] * zPl[1, α, β]^(-n))
    - ((aTumTumZPlR[1 / zPl[1, α, β], α, β, pTum1, L]) * zPl[1, α, β]^(n))
    - ((aTumTumZMiR[zMiR[1, α, β], α, β, pTum1, L]) * zMiR[1, α, β]^(-n))
    - ((aTumTumZMi[1 / zMiR[1, α, β], α, β, pTum1, L]) * zMiR[1, α, β]^(n))
    + (KroneckerDelta[n, 1] + KroneckerDelta[n, L - 1]) *
     wTumTumwTumTum[α, β, pTum1, L]) ]

(*************************************************************************
************)
(************ EXAMPLE CALCULATION WITH α =0.01,
β = 0.1, L=30 - see figure 2 ************)
(*************************************************************************
************)
norma = 0.01;
normb = 0.1;
normL = 30;

probTotal = Table[{n,
    ppProb[n, norma, normb, pTumOpen, normL] +
     ppProb[n, norma, normb, pTumOpen, normL] +
     pmProb[30 - n, norma, normb, pTumOpen, normL] +
     pmProb[n, norma, normb, pTumOpen, normL] +
     2 * pTumProb[n, norma, normb, pTumOpen, normL] +
     2 * pTumProb[30 - n, norma, normb, pTumOpen, normL] +
     TumTumProb[n, norma, normb, pTumOpen, normL]
   }, {n, 1, 29 }];

ppProbTotal = Table[{n,
    ppProb[n, norma, normb, pTumOpen, normL]
   }, {n, 1, 29 }];

normalisationPP[pTumOpen_] := Evaluate[Sum[ppProbTotal[[n]][[2]], {n, 1, 29}]]

pTumOpenSoln =
 Solve[normalisationPP[pTumOp] == 1 / (4 * (1 + (norma / normb))^(2)), pTumOp]
{{pTumOp → 0.239859}}
```

```
pTumOpen = pTumOp /. pTumOpenSoln[[1]]
0.239859
prob[pTumOpen_] := Evaluate[probTotal]
maxSep = 30;
normalisation = 500 000 000 - 200 000;
```

```
(* Compare to simulations -
 simulation data in "sepsn30_a100_b10_500million.txt" *)
seps = {{0.`, 5.756143`18.760131574586925*^6, 5.193239`18.715438309884238*^6,
    4.710785`18.67309328351135*^6, 4.297947`18.633261055699524*^6,
    3.942421`18.595762999500543*^6, 3.635664`18.560583739872087*^6,
    3.375962`18.52839754954035*^6, 3.160833`18.499801550855587*^6,
    2.980525`18.474292768949095*^6, 2.835114`18.452570526571268*^6,
    2.720602`18.434665012986546*^6, 2.631796`18.420252222514897*^6,
    2.566704`18.409375787417524*^6, 2.526261`18.402478217559047*^6,
    2.511869`18.399996986155667*^6, 2.525568`18.40235906622679*^6,
    2.565292`18.409136806785458*^6, 2.626785`18.41942452762628*^6,
    2.716254`18.4339703788782*^6, 2.836728`18.45281769541437*^6,
    2.988595`18.47546706553026*^6, 3.171995`18.501332494069867*^6,
    3.386711`18.529778138345172*^6, 3.640131`18.561117013196693*^6,
    3.938273`18.595305818019497*^6, 4.290893`18.632547684868502*^6,
    4.707618`18.672801214744272*^6, 5.193075`18.71542459485597*^6,
    5.757142`18.760206941467622*^6}, {0.`, 9.8865891`18.99504648466581*^7,
    324524.`18.51124682034175, 309559.`18.49074343504418,
    295651.`18.470779352280662, 282194.`18.450547775560807,
    269317.`18.43026376809094, 256844.`18.409669424849817,
    244550.`18.388367667157304, 232702.`18.366800115926313,
    221018.`18.344427644645926, 209635.`18.32146379280548,
    197949.`18.296553312122178, 186357.`18.270345710501594,
    174765.`18.24245446131418, 163109.`18.212477925126723,
    151430.`18.180211922348942, 139341.`18.14407892298428,
    127344.`18.10497848735792, 115246.`18.061625860672752,
    103067.`18.013119635099006, 90812.`18.958143240475255,
    78580.`18.89531202447579, 66579.`18.82333726787467,
    54767.`18.738518952009134, 43402.`18.63750974262198,
    32501.`18.51189672368043, 22366.`18.349588320562464,
    13276.`18.123067243736568, 5677.`18.754118894225414},
   {0.`, 1.3342105`18.12522435415056*^7, 358258.`18.554195897093287,
    338876.`18.530040812163875, 324531.`18.511256187995873,
    311341.`18.49323631599662, 300272.`18.47751483665306,
    291541.`18.464699639100687, 284433.`18.453979981953953,
    278897.`18.44544384273341, 275358.`18.439897698596074,
    273023.`18.436199234411948, 269742.`18.430948573253463,
    269368.`18.430346001747505, 267215.`18.426860833423206,
    267043.`18.426581198290112, 267052.`18.426595834826074,
    266367.`18.425480419426048, 265072.`18.42336385490124,
    263822.`18.42131100834537, 262366.`18.41890755414453,
    259149.`18.413549537330212, 253972.`18.40478583899871,
    246575.`18.39194904179565, 236859.`18.37448989139067,
    223895.`18.350044395067837, 205878.`18.313609940648742,
    182499.`18.261260489090184, 152632.`18.183645594998218,
    113249.`18.05403437583808}, {0.`, 1.353375`18.131418149787226*^6,
    51588.`18.71254869116463, 53683.`18.729836777783888,
    52825.`18.72283950572435, 53458.`18.72801270666123,
    54311.`18.7348877993031, 53233.`18.726180941970846,
    53993.`18.732337458740908, 52682.`18.7216622539981,
    54146.`18.733566378928238, 53339.`18.72704486927375,
    54891.`18.739501142797028, 53326.`18.726939008339187,
    54222.`18.73417553266432, 52600.`18.72098574415374,
    53508.`18.728418718397233, 53290.`18.726645720240914,
    52938.`18.723767529610377, 53343.`18.727077436678343,
    53619.`18.72931871008454, 54019.`18.73254654026421,
    52512.`18.720258559373, 53876.`18.731395344244454,
    52962.`18.723964376970983, 52776.`18.7224364710724,
    53119.`18.725249890558572, 51355.`18.710582733555444,
    52943.`18.723808546835585, 1.346103`18.129078292146648*^6}};
```

```
ppProbAn = Table[{n, ppProb[n, norma, normb, pTumOpen, normL]}, {n, 1, 29}];

ppProbSim = Table[{sep - 1, seps[[1]][[sep]] / normalisation}, {sep, 2, maxSep}];

Rasterize[Show[ListPlot[ppProbAn, PlotStyle → {Blue, PointSize[0.02]},
    AxesLabel → {"n", "P++(n)"}, PlotRange → {0.0045, 0.012}], ListPlot[
    ppProbSim, PlotStyle → {Red, PointSize[0.013]}]], ImageResolution → 1000]
```

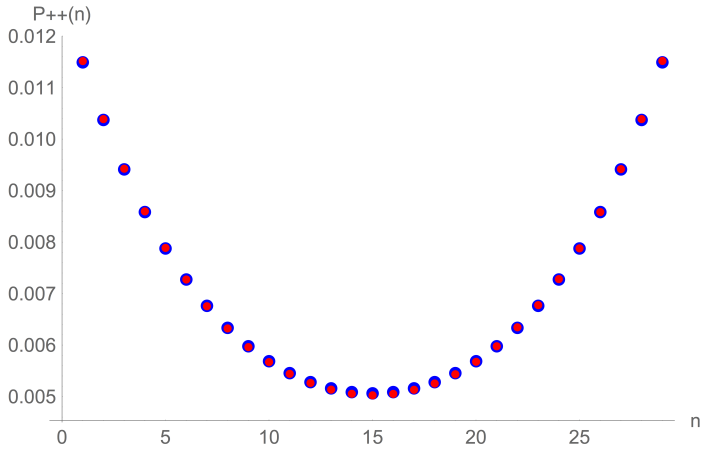


```
pmProbAn = Table[{n, pmProb[n, norma, normb, pTumOpen, normL]}, {n, 1, 29}];

pmProbSim = Table[{sep - 1, seps[[2]][[sep]] / normalisation}, {sep, 2, maxSep}];

Rasterize[Show[ListPlot[pmProbAn, PlotStyle → {Blue, PointSize[0.021]},
    AxesLabel → {"n", "P+-(n)"}, PlotRange → {0, 0.0007}], ListPlot[
    pmProbSim, PlotStyle → {Red, PointSize[0.014]}]], ImageResolution → 1000]
```

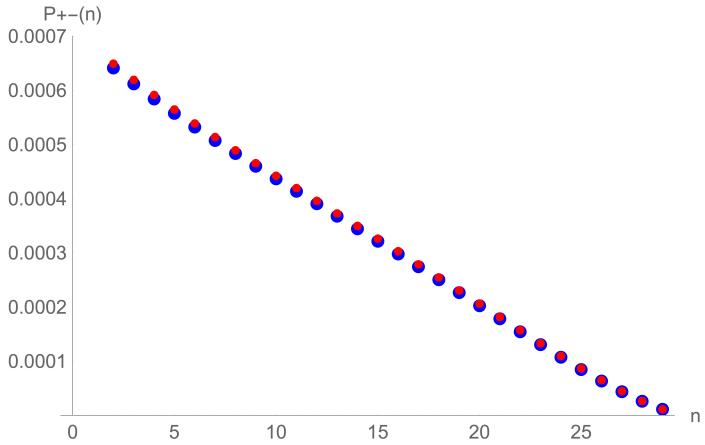


```
pTumProbAn = Table[{n, pTumProb[n, norma, normb, pTumOpen, normL]}, {n, 1, 29}];

pTumProbSim = Table[{sep - 1, seps[[3]][[sep]] / normalisation}, {sep, 2, maxSep}];
```

```
Rasterize[Show[ListPlot[pTumProbAn, PlotStyle → {Blue, PointSize[0.02]},
    AxesLabel → {"n", "P+Tum(n)"}, PlotRange → {0.0002, 0.00075}],
  ListPlot[pTumProbSim, PlotStyle → {Red, PointSize[0.013]}]],
 ImageResolution → 1000]
```

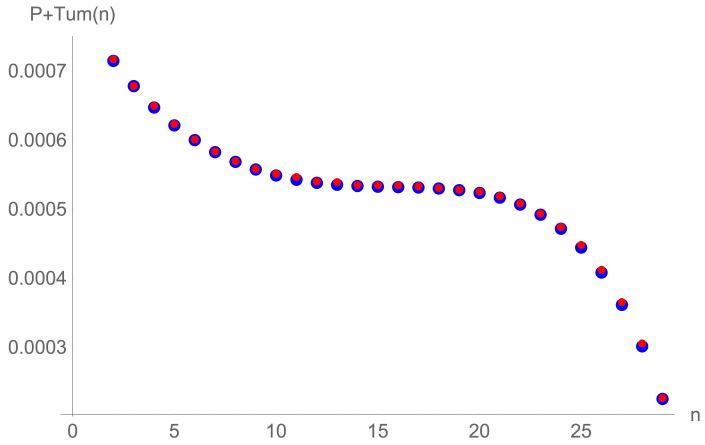


```
tumTumProbAn =
  Table[{n, TumTumProb[n, norma, normb, pTumOpen, normL]}, {n, 1, 29}];

TumTumProbSim =
  Table[{sep - 1, seps[[4]][[sep]] / normalisation}, {sep, 2, maxSep}];

Rasterize[Show[ListPlot[tumTumProbAn, PlotStyle → {Blue, PointSize[0.02]},
    AxesLabel → {"n", "PTumTum(n)"}, PlotRange → All], ListPlot[TumTumProbSim,
    PlotStyle → {Red, PointSize[0.013]}]], ImageResolution → 1000]
```

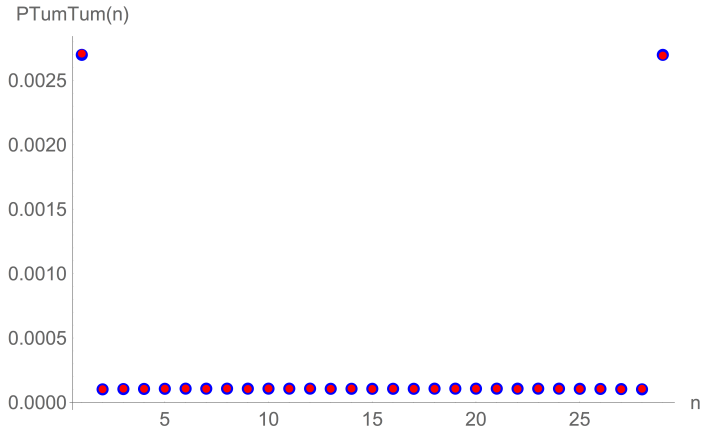

Bibliography

[1] Howard C Berg. *Random walks in biology*. Princeton University Press, 1993.

[2] Sriram Ramaswamy. The mechanics and statistics of active matter. *Annual Review of Condensed Matter Physics*, 1(1):323–345, 2010.

[3] ME Cates. Diffusive transport without detailed balance in motile bacteria: does microbiology need statistical physics? *Rep. Prog. Phys.*, 75(4):042601, 2012.

[4] Jens Elgeti, Roland G Winkler, and Gerhard Gompper. Physics of microswimmers: single particle motion and collective behavior: a review. *Reports on progress in physics*, 78(5):056601, 2015.

[5] Clemens Bechinger, Roberto Di Leonardo, Hartmut Löwen, Charles Reichhardt, Giorgio Volpe, and Giovanni Volpe. Active particles in complex and crowded environments. *Reviews of Modern Physics*, 88(4):045006, 2016.

[6] John Toner and Yuhai Tu. Long-range order in a two-dimensional dynamical XY model: How birds fly together. *Phys. Rev. Lett.*, 75:4326–4329, 1995.

[7] András Czirók and Tamás Vicsek. Collective behavior of interacting self-propelled particles. *Physica A: Statistical Mechanics and its Applications*, 281(1–4):17–29, 2000.

[8] John Toner, Yuhai Tu, and Sriram Ramaswamy. Hydrodynamics and phases of flocks. *Annals of Physics*, 318(1):170 – 244, 2005. Special Issue.

[9] M C Marchetti, J F Joanny, S Ramaswamy, T B Liverpool, J Prost, M Rao, and R A Simha. Hydrodynamics of soft active matter. *Rev. Mod. Phys*, 85:1143–89, 2013.

[10] Antoine Bricard, Jean-Baptiste Caussin, Nicolas Desreumaux, Olivier Dauchot, and Denis Bartolo. Emergence of macroscopic directed motion in populations of motile colloids. *Nature*, 503(7474):95–98, 2013.

[11] S. Chandrasekhar. Stochastic problems in physics and astronomy. *Rev. Mod. Phys.*, 15:1–89, 1943.

[12] Edward Nelson. *Dynamical theories of Brownian motion*, volume 3. Princeton University Press, 1967.

[13] Robert Brown. Xxvii. a brief account of microscopical observations made in the months of june, july and august 1827, on the particles contained in the pollen of plants; and on the general existence of active molecules in organic and inorganic bodies. *Philosophical Magazine Series 2*, 4(21):161–173, 1828.

[14] Philip Pearle, Brian Collett, Kenneth Bart, David Bilderback, Dara Newman, and Scott Samuels. What brown saw and you can too. *American Journal of Physics*, 78(12):1278–1289, 2010.

[15] Geoffrey Grimmett and David Stirzaker. *Probability and random processes*. Oxford University Press, 2001.

[16] Pawel Romanczuk, Markus Bär, Werner Ebeling, Benjamin Lindner, and Lutz Schimansky-Geier. Active brownian particles. *The European Physical Journal Special Topics*, 202(1):1–162, 2012.

[17] Kerson Huang. *Introduction to statistical physics*. CRC press, 2009.

[18] Albert Einstein. *Investigations on the Theory of the Brownian Movement*. Courier Corporation, 1956.

[19] Jeremie Palacci, Stefano Sacanna, Asher Preska Steinberg, David J. Pine, and Paul M. Chaikin. Living crystals of light-activated colloidal surfers. *Science*, 339(6122):936–940, 2013.

[20] Craig W Reynolds. Flocks, herds and schools: a distributed behavioral model. *ACM SIGGRAPH computer graphics*, 21(4):25–34, 1987.

[21] Tamás Vicsek, András Czirók, Eshel Ben-Jacob, Inon Cohen, and Ofer Shochet. Novel type of phase transition in a system of self-driven particles. *Physical review letters*, 75(6):1226, 1995.

[22] Alessandro Attanasi, Andrea Cavagna, Lorenzo Del Castello, Irene Giardina, Tomas S Grigera, Asja Jelić, Stefania Melillo, Leonardo Parisi, Oliver Pohl, Edward Shen, et al. Information transfer and behavioural inertia in starling flocks. *Nature physics*, 10(9):691–696, 2014.

[23] William Bialek, Andrea Cavagna, Irene Giardina, Thierry Mora, Edmondo Silvestri, Massimiliano Viale, and Aleksandra M. Walczak. Statistical mechanics for natural flocks of birds. *Proceedings of the National Academy of Sciences*, 109(13):4786–4791, 2012.

[24] R Aditi Simha and Sriram Ramaswamy. Hydrodynamic fluctuations and instabilities in ordered suspensions of self-propelled particles. *Physical review letters*, 89(5):058101, 2002.

[25] Thomas Speck. Stochastic thermodynamics for active matter. *Europhys. Lett*, 114:30006, 2016.

[26] Cesare Nardini, Étienne Fodor, Elsen Tjhung, Frédéric van Wijland, Julien Tailleur, and Michael E Cates. Entropy production in field theories without time-reversal symmetry: quantifying the non-equilibrium character of active matter. *Physical Review X*, 7(2):021007, 2017.

[27] Sriram Ramaswamy. Active matter. *Journal of Statistical Mechanics: Theory and Experiment*, 2017(5):054002, 2017.

[28] Yaouen Fily and M. Cristina Marchetti. Athermal phase separation of self-propelled particles with no alignment. *Phys. Rev. Lett.*, 108:235702, 2012.

[29] Gabriel S. Redner, Michael F. Hagan, and Aparna Baskaran. Structure and dynamics of a phase-separating active colloidal fluid. *Phys. Rev. Lett.*, 110:055701, 2013.

[30] Xingbo Yang, M Lisa Manning, and M Cristina Marchetti. Aggregation and segregation of confined active particles. *Soft matter*, 10(34):6477–6484, 2014.

[31] AP Solon, ME Cates, and J Tailleur. Active brownian particles and run-and-tumble particles: A comparative study. *The European Physical Journal Special Topics*, 224(7):1231–1262, 2015.

[32] Jérémie Palacci, Cécile Cottin-Bizonne, Christophe Ybert, and Lydéric Bocquet. Sedimentation and effective temperature of active colloidal suspensions. *Physical Review Letters*, 105(8):088304, 2010.

[33] I Theurkauff, C Cottin-Bizonne, J Palacci, C Ybert, and L Bocquet. Dynamic clustering in active colloidal suspensions with chemical signaling. *Physical review letters*, 108(26):268303, 2012.

[34] Ivo Buttinoni, Julian Bialké, Felix Kümmel, Hartmut Löwen, Clemens Bechinger, and Thomas Speck. Dynamical clustering and phase separation in suspensions of self-propelled colloidal particles. *Phys. Rev. Lett.*, 110:238301, Jun 2013.

[35] Sho C Takatori, Wen Yan, and John F Brady. Swim pressure: stress generation in active matter. *Physical review letters*, 113(2):028103, 2014.

[36] Yaouen Fily, Silke Henkes, and M Cristina Marchetti. Freezing and phase separation of self-propelled disks. *Soft matter*, 10(13):2132–2140, 2014.

[37] Jana Schwarz-Linek, Jochen Arlt, Alys Jepson, Angela Dawson, Teun Vissers, Dario Miroli, Teuta Pilizota, Vincent A Martinez, and Wilson CK Poon. Escherichia coli as a model active colloid: a practical introduction. *Colloids and Surfaces B: Biointerfaces*, 137:2–16, 2016.

[38] Howard C Berg. *E. coli in Motion*. Springer, 2004.

[39] Olivier Tenaillon, David Skurnik, Bertrand Picard, and Erick Denamur. The population genetics of commensal escherichia coli. *Nature reviews. Microbiology*, 8(3):207, 2010.

[40] Michael Donnenberg. *E. coli: Genomics, Evolution and Pathogenesis*. Springer, 2002.

[41] CR Calladine. Design requirements for the construction of bacterial flagella. *Journal of theoretical biology*, 57(2):469–489, 1976.

[42] Yoshiyuki Sowa and Richard M Berry. Bacterial flagellar motor. *Quarterly reviews of biophysics*, 41(2):103–132, 2008.

[43] Howard C Berg and Douglas A Brown. Chemotaxis in escherichia coli analysed by three-dimensional tracking. *Nature*, 239:500–4, 1972.

[44] Frederick C. Neidhardt (Ed.). *Escherichia Coli and Salmonella: Cellular and Molecular Biology*. American Society for Microbiology, 1996.

[45] Mark Achtman and Michael Wagner. Microbial diversity and the genetic nature of microbial species. *Nature reviews. Microbiology*, 6(6):431, 2008.

[46] Ekaterina Korobkova, Thierry Emonet, Jose M G Vilar, Thomas S Shimizu, and Philippe Cluzel. From molecular noise to behavioural variability in a single bacterium. *Nature*, 428(6982):574–578, 2004.

[47] Taejin L Min, Patrick J Mears, Lon M Chubiz, Christopher V Rao, Ido Golding, and Yann R Chemla. High-resolution, long-term characterization of bacterial motility using optical tweezers. *Nature methods*, 6(11):831–835, 2009.

[48] Jonathan Saragosti, Pascal Silberzan, and Axel Buguin. Modeling *E. coli* tumbles by rotational diffusion:x implications for chemotaxis. *PLoS ONE*, 7(4):1–6, 04 2012.

[49] Patrick J Mears, Santosh Koirala, Chris V Rao, Ido Golding, and Yann R Chemla. Escherichia coli swimming is robust against variations in flagellar number. *Elife*, 3:e01916, 2014.

[50] Linda Turner, William S Ryu, and Howard C Berg. Real-time imaging of fluorescent flagellar filaments. *Journal of bacteriology*, 182(10):2793–2801, 2000.

[51] Nicholas C Darnton, Linda Turner, Svetlana Rojevsky, and Howard C Berg. On torque and tumbling in swimming escherichia coli. *Journal of bacteriology*, 189(5):1756–1764, 2007.

[52] Howard C Berg and Linda Turner. Cells of escherichia coli swim either end forward. *Proceedings of the National Academy of Sciences*, 92(2):477–479, 1995.

[53] Sherri A. Biondi, John A. Quinn, and Howard Goldfine. Random motility of swimming bacteria in restricted geometries. *AIChE Journal*, 44(8):1923–1929, 1998.

[54] Jaan Männik, Rosalie Driessen, Peter Galajda, Juan E. Keymer, and Cees Dekker. Bacterial growth and motility in sub-micron constrictions. *Proc. Natl. Acad. Sci. USA*, 106(35):14861–14866, 2009.

[55] William B Whitman, David C Coleman, and William J Wiebe. Prokaryotes: the unseen majority. *Proceedings of the National Academy of Sciences*, 95(12):6578–6583, 1998.

[56] Lionel Ranjard and Agnès Richaume. Quantitative and qualitative microscale distribution of bacteria in soil. *Research in microbiology*, 152(8):707–716, 2001.

[57] Sidney Goldstein. On diffusion by discontinuous movements, and on the telegraph equation. *The Quarterly Journal of Mechanics and Applied Mathematics*, 4(2):129–156, 1951.

[58] George H Weiss. The two-state random walk. *Journal of Statistical Physics*, 15(2):157–165, 1976.

[59] Mark J. Schnitzer. Theory of continuum random walks and application to chemotaxis. *Phys. Rev. E*, 48:2553–2568, 1993.

[60] George H Weiss. Some applications of persistent random walks and the telegrapher's equation. *Physica A: Statistical Mechanics and its Applications*, 311:381–410, 2002.

[61] Luca Angelani. Run-and-tumble particles, telegrapher's equation and absorption problems with partially reflecting boundaries. *Journal of Physics A: Mathematical and Theoretical*, 48(49):495003, 2015.

[62] Luca Angelani. Confined run-and-tumble swimmers in one dimension. *Journal of Physics A: Mathematical and Theoretical*, 50(32), 2017.

[63] L Angelani, R Di Leonardo, and M Paulozzi. First-passage time of run-and-tumble particles. *Eur. Phys. J. E*, 37:59, 2014.

[64] F Detcheverry. Non-poissonian run-and-turn motions. *EPL (Europhysics Letters)*, 111(6):60002, 2015.

[65] M E Cates and J Tailleur. Motility-induced phase separation. *Annu. Rev. Condens. Matter*, 6:219–44, 2015.

[66] E Ben-Jacob, I Cohen, and H Levine. Cooperative self-organization of microorganisms. *Adv. Phys.*, 49:395–554, 2010.

[67] J W Costerton, Philip S Stewart, and E P Greenberg. Bacterial Biofilms: A Common Cause of Persistent Infections. *Science*, 284(5418):1318–1322, 1999.

[68] David Davies. Understanding biofilm resistance to antibacterial agents. *Nat Rev Drug Discov*, 2(2):114–122, 2003.

[69] Manuel Simões, Lúcia C Simões, and Maria J Vieira. A review of current and emergent biofilm control strategies. *LWT - Food Science and Technology*, 43(4):573–583, 2010.

[70] Esther Karunakaran, Joy Mukherjee, Bharathi Ramalingam, and Catherine A Biggs. Biofilmology: a multidisciplinary review of the study of microbial biofilms. *Applied microbiology and biotechnology*, 90(6):1869–1881, 2011.

[71] J William Costerton, Zbigniew Lewandowski, Douglas E Caldwell, Darren R Korber, and Hilary M Lappin-Scott. Microbial biofilms. *Annual Reviews in Microbiology*, 49(1):711–745, 1995.

[72] George O'Toole, Heidi B Kaplan, and Roberto Kolter. Biofilm formation as microbial development. *Annual Reviews in Microbiology*, 54(1):49–79, 2000.

[73] Russell D Monds and George A O'Toole. The developmental model of microbial biofilms: ten years of a paradigm up for review. *Trends in Microbiology*, 17(2):73–87, 2009.

[74] Rodrigo Soto and Ramin Golestanian. Run-and-tumble dynamics in a crowded environment: Persistent exclusion process for swimmers. *Phys. Rev. E*, 89(1):012706, 2014.

[75] A. B. Slowman, M. R. Evans, and R. A. Blythe. Jamming and attraction of interacting run-and-tumble random walkers. *Phys. Rev. Lett.*, 116:218101, 2016.

[76] Melissa B Miller and Bonnie L Bassler. Quorum sensing in bacteria. *Annual Reviews in Microbiology*, 55(1):165–199, 2001.

[77] David G Davies, Matthew R Parsek, James P Pearson, Barbara H Iglewski, JW t Costerton, and EP Greenberg. The involvement of cell-to-cell signals in the development of a bacterial biofilm. *Science*, 280(5361):295–298, 1998.

[78] E Lauga and T R Powers. The hydrodynamics of swimming microorganisms. *Rep. Prog. Phys.*, 72:096601, 2009.

[79] Thomas K Wood, Andrés F González Barrios, Moshe Herzberg, and Jintae Lee. Motility influences biofilm architecture in escherichia coli. *Applied microbiology and biotechnology*, 72(2):361–367, 2006.

[80] Fernando Peruani, Andreas Deutsch, and Markus Bär. Nonequilibrium clustering of self-propelled rods. *Phys. Rev. E*, 74:030904, 2006.

[81] Fernando Peruani, Lutz Schimansky-Geier, and Markus Baer. Cluster dynamics and cluster size distributions in systems of self-propelled particles. *The European Physical Journal Special Topics*, 191(1):173–185, 2011.

[82] Fernando Peruani, Tobias Klauss, Andreas Deutsch, and Anja Voss-Boehme. Traffic jams, gliders, and bands in the quest for collective motion of self-propelled particles. *Phys. Rev. Lett.*, 106:128101, 2011.

[83] Ruben van Drongelen, Anshuman Pal, Carl P. Goodrich, and Timon Idema. Collective dynamics of soft active particles. *Phys. Rev. E*, 91:032706, 2015.

[84] Joakim Stenhammar, Adriano Tiribocchi, Rosalind J. Allen, Davide Marenduzzo, and Michael E. Cates. Continuum theory of phase separation kinetics for active brownian particles. *Phys. Rev. Lett.*, 111:145702, 2013.

[85] Raphael Wittkowski, Adriano Tiribocchi, Joakim Stenhammar, Rosalind J Allen, Davide Marenduzzo, and Michael E Cates. Scalar ϕ^4 field theory for active-particle phase separation. *Nat. Commun.*, 5, 2014.

[86] Thomas Speck, Julian Bialké, Andreas M. Menzel, and Hartmut Löwen. Effective cahn-hilliard equation for the phase separation of active brownian particles. *Phys. Rev. Lett.*, 112:218304, 2014.

[87] J. Tailleur and M. Cates. Statistical Mechanics of Interacting Run-and-Tumble Bacteria. *Phys. Rev. Lett*, 100(21):218103, 2008.

[88] A G Thompson, J Tailleur, M E Cates, and R A Blythe. Lattice models of nonequilibrium bacterial dynamics. *J. Stat. Mech.: Theor. Exp.*, 2011(02):P02029, 2011.

[89] Néstor Sepúlveda and Rodrigo Soto. Coarsening and clustering in run-and-tumble dynamics with short-range exclusion. *Phys. Rev. E*, 94:022603, 2016.

[90] Michael F Hagan and Aparna Baskaran. Emergent self-organization in active materials. *Current Opinion in Cell Biology*, 38:74 – 80, 2016.

[91] Julian Bialké, Hartmut Löwen, and Thomas Speck. Microscopic theory for the phase separation of self-propelled repulsive disks. *EPL (Europhysics Letters)*, 103(3):30008, 2013.

[92] T. F. F. Farage, P. Krinninger, and J. M. Brader. Effective interactions in active brownian suspensions. *Phys. Rev. E*, 91:042310, 2015.

[93] Claudio Maggi, Umberto Marini Bettolo Marconi, Nicoletta Gnan, and Roberto Di Leonardo. Multidimensional stationary probability distribution for interacting active particles. *Scientific Reports*, 5:10742, 2015.

[94] Umberto Marini Bettolo Marconi and Claudio Maggi. Towards a statistical mechanical theory of active fluids. *Soft matter*, 11(45):8768–8781, 2015.

[95] Peter Hänggi and Peter Jung. Colored noise in dynamical systems. *Advances in chemical physics*, 89:239–326, 1995.

[96] Peter Jung and Peter Hänggi. Dynamical systems: a unified colored-noise approximation. *Physical review A*, 35(10):4464, 1987.

[97] Étienne Fodor, Cesare Nardini, Michael E. Cates, Julien Tailleur, Paolo Visco, and Frédéric van Wijland. How far from equilibrium is active matter? *Phys. Rev. Lett.*, 117:038103, 2016.

[98] Ronald F Fox. Functional-calculus approach to stochastic differential equations. *Physical Review A*, 33(1):467, 1986.

[99] Ronald Forrest Fox. Uniform convergence to an effective fokker-planck equation for weakly colored noise. *Physical Review A*, 34(5):4525, 1986.

[100] F. P. Kelly. *Reversibility and stochastic networks*. Wiley, New York, 1979.

[101] N.G. Van Kampen. *Stochastic Processes in Physics and Chemistry*. Elsevier, third edition, 2007.

[102] Sean P Meyn and Richard L Tweedie. *Markov chains and stochastic stability*. Springer Science & Business Media, 2012.

[103] Andrei Kolmogoroff. Zur theorie der markoffschen ketten. *Mathematische Annalen*, 112(1):155–160, 1936.

[104] Herbert S Wilf. *generatingfunctionology*. Elsevier, 2013.

[105] Cyril Banderier, Mireille Bousquet-Mélou, Alain Denise, Philippe Flajolet, Daniele Gardy, and Dominique Gouyou-Beauchamps. Generating functions for generating trees. *Discrete mathematics*, 246(1-3):29–55, 2002.

[106] Helmut Prodinger. The kernel method: a collection of examples. *Sém. Lothar. Combin*, 50:B50f, 2004.

[107] Donald E Knuth. The art of computer programming, volume 1: Fundamental algorithms addison-wesley. *Reading, Mass*, 1968.

[108] Mireille Bousquet-Mélou. A method for the enumeration of various classes of column-convex polygons. *Discrete Mathematics*, 154(1-3):1–25, 1996.

[109] Mireille Bousquet-Mélou. Multi-statistic enumeration of two-stack sortable permutations. *the electronic journal of combinatorics*, 5(1):R21, 1998.

[110] Martin R. Evans and Satya N. Majumdar. Diffusion with stochastic resetting. *Phys. Rev. Lett.*, 106:160601, 2011.

[111] S Redner. *A guide to first-passage processes*. Cambridge University Press, Cambridge, UK, 2001.

[112] A. B. Slowman, M. R. Evans, and R. A. Blythe. Exact solution of two interacting run-and-tumble random walkers with finite tumble duration. *Journal of Physics A: Mathematical and Theoretical*, 50:375601, 2017.

[113] James W Demmel. *Applied Numerical Linear Algebra*. SIAM, 1997.

[114] Norman L. Biggs. *Discrete Mathematics*. Oxford University Press, New York, 1990.

[115] J Schnakenberg. Network theory of microscopic and macroscopic behavior of master equation systems. *Reviews of Modern physics*, 48(4):571, 1976.

[116] R Gerd et al. *Nonequilibrium Statistical Physics*. John Wiley & Sons, 2013.

[117] Thomas Muir. *The theory of determinants in the historical order of development*, volume 1. Macmillan and Company, limited, 1906.

[118] Frank Harary. *Graph Theory*. Addison-Wesley, 1969.

[119] Seth Chaiken and Daniel J Kleitman. Matrix tree theorems. *Journal of combinatorial theory, Series A*, 24(3):377–381, 1978.

[120] G Kirchoff. über die auflösung der gleichungen, auf welche man bei der untersuchung der linearen verteilung galvanischer ströme gefuhrt wird. *Ann. Phys. Chem*, 72:497–508, 1847.

[121] G Kirchoff. On the solution of the equations obtained from the investigation of the linear distribution of galvanic currents. *IRE Trans. Circuit Theory*, 5:4–7, 2003.

[122] BO Shubert. A flow-graph formula for the stationary distribution of a Markov chain. *IEEE Transactions on Man and Cybernetics*, pages 1974–1975, 1975.

[123] V Anantharam and P Tsoucas. A proof of the Markov chain tree theorem. *Statistics & Probability Letters*, 8:189–192, 1989.

[124] Christian Maes, Karel Netočný, and Winny O'Kelly de Galway. Low temperature behavior of nonequilibrium multilevel systems. *Journal of Physics A: Mathematical and Theoretical*, 47(3):035002, 2014.

[125] Raffaele Basile, Ramon Grima, and Nikola Popović. A graph-based approach for the approximate solution of the chemical master equation. *Bulletin of mathematical biology*, 75(10):1653–1696, 2013.

[126] J Szavits Nossan. Disordered exclusion process revisited: some exact results in the low-current regime. *Journal of Physics A: Mathematical and Theoretical*, 46(31):315001, 2013.

[127] Christian Maes and Karel Netočný. Heat Bounds and the Blowtorch Theorem. *Annales Henri Poincaré*, 14(5):1193–1202, 2012.

[128] Christian Maes and Winny O'Kelly de Galway. A Low Temperature Analysis of the Boundary Driven Kawasaki Process. *Journal of Statistical Physics*, 153(6):991–1007, 2013.

[129] Katherine Humphreys. A history and a survey of lattice path enumeration. *Journal of Statistical Planning and Inference*, 140(8):2237–2254, 2010.

[130] Jens Elgeti and Gerhard Gompper. Run-and-tumble dynamics of self-propelled particles in confinement. *EPL (Europhysics Letters)*, 109(5):58003, 2015.

[131] Jérémie Gachelin, Gastón Miño, Hélène Berthet, Anke Lindner, Annie Rousselet, and Éric Clément. Non-newtonian viscosity of escherichia coli suspensions. *Physical review letters*, 110(26):268103, 2013.

[132] Nuris Figueroa-Morales, Gastón Leonardo Miño, Aramis Rivera, Rogelio Caballero, Eric Clément, Ernesto Altshuler, and Anke Lindner. Living on the edge: transfer and traffic of e. coli in a confined flow. *Soft Matter*, 11(31):6284–6293, 2015.

[133] Jens Elgeti and Gerhard Gompper. Wall accumulation of self-propelled spheres. *EPL (Europhysics Letters)*, 101(4):48003, 2013.

[134] Xingbo Yang, M Lisa Manning, and M Cristina Marchetti. Aggregation and segregation of confined active particles. *Soft matter*, 10(34):6477–6484, 2014.

[135] Barath Ezhilan, Roberto Alonso-Matilla, and David Saintillan. On the distribution and swim pressure of run-and-tumble particles in confinement. *Journal of Fluid Mechanics*, 781:R4, 2015.

[136] Alexandre P Solon, Y Fily, Aparna Baskaran, Mickael E Cates, Y Kafri, M Kardar, and J Tailleur. Pressure is not a state function for generic active fluids. *Nature Physics*, 11(8):673–678, 2015.

[137] Rodney J Baxter. *Exactly solved models in statistical mechanics*. Elsevier, 1989.

[138] Vladimir Privman. *Nonequilibrium statistical mechanics in one dimension*. Cambridge University Press, 2005.

[139] Richard A Blythe and Martin R Evans. Nonequilibrium steady states of matrix-product form: a solver's guide. *Journal of Physics A: Mathematical and Theoretical*, 40(46):R333, 2007.

[140] Anthony J Wood, Richard A Blythe, and Martin R Evans. Renyi entropy of the totally asymmetric exclusion process. *arXiv preprint arXiv:1708.00303*, 2017.

[141] Persi Diaconis, Susan Holmes, and Radford M Neal. Analysis of a nonreversible markov chain sampler. *Annals of Applied Probability*, pages 726–752, 2000.